Structural and Functional Models of Non-Heme Iron Enzymes

A Study of the 2-His-1-Carboxylate Facial Triad

Structurele en Functionele Modellen van Niet-Heem-IJzerbevattende Enzymen

Een Studie naar de 2-His-1-Carboxylaat Faciale Triade

(met een samenvatting in het Nederlands)

Proefschrift

ter verkrijging van de graad van doctor aan de Universiteit Utrecht
op gezag van de rector magnificus, prof. dr. W. H. Gispen
ingevolge het besluit van het college voor promoties
in het openbaar te verdedigen
op woensdag 31 januari 2007 des middags te 14.30 uur

door

Pieter Cornelis Antonius Bruijnincx

Geboren op 9 april 1979 te Roosendaal

Promotores: Prof. dr. G. van Koten

Prof. dr. R. J. M. Klein Gebbink

Prof. dr. ir. B. M. Weckhuysen

Structural and Functional Models of Non-Heme Iron Enzymes

A Study of the 2-His-1-Carboxylate Facial Triad

Voor mijn ouders

Bruijnincx, Pieter Cornelis Antonius

Title: Structural and Functional Models of Non-Heme Iron Enzymes. A Study of the 2-His-1-carboxylate Facial Triad
Utrecht, Utrecht University, Faculty of Science
Thesis Utrecht University – with ref. – with summary in Dutch –
ISBN–10: 90-393-4438-8
ISBN–13: 978-90-393-4438-5

The work described in this thesis was carried out at the Faculty of Science, Organic Chemistry and Catalysis group, Utrecht University, the Netherlands.

This investigation was financially supported by the National Research School Combination-Catalysis (NRSC-C).

CONTENTS

PREFACE

Aim and Scope of this Thesis

Biological inorganic chemistry is a thriving field at the interface of the chemical and biological sciences.[1] Its primary concern is the correlation of structure with function of all biological processes that involve metal-containing structures, i.e. it is the inorganic chemistry of life.

Biomimetic inorganic chemistry constitutes an important discipline within biological inorganic chemistry and involves the synthesis of small synthetic coordination or organometallic compounds that mimic biological systems.[2] The study of these synthetic analogues, be it structural or functional, provides further insight into the operation of biological structures, such as metalloenzymes, at a molecular level.[1,2] These insights may at the same time lead to the development of, for example, new medications or bio-inspired green catalysts that can contribute to a more sustainable society.[3,4] With respect to the latter application, synthetic inorganic chemists have been particularly interested in the modeling of non-heme iron containing metalloenzymes that are able to activate dioxygen and selectively oxidize organic substrates.[5,6] This challenge has been a long-standing goal in both industry and academia.[4]

In the last decade, a versatile family of mononuclear non-heme iron enzymes has emerged that catalyzes a remarkably divers set of oxidative transformations.[5,7] The enzymes share an active site in which two histidine residues and one carboxylato group occupy one face of the iron coordination sphere. This so-called 2-His-1-carboxylate facial triad has now been established as one of Nature's recurring structural motifs (Figure 1).[8]

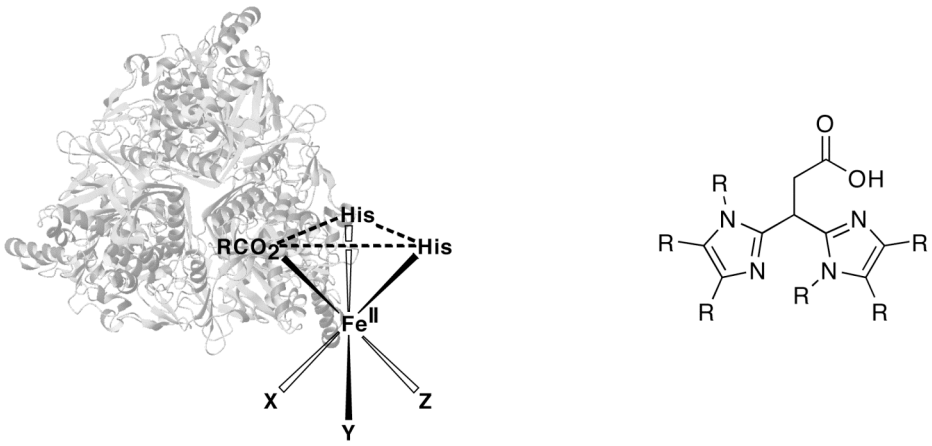

Figure 1. The 2-His-1-carboxylate facial triad and the new family of biomimetic *N*,*N*,*O* ligands studied in this thesis.

The aim of this work was the development of new, structurally faithful model complexes of the mononuclear non-heme iron enzymes that feature the 2-His-1-carboxylate facial triad and the study of these complexes as potential oxidation catalysts. For this purpose, a ligand system was developed that closely resembles this facial triad. The new family of substituted 3,3-bis(1-alkylimidazol-2-yl)propionates was designed to provide the metal center with the biologically relevant donor groups in the appropriate geometry (Figure 1). The iron coordination chemistry of these and related ligands was explored and the reactivity of the obtained complexes was studied. In addition, a few excursions into the coordination chemistry of copper and zinc are reported.

Chapter 1 offers a concise background on the current knowledge concerning non-heme iron enzymes with the 2-His-1-carboxylate facial triad and discusses recent developments in the field.

The new ligand family is introduced in Chapter 2 and a general synthetic route towards these tripodal tridentate *N*,*N*,*O* ligands is presented. The potential of these ligands to facially cap a metal center is illustrated by two crystallographically characterized copper complexes.

In Chapter 3 mononuclear iron-catecholato complexes of the new ligands are synthesized as accurate structural models of the extradiol cleaving catechol dioxygenases, a major subgroup of the 2-His-1-carboxylate family. The dioxygen reactivity of these complexes shows that they can be regarded as functional models as well.

A complementary biomimetic study of the intradiol cleaving catechol dioxygenases is the subject of Chapter 4. The use of a modified ligand system, which differs in the type of anionic oxygen donor group, allowed the synthesis of an accurate structural and functional model of the active site of this closely related group of non-heme iron enzymes.

The practical application of non-heme iron complexes as homogeneous oxidation catalysts was explored in the experiments described in Chapters 5 and 6. Both epoxidation and *cis*-dihydroxylation activity are observed for iron complexes of a neutral ester analogue of the new ligand family. Furthermore, the structure of both dinuclear and mononuclear iron complexes of a simple bidentate ligand and the reactivity of the latter in alkane and alkene oxidations are discussed.

The final two Chapters 7 and 8 concern the structure and reactivity of zinc and copper complexes of the new ligands. Rather unique reactivities of pyruvate and tetrachlorocatechol mediated by zinc and copper complexes, respectively, are described.

References

1. Kraatz, H.-B.; Metzler-Nolte, N. (eds), *Concepts and Models in Bioinorganic Chemistry*. Wiley New York, 2006.
2. Holm, R. H.; Solomon, E. I. *Chem. Rev.* **2004**, *104*, 347-348.
3. Collins, T. J. *Acc. Chem. Res.* **2002**, *35*, 782-790.
4. Tanase, S.; Bouwman, E. *Adv. Inorg. Chem.* **2006**, *58*, 29-75.
5. Costas, M.; Mehn, M. P.; Jensen, M. P.; Que, L., Jr. *Chem. Rev.* **2004**, *104*, 939-986.
6. Tshuva, E. Y.; Lippard, S. J. *Chem. Rev.* **2004**, *104*, 987-1012.
7. Solomon, E. I.; Brunold, T. C.; Davis, M. I.; Kernsley, J. N.; Lee, S-K.; Lehnert, N.; Neese, F.; Skulan, A. J.; Yang, Y-S.; Zhou, J. *Chem. Rev.* **2000**, *100*, 235-349.
8. Koehntop, K. D.; Emerson, J. P.; Que, L., Jr. *J. Biol. Inorg. Chem.* **2005**, *10*, 87-93.

CHAPTER 1

Mononuclear Non-Heme Iron Enzymes with the 2-His-1-Carboxylate Facial Triad: Recent Developments in Enzymology and Modeling Studies

Abstract

The family of non-heme iron enzymes that feature the 2-His-1-carboxylate facial triad at their active site has emerged as a common platform for dioxygen activation in Nature. This Chapter provides a concise background to this interesting group of metalloenzymes and the diverse oxidative transformations they catalyze. Recent developments in this field are discussed.

P. C. A. Bruijnincx, R. J. M. Klein Gebbink, G. van Koten, manuscript in preparation

1.1 Introduction

The oxidation of organic compounds is thermodynamically downhill and large amounts of energy are released in these reactions. However, the ground state of dioxygen in the atmosphere is open-shell, triplet O_2 and the (concerted) reaction of organic substrates, which usually have a singlet ground state, with dioxygen is a spin-forbidden process.[1] On a positive note, this means that spontaneous combustion of organic material, i.e. all forms of live, to carbon dioxide and water is prevented. Another consequence of the spin mismatch and the low one-electron oxidation potential of triplet oxygen is its rather sluggish kinetic reactivity.[2]

Nature has evolved an elegant solution to overcome the kinetic barrier for the activation of dioxygen by using e.g. transition metals. More specifically, several metalloenzymes catalyze the controlled and selective oxidation of organic compounds. The geometry and structural features of the active site and the choice of incorporated metal are very diverse and fully optimized to the function of the protein or enzyme. The correlation of this geometric and electronic structure with function is actually one of the main questions in the field of bioinorganic chemistry.[2,3] The activation of dioxygen on metal sites requires the availability of different redox states. Metalloenzymes capable of dioxygen activation consist mainly of enzymes with copper or iron active sites.[4,5] A wide variety of different mono- or multinuclear iron and copper enzymes have been discovered and found to catalyze major biological transformations.

The iron-containing enzymes that are involved in dioxygen activation can be divided into two groups based on the active site structures, i.e. heme and non-heme containing enzymes. The heme oxygenases have been studied extensively and are well understood, with cytochrome P450 as the prototypical example.[6] The non-heme iron oxygenases can in turn be divided in mononuclear and dinuclear iron enzymes.[2,7,8] Methane monooxygenase is a remarkable example of the latter group and catalyzes the selective oxidation of the most difficult hydrocarbon substrate, i.e. the oxidation of methane to methanol.[8]

However, the mononuclear non-heme iron oxygenases have received the most attention recently, primarily because of the availability of crystal structures of many different enzymes and the stunningly diverse oxidative transformations that these enzyme catalyze.[1,7,9] The wealth of structural data has furthermore established a new common structural motif for the activation of dioxygen.[9] This structural motif consists of a mononuclear iron(II) metal center that is coordinated facially by two histidine residues and one carboxylato ligand from either glutamate or aspartate residue (Figure 1). This structural motif has been coined the 2-His-1-carboxylate facial triad.[10]

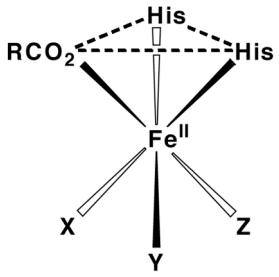

Figure 1. Schematic representation of the 2-His-1-carboxylate facial triad (X, Y, and Z denote weakly bound solvent molecules or vacant sites).

The superfamily of non-heme iron enzymes with this 2-His-1-carboxylate facial triad will be the focus of this Chapter. Several excellent reviews have been devoted (partly) to these enzymes,[1-3,7,9] which address the structural aspects of the enzymes, spectroscopic and theoretical methods and biomimetic modeling studies. Here, we provide a concise background and discuss the recent developments. Indeed, several new discoveries and important advances have appeared since the publication of the comprehensive review by Que et al. at the beginning of 2004.[7] For instance, new examples of enzymes belonging to the superfamily with unique reactivities have been reported. More insight into the mechanistic details and reactive intermediates has been obtained from both enzyme and modeling studies. Sections of this review are devoted to each of these subjects, i.e. the enzymes, biomimetic models, and reactive intermediates.

1.2 The 2-His-1-carboxylate facial triad

Over the last 10 years, there has been an explosion of available crystal structures of non-heme iron enzymes. The 2-His-1-carboxylate facial triad has thus been established in over 30 different structurally characterized enzymes.[9] The active site triad of this superfamily of enzymes can be regarded as one of Nature's recurring motif, like for instance the heme cofactor and iron-sulfur clusters.[10] It is interesting to note that the primary sequence homology amongst the different subfamilies (*vide infra*) is low. This implies that the triad is the result of a convergent evolution of unrelated enzymes and that this particular coordination geometry and choice of metal is favored for different oxidative transformations.[7]

The structural features of the 2-His-1-carboxylate facial triad are exemplified by the resting state of deacetoxycephalosporin C synthase (DAOCS), an enzyme that catalyzes the ring expansion of the thiazolidine ring of penicillin N to afford deacetoxycephalosporin C (Figure 2).[9,11]

One face of the octahedral coordination sphere of the ferrous metal center is occupied by the three endogenous ligands, i.e. two histidines and one aspartate or glutamate residue. In the as-isolated state of the enzymes, the other three coordination sites are either occupied by weakly bound and easily displaceable solvent molecules or are vacant. These three sites are therefore readily available for the binding of dioxygen, substrates, and cofactors. This

flexibility in coordination chemistry at the metal is the primary reason for the diversity in catalyzed oxidative transformations.[7] Small variations in the triad have been observed, such as for instance a bidentate coordination of the carboxylato group in some of the Rieske oxygenases.[7,12]

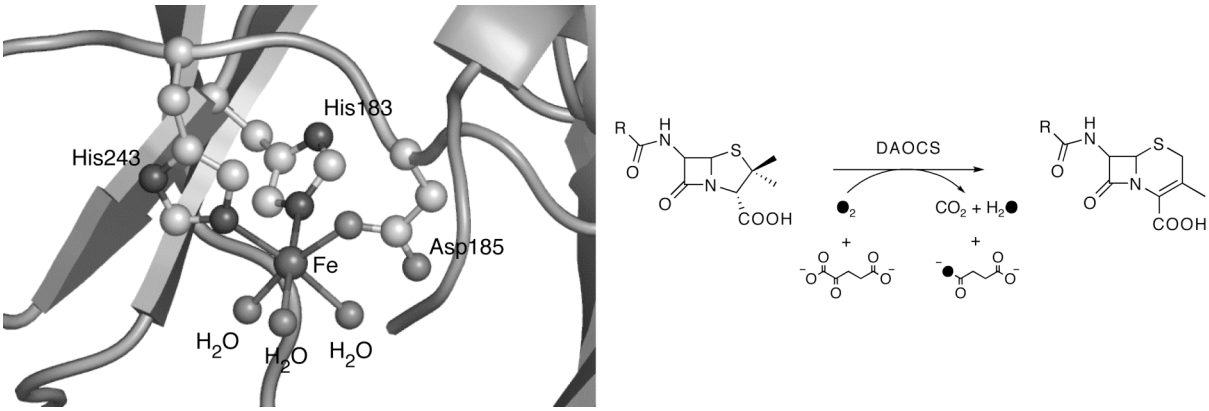

Figure 2. The active site of deacetoxycephalosporin C synthase features the 2-His-1-carboxylate facial triad (protein database accession code: 1RXF.pdb).[13]

Although a very diverse set of reactions are catalyzed by the superfamily of enzymes, some common mechanistic features are shared by all members (Figure 3).[2,3,7,9] First, the typically six-coordinate resting state of the enzyme is rather unreactive towards dioxygen (A). The subsequent binding of substrate or cofactor usually results in the formation of a coordinatively unsaturated, five-coordinate metal center and greatly enhances the dioxygen affinity (B).[3] This coupling of reactivity with substrate binding is a protection mechanism for the enzyme against self-inactivation. In the next step, dioxygen is activated for reaction by direct binding to the metal center (C). The enzymes use two different ways of activating dioxygen and overcoming the low one-electron redox potential of dioxygen by acquiring additional reducing equivalents from either a redox active cofactor or a redox active substrate.[3] The flexibility of the triad allows the binding of dioxygen *trans* to any of the three endogenous residues and the different *trans*-effects have been suggested to modulate the reactivity of the enzyme.[9,10] Dioxygen is then reduced to the peroxide level (D) and from this point on the proposed mechanisms for the different enzymes diverge. In most cases O–O bond cleavage and the formation of a high-valent iron-oxo species is invoked (E). This iron-oxo, be it Fe(IV) or Fe(v), is proposed to be the actual oxidizing species. The assignment of the structure of the oxidizing species is tentative in most cases, but has precedence in both modeling and enzyme studies. Direct evidence for a high-valent iron-oxo species has for instance been reported for the enzyme taurine/α-ketoglutarate dioxygenase[14-17] and several biomimetic oxoiron(IV) complexes have been characterized.[18-20]

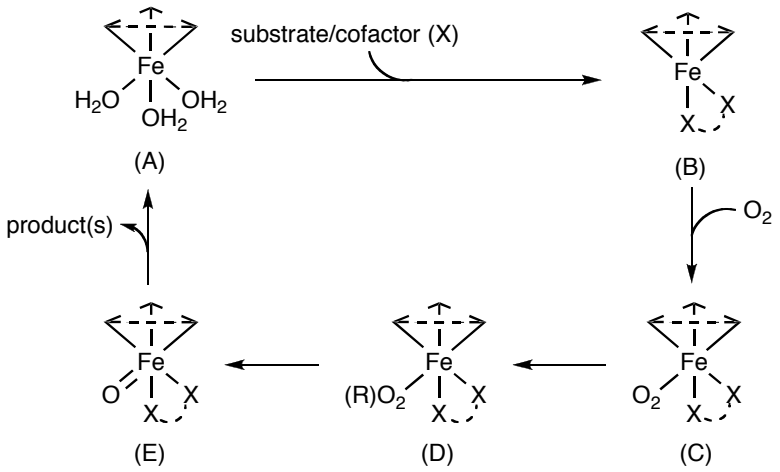

Figure 3. General mechanistic pathway for reactions catalyzed by the 2-His-1-carboxylate facial triad superfamily of non-heme iron(II) enzymes. Picture adapted from Que et al.[9]

The enzymes featuring the 2-His-1-carboxylate facial triad can be classified into five different groups based on their specific requirements for catalysis. These groups are the 1) extradiol cleaving catechol dioxygenases, 2) Rieske oxygenases, 3) α-ketoglutarate dependent enzymes, 4) pterin dependent hydroxylases, and finally 5) a miscellaneous category. The characteristics, recent developments, and illustrative examples of each group will be discussed.

1. Extradiol cleaving catechol dioxygenases. Oxidative ring cleavage is a key metabolic step in the biodegradation of aromatic compounds by bacteria.[21] The common metabolic pathway is the ring fission of catecholic substrates and is catalyzed by the extradiol cleaving catechol dioxygenases.[2,7,21,22] These enzymes utilize a non-heme iron(II) active site (or in a few cases Mn^{II})[23] to cleave the C–C bond next to the two hydroxyl groups with incorporation of both atoms of dioxygen in the substrate (Figure 4). Their intradiol counterparts, which represent a minor pathway, utilize a non-heme iron(III) active site to cleave the C–C bond in between the two hydroxyl groups. The extradiol cleaving dioxygenases are more versatile and in addition to catecholic substrates also accept gentisate, salicylate, hydroquinone and 2-aminophenol.[21] The biological ins and outs of the catechol cleaving dioxygenases have been very recently reviewed comprehensively.[21]

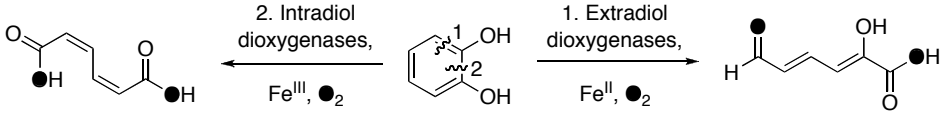

Figure 4. The extradiol and intradiol catechol cleavage pathways catalyzed by the catechol cleaving dioxygenases.

Three evolutionary independent classes of extradiol enzymes have been identified which all share similar active sites and all feature the 2-His-1-carboxylate facial triad.[21] In the

first step of the reaction, the substrate displaces two solvent molecules and binds to the metal to form a five-coordinate species (Figure 5).[3]

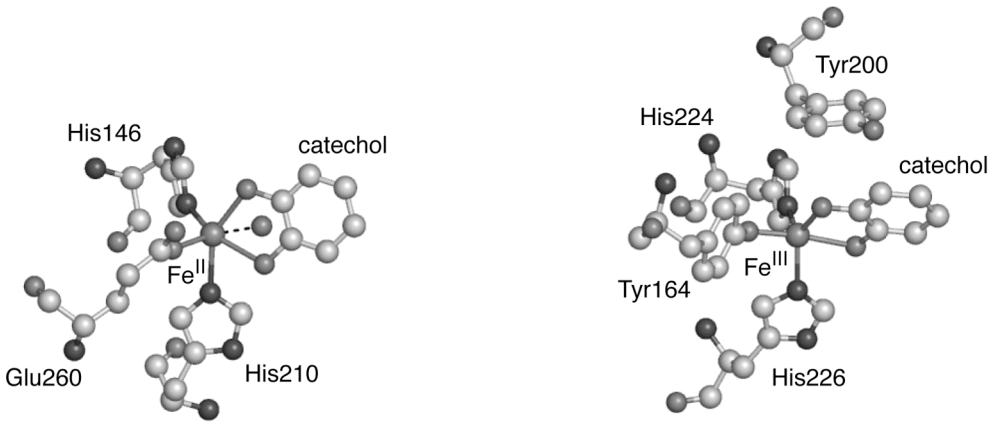

Figure 5. Enzyme–substrate (catechol) complexes of the extradiol enzyme 2,3-dihydroxybiphenyl 1,2-dioxygenase (left, 1KND.pdb) and the intradiol enzyme catechol 1,2-dioxygenase (right, 1DLT.pdb).

The substrate binds as a monoanion in an asymmetric fashion[24] and greatly enhances the affinity of the metal center for dioxygen (Figure 6A).[3] The dioxygen binding results in two subsequent electron transfer steps. First, an iron(III)-superoxide species is formed by one-electron transfer from the metal to dioxygen (B) and in a second step an electron is transferred from the substrate to the metal to form a semiquinonatoiron(II)-superoxide species (C).[7] Evidence for the involvement of a semiquinone species has been obtained from a radical probe substrate analogue[25] and the experimental detection of the initial dioxygen adduct has also been reported.[26] In the next step, a proximal alkylperoxo intermediate is formed (D), which undergoes a Criegee rearrangement (alkenyl migration) to form a seven-membered lactone species and a metal bound hydroxide (E). The latter hydrolyzes the lactone and the ring-opened product is formed.

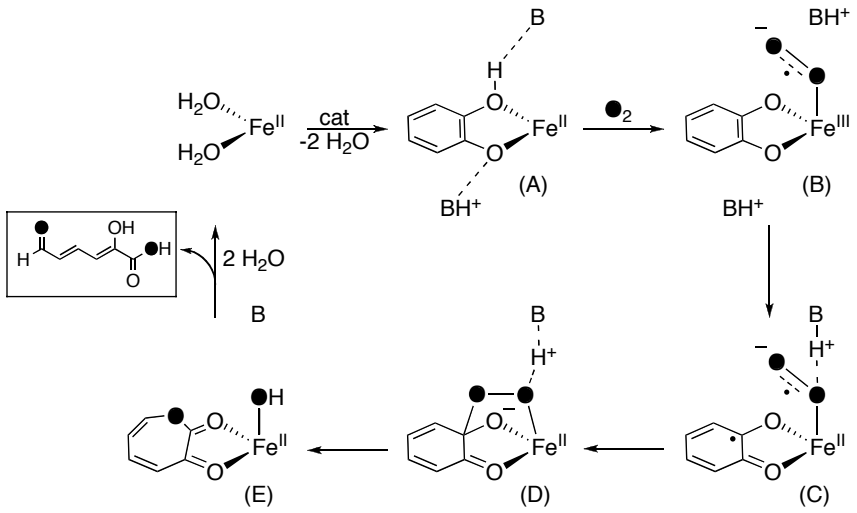

Figure 6. Proposed mechanism for the extradiol type cleavage of catechols (cat). B depicts a conserved second sphere residue.

The origin of the respective regioselectivities of the extradiol and intradiol cleaving catechol dioxygenases is not completely clear and is the subject of current research. The active sites of the enzyme-substrate complexes of the extradiol and intradiol enzymes are rather similar (Figure 5) and also for the intradiol cleaving enzymes a proximal alkylperoxo intermediate is proposed. In the case of intradiol cleavage, however, a different Criegee rearrangement would lead to the formation of an anhydride instead of a lactone. Several different explanations have been offered for the observed difference in regiochemistry. For instance, the exact coordination geometry,[7] stereoelectronic factors,[22] and acid-base chemistry of highly conserved second-sphere residues[27] have been suggested as decisive factors. Site-directed mutagenesis studies have provided considerable evidence that the latter factor determines the final outcome of the cleavage.[26,28,29] The extradiol and intradiol cleaving catechol dioxygenases are described in more detail in Chapters 3 and 4.

2. Rieske oxygenases. A common first step in the biodegradation of aromatic compounds is their conversion into *cis*-dihydroxylated metabolites. The regio- and stereospecific *cis*-dihydroxylation of arenas is catalyzed by Rieske non-heme iron dioxygenases.[7,12] Aromatic hydrocarbons are common contaminants of soil and groundwater and the Rieske dioxygenases provide an attractive way of biodegradation of these pollutants.[30] This, together with the fact that there is little precedent for its unique reactivity in synthetic organic chemistry,[7,31] has spurred a widespread interest in this group of enzymes. Rieske oxygenases have furthermore been shown to be very versatile. Next to *cis*-dihydroxylation, also other oxidations such as monohydroxylations, desaturation, sulfoxidation, O- and N-dealkylation, and amine oxidation are catalyzed.[7,32-35] Examples of some selected reactions catalyzed by Rieske oxygenases are shown in Figure 7.

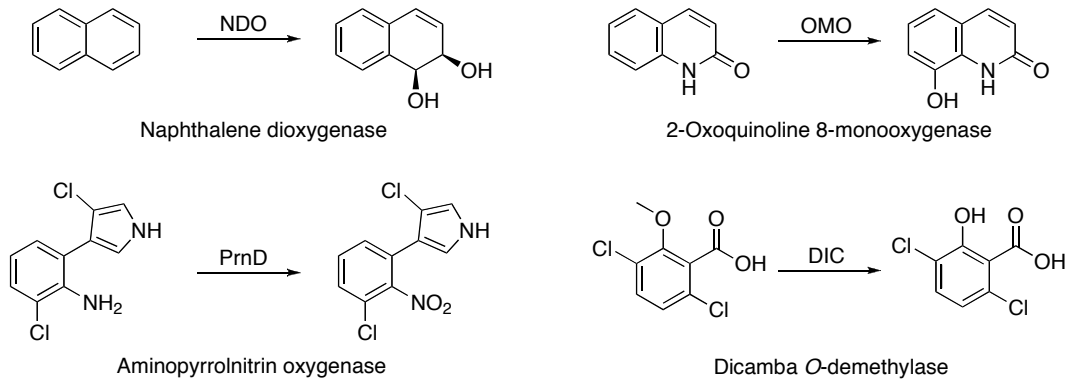

Figure 7. Some examples of reactions catalyzed by different Rieske oxygenases.

The Rieske oxygenases are multicomponent enzymes and consist of a reductase, an oxygenase, and in some cases also a ferredoxin component. Substrate oxidation takes place in the oxygenase component, which contains both a Rieske-type [2Fe-2S] cluster and the mononuclear non-heme iron active site. The Rieske cluster and the non-heme iron center are too far apart in a single subunit to allow for electron transfer. However, the quaternary trimeric structure allows for electron transfer of a Rieske cluster and a mononuclear iron

center from two different subunits. A key role in the electron transfer has been ascribed to a fully conserved aspartic acid residue that bridges between the two metal sites.[36] The two additional electrons needed for the full reduction of dioxygen are supplied by NAD(P)H and shuttled to the iron active site via the reductase and the Rieske cluster. The structural data on the oxygenase component of Rieske oxygenases has long been limited to the crystal structure of naphthalene dioxygenase (NDO).[37,38] Several three-dimensional structures including a dioxygen adduct of an enzyme-substrate analogue complex have been reported. The structural features of the latter complex are depicted in Figure 8.

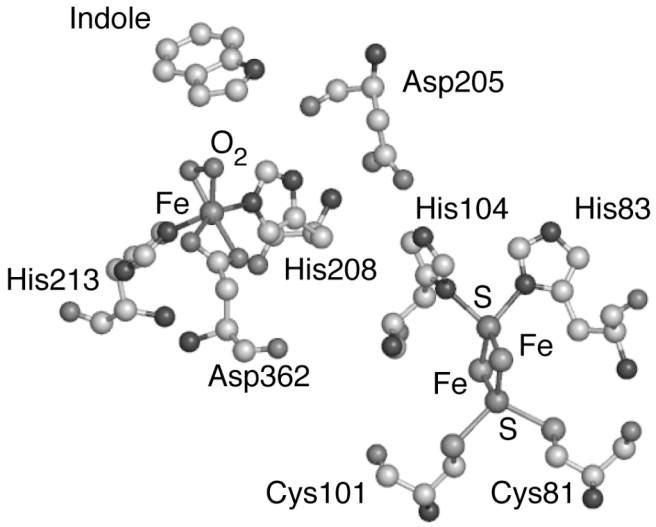

Figure 8. Dioxygen bound side-on to the metal center in naphthalene dioxygenase (1O7N.pdb). The [2Fe-2S] Rieske cluster and a conserved aspartate are also shown.

The structures show that the aspartate residue of the facial triad is bound in a bidentate fashion to the metal center, in a variation of the 2-His-1-carboxylate facial triad. Dioxygen is bound side-on to the iron and is reduced to the peroxide level, based on the O–O bond length of 1.4 Å.[37] Interestingly, the structure of NDO:Fe(II):Indole:NO shows an end-on bound nitric oxide.[39] Nitric oxide is often used as an unreactive analogue of dioxygen, but these results show that one has to be cautious in correlating directly NO binding data to dioxygen binding. In the last two years crystallographic data of five other Rieske oxygenases have been reported. The structures of biphenyl dioxygenase,[40] nitrobenzene dioxygenase,[41] cumene dioxygenase,[42] carbazole-1-9α-dioxygenase,[43] and 2-oxoquinoline 8-monooxygenase[35] show a high structural similarity to naphthalene dioxygenase with all key features present. An interesting variation amongst the reported structures is the binding mode of the aspartate of the facial triad. Whereas a bidentate aspartate was observed in NDO, monodentate binding is found in the enzyme-substrate complex of biphenyl dioxygenase[40] and the as-isolated states of cumene dioxygenase[42] and nitrobenzene dioxygenase.[41] In the latter case, the binding mode changes to bidentate upon substrate binding.

The mechanism of dioxygen activation is believed to be the same for all Rieske oxygenases, regardless of the substrate (Figure 9).[12] The binding of dioxygen to the metal is

enhanced upon substrate binding through the conversion to a five-coordinate metal center,[3] and is furthermore controlled allosterically by the redox state of the Rieske cofactor.[35] A side-on iron-(hydro)peroxide complex is formed upon binding of dioxygen and electron transfer from the Rieske cluster,[7,12] consistent with the crystallographically characterized dioxygen adduct.[37] The iron(III)-(hydro)peroxide intermediate can then either directly attack a substrate or first undergo O–O bond cleavage to yield an HO–Fe(v)=O intermediate. The latter option has been favored by some authors based on isotope labeling experiments with both the enzymes and model complexes, which show oxygen exchange of the active species with labeled water.[7] Others prefer the direct attack of substrate by the side-on (hydro)peroxide species without invoking higher oxidation states of iron.[12] Computational studies implicate a concerted step, where the O–O bond is cleaved concomitantly with the formation of an epoxide. A high activation barrier was found for the mechanism involving O–O bond cleavage prior to attack of the substrate.[44,45] The chemo-, regio-, and stereoselectivity of the specific reactions catalyzed by the different Rieske oxygenases seems determined solely by the specific orientation of the substrate in the binding pocket of the enzyme. Interactions between active site residues and the substrate through, for instance, hydrogen bonds determine this orientation.[12,46]

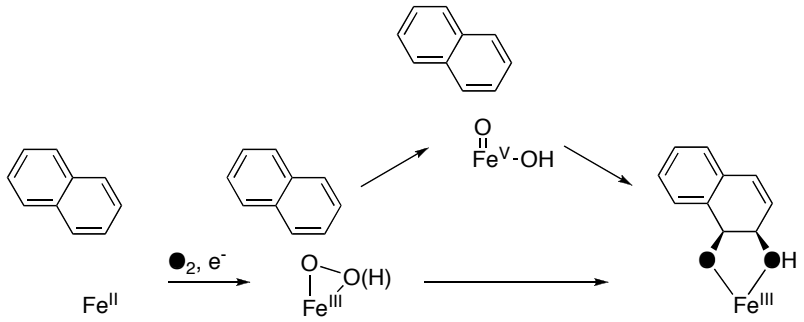

Figure 9. Two possible intermediates in the *cis*-dihydroxylation of naphthalene.

3. α-Ketoglutarate dependent enzymes. The largest subfamily of non-heme iron enzymes with the 2-His-1-carboxylate facial triad couples the oxidative transformation of substrates to the oxidative decarboxylation of the cofactor α-ketoglutarate (α-KG) to carbon dioxide and succinate.[7] This subfamily is not only the largest, but also catalyzes the most diverse set of oxidative transformations. Reactions include hydroxylation, desaturation, ring closure, ring expansion, and many more. The subfamily constitutes probably the most versatile group of oxidizing biological catalysts identified to date.[47] Many of these transformations are at the moment beyond the scope of synthetic organic chemists and are therefore of special chemical interest.[47] Several different reviews have been published recently that are specifically devoted to this subfamily of enzymes.[47-49] Here, we will therefore only address some general features and typical examples. Hydroxylation, for instance, is the most common reactivity observed and its general scheme is shown in Figure 10.

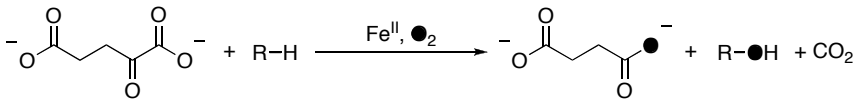

Figure 10. General hydroxylation reaction catalyzed by several α-KG dependent oxygenases.

Two types of hydroxylation reactions have recently received increased attention out of medical interest. Damage of RNA and DNA by nucleotide alkylation results in lesions that are both cytotoxic and mutagenic.[50] Several α-KG dependent oxygenases have been shown to repair these alkylated DNA and RNA bases. *Escherichia coli* AlkB and the homologous human enzyme ABH3 fix the lesion by hydroxylating the alkyl group, after which spontaneous deformylation yields the unmodified base (Figure 11A).[50,51]

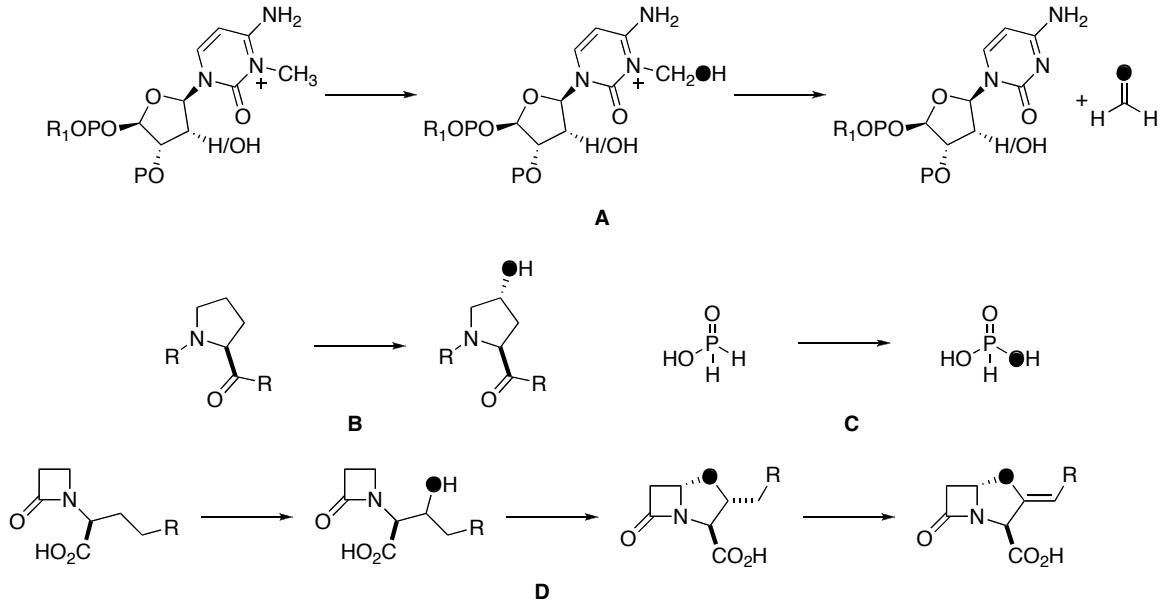

Figure 11. Some selected reactions catalyzed by α-KG dependent oxygenases. A) Nucleobase demethylation by DNA/RNA repair enzyme AlkB; B) Stereospecific proline hydroxylation by proline 4-hydroxylase; C) Hypophosphite hydroxylation by hypophosphite/α-KG dioxygenase HtxA; D) Hydroxylation, ring closure and desaturation reactions in the synthesis of clavulanic acid by clavaminate synthase CAS.

Other, related demethylation reactions catalyzed by α-KG dependent enzymes, such as histone demethylation, have been reported recently.[52,53] The hydroxylation of specific residues of protein side chains and more specifically in oxygen sensing in the cell has also attracted recent interest. Hypoxia-inducible factor (HIF) is responsible for mediating the mammalian response to low oxygen tension (hypoxia). α-KG dependent HIF hydroxylases have been implicated in this hypoxic response and are therefore interesting targets for the development of new therapies for the different diseases associated with this system.[54] Other functions of the α-KG dependent oxygenases include the biosynthesis of antibiotics and plant products, lipid metabolism and biodegradation.[48] Some selected examples are shown in Figure 11.

The crystal structures of many different α-KG dependent oxygenases have been reported.[47] The ternary TauD:Fe(II):α-KG:substrate complex, for instance, shows a five-coordinate metal center with the α-KG cofactor bound in a bidentate way (Figure 12). The cofactor is further held in place by additional interactions of the C5-carboxylate with conserved residues. The primary substrate is not bound directly to the metal center, but is found close to the open coordination site, which is believed to be the site of dioxygen binding. Taurine:α-KG dioxygenase (TauD) catalyzes the hydroxylation of taurine (2-aminoethane-1-sulfonic acid), which leads eventually to sulfite elimination from the product.[14]

The large body of crystallographic data together with spectroscopic studies on especially TauD[14] and CAS[55] have led to the proposal of a common, conserved mechanism for the α-KG dependent oxygenases (Figure 12).[7,14,47,48]

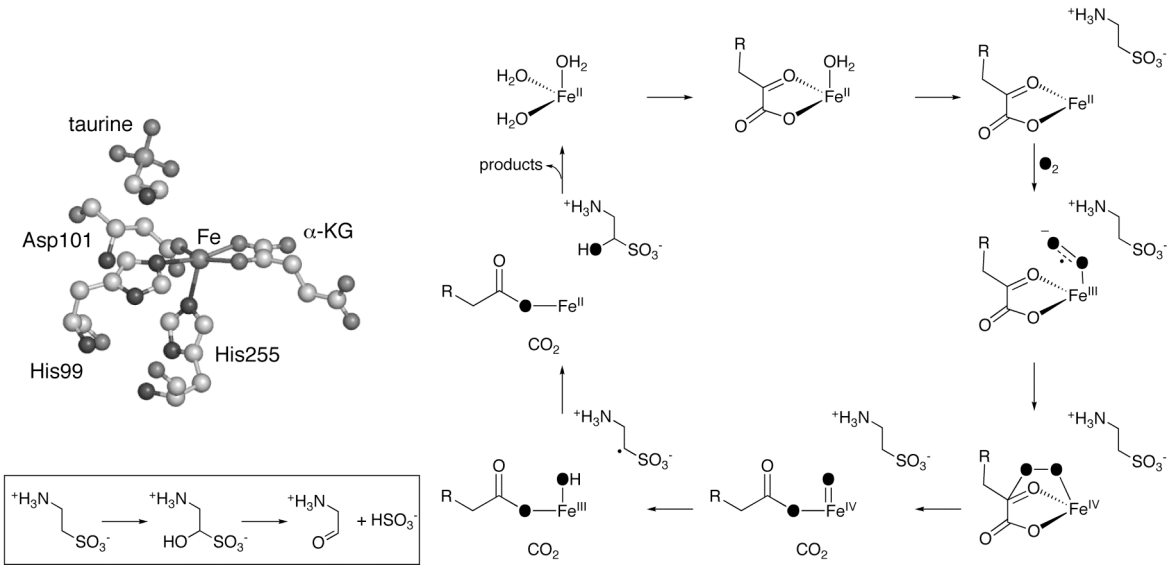

Figure 12. Left: Active site of the ternary TauD:Fe(II):α-KG:taurine complex (1OS7.pdb).[56] Right: Consensus mechanism for α-KG dependent dioxygenases, exemplified for TauD (adapted from ref. 14).

In this general mechanism, an ordered sequential binding of first α-KG (A), then substrate (B) and finally dioxygen is assumed (C). Upon binding of dioxygen, an adduct with significant Fe(III)-superoxide radical anion character is formed.[57] Attack of the carbonyl carbon atom by this species would then result in a cyclic species (D). In the next step, decarboxylation and O–O bond cleavage yield succinate, carbon dioxide and an high-valent Fe(IV)=O species (E), which is the intermediate responsible for the substrate oxidation leading to hydroxylation or a related two-electron oxidation.[14] This ferryl intermediate has been observed experimentally for TauD by rapid freeze-quench Mössbauer,[15] EXAFS,[17] and resonance Raman studies.[16] These studies provided the first direct evidence of the involvement of an iron(IV) intermediate in reactions catalyzed by mononuclear non-heme iron enzymes.

The α-KG-dependent non-heme iron enzymes (4-hydroxyphenyl)pyruvate dioxygenase (HppD)[58] and (4-hydroxy)mandalate synthase (HmaS)[59] form an interesting pair in the sense that they use the same substrate, (4-hydroxyphenyl)pyruvate which itself has an α-keto acid moiety (Figure 13). As a result both atoms of dioxygen are incorporated into the product, similar to the extradiol cleaving dioxygenases. HppD yields the aromatic hydroxylated product homogentisate using an electrophilic attack mechanism followed by an NIH shift, whereas HmaS generates the benzylic hydroxylated product (S)-(4-hydroxy)mandalate via the hydrogen abstraction mechanism.[60] The two enzymes generate the same reactive Fe(IV)=O intermediate, but are able to steer the reaction into two different directions. The decisive factor was found to be the exact orientation of the substrate in the binding pocket.[60]

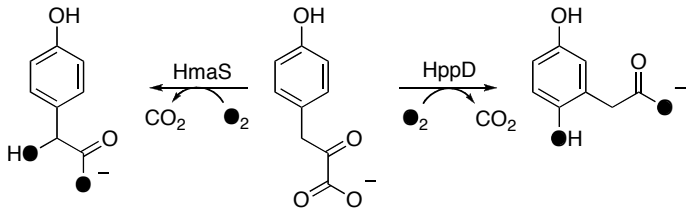

Figure 13. Oxidative transformations of (4-hydroxyphenyl)pyruvate catalyzed by HmaS and HppD.

Recently, a group of non-heme iron enzymes with quite a different reactivity has been discovered.[61] Rather than hydroxylation, these enzymes catalyze the *halogenation* of aliphatic C–H bonds and require Fe(II), α-KG, dioxygen and chloride for activity. The enzymes SyrB2[62] and CmaB[63] are involved in the biosynthesis of the phytotoxin syringomycin E and the phytotoxin precursor coronamic acid, respectively. Syr2B catalyzes the chlorination of a threonine methyl group, whereas CmaB catalyzes the γ-halogenation of L-*allo*-isoleucine as part of a cryptic biological strategy for cyclopropyl ring formation (Figure 14).

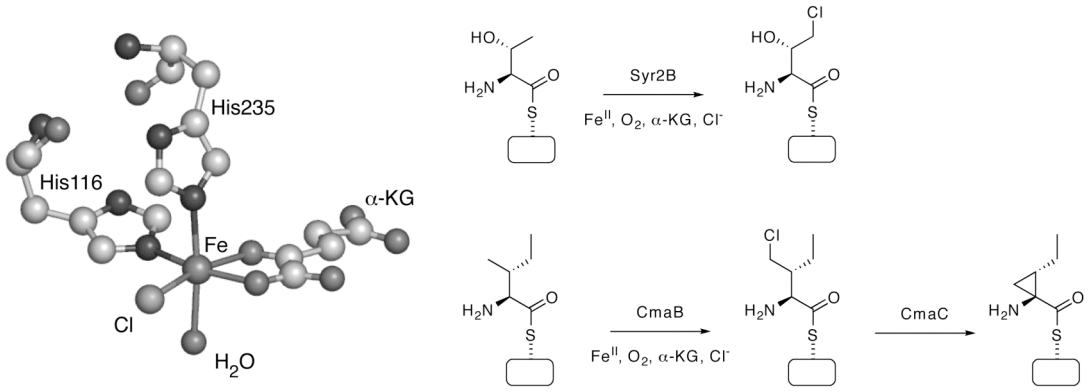

Figure 14. Left: An unprecedented iron scaffold at the active site of Syr2B. Right: The halogenation reactions catalyzed by Syr2B and CmaB.

The crystal structure of the Syr2B:Fe(II):α-KG complex was solved very recently. As a surprising result it presented the first α-KG dependent non-heme iron enzyme *not* coordinated by the 2-His-1-carboxylate facial triad.[64] Instead, the metal was coordinated by α-KG, a chloride anion and only two endogenous ligands. i.e. two histidines (Figure 14). An alanine

replaced the aspartate of the facial triad. The mechanism of halogenation is thought to be similar to the common hydroxylation with chloride abstraction instead of hydroxyl abstraction by the carbon radical in the final step.[64] The non-heme iron halogenation catalysts are not limited to these two enzymes as bioinformatic analysis has provided leads to additional members of this interesting new group.[61]

4. Pterin dependent hydroxylases. A small family of aromatic amino acid hydroxylases requires the cofactor tetrahydrobiopterin (BH_4) for activity.[1,7] Its members phenylalanine hydroxylase (PheH), tyrosine hydroxylase (TyrH), and tryptophan hydroxylase (TrpH) are essential for mammalian physiology.[7] The enzymes catalyze the regiospecific monohydroxylation of their namesake amino acid with concomitant oxidation of the pterin cofactor (Figure 15).

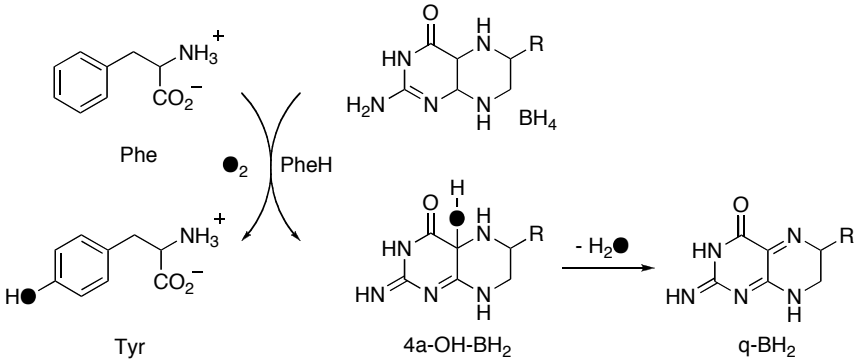

Figure 15. Hydroxylation of phenylalanine to tyrosine catalyzed by phenylalanine hydroxylase (PheH).

This group of enzymes has received considerable attention because of their implication in several neurological and physiological diseases. Several different reviews are available that comprehensively discuss the current state of knowledge of this sub-family.[1,7,15,65,66] The crystal structures of all three enzymes[67-69] show the presence of a mononuclear non-heme iron active site, coordinated by the 2-His-1-carboxylate facial triad and three water molecules. Interestingly, large conformational changes upon substrate binding are observed at the active site in the crystal structure of PheH:Fe(II):BH_4:tha (tha, 3-(2-thienyl)-L-alanine, a substrate analogue).[70] The monodentate glutamate becomes bidentate, water molecules are lost and the pterin-cofactor is displaced towards the iron (Figure 16). All these changes facilitate the binding of dioxygen at the active site.

The plethora of spectroscopic and structural data has led to a consensus about the possible mechanism, although none of the (reactive) intermediates have yet been observed.[1,7,71] First, an pterinperoxo-iron(II) species is formed, which cleaves heterolytically to yield a reactive iron(IV)-oxo intermediate. Finally, the product is formed via electrophilic attack of the substrate.

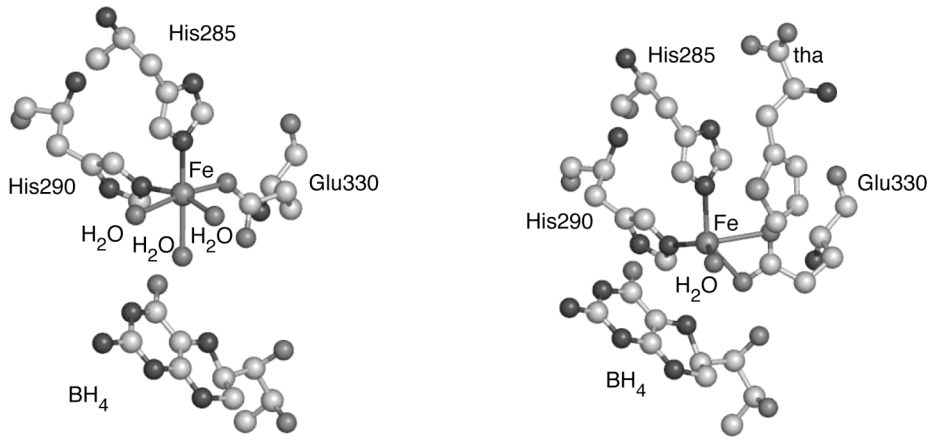

Figure 16. Structural changes upon substrate binding to the active site of phenylalanine hydroxylase. Left: the binary PheH:Fe(II):BH_4 complex (1J8U.pdb); right: the ternary PheH:Fe(II):BH_4:tha complex (1KW0.pdb).

5. Miscellaneous. This category is a diverse collection of enzymes that do not fit into the previous four classes with respect to their specific requirements for catalysis. It is a 'catch-all' category and some very recent discoveries have been included. These newly discovered metalloenzymes catalyze unprecedented chemical reactions and offer a glimpse of the systems and their chemistry, which still are to be discovered.

The enzyme sulfur oxygenase reductase (SOR) for instance, catalyzes a distinctive oxygen-dependent sulfur disproportionation reaction with sulfite, thiosulfate, and hydrogen sulfide as the products (Figure 17).[72]

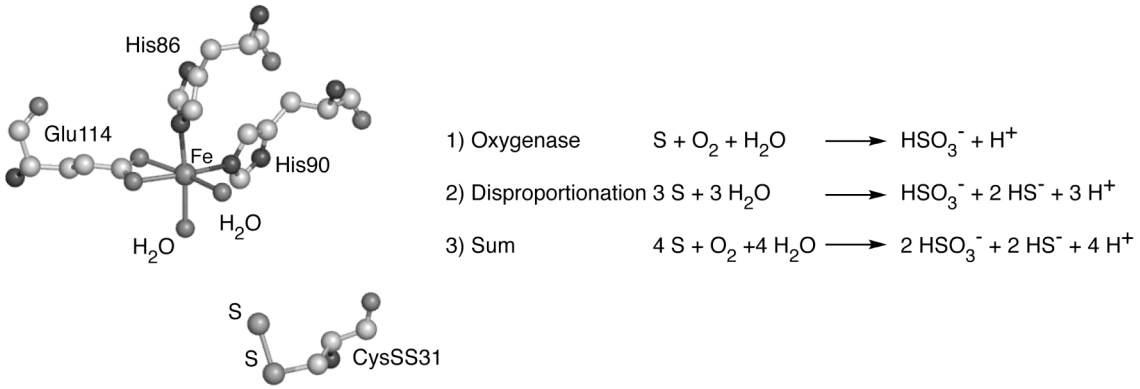

Figure 17. The active site of SOR shows a bidentate glutamate residue and a cysteine persulfide as the substrate binding site (2CB2.pdb).

SOR is one of the few systems known to oxidize elemental sulfur, an essential reaction for ecosystems that use sulfur as the major energy source. The *Acidianus ambivalens* SOR is a complex self-compartmentalizing metalloenzyme that consists of 24 subunits and forms a hollow sphere.[72] A mononuclear non-heme iron site and a cysteine persulfide were found to be important for catalysis. The latter is the probable covalent binding site for linear elemental

sulfur substrate. As previously observed for some of the Rieske dioxygenases, the glutamate of the triad is bound as a bidentate to the metal. Two water molecules complete the distorted octahedral coordination sphere. Since no other redox-active site was found in SOR, the rather complicated sulfur disproportionation chemistry has to take place at the iron active site.

Fosfomycin, or (1*R*,2*S*)-1,2-epoxypropylphosphonic acid, is a clinically useful antibiotic and is for instance used in the treatment of lower urinary tract infections.[73] The last step in the biosynthesis of fosfomycin in *Streptomyces wedmorensis* is the dehydrogenation of (*S*)-2-hydroxypropylphosphonic acid (Hpp) by Hpp epoxidase (HppE) (Figure 18). HppE was recognized as a non-heme iron enzyme belonging to the class featuring the facial triad.[74,75] This reaction is unique in biology since the epoxidation reaction is an oxidative cyclization with retention of the substrate hydroxyl oxygen atom.[74] Usually, in epoxidations such as those catalyzed by cytochrome P450, the incorporated oxygen atom is derived from dioxygen.[6] A catalytic turnover of HppE consumes a stoichiometric amount of NADH with molecular oxygen as the oxidant.[74] Recently, crystal structures of the native enzyme and the enzyme-substrate complex became available.[73] The substrate replaces the two water molecules bound to iron in the as-isolated state consecutively and binds to the metal in a bidentate fashion. Binding of the substrate again activates the metal center for dioxygen activation. The stereo- and regiospecific hydrogen abstraction step is then catalyzed by either an iron(III)-hydroperoxide (Figure 18, path A) or iron(IV)-oxo (path B) species to give a substrate radical intermediate. Cyclization of the radical yields the two-electron oxidized final product.

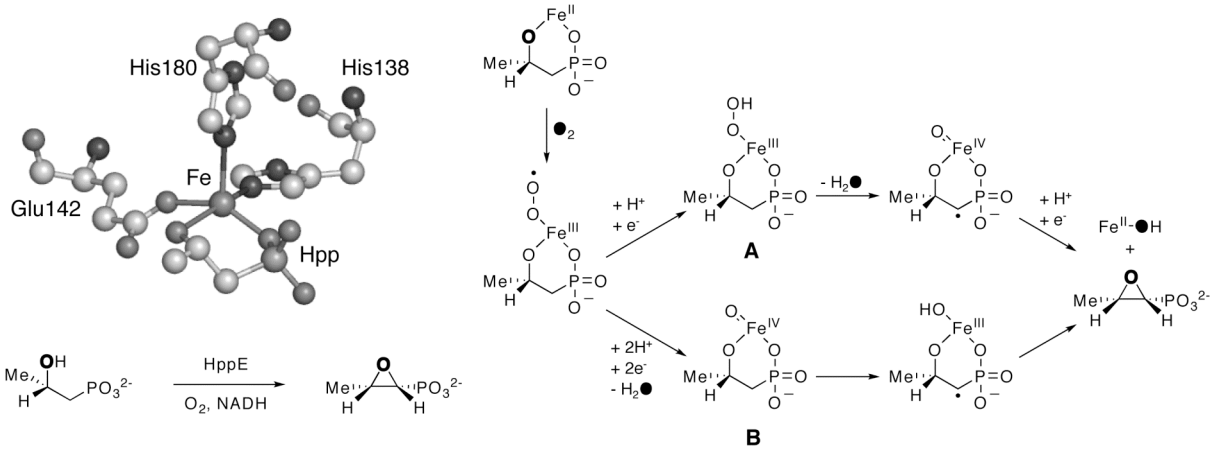

Figure 18. The enzyme-substrate complex of HppE (1ZZ8.pdb) and two possible mechanisms, going through either an iron(III)-hydroperoxide (A) or iron(IV)-oxo species (B).

The enzyme HppE shows similarities with the microbial enzyme isopenicillin N synthase (IPNS). IPNS is a non-heme iron enzyme that catalyzes the double oxidative ring closure of the tripeptide δ-(L-α-aminoadipoyl)-L-cysteinyl-D-valine (acv) to form the bicyclic β-lactam isopenicillin N, the biosynthetic precursor to all penicillins and cephalosporins (Figure 19).[7,76]

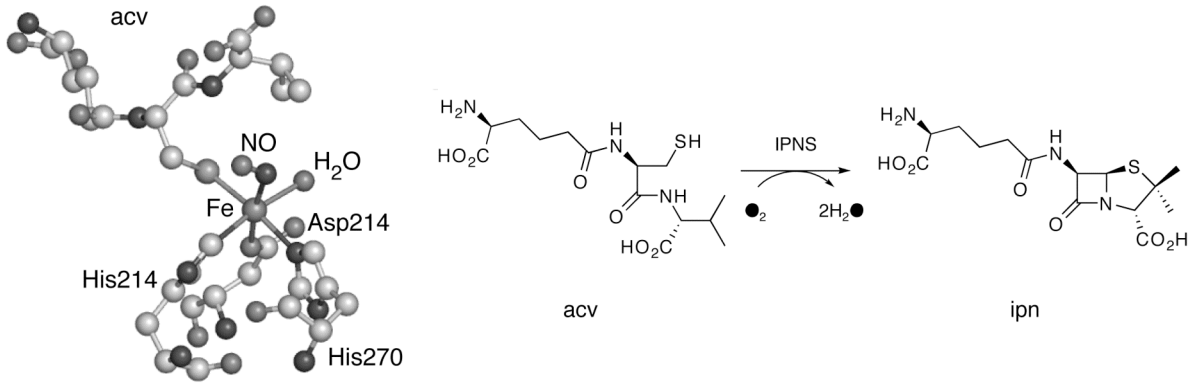

Figure 19. Active site of the ternary IPNS:Fe(II):acv:NO complex and the oxidative double ring closure catalyzed by IPNS.

IPNS shows a high sequence homology to the α-ketoglutarate dependent enzymes, but does not require α-ketoglutarate as cofactor and it does not incorporate oxygen into the product.[7] In the case of IPNS all four electrons required for the reduction of dioxygen to water are provided by the substrate. Crystal structures are available for different stages of the reaction,[77-79] such as for instance the ternary IPNS:Fe(II):acv:NO complex.[79] Nitric oxide (NO) is often used as an unreactive O_2-surrogate to get more insight into the interaction of dioxygen with the metal. Based on this information and comprehensive studies with substrate analogues,[7,76] a mechanism has been proposed. The closure of the β-lactam precedes the formation of the thiazolidine ring, which is mediated by a reactive iron(IV)-oxo intermediate (Figure 19). The enzymology of IPNS and other enzymes involved in the biosynthesis of β-lactam derived compounds has been recently reviewed.[76]

The enzyme 1-aminocyclopropane-1-carboxylic acid oxidase (ACCO) also shows a high sequence homology to the α-ketoglutarate dependent enzymes, but like IPNS does not require α-ketoglutarate as cofactor.[7] ACCO is an enzyme that produces the plant hormone ethylene, which regulates many aspects of plant growth and development. It couples the two-electron oxidation of the unusual amino acid 1-aminocyclopropane-1-carboxylic acid (acc) to give ethylene, CO_2 and HCN.[7] Continuous turnover requires the presence of ascorbate and bicarbonate. Due to the lack of available structural information and the inherent complexity of the system, the mechanism of ACCO is not yet fully understood.[80,81] It is known that the binding of substrate acc activates the iron center in the enzyme for dioxygen by converting it from six- to five-coordinate.[3,82] Indeed, the ternary ACCO:Fe(II):acc:NO complex has been observed by ENDOR spectroscopy.[83] Based on single turnover studies, ascorbate has been ascribed the traditional role of preferred two-electron reductant.[84] In addition, ascorbate might serve a second role by binding at a specific effector site and thus facilitating the formation of the ternary enzyme-substrate-dioxygen complex. Bicarbonate is then proposed to be involved in the generation of the reactive species by a specific protonation step.[84]

The mechanism proposed by Que et al.[84] is shown in Figure 20. Recently, the first crystal structure of ACCO was reported,[85] featuring the 2-His-1-carboxylate facial triad with a

monodentate aspartate residue. This structure will provide a basis for future studies on this convoluted system.

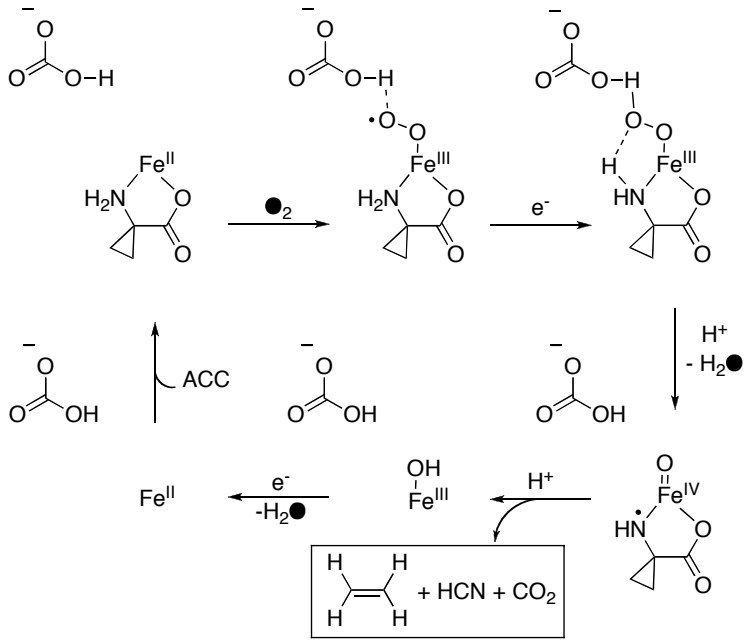

Figure 20. Proposed mechanism for ACCO catalysis. The source of the individual electrons is not well established and not included.

1.3 Biomimetic modeling studies

Many efforts by synthetic inorganic chemists have been devoted to biomimetic modeling studies of the enzymes of the 2-His-1-carboxylate facial triad family. Initial studies focused on the development of functional models of the different subfamilies and employed mostly polydentate all-*N* ligands. Impressive results have been obtained in the modeling of several of the different subfamilies (*vide infra*). The tris(2-pyridylmethyl)amine (tpa), hydridotris(pyrazol-1-yl)borato (Tp), *N*,*N*-bis(2-pyridylmethyl)-*N*,*N*'-dimethyl-1,2-ethylenediamine (bpmen), and 1,4,7-triazacyclononane (tacn) ligands and derivatives thereof have been used as the workhorses in many of these studies (Figure 21).[7]

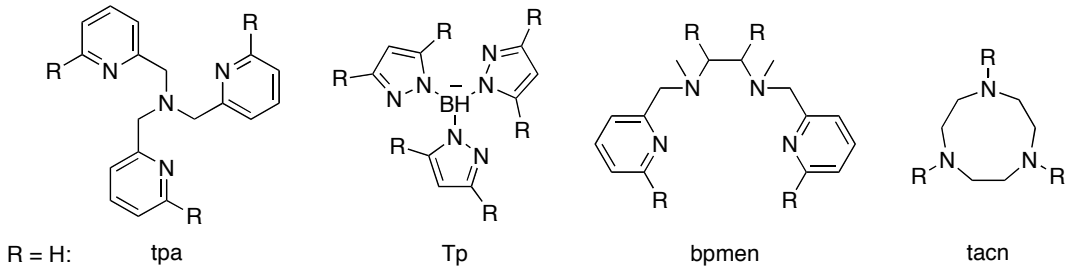

Figure 21. Prominent polydentate all-*N* ligands that have been used in modeling studies of the enzymes with the 2-His-1-carboxylate facial triad. The R groups are drawn at positions, which are commonly modified.

Structural models. Recently, attention has shifted to the design of structural models that more faithfully reproduce the coordination environment of the 2-His-1-carboxylate. Different approaches have been taken to mimic the facial coordination of two imidazole groups and a mono- or bidentate carboxylato group. Burzlaff et al. have studied the iron and zinc coordination chemistry of the bispyrazolylacetates,[86,87] which belong to the family of monoanionic *N*,*N*,*O* heteroscorpionates.[88] The tripodal ligand framework of the bispyrazolylacetates predisposes the three donor groups to facially cap a metal center. The ligands are readily synthesized and the steric properties of the ligand can be varied by the introduction of pyrazole groups with different substitution patterns. Depending on the steric demand of the ligand and the nature of the iron precursor that are used different complexes have been obtained. The most common one is of the $[Fe^{II}L_2]$ type, but also a dimeric species and a mononuclear ferric complex have been reported (Figure 22).[86,87] Recent reports focused on the synthesis of chiral members and an enantiopure heteroscorpionate was reported.[89]

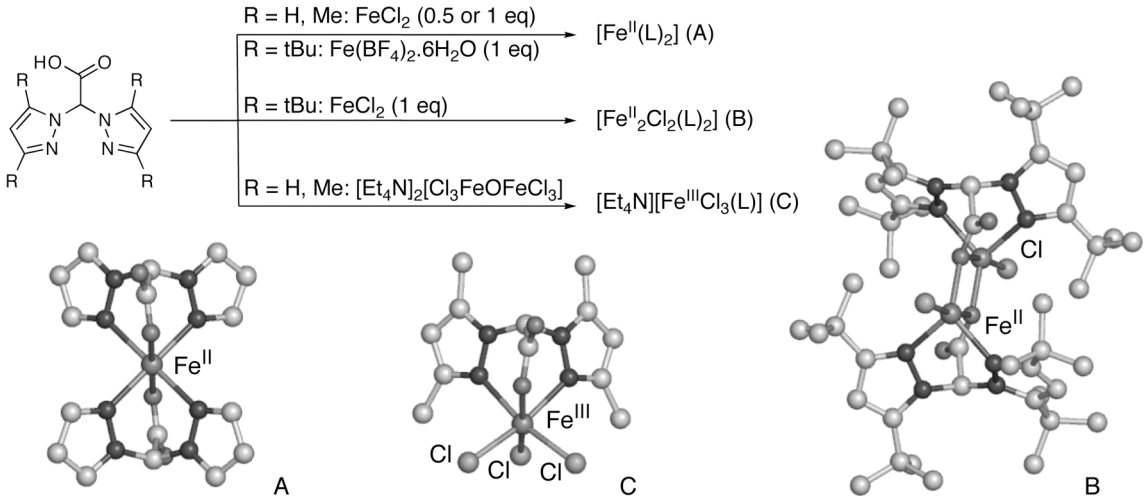

Figure 22. Iron coordination chemistry of the bispyrazolylacetate ligand family.

Que and Tolman et al. have reported recently on a different synthetic strategy to obtain mononuclear iron complexes with an *N*,*N*,*O* donor set.[90] The use of a highly sterically hindered monodentate carboxylato ligand and a bulky diamine allowed the isolation of the mononuclear iron complex $[Fe^{II}Cl(BmaCO_2)(tBu_2Me_2eda)]$ (Figure 23). The structure reveals a carboxylato ligand coordinated in a bidentate fashion, a coordination mode that is found in several different enzymes with the facial triad.

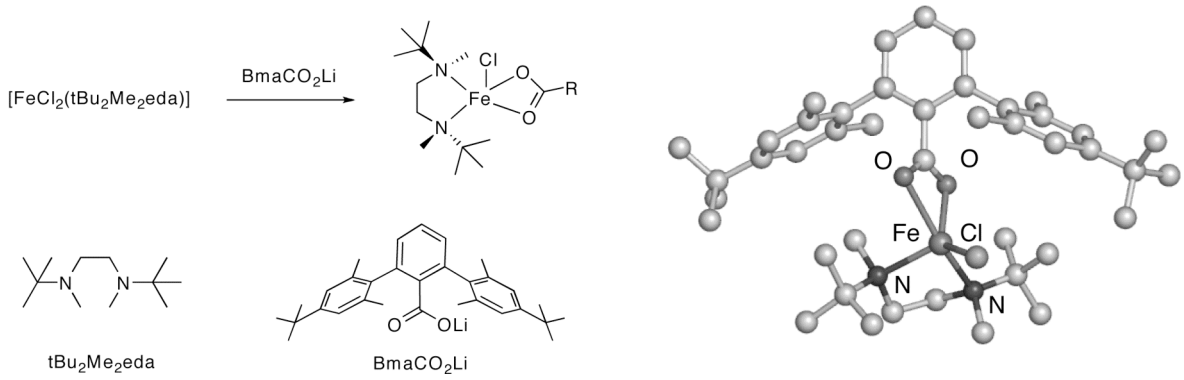

Figure 23. Assembly of a mononuclear iron complex from sterically hindered ligands.

The nitrogen donor atoms in these structural models are distinctly different from the biological systems. The pyrazole rings of the bispyrazolylacetates, for instance, differ both in size, and in chemical and electronic properties from the histidyl imidazole-side found in the biological systems. To resemble also the electronic properties of the facial triad more closely a new tripodal ligand system was developed by the group of Klein Gebbink[91] and that of Burzlaff.[92] The family of substituted 3,3-bis(1-alkylimidazol-2-yl)propionates incorporate the biologically relevant 1-methylimidazole and carboxylate donor groups into a tripodal, monoanionic framework (Figure 24). The facial capping potential of these ligands was illustrated by their copper,[91] rhenium, and manganese[92] complexes.

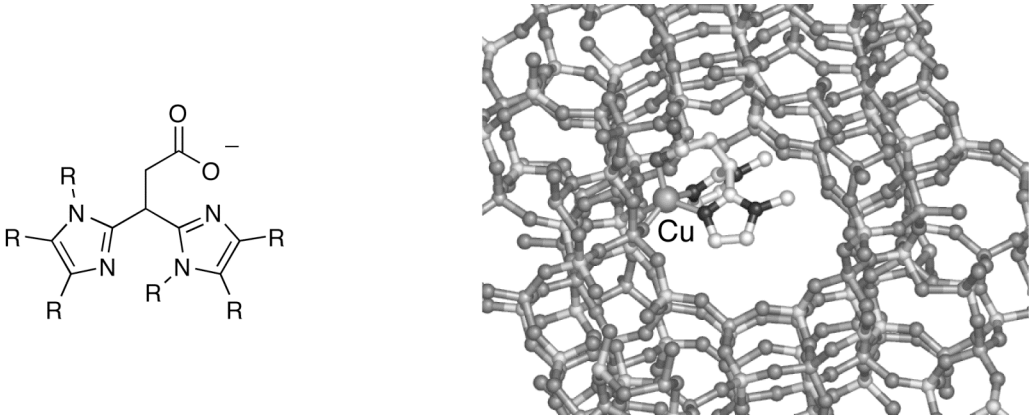

Figure 24. Left: the tripodal *N,N,O* binding 3,3-bis(1-methylimidazol-2-yl)propionate ligand family. Right: Zeolite-immobilized copper complex with the parent ligand.

At the active site of the enzymes with the 2-His-1-carboxylate facial triad, the iron(II) center is facially capped by the three protein residues and the other three sites are either vacant or taken by solvent molecules. This situation is difficult to reproduce in a model system. Indeed, both with the bispyrazolylacetates and 3,3-bis(1-alkylimidazol-2-yl)propionates often coordinatively saturated [FeL_2] type complexes are obtained. Weckhuysen and Klein Gebbink et al. have reported a possible solution to this problem by immobilizing a 1:1 copper(II) complex with 3,3-bis(1-methylimidazol-2-yl)propionate in a

zeolite supercage. The five-coordinate metal was shown to be facially capped by the ligand and still catalytically active in the oxidation of benzyl alcohol (Figure 24).[93] The mononuclearity of the complex, which is difficult to achieve in solution, was illustrated by the lack of activity in the oxidation of catechols, a reaction that typically requires two copper centers in close proximity.

Klein Gebbink et al. also reported recently the first example of homogeneous, mononuclear iron(II/III) complexes of the substituted 3,3-bis(1-alkylimidazol-2-yl)propionates.[94] Iron-catecholato complexes were reported as mimics of the enzyme-substrate complex of the extradiol cleaving dioxygenases (Figure 25). The crystallographically characterized complex [Fe(**L3**)(tcc)(H_2O)] (tcc, tetrachlorocatechol) shows that the structural features of the facial triad are accurately captured by the ligand. Exposure of the complexes with 3,5-di-*tert*-butylcatechol as coligand to dioxygen resulted in (partial) extradiol type cleavage of the catechol. The complexes thus provide the first example of a biomimetic model that incorporates both structural *and* functional properties.

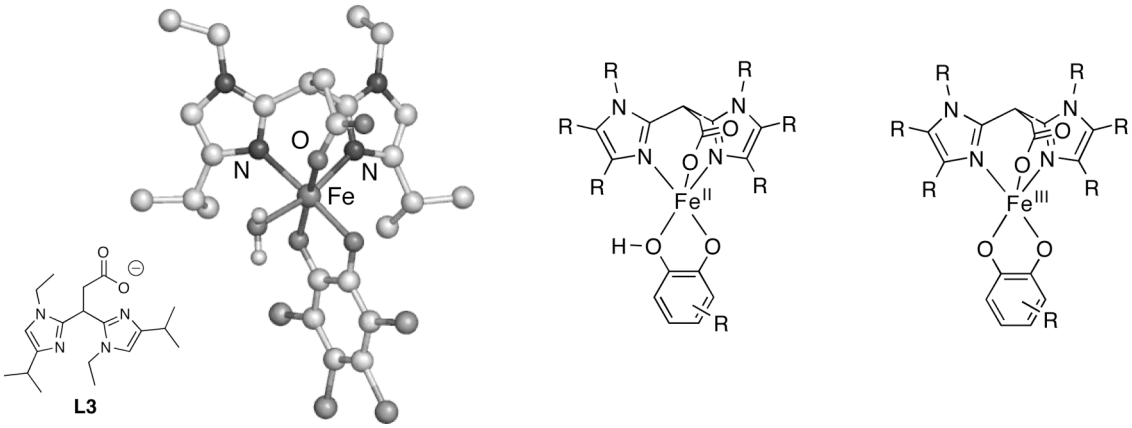

Figure 25. Structural and functional models of the extradiol cleaving catechol dioxygenases.

Functional models. Whereas most of the reports on iron complexes with a mixed donor set ligand have been limited to the structural aspects of the new complexes, *functional* models of all four major subfamilies of the facial triad have been developed as well, mostly with all-*N* ligands.[54] Several ferrous α-keto acid complexes have been reported with the tpa and Tp ligand systems as models of the enzyme-cofactor complex of the α-ketoglutarate dependent oxygenases.[95-98] Most of these complexes show decarboxylation of the α-keto acid upon exposure to dioxygen,[96,98] but the sterically congested [Fe^{II}(bf)($Tp^{iPr,iBu}$)] (bf, benzoylformate) was found not to react.[97] The rate of oxygenation was found to be dependent on the coordination number of the complex, i.e. five-coordinate Tp (N3) complexes reacted much faster than the six-coordinate tpa (N4) complexes, illustrating the importance of a vacant site for dioxygen binding.[7,96] In two cases the oxidative decarboxylation was also coupled to substrate oxidation. Valentine et al. showed that the complex [Fe(bf)(Tp^{Me2})(MeCN)] could effect olefin epoxidation[96] and Que et al. reported the intramolecular aromatic hydroxylation

of one of the phenyl substituents on Tp^{Ph2} upon reaction with dioxygen.[98] Isotope labeling showed that both atoms of $^{18}O_2$ were incorporated in the ligand and benzoic acid, thus mimicking the dioxygenase nature of the enzymes for the first time (Figure 26).

Similar intramolecular arene hydroxylation by mononuclear iron complexes have been observed,[99,100] for instance in the reaction of *tert*-butylhydroperoxide with [Fe(6-Phtpa)(MeCN)$_2$] (6-Phtpa, phenyl appended tpa) (Figure 26).[99] The hydroxylation of the phenyl ring was proposed to proceed via electrophilic attack of the appended arene ring by a high valent iron(IV)-oxo species, similar to the substrate oxidation step in the mechanism of the pterin dependent monooxygenases. These biomimetic studies provided credence to the involvement of iron(IV)-oxo species in the oxidation reactions mediated by the respective enzymes.

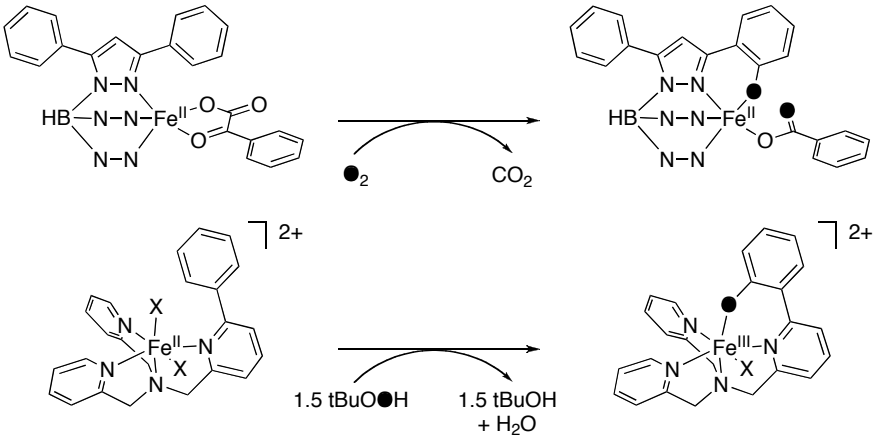

Figure 26. Intramolecular arene hydroxylations that mimic the reactivities of the α-ketoglutarate (top) and pterin (bottom) dependent oxygenases.

Numerous modeling studies have been devoted to the intra- and extradiol ring cleaving catechol dioxygenases.[7,101] Intradiol type cleavage is reported in by far the majority of cases, whereas examples of biomimetic systems capable of extradiol type cleavage are actually quite limited.[7] Funabiki et al. presented the first example of extradiol type cleavage by a combination of $FeCl_2$ or $FeCl_3$ and pyridine/bipyridine.[102] The active species in this complicated mixture could not be readily discerned and future studies, therefore, focused on the reactivity of isolated ferric iron-catecholato complexes of the type [Fe^{III}(dtbc)(L)] (dtbc, 3,5-di-tertbutylcatechol). The highest selectivity for extradiol cleavage is generally obtained with tridentate ligands such as tacn,[103,104] Me_3-tacn,[105] and Tp,[106] which illustrate the importance of a vacant site at the metal center. Bugg et al. reported that the combination of $FeCl_2$/tacn was more selective towards extradiol cleavage than $FeCl_3$/tacn,[103] a finding consistent with the presence of a ferrous ion at the enzyme active site. The first example of extradiol type cleavage with a complex built with a *mixed* donor set ligand similar to the 2-His-1-carboxylate facial triad was reported by Klein Gebbink et al.[94] The modeling studies on the extradiol cleaving dioxygenases are discussed in more detail in Chapter 3.

The functional models described above in most cases display stoichiometric, so-called 'single turnover' reactivities. Functional modeling studies on the Rieske dioxygenases, however, have actually resulted in the discovery of a family of *catalysts* capable of *cis*-dihydroxylation.[107] Ferrous complexes of the ligands tpa and bpmen provided the first example of *cis*-dihydroxylation catalyzed by a non-biological iron complex,[108] a reaction that usually requires reagents such as OsO_4. Even enantioselective *cis*-dihydroxylation with an ee up to 82% has been reported using a chiral analogue of bpmen.[109] The complexes use hydrogen peroxide as oxidant and catalyze the oxidation of a range of olefins with high efficiency. At the same time, these complexes catalyze olefin epoxidation and the actually observed epoxide to *cis*-diol ratios differ widely amongst the reported examples.[107] These two reactions were found to be closely related and the availability of two *cis*-positioned vacant sites was proposed as a necessary requirement for both types of reactivities.[110] The product ratio was found to be dependent on the adopted ligand topology and the spin state of the metal center.[110,111] These factors influence the fate of an implicated Fe^{III}–OOH intermediate such that low spin intermediates generally yield more epoxide and high-spin intermediates more *cis*-diol. Two pathways have been proposed for these two types of complexes, i.e. a water-assisted (wa) pathway for the epoxide selective catalysts and a non-water-assisted (nwa) pathway for the diol selective catalysts (Figure 27).[107,110]

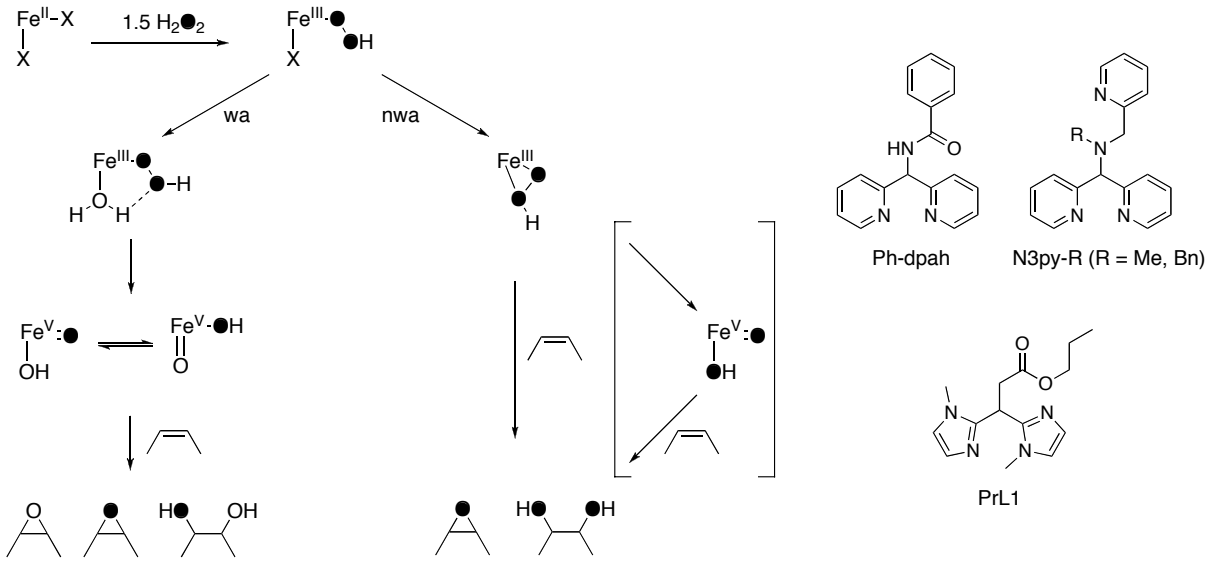

Figure 27. Left: Proposed pathways for the oxidation of olefins by non-heme iron catalysts. Right: Selected new ligand systems capable of *cis*-dihydroxylation.

Isotopic labeling studies have proven particularly insightful and the mechanistic considerations rely heavily on the results obtained from these experiments. Labeling experiments suggest that in the wa-pathway O–O cleavage must occur prior to substrate oxidation and hence a HO–Fe^{V}=O oxidant is proposed. Computational studies suggest that epoxidation or *cis*-dihydroxylation results from initial attack of the olefin by the oxidant oxide or hydroxide, respectively.[112] The mechanism of the nwa-pathway is less clear and direct attack of the olefin by the Fe^{III}–OOH intermediate has been suggested.[113] The nature of the

two oxidants, however, differs significantly. Competition experiments have shown that the oxidant in the wa-pathway has an electrophilic character, whereas in the nwa-pathway a nucleophilic oxidant is generated.[114]

In addition to the tpa and bpmen complexes and derivatives thereof, other complexes capable of *cis*-dihydroxylation have also been reported (Figure 27).[115-118] The iron complex derived from N3py-R reported by Feringa et al. shows comparable reactivity to the original tpa and bmpen systems.[116] Interestingly, the stereoselectivity of the reaction was solvent-dependent, i.e. *cis*- or *trans*-diol was obtained from acetonitrile or acetone solutions, respectively. Recently, examples have been reported that use tridentate ligands with an *N*,*N*,*O* donor set. Oldenburg et al. use the ligand Ph-dpah to obtain the most selective *cis*-dihydroxylation catalyst to date[117] and in a related contribution Klein Gebbink et al. showed that iron complexes of PrL1 also show good epoxidation and *cis*-dihydroxylation activity.[115] More details on functional models of the Rieske dioxygenases can be found in Chapter 5.

The insights obtained from enzymology and functional models have played an important role in the design of bio-inspired oxidation catalysts. The family of *cis*-dihydroxylation/epoxidation catalysts mentioned before is just one example of many biomimetic, non-heme iron oxidation catalysts that use hydrogen peroxide as the oxidant. This topic has been reviewed very recently and will not be discussed here.[119]

1.4 Reaction intermediates

In many of the above studies of both the enzymes and the model systems high-valent iron-oxo intermediates are invoked. Several efforts have been specifically devoted to the study, isolation and characterization of these species to get more insight into the spectroscopic and chemical properties of these intermediates. These studies are discussed below.

Iron(III)-hydroperoxide and -peroxide species. Iron(III)-hydroperoxide ($Fe^{III}OOH$) and iron(III)-peroxide ($Fe^{III}O_2$) species are often invoked as intermediates between the initial binding of dioxygen to iron and the formation of the actual, active oxidant in many different heme and non-heme iron biomolecules.[7] Examples for the latter category include, for instance, the crystallographically observed side-on bound O_2 adduct of naphthalene dioxygenase.[37] In the Rieske dioxygenases, the group of enzymes to which naphthalene dioxygenase belongs, this intermediate has been proposed by some authors to be the actual oxidant rather than a precursor to a high valent iron-oxo oxidant (*vide infra*).[12,44]

Since the first report of the generation of an $Fe^{III}OOH$ intermediate with a model compound by Mascharak et al.,[120] a number of mononuclear, non-heme iron(III)-(hydro)peroxide complexes have been constructed with different, mostly neutral, polydentate ligands such as N4py,[121] tpa,[122] H_2bbpa,[123] Rtpen,[124] and bispidine-derived[125] ligands (Figure 28).[7,126] These species can be generated by the reaction of an iron(II) precursor with H_2O_2 at

low temperature. They have been characterized by a variety of spectroscopic techniques including resonance Raman, UV-Vis, EPR, Mössbauer, and XAS spectroscopy and by mass spectrometric methods.[121,124,126-128]

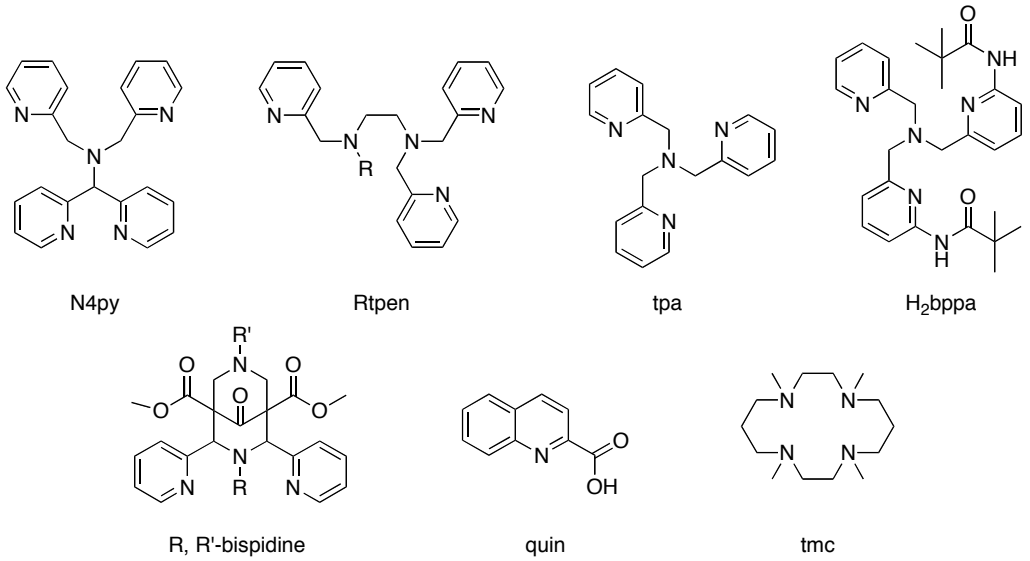

Figure 28. Some selected ligand systems that have been used to generate iron(III)-(hydro)peroxide complexes.

A crystallographically characterized example of a mononuclear non-heme iron(III)-(hydro)peroxide is, however, still lacking. The only example of a iron(III)-peroxide complex is the peroxocarbonate complex $[Ph_4P][Fe^{III}(\kappa^2\text{-}CO_4)(quin)_2]$ that results from the reaction of an iron-hydroperoxide precursor with carbon dioxide (Figure 29, left).[129]

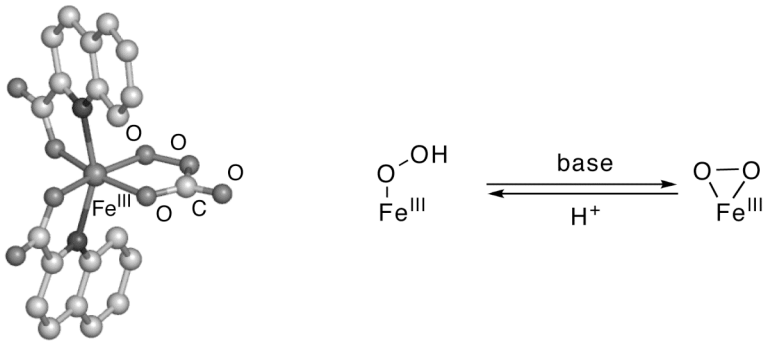

Figure 29. Left: Only available molecular structure of a mononuclear iron complex with a peroxide group $[Ph_4P][Fe^{III}(quin)_2(\kappa^2\text{-}CO_4)]$. Right: Edge-on $[Fe^{III}(\eta^1\text{-}OOH)]^{n+}$ to side-on $[Fe^{III}(\eta^2\text{-}O_2)]^{(n-1)+}$ conversion.

The initially formed $[Fe^{III}(\eta^1\text{-}OOH)(L)]^{n+}$ complexes are generally low-spin, purple-blue species with one LMCT absorption in the visible region at about 550-600 nm. High spin $[Fe^{III}(\eta^1\text{-}OOH)(L)]^{n+}$ complexes have also been obtained with the sterically hindered H_2bppa ligand and the anionic quin ligand (Figure 28).[123,129]

Some complexes, such as for example $[Fe^{III}(\eta^1\text{-}OOH)(N4py)]^{2+}$,[121,130] but not all[125] show reversible acid-base chemistry (Figure 29). The addition of base results in the formation of the conjugate base of the complex. A side-on bound η^2-peroxide structure is proposed for the conjugate base, based on resonance Raman, Mössbauer, and DFT studies (Figure 29, right).[121,125] The $[Fe^{III}(\eta^2\text{-}O_2)(L)]^{(n-1)+}$ complexes are high-spin ferric complexes and display a red-shifted electronic transition compared to their protonated counterparts.

Most studies have focused on the structural description of the side-on $[Fe^{III}(\eta^2\text{-}O_2)]^{(n-1)+}$ complexes and less is known about their reactivity. These species seem to be rather unreactive towards organic substrates,[2,7,131] however, and only nucleophilic oxidation reactions have been reported. The complex $[Fe^{III}(\eta^2\text{-}O_2)(tmc)]^+$ was, for example found to be active in the deformylation of aldehydes, a typical nucleophilic reaction.[132,133] The low reactivity is consistent with the electronic description of a side-on bound peroxide to a ferric metal center, which indicates no activation or weakening of the O–O bond.[2]

A recent study showed that several different $[Fe^{III}(\eta^1\text{-}OOH)]^{n+}$ complexes were not capable of deformylating aldehydes at low temperatures nor were they active in electrophilic reactions such as sulfide and olefin oxidation.[133] Substrate conversion was only observed upon warming of the reaction mixtures. These results indicate that also an $[Fe^{III}(\eta^1\text{-}OOH)]^{n+}$ complex seems a sluggish oxidant and, therefore, cannot not be the active species in sulfoxidation, epoxidation or alkane hydroxylation reactions.[133]

High-valent non-heme iron-oxo species. In many of the above reactions catalyzed by the enzymes with the 2-His-1-carboxylate facial triad and in the model systems, a high-valent iron(IV)-oxo intermediate is brought into play as the reactive oxidizing species. Such species have been previously characterized in several heme-containing iron enzymes and recently, for the first time a high-valent iron(IV)-oxo species has been detected directly in the mononuclear non-heme iron enzyme TauD.[14] This important finding shows that this species is also viable in an enzyme with a non-heme iron active site. At the same time, synthetic efforts were aimed at the development of model systems with an Fe(IV)=O group. In 2000, the first evidence for such a species in a mononuclear non-heme iron environment was presented, albeit in low yield.[134] Subsequently, in a landmark paper in 2003 Que et al. presented the high-yield synthesis and spectroscopic properties of the non-heme iron complex $[Fe^{IV}(O)(tmc)(MeCN)](OTf)_2$ with a terminal iron(IV)-oxo species.[19] The remarkable stability of this species even allowed crystallization and determination of a high-resolution crystal structure of the complex (Figure 30). After this initial report, several more examples have appeared of iron(IV)-oxo complexes. The crystal structure of one of these, $[Fe^{IV}(O)(N4py)](ClO_4)_2$ has also been determined.[18]

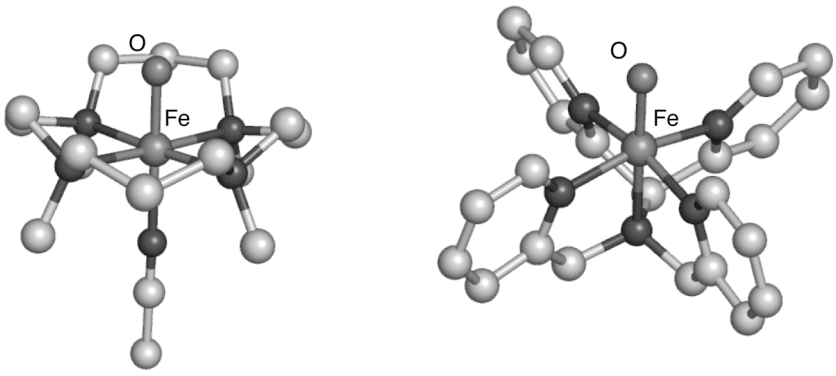

$[Fe^{IV}(O)(tmc)(MeCN)]^{2+}$ $[Fe^{IV}(O)(N4py)]^{2+}$

Figure 30. Molecular structures of the cations of the two crystallographically characterized Fe(IV)=O complexes.

These results incited many experimental and theoretical studies[20,135] into the spectroscopic properties,[136-138] coordination chemistry[139,140] and reactivity[141-144] of these high-valent iron complexes. Several routes have been developed to obtain the desired high-valent complexes. These generally involve the reaction of an iron(II) precursor with oxidants like peracids,[145] iodosylbenzene,[19] peroxides,[146] and even an example has been reported that uses dioxygen[147] as the oxidant. The pale-green species are generally characterized by an electronic absorption with low-intensity in the near-IR region (associated with a ligand field transition[136]), an $S = 1$ ground state, and a short Fe–O bond of about 1.65 Å.[20]

Recently, the formation of iron(IV)-oxo complexes in aqueous solution under various conditions has been reported.[137,148,149] The generation of such a species and the study of its reactivity provided critical insight into the nature of the oxidant in the classical Fenton reaction, i.e. the reaction between Fe^{II} and H_2O_2 in water. An Fe(IV)=O species has sometimes been invoked as an alternative to the hydroxyl radical as the reactive oxidant, but studies on the reactivity of iron(IV)-oxo complexes under Fenton conditions unambiguously ruled out the involvement of this species as the actual oxidant.[149]

The reactivity of the iron(IV)-oxo complexes was furthermore tested in various reactions and the complexes were found to be active in, for instance alkane hydroxylation,[141,150] olefin epoxidation,[141,145] alcohol oxidation,[151] and sulfide oxidation.[147,152] The complex $[Fe^{IV}(O)(N4py)](ClO_4)_2$ was even found to be capable of oxidizing the unactivated C–H bonds of cyclohexane at room temperature.[150] This result shows that the Fe(IV)=O unit has sufficient oxidizing power to cleave aliphatic C–H bonds[150] and it has been calculated to be even more reactive than the corresponding iron(IV)-oxo porphyrin cation radical of P450 (Compound I).[153] In conclusion, the development, characterization, and reactivity studies on biomimetic iron(IV)-oxo complexes has provided strong credence to the mechanisms proposed for the non-heme iron enzymes.

A high valent Fe(V)=O oxidant has been proposed by some authors for the oxygen activation mechanism of the Rieske dioxygenases only (*vide supra*).[7] In contrast to the structurally characterized Fe(IV)=O species, no direct evidence has been reported yet for the

proposed HO–Fe(V)=O oxidant. Mechanistic studies, in particular isotopic labeling experiments, on bio-inspired *cis*-dihydroxylation[107] and alkane hydroxylation catalysts,[116,154] however, strongly implicate the involvement of such an oxidant in these systems. The involvement of an iron(V)-oxo has also been suggested in the self-hydroxylation of different perbenzoic acids by a non-heme iron complex[155] and in a regioselective ligand oxidation.[156] Although no iron(V)-oxo species have been identified spectroscopically, a mononuclear non-heme iron(V)-nitrido complex has been observed, which was generated by the photolysis of a ferric bis(azido) complex.[157,158] The isolation and spectroscopic or structural characterization of an analogues oxo species, however, still awaits.

1.5 Concluding remarks

The recent explosion in crystallographically characterized non-heme iron enzymes has firmly established the 2-His-1-carboxylate facial triad as a common platform for dioxygen activation in Nature. The breadth of oxidative transformations is stunning and many reactions do not have a precedent in synthetic organic chemistry. New members of the family are reported at a remarkable pace, which illustrates both the ubiquity and the versatility of the triad. This holds great promise for the future and without a doubt new systems that mediate exciting new chemistry will be discovered. For these reactivities to be of practical interest the mechanisms have to be understood at the molecular level. Great strides have been made by complementary, parallel studies of enzymes and their biomimetic model complexes, with notable achievements such as the detection and crystallization of iron(IV)-oxo species. Many questions still remain, however, that concern the steps following initial dioxygen binding and lead to product formation. The elaborate studies of synthetic functional analogues have contributed greatly to our understanding of these enzymes. The recent developments towards the synthesis of even more precise high-fidelity structural models promise further progress in this field and may even ultimately lead to the development of synthetically useful catalysts.

1.6 References & Notes

1. Abu-Omar, M. M.; Loaiza, A.; Hontzeas, N. *Chem. Rev.* **2005**, *105*, 2227-2252.
2. Solomon, E. I.; Brunold, T. C.; Davis, M. I.; Kernsley, J. N.; Lee, S-K.; Lehnert, N.; Neese, F.; Skulan, A. J.; Yang, Y-S.; Zhou, J. *Chem. Rev.* **2000**, *100*, 235-349.
3. Neidig, M. L.; Solomon, E. I. *Chem. Commun.* **2005**, 5843-5863.
4. Solomon, E. I.; Chen, P.; Metz, M.; Lee, S.-K.; Palmer, A. E. *Angew. Chem. Int. Ed.* **2001**, *40*, 4570-4590.
5. Holm, R. H.; Kennepohl, P.; Solomon, E. I. *Chem. Rev.* **1996**, *96*, 2239-2314.
6. Denisov, I. G.; Makris, T. M.; Sligar, S. G.; Schlichting, I. *Chem. Rev.* **2005**, *105*, 2253-2277.
7. Costas, M.; Mehn, M. P.; Jensen, M. P.; Que, L., Jr. *Chem. Rev.* **2004**, *104*, 939-986.
8. Tshuva, E. Y.; Lippard, S. J. *Chem. Rev.* **2004**, *104*, 987-1012.
9. Koehntop, K. D.; Emerson, J. P.; Que, L., Jr. *J. Biol. Inorg. Chem.* **2005**, *10*, 87-93.
10. Que, L., Jr. *Nat. Struct. Biol.* **2000**, *7*, 182-184.

11. Valegård, K.; Terwisscha van Scheltinga, A. C.; Lloyd, M. D.; Hara, T.; Ramaswamy, S.; Perrakis, A.; Thompson, A.; Lee, H.-J.; Baldwin, J. E.; Schofield, C. J.; Hajdu, J.; Andersson, I. *Nature* **1998**, *394*, 805-809.
12. Ferraro, D. J.; Gakhar, L.; Ramaswamy, S. *Biochem. Biophys. Res. Commun.* **2005**, *338*, 175-190.
13. Delano, W. L. *The Pymol Molecular Graphics System*, Delano Scientific: San Carlos, CA, USA, 2002.
14. Bollinger, J. M., Jr.; Price, J. C.; Hoffart, L. M.; Barr, E. W.; Krebs, C. *Eur. J. Inorg. Chem.* **2005**, 4245-4254.
15. Price, J. C.; Barr, E. W.; Tirupati, B.; Bollinger, J. M., Jr.; Krebs, C. *Biochemistry* **2003**, *42*, 7497-7508.
16. Proshlyakov, D. A.; Henshaw, T. F.; Monterosso, G. R.; Ryle, M. J.; Hausinger, R. P. *J. Am. Chem. Soc.* **2004**, *126*, 1022-1023.
17. Riggs-Gelasco, P. J.; Price, J. C.; Guyer, J. C.; Brehm, J. H.; Barr, E. W.; Bollinger, J. M., Jr.; Krebs, C. *J. Am. Chem. Soc.* **2004**, *126*, 8108-8109.
18. Klinker, E. J.; Kaizer, J.; Brennessel, W. W.; Woodrum, N. L.; Cramer, C. J.; Que, L., Jr. *Angew. Chem. Int. Ed.* **2005**, *44*, 3690-3694.
19. Rohde, J.-U.; In, J.-H.; Lim, M. H.; Brennessel, W. W.; Bukowski, M. R.; Stubna, A.; Münck, E.; Nam, W.; Que, L., Jr. *Science* **2003**, *299*, 1037-1039.
20. Shan, X. P.; Que, L. *J. Inorg. Biochem.* **2006**, *100*, 421-433.
21. Vaillancourt, F. H.; Bolin, J. T.; Eltis, L. D. *Crit. Rev. Biochem. Mol. Biol.* **2006**, *41*, 241-267.
22. Bugg, T. D. H.; Lin, G. *Chem. Commun.* **2001**, 941-952.
23. Que, L., Jr.; Reynolds, M. F. *Met. Ions Biol. Syst.* **2000**, *37*, 505-525.
24. Vaillancourt, F. H.; Barbosa, C. J.; Spiro, T. G.; Bolin, J. T.; Blades, M. W.; Turner, R. F. B.; Eltis, L. D. *J. Am. Chem. Soc.* **2002**, *124*, 2485-2496.
25. Spence, E. L.; Langley, G. J.; Bugg, T. D. H. *J. Am. Chem. Soc.* **1996**, *118*, 8336-8343.
26. Groce, S. L.; Lipscomb, J. D. *Biochemistry* **2005**, *44*, 7175-7188.
27. Zhang, J.; Zheng, H.; Groce, S. L.; Lipscomb, J. D. *J. Mol. Cat. A* **2006**, *251*, 54-65.
28. Groce, S. L.; Lipscomb, J. D. *J. Am. Chem. Soc.* **2003**, *125*, 11780-11781.
29. Mendel, S.; Arndt, A.; Bugg, T. D. H. *Chem. Commun.* **2005**, 666-668.
30. Gibson, D. T.; Parales, R. E. *Curr. Op. Biotech.* **2000**, *11*, 236-243.
31. Boyd, D. R.; Bugg, T. D. H. *Chem. Commun.* **2006**, 181-192.
32. Gibson, D. T.; Resnick, S. M.; Lee, K.; Brand, J. M.; Torok, D. S.; Wackett, L. P.; Schocken, M. J.; Haigler, B. E. *J. Bacteriol.* **1995**, *177*, 2615-2621.
33. Herman, P. L.; Behrens, M.; Chakraborty, S.; Chrastil, B. M.; Barycki, J.; Weeks, D. P. *J. Biol. Chem.* **2005**, *280*, 24759-24767.
34. Lee, J.; Zhao, H. *Angew. Chem. Int. Ed.* **2006**, *45*, 622-625.
35. Martins, B. M.; Svetlitchnaia, T.; Dobbek, H. *Structure* **2005**, *13*, 817-824.
36. Tarasev, M.; Pinto, A.; Kim, D.; Elliot, S. J.; Ballou, D. P. *Biochemistry* **2006**, *45*, 10208-10216.
37. Karlsson, A.; Parales, J. V.; Parales, R. E.; Gibson, D. T.; Eklund, H.; Ramaswamy, S. *Science* **2003**, *299*, 1039-1042.
38. Kauppi, B.; Lee, K.; Carredano, E.; Parales, R. E.; Gibson, D. T.; Eklund, H.; Ramaswamy, S. *Structure* **1998**, *6*, 571-586.
39. Karlsson, A.; Parales, J. V.; Parales, R. E.; Gibson, D. T.; Eklund, H.; Ramaswamy, S. *J. Biol. Inorg. Chem.* **2005**, *10*, 483-489.
40. Furusawa, Y.; Nagarajan, V.; Tanokura, M.; Masai, E.; Fukuda, M.; Senda, T. *J. Mol. Biol.* **2004**, *342*, 1041-1052.
41. Friemann, R.; Ivkovic-Jensen, M. M.; Lessner, D. J.; Yu, C. L.; Gibson, D. T.; Parales, R. E.; Eklund, H.; Ramaswamy, S. *J. Mol. Biol.* **2005**, *348*, 1139-1151.

42. Dong, X.; Fushinobu, S.; Fukuda, E.; Terada, T.; Nakamura, S.; Shimizu, K.; Nojiri, H.; Omori, T.; Shoun, H.; Wakagi, T. *J. Bacteriol.* **2005**, *187*, 2483-2490.
43. Nojiri, H.; Ashikawa, Y.; Noguchi, H.; Nam, J. W.; Urata, M.; Fujimoto, Z.; Uchimura, H.; Terada, T.; Nakamura, S.; Shimizu, K.; Yoshida, T.; Habe, H.; Omori, T. *J. Mol. Biol.* **2005**, *351*, 355-370.
44. Bassan, A.; Blomberg, M. R. A.; Siegbahn, P. E. M. *J. Biol. Inorg. Chem.* **2004**, *9*, 439-452.
45. Bassan, A.; Borowski, T.; Siegbahn, P. E. M. *Dalton Trans.* **2004**, 3153-3162.
46. Ferraro, D. J.; Okerlund, A. L.; Mowers, J. C.; Ramaswamy, S. *J. Bacteriol.* **2006**, *188*, 6986-6994.
47. Clifton, I. J.; McDonough, M. A.; Ehrismann, D.; Kershaw, N. J.; Granatino, N.; Schofield, C. J. *J. Inorg. Biochem.* **2006**, *100*, 644-669.
48. Hausinger, R. P. *Crit. Rev. Biochem. Mol. Biol.* **2004**, *39*, 21-68.
49. Hewitson, K. S.; Granatino, N.; Welford, W. D.; McDonough, M. A.; Schofield, C. J. *Phil. Trans. R. Soc. A* **2005**, *363*, 807-828.
50. Yu, B.; Edstrom, W. C.; Benach, J.; Hamuro, Y.; Weber, P. C.; Gibney, B. R.; Hunt, J. F. *Nature* **2006**, *439*, 879-884.
51. Sundheim, O.; Vågbø, C. B.; Bjøras, M.; Sousa, M. M. L.; Talstad, V.; Aas, P. A.; Drabløs, F.; Krokan, H. E.; Tainer, J. A.; Slupphaug, G. *EMBO J.* **2006**, *25*, 3389-3397.
52. Cloos, P. A. C.; Christensen, J.; Agger, K.; Maiolica, A.; Rappsilber, J.; Antal, T.; Hansen, K. H.; Helin, K. *Nature* **2006**, *442*, 307-311.
53. Tsukada, Y.-I.; Fang, J.; Erdjument-Bromage, H.; Warren, M. E.; Borchers, C. H.; Tempst, P.; Zhang, Y. *Nature* **2006**, *439*, 811-816.
54. McDonough, M. A.; Li, V.; Flashman, E.; Chowdhury, R.; Mohr, C.; Liénard, B. M. R.; Zondlo, J.; Oldham, N. J.; Clifton, I. J.; Lewis, J.; McNeill, L. A.; Kurzeja, R. J. M.; Hewitson, K. S.; Yang, E.; Jordan, S.; Syed, R. S.; Schofield, C. J. *Proc. Natl. Acad. Sci. U. S. A.* **2006**, *103*, 9814-9819.
55. Pavel, E. G.; Zhou, J.; Busby, R. W.; Gunsior, M.; Townsend, C. A.; Solomon, E. I. *J. Am. Chem. Soc.* **1998**, *120*, 743-753.
56. O'Brien, J. R.; Schuller, D. J.; Yang, V. S.; Dillard, B. D.; Lanzilotta, W. N. *Biochemistry* **2003**, *42*, 5547-5554.
57. Schenk, G.; Pau, M. Y. M.; Solomon, E. I. *J. Am. Chem. Soc.* **2004**, *126*, 505-515.
58. Moran, G. R. *Arch. Biochem. Biophys.* **2005**, *433*, 117-128.
59. Choroba, O. W.; Wiliams, D. H.; Spencer, J. B. *J. Am. Chem. Soc.* **2000**, *122*, 5389-5390.
60. Neidig, M. L.; Decker, A.; Choroba, O. W.; Huang, F.; Kavana, M.; Moran, G. R.; Spencer, J. B.; Solomon, E. I. *Proc. Natl. Acad. Sci. U. S. A.* **2006**, *103*, 12966-12973.
61. Vaillancourt, F. H.; Yeh, E.; Vosburg, D. A.; Garneau-Tsodikova, S.; Walsh, C. T. *Chem. Rev.* **2006**, *106*, 3364-3378.
62. Vaillancourt, F. H.; Yin, J.; Walsh, C. T. *Proc. Natl. Acad. Sci. U. S. A.* **2005**, *102*, 10111-10116.
63. Vaillancourt, F. H.; Yeh, E.; Vosburg, D. A.; O'Connor, S. E.; Walsh, C. T. *Nature* **2005**, *436*, 1191-1194.
64. Blasiak, L. C.; Vaillancourt, F. H.; Walsh, C. T.; Drennan, C. L. *Nature* **2006**, *440*, 368-371.
65. Fitzpatrick, P. F. *Annu. Rev. Biochem.* **1999**, *68*, 355-381.
66. Flatmark, T.; Stevens, R. C. *Chem. Rev.* **1999**, *99*, 2137-2160.
67. Goodwill, K. E.; Sabatier, C.; Marks, C.; Raag, R.; Fitzpatrick, P. F.; Stevens, R. C. *Nat. Struct. Biol.* **1997**, *4*, 578-585.
68. Kobe, B.; Jennings, I. G.; House, C. M.; Michell, B. J.; Goodwill, K. E.; Santarsiero, B. D.; Stevens, R. C.; Cotton, R. G. H.; Kemp, B. E. *Nat. Struct. Biol.* **1999**, *6*, 442-448.
69. Wang, L.; Erlandsen, H.; Haavik, J.; Knappskog, P. M.; Stevens, R. C. *Biochemistry* **2002**, *41*, 12569-12574.
70. Andersson, O. A.; Flatmark, T.; Hough, E. *J. Mol. Biol.* **2002**, *320*, 1095-1108.

71. Klinman, J. P. *J. Biol. Inorg. Chem.* **2001**, *6*, 1-13.
72. Urich, T.; Gomes, C. M.; Kletzin, A.; Frazão, C. *Science* **2006**, *311*, 996-1000.
73. Higgins, L. J.; Yan, F.; Liu, P.; Liu, H.-W.; Drennan, C. L. *Nature* **2005**, *437*, 838-844.
74. Liu, P.; Liu, A.; Yan, F.; Wolfe, M. D.; Lipscomb, J. D.; Liu, H.-W. *Biochemistry* **2003**, *42*, 11577-11586.
75. Yan, F.; Munos, J. W.; Liu, P.; Liu, H.-W. *Biochemistry* **2006**, *45*, 11473-11481.
76. Kershaw, N. J.; Caines, M. E. C.; Sleeman, M. C.; Schofield, C. J. *Chem. Commun.* **2006**, 4251-4263.
77. Burzlaff, N. I.; Rutledge, P. J.; Clifton, I. J.; Hensgens, C. M. H.; Pickford, M.; Adlington, R. M.; Roach, P. L.; Baldwin, J. E. *Nature* **1999**, *401*, 721-724.
78. Roach, P. L.; Clifton, I. J.; Hensgens, C. M. H.; Shibata, N.; Long, A. J.; Strange, R. W.; Hasnain, S. S.; Schofield, C. J.; Baldwin, J. E.; Hajdu, J. *Eur. J. Biochem.* **1996**, *242*, 736-740.
79. Roach, P. L.; Clifton, I. J.; Hensgens, C. M. H.; Shibata, N.; Schofield, C. J.; Hajdu, J.; Baldwin, J. E. *Nature* **1997**, *387*, 827-830.
80. Brunhuber, N. M. W.; Mort, J. L.; Christoffersen, R. E.; Reich, N. O. *Biochemistry* **2000**, *39*, 10730-10738.
81. Thrower, J. S.; Blalock, R., III; Klinman, J. P. *Biochemistry* **2001**, *40*, 9717-9724.
82. Zhou, J.; Rocklin, A. M.; Lipscomb, J. D.; Que, L., Jr.; Solomon, E. I. *J. Am. Chem. Soc.* **2002**, *124*, 4602-4609.
83. Tierney, D. L.; Rocklin, A. M.; Lipscomb, J. D.; Que, L., Jr.; Hoffman, B. M. *J. Am. Chem. Soc.* **2005**, *127*, 7005-7013.
84. Rocklin, A. M.; Kato, K.; Liu, H.-W.; Que, L., Jr.; Lipscomb, J. D. *J. Biol. Inorg. Chem.* **2004**, *9*, 171-182.
85. Zhang, Z.; Ren, J.-S.; Clifton, I. J.; Schofield, C. J. *Chem. Biol.* **2004**, *11*, 1383-1394.
86. Beck, A.; Barth, A.; Hübner, E.; Burzlaff, N. *Inorg. Chem.* **2003**, *42*, 7182-7188.
87. Beck, A.; Weibert, B.; Burzlaff, N. *Eur. J. Inorg. Chem.* **2001**, 521-527.
88. Otero, A.; Fernández-Baeza, J.; Antiñolo, A.; Tejeda, J.; Lara-Sánchez, A. *Dalton Trans.* **2004**, 1499-1510.
89. Peters, L.; Burzlaff, N. *Polyhedron* **2004**, *23*, 245-251.
90. Friese, S. J.; Kucera, B. E.; Que, L., Jr.; Tolman, W. B. *Inorg. Chem.* **2006**, *45*, 8003-8005.
91. Bruijnincx, P. C. A.; Lutz, M.; Spek, A. L.; van Faassen, E. E.; Weckhuysen, B. M.; van Koten, G.; Klein Gebbink, R. J. M. *Eur. J. Inorg. Chem.* **2005**, 779-787 (Chapter 2 of this thesis).
92. Peters, L.; Hübner, E.; Burzlaff, N. *J. Organomet. Chem.* **2005**, *690*, 2009-2016.
93. Kervinen, K.; Bruijnincx, P. C. A.; Beale, A. M.; Mesu, J. G.; van Koten, G.; Klein Gebbink, R. J. M.; Weckhuysen, B. M. *J. Am. Chem. Soc.* **2006**, *128*, 3208-3217.
94. Bruijnincx, P. C. A.; Lutz, M.; Spek, A. L.; Hagen, W. R.; Weckhuysen, B. M.; van Koten, G.; Klein Gebbink, R. J. M. *J. Am. Chem. Soc.*, accepted for publication (Chapter 3 of this thesis).
95. Chiou, Y.-M.; Que, L., Jr. *J. Am. Chem. Soc.* **1995**, *117*, 3999-4013.
96. Ha, E. H.; Ho, R. Y. N.; Kisiel, J. F.; Valentine, J. S. *Inorg. Chem.* **1995**, *34*, 2265-2266.
97. Hikichi, S.; Ogihara, T.; Fujisawa, K.; Kitajima, N.; Akita, M.; Moro-oka, Y. *Inorg. Chem.* **1997**, *36*, 4539-4547.
98. Mehn, M. P.; Fujisawa, K.; Hegg, E. L.; Que, L., Jr. *J. Am. Chem. Soc.* **2003**, *125*, 7828-7842.
99. Jensen, M. P.; Lange, S. J.; Mehn, M. P.; Que, E. L.; Que, L., Jr. *J. Am. Chem. Soc.* **2003**, *125*, 2113-2128.
100. Mekmouche, Y.; Ménage, S.; Toia-Duboc, C.; Fontecave, M.; Galey, J.-B.; Lebrun, C.; Pécaut, J. *Angew. Chem. Int. Ed.* **2001**, *40*, 949-952.
101. Yamahara, R.; Ogo, S.; Masuda, H.; Watanabe, Y. *J. Inorg. Biochem.* **2002**, *88*, 284-294.
102. Funabiki, T.; Mizoguchi, A.; Sugimoto, T.; Tada, S.; Tsuji, M.; Sakamoto, H.; Yoshida, S. *J. Am. Chem. Soc.* **1986**, *108*, 2921-2932.
103. Lin, G.; Reid, G.; Bugg, T. D. H. *J. Am. Chem. Soc.* **2001**, *123*, 5030-5039.
104. Dei, A.; Gatteschi, D.; Pardi, L. *Inorg. Chem.* **1993**, *32*, 1389-1395.
105. Jo, D.-H.; Que, L., Jr. *Angew. Chem. Int. Ed.* **2000**, *39*, 4284-4287.

106. Ogihara, T.; Hikichi, S.; Akita, M.; Moro-oka, Y. *Inorg. Chem.* **1998**, *37*, 2614-2615.
107. Oldenburg, P. D.; Que, L., Jr. *Catal. Today* **2006**, *117*, 15-21.
108. Chen, K.; Que, L., Jr. *Angew. Chem. Int. Ed.* **1999**, *38*, 2227-2229.
109. Costas, M.; Tipton, A. K.; Chen, K.; Jo, D.-H.; Que, L., Jr. *J. Am. Chem. Soc.* **2001**, *123*, 6722-6723.
110. Chen, K.; Costas, M.; Kim, J.; Tipton, A. K.; Que, L., Jr. *J. Am. Chem. Soc.* **2002**, *124*, 3026-3035.
111. Mas-Ballesté, R.; Costas, M.; van den Berg, T.; Que, L., Jr. *Chem. Eur. J.* **2006**, *12*, 3026-3035.
112. Bassan, A.; Blomberg, M. R. A.; Siegbahn, P. E. M.; Que, L., Jr. *Angew. Chem. Int. Ed.* **2005**, *44*, 2939-2941.
113. Quiñonero, D.; Morokuma, K.; Musaev, D.; Mas-Ballesté, R.; Que, L., Jr *J. Am. Chem. Soc.* **2005**, *127*, 6548-6549.
114. Fujita, M.; Costas, M.; Que, L., Jr. *J. Am. Chem. Soc.* **2003**, *125*, 9912-9913.
115. Bruijnincx, P. C. A.; Buurmans, I. L. C.; Gosiewska, S.; Lutz, M.; Spek, A. L.; van Koten, G.; Klein Gebbink, R. J. M. *to be submitted* (Chapter 5 of this thesis).
116. Klopstra, M.; Roelfes, G.; Hage, R.; Kellogg, R. M.; Feringa, B. L. *Eur. J. Inorg. Chem.* **2004**, 846-856.
117. Oldenburg, P. D.; Shteinman, A. A.; Que, L., Jr. *J. Am. Chem. Soc.* **2005**, *127*, 15673-15674.
118. Rotthaus, O.; Le Roy, S.; Tomas, A.; Barkigia, K. M.; Artaud, I. *Inorg. Chim. Acta* **2004**, *357*, 2211-2217.
119. Tanase, S.; Bouwman, E. *Adv. Inorg. Chem.* **2006**, *58*, 29-75.
120. Guajardo, R. J.; Hudson, S. E.; Brown, S. J.; Mascharak, P. K. *J. Am. Chem. Soc.* **1993**, *115*, 7971-7977.
121. Roelfes, G.; Vrajmasu, V.; Chen, K.; Ho, R. Y. N.; Rohde, J.-U.; Zondervan, C.; la Crois, R. M.; Schudde, E. P.; Lutz, M.; Spek, A. L.; Hage, R.; Feringa, B. L.; Münck, E.; Que, L., Jr. *Inorg. Chem.* **2003**, *42*, 2639-2653.
122. Ho, R. Y. N.; Roelfes, G.; Feringa, B. L.; Que, L., Jr. *J. Am. Chem. Soc.* **1999**, *121*, 264-265.
123. Wada, A.; Ogo, S.; Nagamoto, S.; Kitagawa, T.; Watanabe, Y.; Jitsukawa, K.; Masuda, H. *Inorg. Chem.* **2002**, *42*, 616-618.
124. Hazell, A.; McKenzie, C. J.; Nielsen, L. P.; Schindler, S.; Weitzer, M. *J. Chem. Soc., Dalton Trans.* **2002**, 310-317.
125. Bukowski, M. R.; Comba, P.; Limberg, C.; Merz, M.; Que, L., Jr.; Wistuba, T. *Angew. Chem. Int. Ed.* **2004**, *43*, 1283-1287.
126. Girerd, J.-J.; Banse, F.; Simaan, A. J. *Struct. Bonding* **2000**, *97*, 145-177.
127. Koehntop, K. D.; Rohde, J.-U.; Costas, M.; Que, L., Jr. *Dalton Trans.* **2004**, 3191-3198.
128. Simaan, A. J.; Döpner, S.; Banse, F.; Bourcier, S.; Bouchoux, G.; Boussac, A.; Hildebrandt, P.; Girerd, J.-J. *Eur. J. Inorg. Chem.* **2000**, 1627-1633.
129. Hashimoto, K.; Nagamoto, S.; Fujinami, S; Furutachi, H.; Ogo, S.; Suzuki, M.; Uehara, A.; Maeda, Y.; Watanabe, Y.; Kitagawa, T. *Angew. Chem. Int. Ed.* **2002**, *41*, 1202-1205.
130. Jensen, K. B.; McKenzie, C. J.; Nielsen, L. P.; Pedersen, J. Z.; Svendsen, H. M. *Chem. Commun.* **1999**, 1313-1314.
131. Neese, F.; Solomon, E. I. *J. Am. Chem. Soc.* **1998**, *120*, 12829-12848.
132. Annaraj, J.; Suh, Y.; Seo, M. S.; Kim, S. O.; Nam, W. *Chem. Commun.* **2005**, 4529-4531.
133. Park, M. J.; Lee, J.; Suh, Y.; Kim, J.; Nam, W. *J. Am. Chem. Soc.* **2006**, *128*, 2630-2634.
134. Grapperhaus, C. A.; Mienert, B.; Bill, E.; Weyhermüller, T.; Wieghardt, K. *Inorg. Chem.* **2000**, *39*, 5306-5317.
135. Decker, A.; Clay, M. D.; Solomon, E. I. *J. Inorg. Biochem.* **2006**, *100*, 697-706.
136. Decker, A.; Rohde, J.-U.; Que, L., Jr.; Solomon, E. I. *J. Am. Chem. Soc.* **2004**, *126*, 5378-5379.
137. Sastri, C. V.; Park, M. J.; Ohta, T.; Jackson, T. A.; Stubna, A.; Seo, M. S.; Lee, J.; Kim, J.; Kitagawa, T.; Münck, E.; Que, L., Jr.; Nam, W. *J. Am. Chem. Soc.* **2005**, *127*, 12494-12495.
138. Rohde, J.-U.; Torelli, S.; Shan, X.; Lim, M. H.; Klinker, E. J.; Kaizer, J.; Chen, K.; Nam, W.; Que, L., Jr. *J. Am. Chem. Soc.* **2004**, *126*, 16750-16761.
139. Rohde, J.-U.; Stubna, A.; L., Bominaar. E.; Münck, E.; Nam, W.; Que, L., Jr. *Inorg. Chem.* **2006**, *45*, 6435-6445.
140. Rohde, J.-U.; Que, L., Jr. *Angew. Chem. Int. Ed.* **2005**, *44*, 2255-2258.

141. Martinho, M.; Banse, F.; Bartoli, J.-F.; Mattioli, T. A.; Battioni, P.; Horner, O.; Bourcier, S.; Girerd, J.-J. *Inorg. Chem.* **2005**, *44*, 9592-9596.
142. Sastri, C. V.; Oh, K.; Lee, Y. J.; Seo, M. S.; Shin, W.; Nam, W. *Angew. Chem. Int. Ed.* **2006**, *45*, 3992-3995.
143. Seo, M. S.; In, J.-H.; Kim, S. O.; Oh, N. Y.; Hong, J.; Kim, J.; Que, L., Jr.; Nam, W. *Angew. Chem. Int. Ed.* **2004**, *43*, 2417-2420.
144. Furutachi, H.; Hashimoto, K.; Nagamoto, S.; Endo, T.; Fujinami, S.; Watanabe, Y.; Kitagawa, T.; Suzuki, M. *J. Am. Chem. Soc.* **2005**, *127*, 4550-4551.
145. Lim, M. H.; Rohde, J.-U.; Stubna, A.; Bukowski, M. R.; Costas, M.; Ho, R. Y. N.; Münck, E.; Nam, W.; Que, L., Jr. *Proc. Natl. Acad. Sci. U. S. A.* **2003**, *100*, 3665-3670.
146. Jensen, M. P.; Costas, M.; Ho, R. Y. N.; Kaizer, J.; Mairata i Payeras, A.; Münck, E.; Que, L., Jr.; Rohde, J.-U.; Stubna, A. *J. Am. Chem. Soc.* **2005**, *127*, 9117-9128.
147. Kim, S. O.; Sastri, C. V.; Seo, M. S.; Kim, J.; Nam, W. *J. Am. Chem. Soc.* **2005**, *127*, 4178-4179.
148. Bautz, J.; Bukowski, M. R.; Kerscher, M.; Stubna, A.; Comba, P.; Lienke, A.; Münck, E.; Que, L., Jr. *Angew. Chem. Int. Ed.* **2006**, *45*, 5681-5684.
149. Pestovsky, O.; Stoian, S.; Bominaar, E. L.; Shan, X.; Münck, E.; Que, L., Jr.; Bakac, A. *Angew. Chem. Int. Ed.* **2005**, *44*, 6871-6874.
150. Kaizer, J.; Klinker, E. J.; Oh, N. Y.; Rohde, J.-U.; Song, W. J.; Stubna, A.; Kim, J.; Münck, E.; Nam, W.; Que, L., Jr. *J. Am. Chem. Soc.* **2004**, *126*, 472-473.
151. Oh, N. Y.; Suy, Y.; Park, M. J.; Seo, M. S.; Kim, J.; Nam, W. *Angew. Chem. Int. Ed.* **2005**, *44*, 4235-4239.
152. Sastri, C. V.; Seo, M. S.; Park, M. J.; Kim, K. M.; Nam, W. *Chem. Commun.* **2005**, 1405-1407.
153. Kumar, D.; Hirao, H.; Que, L., Jr.; Shaik, S. *J. Am. Chem. Soc.* **2205**, *127*, 8026-8027.
154. Chen, K.; Que, L., Jr. *J. Am. Chem. Soc.* **2001**, *123*, 6327-6337.
155. Oh, N. Y.; Seo, M. S.; Lim, M. H.; Consugar, M. B.; Park, M. J.; Rohde, J.-U.; Han, J.; Kim, K. M.; Kim, J.; Que, L., Jr.; Nam, W. *Chem. Commun.* **2005**, 5644-5646.
156. Nielsen, A.; Larsen, F. B.; Bond, A. D.; McKenzie, C. J. *Angew. Chem. Int. Ed.* **2006**, *45*, 1602-1606.
157. Aliaga-Alcalde, N.; DeBeer George, S.; Mienert, B.; Bill, E.; Wieghardt, K.; Neese, F. *Angew. Chem. Int. Ed.* **2005**, *44*, 2908-2912.
158. Meyer, K.; Bill, E.; Weyhermüller, T.; Wieghardt, K. *J. Am. Chem. Soc.* **1999**, *121*, 4859-4876.

CHAPTER 2

A New Family of Biomimetic *N,N,O* Ligands.

Synthesis, Structures and Cu^{II} Coordination Complexes

Abstract

A new family of substituted 3,3-bis(1-alkylimidazol-2-yl)propionates has been developed to mimic the 2-His-1-carboxylate facial triad. A general synthetic route towards these tridentate, tripodal *N,N,O* ligands, bearing one carboxylato group and two of the biologically relevant 1-methylimidazole moieties, is presented. The potential of these ligands to facially cap a metal center was studied using copper(II) as a probe metal. The two ligands were found to coordinate facially through all donor atoms and two isostructural mononuclear copper(II) complexes of the type $[Cu^{II}L_2]$ were obtained and crystallographically characterized.

P. C. A. Bruijnincx, M. Lutz, A. L. Spek, E. E. van Faassen, B. M. Weckhuysen, G. van Koten, R. J. M. Klein Gebbink, *Eur. J. Inorg. Chem.* **2005**, 779-787

2.1 Introduction

The study of synthetic active site analogues has made a vast contribution to the understanding of the structure-function relationship of many metalloenzymes, as has been highlighted recently in a thematic review issue.[1] In particular, the use of tripodal ligand systems has received much attention, the most well known example probably being the tris(pyrazolyl)borates.[2,3] Despite their remarkable versatility and the impressive results that have been obtained, these "scorpionates" also illustrate two of the drawbacks associated with many of the reported tripodal ligands. First, most ligand systems are fully symmetrical and provide, for instance, an all-*N* donor set. Second, the *N* donor groups are often found to be non-biologically relevant heterocycles (such as pyrazole or pyridine), which differ both in size, and chemical and electronic properties from the histidyl imidazole-side chain found in biological systems. Since the coordination environment of many metalloenzyme active sites is made up of different donor groups, the interest of synthetic chemists has shifted towards the design of *mixed* ligand systems incorporating different functionalities, i.e. "heteroscorpionates".[4-7]

We are particularly interested in a group of enzymes exhibiting the so-called 2-His-1-carboxylate motif at their active site.[8-10] This structural motif is found in many crystallographically characterized mononuclear non-heme iron enzymes,[11] like deacetoxycephalosporin C synthase (DAOCS)[12] and naphthalene 1,2-dioxygenase (NDO),[13] in which two histidines and one carboxylato group occupy one face of the iron(II) coordination environment. The same facial capping by two histidines and one carboxylato group is found in some zinc containing enzymes, e.g. carboxypeptidase and thermolysin.[14,15] This triad is therefore an interesting target for structural and functional modeling.

Most modeling efforts aimed at mimicking this facial triad used either the tridentate trispyrazolylborato *N,N,N* or the tetradentate tris(2-pyridylmethyl)amine *N,N,N,N'* ligands.[11,14,15] However, suitable structural mimics of this triad should preferably be tridentate, tripodal, monoanionic ligand systems with a potentially facially coordinating *N,N,O* donor set. Such *N,N,O* ligands are relatively rare and, to the best of our knowledge, only three tridentate examples have been reported of these mixed ligands bearing a carboxylate group. The bispyrazolylacetates were introduced by Otero et al.[16] and have been studied by Burzlaff et al. as mimics of the 2-His-1-carboxylate motif.[17-20] A drawback of this system is the use of biologically non-relevant pyrazole groups as the two *N* donor groups. The second example is the bis(imidazole)propionate ligand (Hbip) already reported in the late 1970s by Joseph et al.[21] This ligand system, however, suffers from a difficult synthetic route, complicating acid-base chemistry, and limited solubility in non-aqueous media. Parkin, finally, indirectly constructed an *N,N,O* donor set by the insertion of carbon dioxide or formaldehyde into the B–H bond of a bis(pyrazol-1-yl)hydroborato zinc complex.[22,23]

We are interested in biomimetic ligand systems which in principle could accommodate the desired facial coordination geometry and would incorporate the biologically relevant *N,N,O* donor atom set. A further requirement would be the access to a straightforward

synthetic route, which would allow for facile modification of the *N,N,O* ligands and therefore tuneability of their physical properties. With this in mind, we have developed new *N,N,O* ligands, i.e. bis(1-methylimidazol-2-yl)propionate (**L1**) (**1**) and bis(1-methylbenzimidazol-2-yl)propionate (**L2**) (**2**), incorporating the biomimetic 1-methylimidazole and carboxylate groups in a tripodal, monoanionic, tridentate ligand framework (Figure 1).

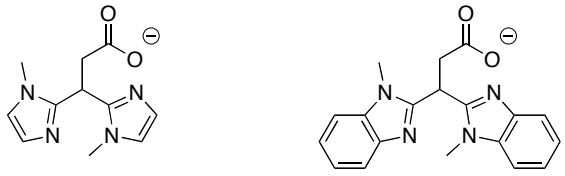

L1 **L2**

Figure 1. *N,N,O* ligands **L1** and **L2**.

These *N,N,O* ligands are also of interest in connection with the biomimetic study of copper proteins. Various (polynuclear) copper enzymes are known in which the metal centers are found in an imidazole-rich coordination environment.[24] Furthermore, copper(II) can be used as a probe metal to test the ability of the ligands to facially cap a metal center.[25] Herein, we describe the synthesis and structural characterization of two new *N,N,O* ligands, **L1** and **L2**, and their copper(II) coordination complexes.

2.2 Results

Synthesis and structural characterization of the *N,N,O* ligands. A general synthetic route for the bis(1-methylimidazol-2-yl)- and bis(1-methylbenzimidazol-2-yl)propionates was developed (Scheme 1). This route is based on the readily available bis(1-methylimidazol-2-yl)methane framework. Both bis(1-methylimidazol-2-yl)methane (**5**)[26,27] and bis(1-methylbenzimidazol-2-yl)methane (**6**)[28] can be easily synthesized on a multigram scale.

Lithiation of **5** and **6** at the bridging methylene group with *n*-butyllithium at – 78 °C in THF and subsequent dropwise addition of propyl bromoacetate resulted in the clean formation of the propyl esters Pr**L1** (**7**) and Pr**L2** (**8**). Basic hydrolysis of these ligand precursors in THF with one equivalent of a potassium hydroxide solution in water gave the potassium salts of 3,3-bis(1-methylimidazol-2-yl)propionic acid, K[**L1**] (**1b**), and 3,3-bis(1-methylbenzimidazol-2-yl)propionic acid, K[**L2**] (**2b**), in quantitative yields. Likewise, treatment of the esters with $[Bu_4N]OH$ resulted in the quantitative formation of the tetrabutylammonium salts $[Bu_4N]$[**L1**] (**1c**) and $[Bu_4N]$[**L2**] (**2c**). Subsequent addition of one equivalent of hydrochloric acid to a solution of the hydrolyzed esters and purification via recrystallization gave 3,3-bis(1-methylimidazol-2-yl)propionic acid, H**L1** (**1a**), and 3,3-bis(1-methylbenzimidazol-2-yl)propionic acid, H**L2** (**2a**), in good yields. The propionate salts **1b**/**1c** and **2b**/**2c** are very hygroscopic and can only be obtained as fine powders if they are completely solvent free. This is also reflected in the IR spectra of the compounds. The exact

position of the bands depends on the amount of water present in the sample or accumulated during measurement. The carboxylato group asymmetric stretch vibrations $\nu_{as}(COO^-)$ can be found at 1702 (**1a**) and 1716 cm^{-1} (**2a**) for the acids and at 1581 (**1b**/**1c**) and 1597 (**2c**) for the K- and Bu_4N-salts. The $\nu_{as}(COO^-)$ of **2b** is split into two bands of equal intensity at 1582 and 1598 cm^{-1}. The symmetric stretch vibration $\nu_s(COO^-)$ is less intense and could only be unambiguously identified for the potassium salts **1b** and **2b** (1393 and 1386 cm^{-1}, respectively).

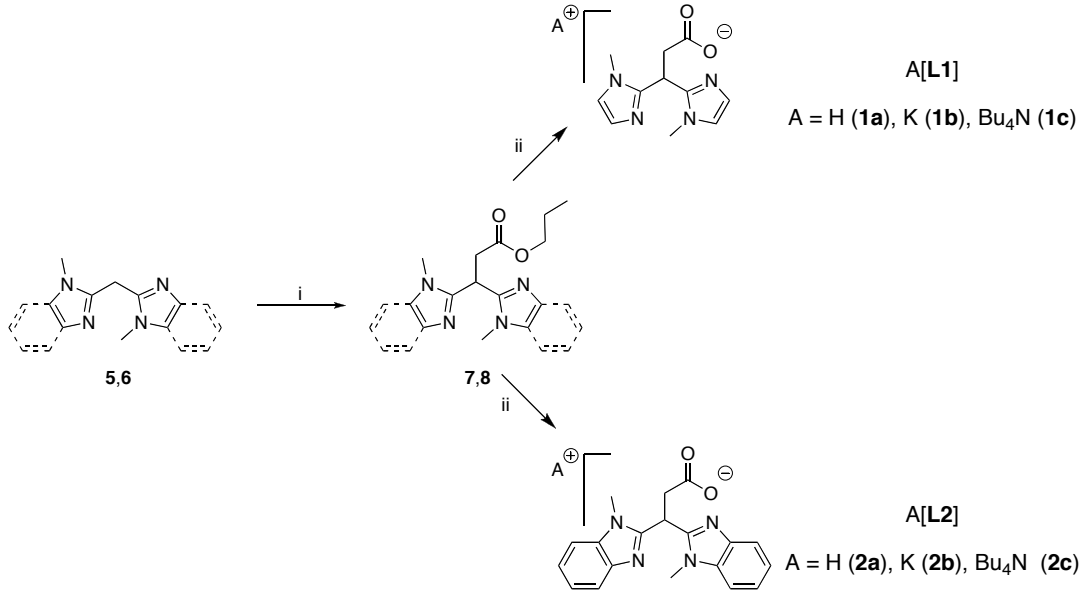

Scheme 1. i) a. *n*-butyllithium, – 78 °C, 1h; b. propyl bromoacetate, – 78 °C → rt, overnight; ii) a. 1 eq KOH, rt, 3h; b. 1 eq HCl (**1a**/**2a**); 1 eq KOH, rt, 3h (**1b**/**2b**); 1 eq [Bu_4N]OH, rt, 3h (**1c**/**2c**).

The molecular structures of acids **1a** and **2a** were studied by single crystal X-ray diffraction (Figure 2). Suitable single crystals of H**L1** (**1a**) were obtained by slow vapor diffusion of diethyl ether into a methanolic solution. Recrystallization of the crude product from ethanol/water (95/5) resulted in the formation of a different crystalline phase.[29] Single crystals of H**L2** (**2a**) were obtained by slow cooling of a hot, saturated solution of **2a** in methanol.

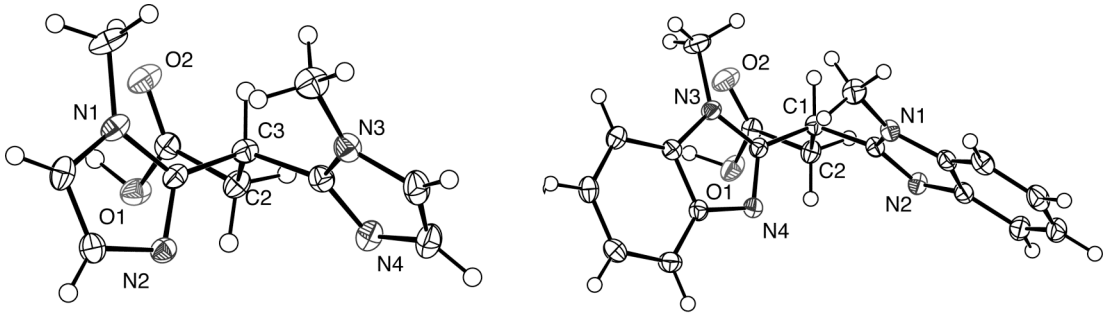

Figure 2. Molecular structures of H**L1**·MeOH (**1a**, left) and H**L2** (**2a**, right) in the crystals. The co-crystallized solvent molecule in H**L1**·MeOH has been omitted for clarity. Displacement ellipsoids are drawn at the 50% probability level.

The molecular structures of the acids **1a** and **2a** are very similar and their solid state structures clearly show the general predisposition of tripodal ligands towards facial capping of a metal center.[14] Rotation around a single C–C bond, i.e. C2–C3 in **1a**, will orient the *N,N,O* lone pairs to a virtual metal center in a facial manner. Interestingly, **1a** and **2a** do not crystallize as zwitterions; the carboxylate oxygen atom O1 is protonated, the imidazole nitrogen atoms are not protonated. Thus, atom O1 can act as hydrogen bond donor and the imidazole nitrogen atoms as hydrogen bond acceptors. In the solid state, molecules of H**L1** (**1a**) form an infinite hydrogen bonded chain along the crystallographic *c*-axis (Figure 3, Table 1). The co-crystallized methanol solvent molecule is also participating as a hydrogen bond donor with imidazole nitrogen N4 as acceptor. Consequently, both imidazole nitrogens are involved in for hydrogen bonding.

In the crystal structure of **2a**, there are no co-crystallized solvent molecules and therefore only imidazole nitrogen N4 accepts hydrogen bonds to form a one-dimensional hydrogen bonded chain along the crystallographic *c*-axis (Figure 3, Table 1). In both crystal structures the carbonyl oxygen atom O2 is not involved in strong hydrogen bonds. Weak C–H···O and C–H···N interactions involve O2 in both structures and nitrogen N2 of compound **2a**. π-π Stacking interactions between the aromatic systems of the (N1,N2,C4–C10)-benzimidazole rings with average interplanar distances of 3.40 and 3.49 Å are also observed for **2a**.

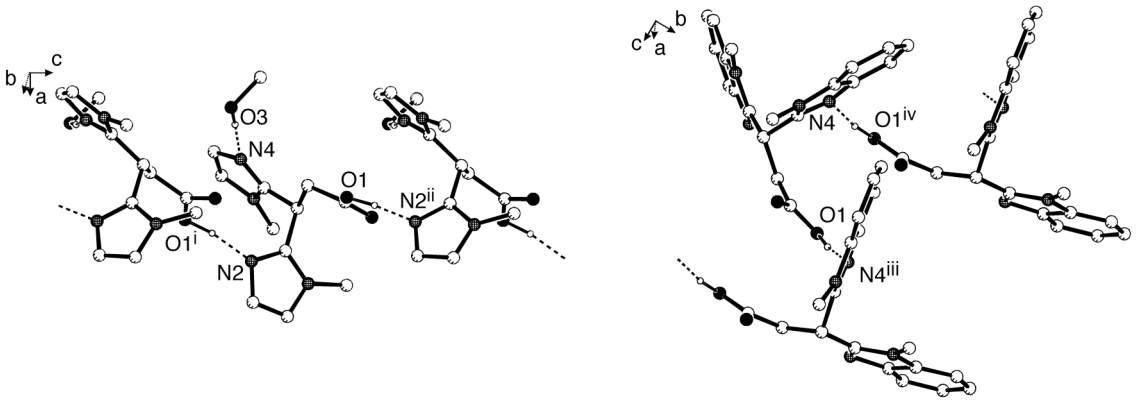

Figure 3. Hydrogen bonding patterns in H**L1** (**1a**) (left) and H**L2** (**2a**) (right). C–H hydrogen atoms have been omitted for clarity. Symmetry operations: i: x, 1/2 – y, z – 1/2; ii: x, 1/2 – y, z + 1/2; iii: x, 3/2 – y, z + 1/2; iv: x, 3/2 – y, z – 1/2.

Table 1. Selected hydrogen bond lengths (Å) and angles (°) for H**L1**·MeOH (**1a)** and H**L2** (**2a**). Symmetry operations: i: x, 1/2 – y, z + 1/2; ii: x, 3/2 – y, z + 1/2

	Donor–H ··· Acceptor	D–H	H ··· A	D ··· A	D–H ··· A
1a	O1–H1O···N2^{i}	1.02(2)	1.65(2)	2.6649(13)	171(2)
	O3–H3O···N4	0.86(2)	2.01(2)	2.8589(16)	171.8(17)
2a	O1–H10···N4^{ii}	1.02(2)	1.65(2)	2.6659(13)	171(2)

Synthesis of Cu(II) complexes. To investigate the facial capping potential of the new *N,N,O* ligands, their coordination chemistry towards copper(II) cations was investigated. Two new, neutral copper complexes of the type $[CuL_2]$ were synthesized and characterized by X-ray crystallography, IR, UV-Vis and EPR spectroscopy, and ESI-MS. The mononuclear copper complex $[Cu(\mathbf{L1})_2]\cdot 2H_2O$ (**3**) was obtained by reaction of one equivalent of $CuCl_2\cdot 2H_2O$ with two equivalents of K[**L1**] (**1b**) in hot ethanol. Complex **4**, identified as $[Cu(\mathbf{L2})_2]$, with a comparable coordination environment was isolated when $CuCl_2\cdot 2H_2O$ was reacted with two equivalents of K[**L2**] (**2b**) in hot ethanol. In both cases, blue single crystals suitable for X-ray diffraction analyses crystallized after several weeks. The complexes can also be obtained directly as powders, nicely illustrating how the judicious choice of solvent and ligand cation can simplify isolation and purification (*vide infra*). In this way, reaction of $CuCl_2$ with two equivalents of $[Bu_4N][\mathbf{L2}]$ (**2c**) in dry methanol resulted in the formation of the pale blue precipitate $[Cu(\mathbf{L2})_2]$. Separation by centrifugation and purification by simple washings with dichloromethane allowed for the facile isolation of the copper complex.

Crystal structure of $[Cu(L1)_2]\cdot 2H_2O$ (3). Two monoanionic **L1** ligands were found to be arranged centrosymmetrically around the copper ion, coordinating through all three donor groups, i.e. two 1-methylimidazole nitrogens and one carboxylato oxygen each, resulting in an elongated octahedral geometry (Figure 4). The four 1-methylimidazole imine nitrogen atoms occupy the equatorial plane (Cu–N 2.0109(18) and 1.9929(18) Å) and the two carboxylato oxygen atoms are located in the axial positions (Cu–O 2.4004(17) Å). Crystallographic data and selected bond lengths and angles are given in Tables 2 and 3. The Cu–N bond lengths are similar to those found in other CuN_4O_2 chromophores with imidazole nitrogen donors.[30-33] The Cu–O bonds are, however, shorter than those found in, for instance, bis(acetato)tetrakis(imidazole)copper(II),[30] due to ligand constraints.

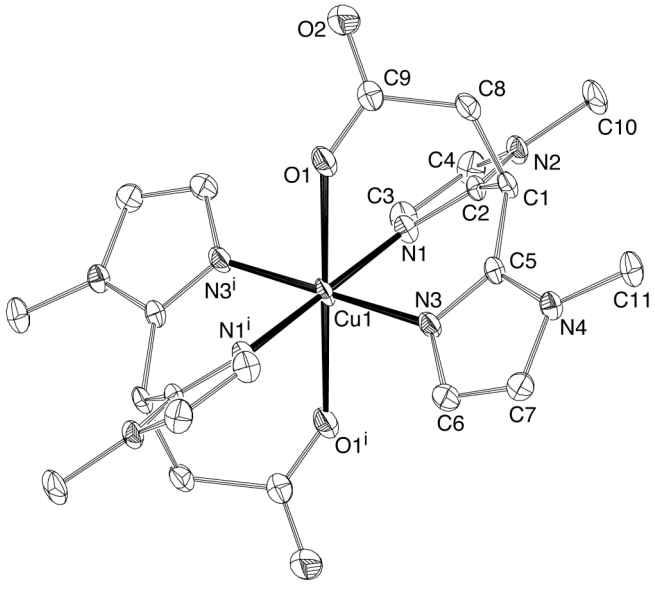

Figure 4. Molecular structure of $[Cu(\mathbf{L1})_2]\cdot 2H_2O$ (**3**) in the crystal. Hydrogen atoms and non-coordinated water molecules have been omitted for clarity. Displacement ellipsoids are drawn at the 50% probability level.

The non-coordinated water molecules are involved in a one-dimensional hydrogen bonded network. Two water molecules connect two neighboring octahedrons, each water molecule forming two hydrogen bonds to the non-coordinated oxygen atoms of the carboxylate group. This results in the formation of infinite linear chains in the direction of the crystallographic *a*,*b*,*c*-diagonal as shown in Figure 5. The OH stretching vibrations characteristic for hydrogen bonded water molecules are present in the IR spectrum of **3** at 3347 cm^{-1}. A related $[CuL_2]$ structure was recently reported for $[Cu(bdmpza)_2]\cdot 2H_2O$ (bdmpza = bis(3,5-dimethylpyrazol-1-yl)acetate) by Reedijk et al. in which the two co-crystallized water molecules play an identical role.[34] Copper(II) complexes of the related Hbip ligand have also been reported, but no facial capping of the ligand through all donor atoms was observed.[35-37]

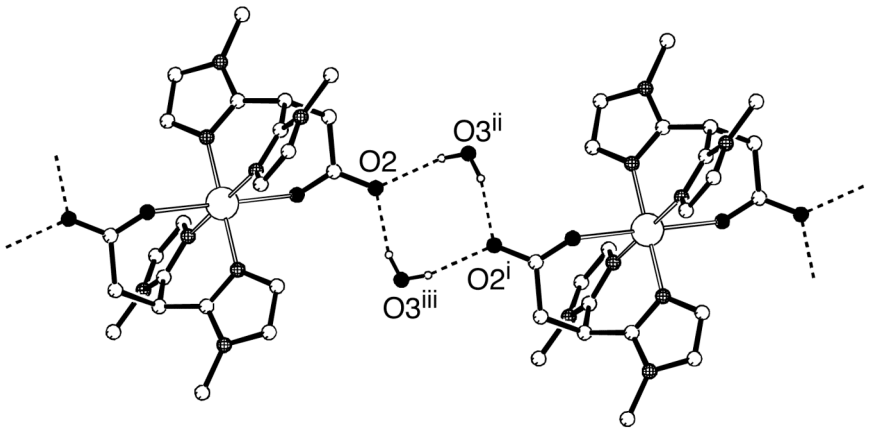

Figure 5. Hydrogen bonding network of **3** resulting in infinite linear chains. C–H hydrogen atoms have been omitted for clarity. Symmetry operations: i: – x, – y, – z; ii: – x, 1 – y, – z; iii: x, y – 1, z.

Table 2. Selected bond lengths (Å) and angles (°) for $[Cu(\mathbf{L1})_2]\cdot 2H_2O$ (**3**) and $[Cu(\mathbf{L2})_2]\cdot 3.12H_2O\cdot 1.74EtOH$ (**4**)

$[Cu(\mathbf{L1})_2]\cdot 2H_2O$ (**3**)		$[Cu(\mathbf{L2})_2]\cdot 3.12H_2O\cdot 1.74EtOH$ (**4**)	
Cu1–N1	2.0109(18)	Cu1–N1	2.0086(15)
Cu1–N3	1.9929(18)	Cu1–N11	2.0151(15)
Cu1–O1	2.4004(17)	Cu1–O24	2.3475(14)
N1–Cu1–N3	86.45(8)	N1–Cu1–N11	85.58(6)
N3–Cu1–$N1^i$	93.55(8)	N11–Cu1–$N1^i$	94.42(6)
N1–Cu1–O1	85.68(7)	N1–Cu1–O24	89.23(6)
N3–Cu1–O1	86.23(7)	N11–Cu1–O24	87.80(6)
$N1^i$–Cu1–O1	94.32(7)	$N1^i$–Cu1–O24	90.77(6)
$N3^i$–Cu1–O1	93.77(7)	$N11^i$–Cu1–O24	92.20(6)

Crystal structure of [Cu(L2)$_2$]·3.12H$_2$O·1.74EtOH (4). **4** was found to have a comparable copper geometry as in **3** (Figure 6). Crystallographic data and selected bond lengths and angles are given in Tables 2 and 3. The replacement of 1-methylimidazole for 1-methylbenzimidazole hardly affects the *N,N,O* tridentate coordination to the copper center. However, the Cu–O bond in **4** (2.3476(14) Å) is significantly shorter than the one found in **3** (2.4005(18) Å). The Cu–N bond lengths compare well to the only other crystallographically characterized CuN_4O_2 chromophore with four benzimidazole donor groups.[38]

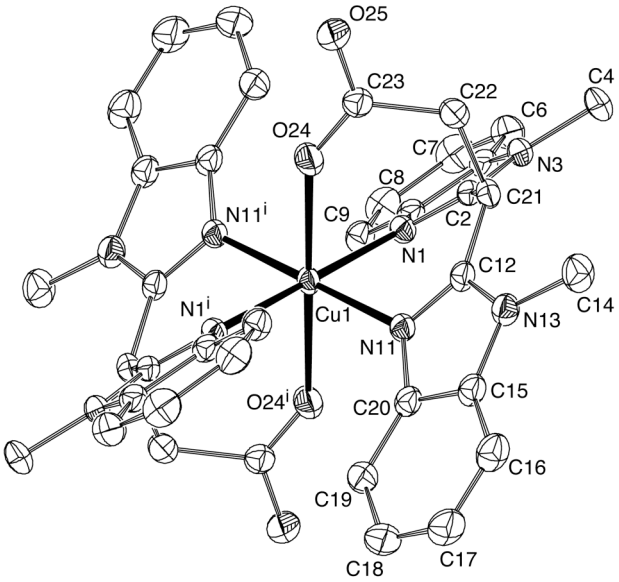

Figure 6. Molecular structure of [Cu(**L2**)$_2$]·3.12H$_2$O·1.74EtOH (**4**) in the crystal. Hydrogen atoms and solvent molecules have been omitted for clarity. Displacement ellipsoids are drawn at the 50% probability level.

Also, the hydrogen bonding pattern is similar to the one found in **3**. Again two water molecules connect the octahedrons via four hydrogen bonds to form an infinite chain in the direction of the crystallographic *c*-axis. Yet, the water molecules here also act as hydrogen bond acceptors for co-crystallized ethanol molecules (Figure 7). Additionally, there are water molecules present in the crystal structure, which do not participate in the hydrogen bonding. The latter water and ethanol molecule positions in the crystal lattice are not fully occupied (probably due to evaporation), hence the non-integer coefficients in the structural formulation of [Cu(**L2**)$_2$]·3.12H$_2$O·1.74EtOH.

ESI-MS. The ESI mass spectra of **3** and **4** dissolved in a methanol/acetonitrile mixture were recorded and very clean spectra were obtained for both complexes. Also, reference spectra of K[**L1**] (**1b**) and K[**L2**] (**2b**) were recorded for comparison. For complex [Cu(**L1**)$_2$]·2H$_2$O (**3**) only two, equally intense peaks were detected. The peak at *m/z* 551.78 corresponds to the {[Cu(**L1**)$_2$] + Na}$^+$ adduct ion, while the peak at *m/z* 529.96 is assigned to {[Cu(**L1**)$_2$] + H}$^+$. The same adduct ions were found for compound **4**, giving an *m/z* of 752.14 for {[Cu(**L2**)$_2$] + Na}$^+$ and 730.25 for {[Cu(**L2**)$_2$] + H}$^+$. The observed copper isotope

patterns were in good agreement with the calculated ones and, furthermore, no free ligand was found in the spectra of both complexes. These data strongly suggest the prevalence of the $[CuL_2]$ motif and show the complexes $[Cu(\mathbf{L1})_2]$ and $[Cu(\mathbf{L2})_2]$ as predominant species in solution.

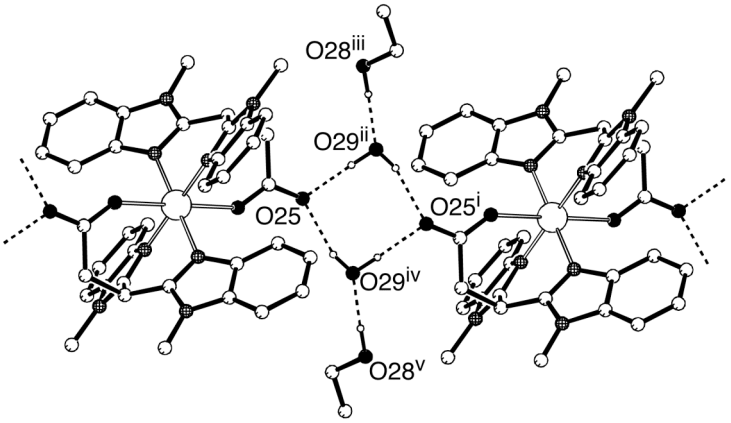

Figure 7. Hydrogen bonding network of **4** resulting in infinite linear chains. C–H hydrogens and water molecules that do not participate in the hydrogen bonding, have been omitted for clarity. Symmetry operations: i: 1 – x, 1 – y, – z; ii: x, 1/2 – y, z – 1/2; iii: x – 1, 1/2 – y, z – 1/2; iv: 1 – x, y + 1/2, 1/2 – z; v: 2 – x, y + 1/2, 1/2 – z.

Electronic absorption and EPR spectra. The UV-Vis spectrum of **3** in methanol shows three absorption bands at 215, 293 (sh), and 587 nm. The first two bands are also present in reference spectra of the ligand and are therefore assigned to intraligand transitions. The broad absorption centered at 587 nm is assigned to a d–d transition of the copper(II) center. The d–d band for **4** in methanol was found around 666 nm and four intraligand transitions could be detected (228, 252, 271 and 284 nm). Changing the nitrogen donor groups from imidazole to benzimidazole affects the ligand field splitting parameter and results in a red-shift of about 80 nm for complex **4** with respect to complex **3**. This red shift reflects the smaller axial Jahn-Teller distortion and corresponds to the shorter Cu–O bond as found in the crystal structure of complex **4**. The spectral parameters are in the range expected for d–d transitions of tetragonally distorted monomeric CuN_4O_2 chromophores.[30]

The complexes **3** and **4** were studied by EPR spectroscopy as powders at room temperature and as frozen solutions at 77 K (Figure 8). The solid state EPR spectra of both complexes at room temperature display broad features due to dipolar coupling of the Cu(II) centers, but are typically axial with $g_\perp = 2.06$ and $g_{||} = 2.22$ for **3**, and $g_\perp = 2.06$ and $g_{||} = 2.25$ for **4**. The hyperfine splitting of the spectrum with the Cu(II) ion was observed in the parallel region in both cases with $A_{||} = 200$ G (**3**) and $A_{||} = 177$ G (**4**), the latter being better resolved. This smaller hyperfine coupling $A_{||}$ of complex **4** is in line with the red shift observed in the UV-Vis spectra. An EPR spectrum of a frozen solution of **3** in methanol/water (1:5 v/v) was also recorded and again an EPR envelope typical for an axially elongated mononuclear Cu(II) species was observed ($g_\perp = 2.04$, $g_{||} = 2.24$, $A_{||} = 193$ G). Additional superhyperfine splitting due to interaction with the ^{14}N nuclei of the ligands is resolved, consistent with four

equivalent nitrogens in the equatorial plane ($A_{\perp}$= 15.5 G). A frozen methanolic solution of **4** gave a similar EPR spectrum. Again, both the hyperfine and superhyperfine couplings were resolved and the relevant parameters in this case are $g_{\perp}$ = 2.05, $g_{||}$= 2.25, $A_{||}$ = 187 G, and $A_{\perp}$ = 14.5 G. The EPR data of the powders and the frozen solutions are consistent with the structure description derived from the X-ray analyses and the ESI-MS measurements, respectively. The spectral parameters for **3** and **4** are characteristic of tetragonally elongated monomeric copper(II) complexes[39] and are comparable to the EPR parameters obtained for CuN_4O_2 chromophores with four imidazole nitrogen-donors.[30-33]

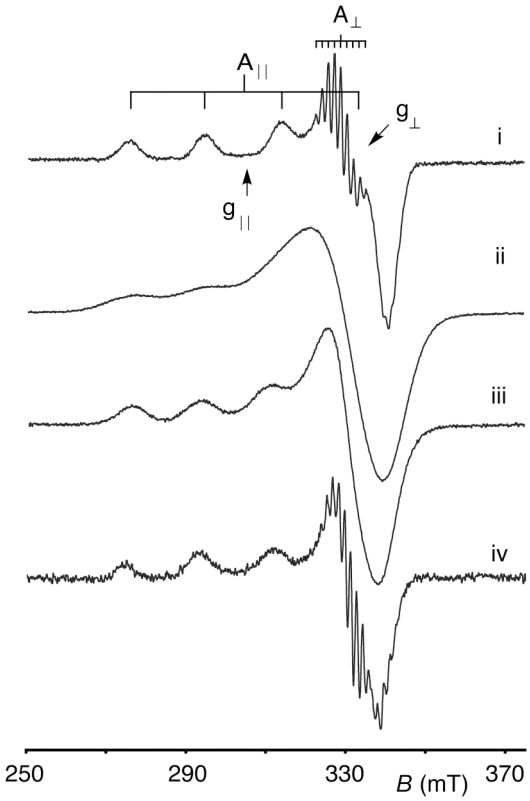

Figure 8. EPR spectra of **3** and **4**: i) frozen methanol/water solution of **3** at 77K; ii) solid **3** at rt; iii) solid **4** at rt; iv) frozen methanol solution of **4** at 77K.

2.3 Discussion

A relatively straightforward, high yielding, two-step route for the synthesis of two new *N,N,O* ligands on a multigram scale has been developed. Ligands **L1** and **L2** can be regarded as parent ligands, as the synthetic route offers the possibility of further expansion of this series of ligands. For instance, the bis(heteroaryl)methane synthesis (**5** and **6**)[26-28] allows for the incorporation of (poly)substituted (benz)imidazoles; thus introduction of other functionalities and further modification of this *N,N* backbone is feasible. Both physical properties like solubility, ease of crystallization, and steric requirements as well as the electronic properties of the ligand can therefore be controlled by design. Alterations in the

fourth substituent of the central carbon atom (C3 (**1a**) and C1 (**2a**) in Figure 2) and the type of introduced electrophile offer further possibilities for structural variation.

The two cation series of ligands, A[**L1**] and A[**L2**] (A = H, K, and [Bu_4N]), were developed to vary the solubility of one single member of a ligand family and simplify the syntheses and purification of different metal complexes. The reaction of a monoanionic ligand with a metal salt generally results in the formation of two new salts, *i.e.* the desired complex and an (inorganic) byproduct. The solubility properties of both the desired complex and the byproduct are often comparable and this then hampers purification. Choosing the right cation allows control over the solubility properties of the formed byproduct and therefore purification of the desired metal complexes can in principle be achieved by a simple washing procedure. An example of this approach is described here for the synthesis of [Cu(**L2**)$_2$] (**4**). The solubility properties of the [Bu_4N]-ligands (**1c**,**2c**) also allow the use of relatively apolar solvents, solvents in which the potassium salts (**1b**,**2b**) and acids (**1a**,**2a**) are insoluble.

2.4 Conclusions

The ligands **L1** and **L2** were designed to provide a transition metal with a facial donor array of one carboxylato and two imidazole groups, as found in the enzymes exhibiting the 2-His-1-carboxylate motif.[11,15] Using copper(II) as a probe, the neutral [CuL_2] complexes **3** and **4** nicely illustrate the facial *N*,*N*,*O* capping potential of both new ligands. This facial capping of the *N*,*N*,*O* ligands **L1** and **L2** renders this new family of ligands suitable candidates for mimicking the 2-His-1-carboxylate motif.

2.5 Experimental Section

Air-sensitive reactions were carried out under an atmosphere of dry, oxygen-free N_2 using standard Schlenk techniques. THF was dried over sodium benzophenone ketyl and distilled under N_2 prior to use. Methanol was dried over magnesium methoxide and distilled under N_2 prior to use. ^1H and $^{13}C\{^1H\}$ NMR spectra were recorded on a Varian Inova 300 spectrometer at 300 and 75 MHz, respectively, operating at 25 °C. Elemental microanalyses were carried out by the Microanalytisches Laboratorium Dornis & Kolbe, Mulheim a.d. Ruhr, Germany. Infrared spectra were recorded on a Perkin Elmer Spectrum One FT-IR instrument. ESI-MS spectra were recorded on a Micromass LC-TOF mass spectrometer by the Biomolecular Mass Spectrometry group, Utrecht University. UV-Vis spectra were recorded on a Cary 50 Varian spectrometer. EPR spectra were measured on a modified Bruker ESP300 spectrometer equipped with an ER4103TM cavity (TM_{110} mode with unloaded Q = 12000). The microwave frequency was near 9.52 GHz and the spectrometer settings involved 4 Gauss field modulation. Bis(1-methylimidazol-2-yl)methane and bis(1-methylbenzimidazol-2-yl)methane were prepared according to literature procedures.[26-28] All other chemicals were commercially obtained and used as received.

Propyl 3,3-bis(1-methylimidazol-2-yl)propionate PrL1 (7): A solution of n-butyllithium in hexanes (18 mL, 28.8 mmol, 1.6 M in hexanes) was added dropwise to a stirred solution of bis(1-methylimidazol-2-yl)methane

(**5**) (5.02 g, 28.5 mmol) in THF (150 mL) at – 78 °C. The solution was stirred for 1 hour at – 78 °C, followed by the dropwise addition of propyl bromoacetate (3.8 mL, 29 mmol). The temperature was allowed to rise to room temperature overnight, resulting in a yellow-white suspension. The reaction mixture was quenched with H_2O (25 mL) and all volatiles were evaporated *in vacuo*. The water layer was extracted with ethyl acetate (4 × 30 mL) and the combined organic layers were dried over magnesium sulfate, filtered and evaporated to dryness. The product was obtained as a yellow oil, which solidifies upon standing (6.51 g, 83%). This product can be purified by column chromatography (silica, eluent ethyl acetate:methanol = 9:1), but the crude product is pure enough for further use. ^{1}H NMR (300 MHz, $CDCl_3$, 25 °C): δ = 0.82 (t, 3H, *J* = 7.8 Hz, $OCH_2CH_2CH_3$), 1.54 (sextet, 2H, *J* = 7.5 Hz, $OCH_2CH_2CH_3$), 3.28 (d, 2H, *J* = 7.8 Hz, $CHCH_2$), 3.46 (s, 6H, NCH_3), 3.96 (t, 2H, *J* = 6.9 Hz, $OCH_2CH_2CH_3$), 4.94 (t, 1H, *J* = 7.8 Hz, $CHCH_2$), 6.72 (s, 2H, H_{im}), 6.88 (s, 2H, H_{im}) ppm. ^{13}C{^{1}H} NMR (75 MHz, $CDCl_3$, 25 °C): δ = 10.2, 21.8, 32.8, 34.4, 36.3, 66.3, 121.9, 127.2, 145.2, 171.2 ppm. IR (solid) ν = 3099.1, 2967.2, 1727.1, 1492.3, 1282.9, 1189.7, 1174.9, 1129.8, 744.0 cm^{-1}. Anal. for $C_{14}H_{20}N_4O_2$ (276.33): calc. C 60.85, H 7.30, N 20.28; found C 60.74, H 7.22, N 20.18.

Propyl 3,3-bis(1-methylbenzimidazol-2-yl)propionate PrL2 (8): Compound **8** was synthesized using the procedure described above for compound **7**. The product was obtained as an off-white solid (2.89 g, 92%). This product can be purified by column chromatography (silica, eluent ethyl acetate:methanol = 7:1), but the crude product is pure enough for further use. ^{1}H NMR (300 MHz, $CDCl_3$, 25 °C): δ = 0.86 (t, 3H, *J* = 7.5 Hz, $OCH_2CH_2CH_3$), 1.58 (sextet, 2H, *J* = 7.2 Hz, $OCH_2CH_2CH_3$), 3.61 (d, 2H, *J* = 7.5 Hz, $CHCH_2$), 3.76 (s, 6H, NCH_3), 4.02 (t, 2H, *J* = 6.3 Hz, $OCH_2CH_2CH_3$), 5.45 (t, 1H, *J* = 7.5 Hz, $CHCH_2$), 7.26 (m, 6H, $H_{benzimid}$), 7.76 (s, 2H, $H_{benzimid}$) ppm. ^{13}C{^{1}H} NMR (75 MHz, $CDCl_3$, 25 °C): δ = 10.2, 21.8, 30.3, 35.9, 36.2, 66.6, 109.2, 119.7, 122.2, 122.8, 136.4, 142.1, 151.2, 170.9 ppm. IR (solid) ν = 2973.2, 1733.9, 1467.1, 1439.7, 1389.1, 1179.2, 733.7 cm^{-1}. Anal. for $C_{22}H_{24}N_4O_2$ (376.45): calc. C 70.19, H 6.43, N 14.88; found C 69.98, H 6.41, N 14.69.

3,3-Bis(1-methylimidazol-2-yl)propionic acid HL1 (1a): To a solution of ester **7** (2.24 g, 8.1 mmol) in THF (20 mL) was added one equivalent of potassium hydroxide in water (8.20 mL, 0.989 M, 8.1 mmol) and the solution was stirred for 3 h at room temperature. Subsequently, one equivalent of a hydrochloric acid solution in water (8.11 mL, 1 M, 8.1 mmol) was added to the hydrolyzed reaction mixture. Evaporation of the solvents resulted in a white mixture of product and potassium chloride. Most of the KCl was removed after extraction of the powder with dry methanol (3 × 15 mL). Evaporation of the solvent and recrystallization from EtOH/H_2O (95:5) gave the product as colorless crystals of composition H**L1**·4H_2O (1.6 g, 65%). Single crystals of the composition H**L1**·MeOH were obtained by slow diffusion of diethyl ether in a concentrated solution of **1a** in methanol. ^{1}H NMR (300 MHz, CD_3OD, 25 °C): δ = 3.16 (d, 2H, *J* = 7.8 Hz, $CHCH_2$), 3.62 (s, 6H, NCH_3), 5.00 (t, 1H, *J* = 7.2 Hz, $CHCH_2$), 6.99 (s, 2H, H_{im}), 7.11 (s, 2H, H_{im}) ppm. ^{13}C{^{1}H} NMR (75 MHz, CD_3OD, 25 °C): δ = 33.6, 33.9, 38.9, 123.9, 125.9, 146.8, 175.2 ppm. IR (solid) ν = 3130.0, 1701.5, 1491.2, 1348.4, 1285.6, 1266.7, 1220.9, 1135.5, 772.3 cm^{-1}. Anal. for $C_{11}H_{14}N_4O_2$·4H_2O (306.32): calc. C 43.13, H 7.24, N 18.29; found C 43.31, H 7.16, N 18.34.

3,3-Bis(1-methylbenzimidazol-2-yl)propionic acid HL2 (2a): The acid **2a** was synthesized using the procedure as described above for the acid **1a**. KCl could in this case be removed by washing the product with water (3 × 20 mL). Recrystallization from methanol gave the product as colorless crystals (0.59 g, 64%). Slow cooling of a hot saturated solution of **2a** in methanol resulted in crystals suitable for X-ray analysis. ^{1}H NMR

(300 MHz, CD_3OD, 25 °C): δ = 3.53 (d, 2H, *J* = 7.2 Hz, CHCH_2), 3.78 (s, 6H, NCH_3), 5.40 (t, 1H, *J* = 7.2 Hz, C*H*CH_2), 7.28 (m, 4H, $H_{benzimid}$), 7.48 (d, 2H, *J* = 7.2 Hz, $H_{benzimid}$) 7.63 (d, 2H, *J* = 7.2 Hz, $H_{benzimid}$) ppm. $^{13}C\{^1H\}$ NMR (75 MHz, CD_3OD, 25 °C): δ = 30.5, 35.3, 37.6, 111.0, 119.6, 123.6, 124.3, 137.3, 142.7, 153.5, 174.4 ppm. IR (solid) ν = 2934.4, 1716.3, 1467.8, 1392.8, 1332.3, 1282.8, 762.1, 739.6 cm^{-1}. Anal. for $C_{19}H_{18}N_4O_2$ (334.37): calc. C 68.25, H 5.43, N 16.76; found C 68.15, H 5.49, N 16.83.

General procedure for the synthesis of the potassium and tetrabutylammonium salts 1b/c and 2b/c: To a solution of the appropriate ester **7** or **8** in THF (20 mL) was added one mole equivalent of a KOH or $[Bu_4N]OH$ solution in water (volumetric standard) and the reaction mixture was stirred for 3 hours at room temperature. Evaporation of the solvents resulted in an oil. Repeated azeotropic drying of the oil with toluene gave the desired product as a powder in quantitative yield.

Potassium 3,3-bis(1-methylimidazol-2-yl)propionate K[L1] (1b): Yellowish powder (1.97 g). ^1H NMR (300 MHz, CD_3OD, 25 °C): δ = 3.08 (d, 2H, *J* = 7.2 Hz, CHCH_2), 3.52 (s, 6H, NCH_3), 4.92 (t, 1H, *J* = 7.2 Hz, C*H*CH_2), 6.83 (s, 2H, H_{im}), 6.95 (s, 2H, H_{im}) ppm. $^{13}C\{^1H\}$ NMR (75 MHz, CD_3OD, 25 °C): δ = 35.2, 35.6, 41.1, 123.2, 127.1, 148.3, 178.6 ppm. IR (solid) ν = 1580.2, 1393.0, 665.2 cm^{-1}. Anal. for $C_{11}H_{13}KN_4O_2$ (272.34): calc. C 48.51, H 4.81, N 20.57; found C 48.36, H 4.92, N 20.47. ESI-MS: *m/z* = 311.08 {$[KL1 + K]^+$, calc. 311.03), 583.04 {$[2(KL1) + K]^+$, calc. 583.10}.

Tetrabutylammonium 3,3-bis(1-methylimidazol-2-yl)propionate [Bu_4N][L1] (1c): White powder (1.97 g). ^1H NMR (300 MHz, $CDCl_3$, 25 °C): δ = 0.92 (m, 12H, $CH_2CH_2CH_2CH_3$), 1.35 (m, 8H, $CH_2CH_2CH_2CH_3$), 1.57 (m, 8H, $CH_2CH_2CH_2CH_3$), 3.06 (d, 2H, *J* = 6.5 Hz, CHCH_2), 3.26 (m, 8H, C$H_2CH_2CH_2CH_3$), 3.58 (s, 6H, NCH_3), 5.08 (t, 1H, *J* = 6.5 Hz, C*H*CH_2), 6.65 (s, 2H, H_{im}), 6.77 (s, 2H, H_{im}) ppm. $^{13}C\{^1H\}$ NMR (75 MHz, $CDCl_3$, 25 °C): δ = 13.7, 19.7, 24.0, 33.0, 35.2, 40.8, 58.6, 120.8, 126.5, 148.9, 174.7 ppm. IR (solid) ν = 2962.5, 2936.7, 1581.6, 1489.7, 1363.2, 1280.6, 1128.0, 770.5 cm^{-1}. Anal. for $C_{27}H_{49}N_5O_2$ (475.71): calc. C 68.17, H 10.38, N 14.72; found C 67.89, H 10.31, N 14.63.

Potassium 3,3-bis(1-methylbenzimidazol-2-yl)propionate K[L2] (2b): Yellowish powder (2.27 g). ^1H NMR (300 MHz, CD_3OD, 25 °C): δ = 3.35 (d, 2H, *J* = 7.2 Hz, 2H, CHCH_2), 3.78 (s, 6H, NCH_3), 5.40 (t, 1H, *J* = 7.2 Hz, C*H*CH_2), 7.23 (m, 4H, $H_{benzimid}$), 7.44 (d, 2H, *J* = 7.8 Hz, $H_{benzimid}$), 7.61 (d, 2H, *J* = 7.8 Hz, $H_{benzimid}$) ppm. $^{13}C\{^1H\}$ NMR (75 MHz, CD_3OD, 25 °C): δ = 29.3, 35.4, 39.8, 109.6, 118.4, 122.0, 122.7, 136.2, 141.8, 153.6, 176.8 ppm. IR (solid) ν = 1598.0, 1581.9, 1385.7, 1282.7, 737.8 cm^{-1}. Anal. for $C_{19}H_{17}KN_4O_2$ (372.46): calc. C 61.27, H 4.60, N 15.04; found C 61.05, H 4.68, N 14.86. ESI-MS: *m/z* = 327.18 {$[BenzMIm_2C_2H_2 + K]^+$, calc. 327.10), 411.12 {$[KL2 + K]^+$, calc. 411.06}, 783.19 {$[2(KL2) + K]^+$, calc. 783.16)}.

Tetrabutylammonium 3,3-bis(1-methylbenzimidazol-2-yl)propionate [Bu_4N][L2] (2c): Yellow powder (1.52 g). ^1H NMR (300 MHz, $CDCl_3$, 25 °C): δ = 0.92 (t, 12H, *J* = 7.2 Hz, $CH_2CH_2CH_2CH_3$), 1.33 (m, 8H, $CH_2CH_2CH_2CH_3$), 1.53 (m, 8H, $CH_2CH_2CH_2CH_3$), 3.19 (m, 8H, C$H_2CH_2CH_2CH_3$), 3.37 (d, 2H, *J* = 6.6 Hz, CHCH_2), 3.82 (s, 6H, NCH_3), 5.58 (t, 1H, *J* = 6.3 Hz, C*H*CH_2), 7.20 (m, 6H, $Hb_{enzimid}$), 7.65 (m, 2H, $H_{benzimid}$) ppm. $^{13}C\{^1H\}$ NMR (75 MHz, $CDCl_3$, 25 °C): δ = 13.6, 19.6, 23.9, 30.2, 36.2, 39.5, 58.6, 109.1, 119.3, 121.3, 121.9, 136.4, 142.4, 154.3, 174.1 ppm. IR (solid) ν = 2960.0, 2874.0, 1596.5, 1465.8, 1380.2, 1275.5, 736.1 cm^{-1}. Anal. for $C_{35}H_{53}N_5O_2$ (575.83): calc. C 73.00, H 9.28, N 12.16; found C 72.89, H 9.38, N 12.22.

Table 3. Crystallographic data for compounds **1a**, **2a**, **3**, and **4**

	1a	**2a**	**3**	**4**
formula	$C_{11}H_{14}N_4O_2{\cdot}CH_3OH$	$C_{19}H_{18}N_4O_2$	$C_{22}H_{26}CuN_8O_4{\cdot}2H_2O$	$C_{38}H_{34}CuN_8O_4{\cdot}$ 1.74EtOH$\cdot$3.12H_2O
fw	266.30	334.37	566.08	866.64
crystal size (mm)	0.06 × 0.30 × 0.43	0.18 × 0.42 × 0.42	0.12 × 0.12 × 0.18	0.09 × 0.15 × 0.33
crystal syst	Monoclinic	Monoclinic	Triclinic	Monoclinic
space group	$P2_1/c$ (no. 14)	$P2_1/c$ (no. 14)	$P\bar{1}$ (no. 2)	$P2_1/c$ (no. 14)
a (Å)	14.8340(10)	8.5910(1)	8.3128(9)	8.5293(1)
b (Å)	8.2221(6)	22.8189(2)	8.3514(9)	18.8885(2)
c (Å)	10.6605(7)	8.2417(1)	9.9368(17)	12.6452(2)
α (deg)	90	90	96.457(13)	90
β (deg)	91.652(6)	102.7895(6)	94.540(10)	100.3961(4)
γ (deg)	90	90	118.353(8)	90
V (Å^3)	1299.69(15)	1575.59(3)	596.27(14)	2003.77(4)
Z	4	4	1	2
D_{calc} (g/cm^3)	1.361	1.410	1.576	1.436
μ (mm^{-1})	0.100	0.095	0.973	0.612
abs. corr. range	0.90 - 1.00	–	0.69-0.89	0.88-0.94
collected refl.	26945	29513	8358	31917
unique refl.	2975	3623	2708	4591
parameter/ restraints	183 / 0	232 / 0	179 / 0	280 / 0
R1/wR2 [I>2σ(I)]	0.0358 / 0.0869	0.0370 / 0.0957	0.0410 / 0.1018	0.0379 / 0.1033
R1/wR2 [all refl.]	0.0485 / 0.0928	0.0429 / 0.1000	0.0500 / 0.1072	0.0494 / 0.1106
S	1.046	1.032	1.085	1.065
Min/max res.dens (e/Å^3)	– 0.21 / 0.23	– 0.28 / 0.29	– 0.90 / 0.73	– 0.49 / 0.51

[Cu(L1)$_2$]·2H$_2$O (3): To a colorless solution of K[**L1**] (**1b**) (414 mg, 1.52 mmol) in hot ethanol (20 mL) was added a solution of $CuCl_2{\cdot}2H_2O$ (129 mg, 0.76 mmol) in hot ethanol (10 mL). The solution immediately turned dark blue and the reaction mixture was heated to reflux for one hour. Upon cooling of the solution to room temperature a white precipitate formed (KCl). The solution was filtered and concentrated *in vacuo*. The resulting dark blue powder was recrystallized from a minimal amount of refluxing ethanol and cooled to 4 °C to give the title compound as blue crystals (201 mg, 47%). Single crystals formed after three weeks from a concentrated solution of **3** in ethanol upon standing. Anal. for $C_{22}H_{26}CuN_8O_4{\cdot}2H_2O$ (566.06): calc. C 46.86, H 5.34, N 19.80; found C 46.60, H 5.44, N 19.72. IR (solid) ν = 3347.5, 3275.9, 3126.5, 1582.1, 1506.9, 1383.9, 1289.8, 1153.1, 745.9 cm^{-1}. UV-Vis (methanol): λ_{max} = 215, 219, 587 nm. ESI-MS: *m/z* = 529.96 {[Cu(L1)$_2$ + H]$^+$, calc. 530.14}, 551.78 {[Cu(L1)$_2$ + Na]$^+$, calc. 552.13}.

[Cu(L2)$_2$] (4): To a colorless solution of [Bu_4N][**L2**] (**2c**) (470 mg, 0.82 mmol) in hot, dry methanol (20mL) was added a solution of $CuCl_2$ (55 mg, 0.41 mmol) in hot, dry methanol (10 mL). Immediately the solution turned green-blue and the reaction mixture was refluxed for one hour, during which a pale blue precipitate formed. The reaction mixture was allowed to cool to room temperature and the precipitate was collected via centrifugation. The crude product was washed with methanol (1 × 10 mL) and dichloromethane (3 × 10 mL) and dried *in vacuo*. The title compound was isolated as a light blue powder (162 mg, 54%). Slow evaporation of a concentrated solution of **4** in ethanol resulted in the formation of single crystals of the composition [Cu(**L2**)$_2$]·3.12H_2O·1.74EtOH formed after six weeks. Anal. for $C_{38}H_{34}CuN_8O_4$ (730.27): calc. C 62.50, H 4.69, N 15.34; found C 62.36, H 4.62, N 15.23. IR (solid) ν = 3349.8, 1583.1, 1458.0, 1385.5, 1304.1, 1284.8, 742.8 cm^{-1}. UV-Vis (methanol): λ_{max} = 228, 252, 271, 666 nm. ESI-MS: *m/z* = 730.25 {$[Cu(L2)_2 + H]^+$, calc. 730.21}, 752.14 {$[Cu(L2)_2 + Na]^+$, calc. 752.19}.

X-ray crystal structure determinations of 1a, 2a, 3 and 4. X-ray intensities were measured on a Nonius KappaCCD diffractometer with rotating anode (graphite monochromator, λ = 0.71073 Å) at a temperature of 150 K. The structures were solved with Direct Methods (compounds **1a**,[40] **2a**,[41] and **4**[40]) or automated Patterson methods (compound **3**[42]). The structures were refined with SHELXL-97[43] against F^2 of all reflections up to $(\sin\theta/\lambda)_{max}$ = 0.65 $Å^{-1}$. Structure calculations, drawings, and checking for higher symmetry was performed with the PLATON[44] package. Further details are given in Table 3. In crystal structures **1a**, **2a**, and **3** all hydrogen atoms were located in the difference Fourier map. C–H hydrogens were refined as rigid groups. O–H hydrogens were refined freely with isotropic displacement parameters. In crystal structure **4**, the position of water molecule O29 is fully occupied. Water molecule O30 was refined with an occupancy of 56% and the ethanol molecule with an occupancy of 87%. All hydrogen atoms were located in the difference Fourier map. C–H hydrogens were refined as rigid groups. O–H hydrogens were kept fixed in the located position.

2.6 References

1. Holm, R. H.; Solomon, E. I. (Eds.) *Chem. Rev.* **2004**, *104*, 347-1200.
2. Edelmann, F. T. *Angew. Chem. Int. Ed.* **2001**, *40*, 1656-1660.
3. Trofimenko, S. *Chem. Rev.* **1993**, *93*, 943-980.
4. Hammes, B. S.; Carrano, C. J. *Inorg. Chem.* **1999**, *38*, 4593-4600.
5. Karambelkar, V. V.; Krishnamurthy, D.; Stern, C. L.; Zakharov, L. N.; Rheingold, A. L.; Goldberg, D. P. *Chem. Commun.* **2002**, 2772-2773.
6. Otero, A.; Fernandez-Baeza, J.; Antinolo, A.; Tejeda, J.; Lara-Sanchez, A. *Dalton Trans.* **2004**, 1499-1510.
7. Trosch, A.; Vahrenkamp, H. *Eur. J. Inorg. Chem.* **1998**, 827-832.
8. Hegg, E. L.; Que, L. *Eur. J. Biochem.* **1997**, *250*, 625-629.
9. Lange, S. J.; Que, L., Jr. *Curr. Opin. Chem. Biol.* **1998**, *2*, 159-172.
10. Que, L., Jr. *Nat. Struct. Biol.* **2000**, *7*, 182-184.
11. Costas, M.; Mehn, M. P.; Jensen, M. P.; Que, L. *Chem. Rev.* **2004**, *104*, 939-986.
12. Valegard, K.; van Scheltinga, A. C. T.; Lloyd, M. D.; Hara, T.; Ramaswamy, S.; Perrakis, A.; Thompson, A.; Lee, H. J.; Baldwin, J. E.; Schofield, C. J.; Hajdu, J.; Andersson, I. *Nature* **1998**, *394*, 805-809.
13. Kauppi, B.; Lee, K.; Carredano, E.; Parales, R. E.; Gibson, D. T.; Eklund, H.; Ramaswamy, S. *Structure* **1998**, *6*, 571-586.

14. Parkin, G. *Chem. Commun.* **2000**, 1971-1985.
15. Parkin, G. *Chem. Rev.* **2004**, *104*, 699-767.
16. Otero, A.; Fernandez-Baeza, J.; Tejeda, J.; Antinolo, A.; Carrillo-Hermosilla, F.; Diez-Barra, E.; Lara-Sanchez, A.; Fernandez-Lopez, M.; Lanfranchi, M.; Pellinghelli, M. A. *J. Chem. Soc., Dalton Trans.* **1999**, 3537-3539.
17. Beck, A.; Barth, A.; Hubner, E.; Burzlaff, N. *Inorg. Chem.* **2003**, *42*, 7182-7188.
18. Beck, A.; Weibert, B.; Burzlaff, N. *Eur. J. Inorg. Chem.* **2001**, 521-527.
19. Hegelmann, I.; Beck, A.; Eichhorn, C.; Weibert, B.; Burzlaff, N. *Eur. J. Inorg. Chem*. **2003**, 339-347.
20. Muller, R.; Hubner, E.; Burzlaff, N. *Eur. J. Inorg. Chem.* **2004**, 2151-2159.
21. Joseph, M.; Leigh, T.; Swain, M. L. *Synthesis* **1977**, 459-461.
22. Dowling, C.; Parkin, G. *Polyhedron* **1996**, *15*, 2463-2465.
23. Ghosh, P.; Parkin, G. *J. Chem. Soc., Dalton Trans.* **1998**, 2281-2283.
24. Valentine, J. S. (Ed), *Copper-containing proteins*. Academic Press: Amsterdam, 2002.
25. Gazo, J.; Bersuker, I. B.; Garaj, J.; Kabesova, M.; Kohout, J.; Langfelderova, H.; Melnik, M.; Serator, M.; Valach, F. *Coord. Chem. Rev.* **1976**, *19*, 253-297.
26. Braussaud, N.; Ruther, T.; Cavell, K. J.; Skelton, B. W.; White, A. H. *Synthesis* **2001**, 626-632.
27. Lucas, P.; El Mehdi, N.; Ho, H. A.; Belanger, D.; Breau, L. *Synthesis* **2000**, 1253-1258.
28. Elgafi, S.; Field, L. D.; Messerle, B. A.; Turner, P.; Hambley, T. W. *J. Organomet. Chem.* **1999**, *588*, 69-77.
29. Bruijnincx, P. C. A.; Lutz, M.; Klein Gebbink, R. J. M. *unpublished results*.
30. Abuhijleh, A. L.; Woods, C. *Inorg. Chim. Acta* **1992**, *194*, 9-14.
31. Baesjou, P. J.; Driessen, W. L.; Challa, G.; Reedijk, J. *J. Mol. Cat. A: Chem*. **1996**, *110*, 195-210.
32. Barszcz, B.; Glowiak, T.; Jezierska, J. *Polyhedron* **1999**, *18*, 3713-3721.
33. Place, C.; Zimmermann, J. L.; Mulliez, E.; Guillot, G.; Bois, C.; Chottard, E. C. *Inorg. Chem.* **1998**, *37*, 4030-4039.
34. Kozlevcar, B.; Gamez, P.; de Gelder, R.; Driessen, W. L.; Reedijk, J. *Eur. J. Inorg. Chem*. **2003**, 47-50.
35. Akriff, Y.; Server-Carrio, J.; Sancho, A.; Garcia-Lozano, J.; Escriva, E.; Folgado, J. V.; Soto, L. *Inorg. Chem*. **1999**, *38*.
36. Akriff, Y.; Server-Carrio, J.; Sancho, A.; Garcia-Lozano, J.; Escriva, E.; Soto, L. *Inorg. Chem.* **2001**, *40*, 6832-6840.
37. Sancho, A.; Gimeno, B.; Amigo, J. M.; Ochando, L. E.; Debaerdemaeker, T.; Folgado, J. V.; Soto, L. *Inorg. Chim. Acta* **1996**, *248*, 153-158.
38. Isele, K.; Broughton, V.; Matthews, C. J.; Williams, A. F.; Bernardinelli, G.; Franz, P.; Decurtins, S. *J. Chem. Soc., Dalton Trans.* **2002**, 3899-3905.
39. Hathaway, B. J.; Billing, D. E. *Coord. Chem. Rev.* **1970**, *5*, 143-207.
40. Altomare, A.; Burla, M. C.; Camalli, M.; Cascarano, G. L.; Giacovazzo, C.; Guagliardi, A.; Moliterni, A. G. G.; Polidori, G.; Spagna, R. *J. Appl. Cryst.* **1999**, *32*, 115-119.
41. Sheldrick, G. M. *SHELXS-97. Program for crystal structure solution*, University of Gottingen: Germany, 1997.
42. Beurskens, P. T.; Admiraal, G.; Beurskens, G.; Bosman, W. P.; Garcia-Granda, S.; Gould, R. O.; Smits, J. M. M.; Smykalla, C. *The DIRDIF99 program system*, Technical Report of the Crystallography Laboratory, University of Nijmegen: The Netherlands, 1999.
43. Sheldrick, G. M. *SHELXL-97. Program for crystal structure refinement*, University of Gottingen: Germany, 1997.
44. Spek, A. L. *J. Appl. Cryst.* **2003**, *36*, 7-13.

CHAPTER 3

Modeling the 2-His-1-Carboxylate Facial Triad: Iron-Catecholato Complexes as Structural and Functional Models of the Extradiol Cleaving Dioxygenases

Abstract

The synthesis of mononuclear iron(II)- and iron(III)-catecholato complexes with three members of the new family of substituted 3,3-bis(1-alkylimidazol-2-yl)propionates as models of the active site of the extradiol cleaving dioxygenases is described. The structure of the mononuclear complex [Fe(**L3**)(tcc)(H_2O)] was determined by single crystal X-ray diffraction and can be regarded as a close structural model of the enzyme-substrate complex. The dioxygen reactivity of the complexes proceeds in two steps. In the first step the iron(II)-catecholato complexes convert rapidly to the corresponding iron(III) complexes, which then, in a second and slower step, exhibit both oxidative cleavage and auto-oxidation of the substrate. Extradiol *and* intradiol cleavage are obtained in roughly equal amounts in non-coordinating solvents.

P. C. A. Bruijnincx, M. Lutz, A. L. Spek, W. R. Hagen, B. M. Weckhuysen, G. van Koten, R. J. M. Klein Gebbink, *J. Am. Chem. Soc.*, accepted for publication

3.1 Introduction

Extradiol cleaving catechol dioxygenases catalyze the oxidative cleavage of catechols at the aromatic C–C bond adjacent to the catechol oxygens.[1-3] These enzymes are part of a superfamily of enzymes that share a common structural motif at the active site, the so-called 2-His-1-carboxylate facial triad.[4-6] Over the last decade, this structural motif has emerged as a new common platform for dioxygen activation in biology.[1,7] It consists of a mononuclear non-heme iron(II) center, which is coordinated by three endogenous ligands (two His and one Glu or Asp) in a facial manner, thereby leaving the other three coordination sites vacant and available for the binding of exogenous ligands such as dioxygen, substrate, and/or cofactor (Figure 1).[1,5,7] The flexibility in coordination chemistry at the metal center is reflected in the stunningly diverse oxidative transformations that the enzymes of this superfamily catalyze and new types of reactivity based on this platform keep being discovered.[8] The reactivity of these enzymes ranges from the biosynthesis of isopenicillins via heterocyclic ring formation[9,10] to the *cis*-dihydroxylation of arene double bonds.[11,12]

Many studies have been devoted to the structural and functional modeling of this superfamily of enzymes. The most prominent polydentate ligands that have been studied in this respect are the tpa, bpmcn,[13-20] (Me_3-)tacn,[18,21,22] and $Tp^{R,R'}$[23-27] ligand systems.[28] Indeed, impressive results have been reported in mimicking both the structural and/or functional features of the enzymes under scrutiny. However, the ligands employed in these studies provide the metal center with an all *N* donor set that does not accurately reflect the N_{im},N_{im},O_{carb} ligand environment found at the active site of the enzymes. For this reason, attention has shifted to the development of mixed ligand systems.[29-31] In order to more closely mimic the 2-His-1-carboxylate facial triad, models should preferably contain tridentate, tripodal *N,N,O* ligands with a monoanionic carboxylate group. Such ligands are rare and only very few such *N,N,O* iron complexes have been reported, see e.g. the bispyrazolylacetates studied by Burzlaff et al.[29,30] We recently reported the synthesis and facial capping potential of the substituted bis(1-alkylimidazol-2-yl)propionate framework, a family of monoanionic, tridentate, tripodal ligands that include the biologically relevant carboxylate and imidazole donor groups.[32,33,34] To examine their use as mimics of the 2-His-1-carboxylate facial triad superfamily, we set out to study these ligands and their iron complexes with respect to the extradiol cleaving catechol dioxygenases (Figure 1).

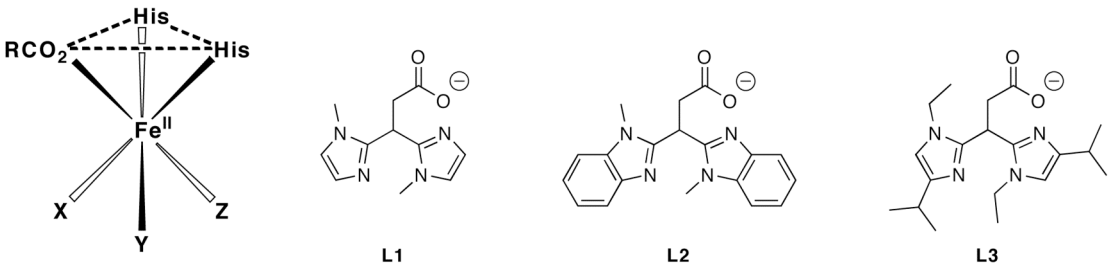

Figure 1. The 2-His-1-carboxylate facial triad and ligands **L1**, **L2**, and **L3**.

The oxidative cleavage of catechols is a key step in the biodegradation of aromatic compounds. In general, the responsible catechol dioxygenases can be divided in two classes, based on the position of the catechol ring cleavage (Figure 2).[1] The extradiol dioxygenases represent the more common metabolic pathway in which the C–C bond adjacent to the catechol oxygens is cleaved. These enzymes are characterized by a non-heme iron(II) active site coordinated by the 2-His-1-carboxylate facial triad.[4,5,7] The intradiol dioxygenases use a non-heme iron(III) cofactor with a His_2Tyr_2 donor set around the metal center and cleave the C–C bond of the enediol functionality.[35]

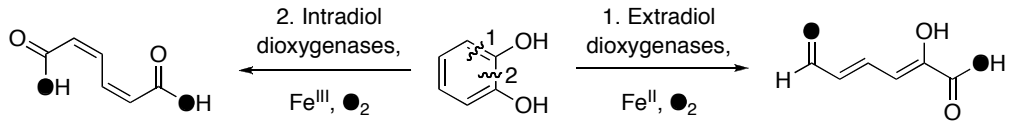

Figure 2. Catechol cleavage by the extradiol and intradiol dioxygenases.

The mechanisms by which these two types of enzymes catalyze the regioselective oxidative ring cleavage are not fully understood. How the enzymes differentiate between the two possible reaction pathways and what the decisive factors for reactivity are, is currently under active investigation.[1,2,36,37]

To address these questions, the use of accurate model complexes can give more insight into the factors governing the regioselectivity of the cleavage. Since the enzymes utilize an ordered mechanism with substrate binding before dioxygen activation,[6,38] isolated iron-catecholato complexes serve as an excellent starting point to model the chemistry of this enzyme-substrate complex. Most of the reported mimics of the catechol dioxygenases make use of tetradentate ligands and display intradiol activity.[1,2,39] Only a few iron complexes have been reported to give extradiol type cleavage products.[22,27,40-43] The system reported by Funabiki, a mixture of $FeCl_2$ or $FeCl_3$ with pyridine/bipyridine, was the first example of a functional mimic of the extradiol dioxygenases.[44] Que et al. communicated the quantitative extradiol cleavage of an isolated [Fe^{III}(Cl)(dtbc)(Me_3-tacn)] complex (dtbc = 3,5-di-*tert*-butylcatecholato dianion)[42] and, along a similar vein, Bugg et al. reported the extradiol type cleavage of catechol using mixtures of tacn, pyridine and either $FeCl_2$ or $FeCl_3$.[22] In both cases, the use of tridentate ligands that facially cap the metal center was of prime importance. There are, however, no examples reported to date of iron complexes with a mixed donor ligand, which would more accurately reflect the active site of the enzymes that elicit extradiol type cleavage.

In this Chapter, we describe the first mononuclear iron(II/III)-catecholato complexes with tridentate ligands of the new substituted bis(1-alkylimidazol-2-yl)propionate ligand family as structural and functional mimics of the extradiol cleaving catechol dioxygenases. The synthesis and structural characterization of these complexes, as well as their dioxygen reactivity and product selectivity will be discussed. These studies provide further insight into the factors governing the observed cleavage pathways of the extradiol catechol cleaving enzymes.

3.2 Results

Synthesis of ligands L1-L3. The potassium salts of ligands **L1** (3,3-bis(1-methylimidazol-2-yl)propionate) and **L2** (3,3-bis(1-methylbenzimidazol-2-yl)propionate) were synthesized according to the general synthetic route previously developed by our group for substituted 3,3-bis(1-alkylimidazol-2-yl)propionates.[32] K[**L3**] (**L3** = 3,3-bis(1-ethyl-4-isopropylimidazol-2-yl)propionate) is a new member of this ligand family and was synthesized according to the same synthetic strategy in four steps, starting from 1-ethyl-4-isopropylimidazole. The synthesis of **L3** is depicted in Scheme 1. **L3** is a sterically more demanding *N,N,O* ligand and the organic substituents on the imidazole-rings increase the solubility of its metal complexes in apolar and non-coordinating solvents.

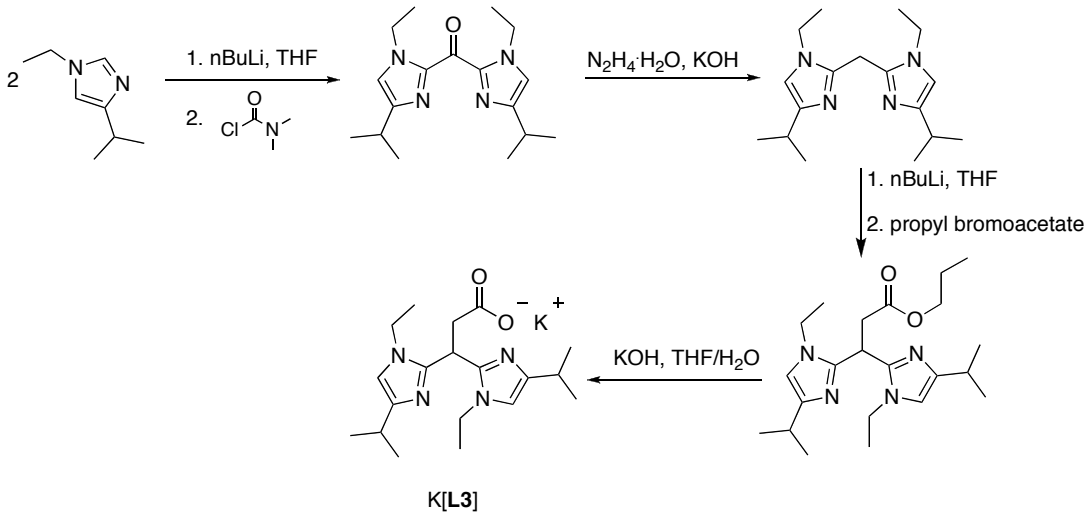

Scheme 1. Synthesis of ligand K[**L3**].

Synthesis and characterization of iron(II)-catecholato complexes. Fe(II)-catecholato complexes with three tridentate, monoanionic *N,N,O* ligands **L1**, **L2**, and **L3** and two differently substituted catechols (H_2tcc and H_2dtbc) were synthesized (Chart 1).

Chart 1. Iron(II)- and iron(III)-catecholato complexes (see Figure 1 for the structures of **L1**-**L3**).

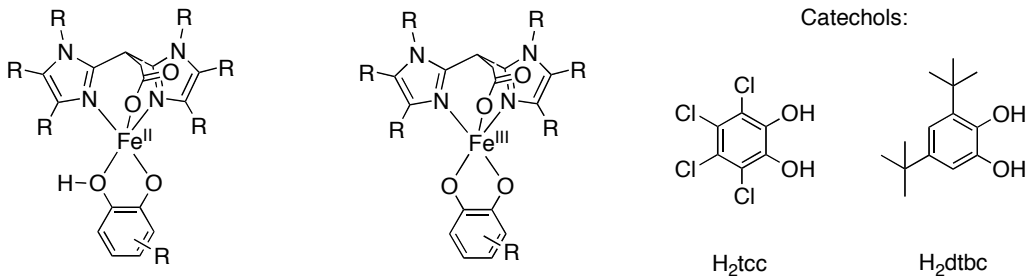

[Fe^{II}(**L1**)(Htcc)] (**1**) [Fe^{III}(**L1**)(tcc)] (**4**) [Fe^{III}(**L1**)(dtbc)] (**7**)
[Fe^{II}(**L2**)(Htcc)] (**2**) [Fe^{III}(**L2**)(tcc)] (**5**) [Fe^{III}(**L2**)(dtbc)] (**8**)
[Fe^{II}(**L3**)(Htcc)] (**3**) [Fe^{III}(**L3**)(tcc)] (**6**) [Fe^{III}(**L3**)(dtbc)] (**9**)

Complexes of the type [Fe^{II}(**L**)(Htcc)] (**1-3**) were synthesized by the addition of a methanolic solution of equimolar amounts of H_2tcc and Et_3N to a methanolic solution containing equimolar amounts of $Fe(OTf)_2 \cdot 2MeCN$ and K[**L**] under argon. Upon addition of the catechol/base solution an immediate and drastic color change from yellow to deep red-purple was observed. These products are sensitive towards air. The compounds could be isolated as purple (**L1**, **L2**) or burgundy-red powders (**L3**) in 40-72% yield.

The complexes are obtained as neutral species of the composition [Fe^{II}(**L**)(Htcc)], as both the tridentate ligand and a monoanionic catecholato ligand neutralize the +2 charge of the ferrous ion. The [Fe^{II}(**L**)(Htcc)] complexes **1-3** are paramagnetic and their solution magnetic moments were determined by Evans' NMR method.[45,46] The iron(II) complexes afforded magnetic moments in the range of 5.2-5.3 μ_B, consistent with a high spin configuration of the ferrous complexes. Elemental analyses confirm the composition of the five-coordinate iron(II) complexes. The ESI-MS spectra of the complexes show one predominant peak corresponding to the mononuclear, one-electron oxidized [Fe^{III}(**L**)(Htcc)]$^+$ ion with expected isotope pattern. Since initially the samples were shortly handled on air before the measurement, we also measured ESI-MS spectra of the complex under anaerobic conditions and similar spectra with the same [Fe^{III}(**L**)(Htcc)]$^+$ ion were observed. The oxidation of the complex seems a consequence of the conditions of the mass spectrometric measurement. The electronic spectra of these complexes are characterized by one single absorption band in the visible region at approximately 600 nm, accounting for their purplish color (Table 1). Whereas the [Fe^{II}(**L**)(Htcc)] complexes are fairly stable and can be isolated, the analogous [Fe^{II}(**L**)(Hdtbc)] complexes were found to be extremely O_2-sensitive. These complexes were synthesized *in situ* following the same procedure as described above, affording yellow-brown solutions. However, attempts to isolate these Fe(II)-complexes failed, because of their extremely fast oxidation with dioxygen yielding the corresponding [Fe^{III}(**L**)(dtbc)] complexes (*vide infra*).

Table 1. Absorption maxima of bands observed in the UV-Vis spectra of the iron-catecholato complexes [λ_{max}, (ε [M^{-1} cm^{-1}])]

	L1	**L2**	**L3**
	(**1**)	(**2**)	(**3**)
Fe^{II}-Htcc	597 (3300)	603 (2400)	606 (5000)
	(**4**)	(**5**)	(**6**)
Fe^{III}-tcc	490 (1600), 626 (2300)	480 (1400), 663 (2100)	492 (1600), 667 (2400)
	(**7**)	(**8**)	(**9**)
Fe^{III}-dtbc	490 (2000), 790 (3000)	504 (2900), 822 (4200)	521 (2400), 807 (3200)

Synthesis and characterization of iron(III)-catecholato complexes. [Fe^{III}(**L**)(tcc)] and [Fe^{III}(**L**)(dtbc)] complexes (**4-9**) were synthesized by the addition of a methanolic catechol solution with two equivalents of Et_3N to a methanolic solution containing equimolar amounts

of $Fe(NO_3)_3 \cdot 9H_2O$ and K[**L**] under argon. The red (**L1**, **L2**) or yellow (**L3**) solutions immediately turned dark blue in the case of the tcc complexes and dark purple-blue in the case of the dtbc complexes. The [Fe^{III}(**L**)(tcc)] complexes **4-6** were isolated as air-stable blue-black powders. Although the [Fe^{III}(**L**)(dtbc)] complexes **7-9** are still sensitive towards oxidation by air, they could nevertheless be isolated as purple-black powders. All complexes were obtained in good to excellent yields (72-95%). Again, like the Fe(II) complexes, the complexes **4-9** were obtained as neutral, five-coordinate complexes, in which the monoanionic tridentate ligand and a dianionic, chelated catecholato ligand carry the negative charges. The ESI-MS spectra of **4-9** show the $[M+H]^+$ ions as the major peaks, confirming their formulation as mononuclear species.

Complexes **4-9** exhibit EPR spectra that indicate that these are all high-spin ferric complexes (data given in Table 2). The EPR spectra of [Fe^{III}(**L3**)(tcc)] (**6**) and [Fe^{III}(**L3**)(dtbc)] (**9**) are shown in Figure 3. The spectrum of [Fe^{III}(**L3**)(tcc)] (**6**) is typical for an $S = 5/2$ system ($E/D = 0.117$) with peaks at $g = 8.3$, 5.4 and 3.3 resulting from the ground and middle Kramers doublets. The signal at 4.3 can be assigned to a small rhombic ferric impurity. A similar spectrum is obtained for [Fe^{III}(**L3**)(dtbc)] (**9**) with $g = 9.0$, 5.2, and 3.9 ($E/D = 0.190$). The EPR envelope of **9** shows an additional feature possibly of a low-spin Fe(III) species ($S = 1/2$, $g = 2.00$, 2.00 and 1.97). This feature arises from a minority species, accounting for less than 10% of the total spin concentration according to spectral simulations.

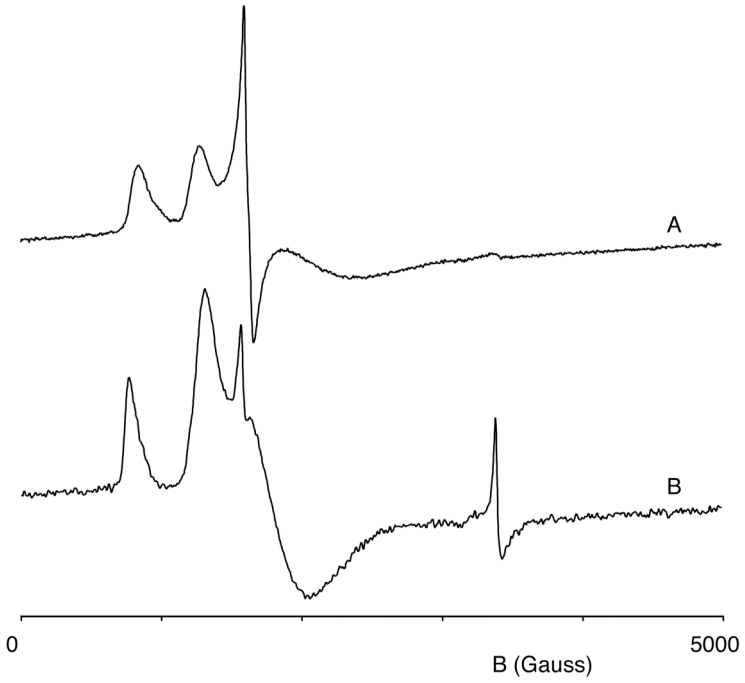

Figure 3. X-band EPR spectra of 2mM [Fe^{III}(**L3**)(tcc)] (**6**) (A) and [Fe^{III}(**L3**)(dtbc)] (**9**) (B) recorded in frozen methanol solution at 22.5 and 15 K, respectively. Typical EPR conditions: microwave frequency 9.63 GHz, microwave power 0.5 mW, modulation amplitude 12.5 G, modulation frequency 100 kHz, sweep width 5000 G.

Table 2. EPR data for complexes **4-9**[a]

Complex	*g* values[b]	*E*/*D*
[Fe^{III}(**L1**)(tcc)] (**4**)	4.5, 4.2, 4.0	0.290
[Fe^{III}(**L2**)(tcc)] (**5**)	8.0, 5.7, 3.7	0.097
[Fe^{III}(**L3**)(tcc)] (**6**)	8.3, 5.6, 3.4	0.117
[Fe^{III}(**L1**)(dtbc)] (**7**)[c]	8.3, 5.6, 3.4	0.117
[Fe^{III}(**L2**)(dtbc)] (**8**)[c]	8.1, 5.7, 3.6	0.104
[Fe^{III}(**L3**)(dtbc)] (**9**)[c]	9.0, 5.1, 3.6	0.190

[a] EPR spectra were recorded on 2 mM complex solution in frozen methanol at 15 (**4**, **5**, **7**-**9**) and 22.5 K (**6**). [b] effective *g* values and rhombicities were determined with the program RHOMBO.[47] [c] *g* values of the major species, a minor low spin Fe(III) species is also observed (g ≈ 2.00, 2.00, 1.97); the minor species accounts in each case for < 10% of the total spin.

The electronic spectra of the [Fe^{III}(**L**)(dtbc)] complexes (**7**-**9**) in methanol are dominated by two moderately intense absorption bands in the 400-1100 nm region (Table 1, Figure 4). Que et al. showed that these bands are highly characteristic of catecholato-to-iron(III) charge transfer bands and that the lower energy absorption can be correlated to the Lewis acidity of the Fe(III) metal center.[48] In our case, the lower energy absorptions are quite blue-shifted compared to iron(III)-catecholato complexes with *N*-polydentate ligands. They are found between 790 and 822 nm and reflect the reduced Lewis acidity arising from the coordination of a *N,N,O* donor set involving the hard carboxylato-oxygen anion. Similar values (λ_{max} = 520, 788 nm) were reported for [Fe^{III}(bpg)(dtbc)] in which the tetradentate bpg ligand also contains one carboxylate group.[48]

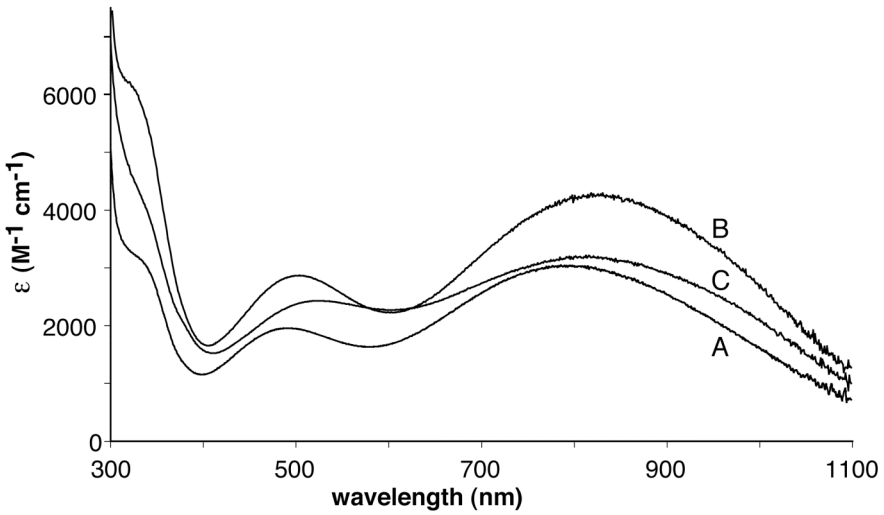

Figure 4. UV-Vis absorption spectra of [Fe^{III}(**L1**)(dtbc)] (**7**) (A), [Fe^{III}(**L2**)(dtbc)] (**8**) (B), and [Fe^{III}(**L3**)(dtbc)] (**9**) (C). All spectra were recorded in methanol solution.

The [Fe^{III}(**L**)(tcc)] complexes (**4-6**) display similar absorption spectra, but exhibit a further blue-shift of the lower energy LMCT band to 626-667 nm. The lower energy absorption band is reported to shift to higher energy as the substituents on the catecholate change from electron donating to electron withdrawing, as is the case here.[48,49] Interestingly, in non-coordinating solvents such as dichloromethane, a broader, less resolved feature is observed for each of the [Fe^{III}(**L**)(dtbc)] complexes, *i.e.* the two LMCT-bands have broadened and are shifted towards each other. Upon titration of dichloromethane solutions of these complexes with pyridine, the two distinct LMCT bands are restored at 535 and 800 nm and after the addition of 500 eq of pyridine a spectrum very similar to the spectrum recorded in pure methanol is observed (Figure 5). This spectral change is in each case accompanied by a distinct color change from blue to purple. The same titration experiments with pyridine of a methanolic solution of the [Fe^{III}(**L**)(dtbc)] complexes did not result in a significant change. This data suggests that the Fe(III) complexes are five-coordinate, unsaturated complexes in non-coordinating media with a vacant coordination site accessible for binding to Lewis bases such as pyridine. In (weakly) coordinating solvents this vacant site is occupied by a solvent molecule. These findings correspond well with the observations made by Moro-oka et al., who reported that upon dissolution of the purple species [Fe^{III}(Tp^{iPr2})(dtbc)(MeCN)] in toluene, a blue solution with coordinatively unsaturated [Fe^{III}(Tp^{iPr2})(dtbc)] is obtained.[27]

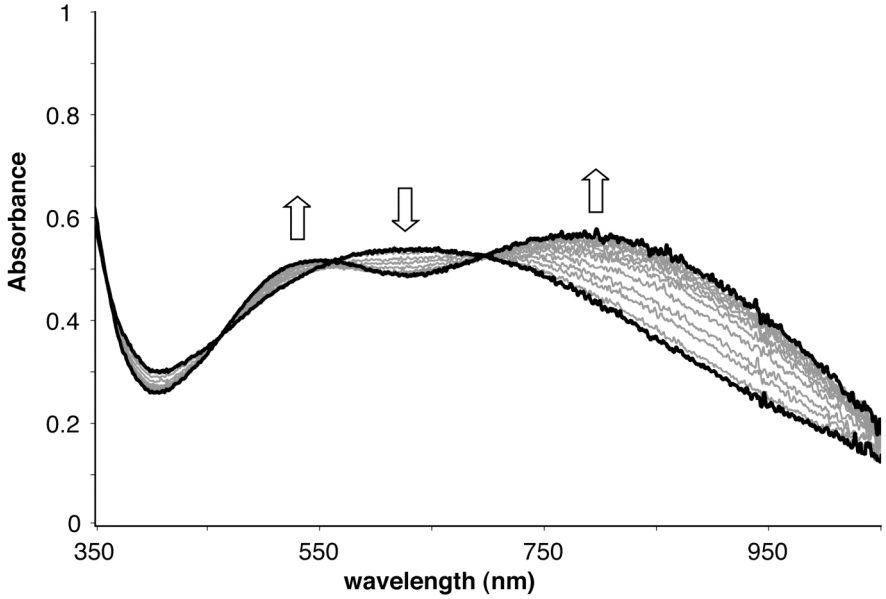

Figure 5. Titration of a solution of [Fe^{III}(**L3**)(dtbc)] in dichloromethane with pyridine. The features at 535 and 800 nm increase upon addition of pyridine (0-500 eq).

Crystal structure of [Fe(L3)(tcc)(H_2O)]. Blue-purple crystals of **6** suitable for X-ray diffraction were obtained by slow evaporation of a dichloromethane/hexanes solution under ambient conditions. Upon crystallization, the complex picked up a water molecule and a six-coordinate iron complex is obtained.[50] The molecular structure of **6** is depicted in Figure 6, with selected bond lengths and angles presented in Table 3.

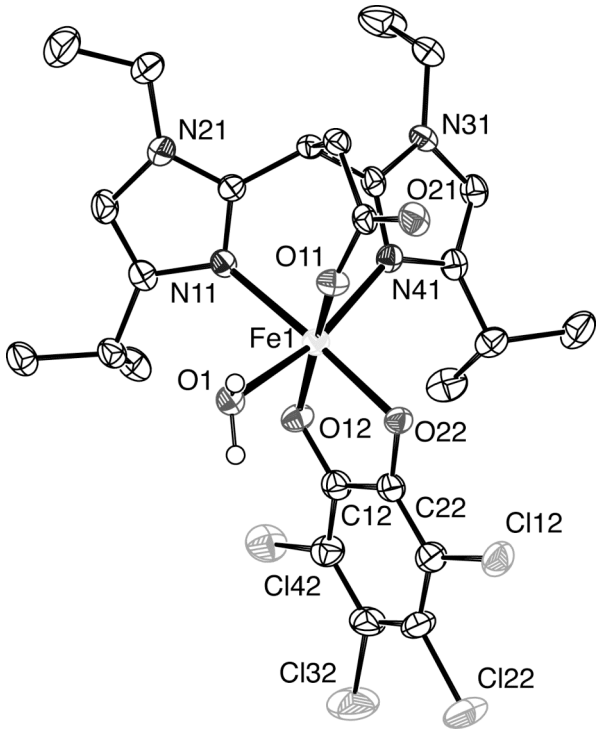

Figure 6. Molecular structure of [Fe(**L3**)(tcc)(H_2O)] (**6**) in the crystal. All C–H hydrogen atoms have been omitted for clarity. Displacement ellipsoids are drawn at the 50% probability level.

Table 3. Selected bond lengths (Å) and angles (°) for **6**

	Bond length		Angle		Angle
Fe1–N11	2.130(2)	O22–Fe1–N11	177.02(7)	N41–Fe1–O11	88.03(8)
Fe1–N41	2.127(2)	O11–Fe1–O12	169.01(8)	N41–Fe1–N11	83.47(8)
Fe1–O11	1.9516(18)	O1–Fe1–N41	165.65(9)	N41–Fe1–O12	101.40(8)
Fe1–O12	1.9231(18)			N41–Fe1–O22	99.15(8)
Fe1–O22	2.0009(18)				
Fe1–O1	2.143(2)	O11–Fe1–O22	90.40(7)	O1–Fe1–O11	81.16(9)
C12–O12	1.325(3)	O11–Fe1–N11	91.10(8)	O1–Fe1–O12	90.39(9)
C22–O22	1.330(3)	O12–Fe1–O22	82.60(8)	O1–Fe1–O22	90.39(7)
		O12–Fe1–N11	95.53(8)	O1–Fe1–N11	87.30(8)

The iron(III) metal center in **6** is coordinated by the three donor atoms of the *N,N,O* ligand. A chelated tetrachlorocatecholato ligand and a water molecule complete the distorted octahedral coordination sphere. The ligand thus provides a facial array of two imidazole N_ε donors and one *O* donor of a monoanionic carboxylato ligand, identical to the facial motif encountered in the 2-His-1-carboxylate facial triad. The Fe–N11 and Fe–N41 bonds at 2.130(2) and 2.127(2) Å are identical within error, despite the different ligands positioned *trans* to the imidazole *N* ligands. The Fe-N_{im} bond lengths are longer than those reported for

the complexes [Fe(tcc)(bpia)](ClO_4) (2.081 Å) and [Fe(tcc)(bpba)](ClO_4) (2.083 Å), which contain a 1-methylimidazole or benzimidazole group *trans* to a tetrachlorocatecholato oxygen, respectively.[49]

The Fe1–O11 carboxylato bond length (1.9516(18) Å) is fairly short, indicating a strong interaction of the carboxylate oxygen with the metal center. This bond length can be compared to the one in [Fe^{III}(bpg)(dtbc)] (1.994 Å),[51] in which a carboxylato group is also located *trans* to a catecholato-oxygen, and the one in [Et_4N][Fe^{III}(bdmpza)Cl_3] (2.049 Å), which contains the tripodal bis(3,5-dimethylpyrazol-2-yl)acetate ligand.[29] The C12–O12 and C22–O22 bond lengths in the tcc moiety are essentially equal (1.325(3) and 1.330(3) Å, respectively) and are similar to those found in the other Fe(III)-tetrachlorocatecholato complexes.[49,52,53] Together with the regular C–C bond lengths of the aromatic ring, it is clear that the catecholato ligand is bound as a *O,O*-dianion. No evidence for the manifestation of partial semiquinone character of the catecholato ligand is found. However, there is an asymmetry in the binding of the catecholate to the iron center with Fe–O bond lengths of 1.9231(18) and 2.0009(18) Å (Δr_{Fe-O} = 0.078 Å). Rather surprising is the observation that the shorter Fe1–O12 bond length is the one *trans* to the carboxylato ligand, while the longer Fe1–O22 is *trans* to the weaker imidazole nitrogen donor atom. The asymmetric binding of dianionic catecholates to iron has been described before, but in all cases the strongest interaction was found *trans* to the weakest donor ligand and could therefore be at least partly attributed to a *trans* influence.[18,49,51,54] In the complex [Fe^{III}(bpg)(dtbc)] for instance, the asymmetrically chelated dtbc ligand shows a considerably shorter Fe–O_{cat} bond length (Fe–O_{cat} = 1.889 Å) *trans* to the weaker tertiary amine donor than the one positioned *trans* to the carboxylato functionality (Fe–O_{cat} = 1.989 Å).[51] In the case of complex **6**, the observed asymmetry in bond lengths seems counterintuitive, but can be partly attributed to the involvement of several of the donor atoms in hydrogen bonding interactions. This weakens the donor strength of these *trans* ligands to the effect that the Fe–O binding sequence becomes inverted. In fact, the water molecule is engaged in two hydrogen bonds, resulting in the formation of dimers of **6** in the solid state (Figure 7, Table 4); hydrogen atom H2O is inter-molecularly bonded to tetrachlorocatechol oxygen O22a, while hydrogen atom H1O is bonded inter-molecularly to the non-coordinated carboxylato oxygen O21a. The unusual Fe-catecholato bond lengths can thus be rationalized by the involvement of both the carbonyl oxygen of the carboxylato group and one of the tetrachlorocatecholate oxygens, O22, as hydrogen bond acceptors. Interestingly, this asymmetric binding of a catecholato dianion to an Fe-center is also found at the active site of the intradiol cleaving catechol dioxygenases, which require Fe(III) as a cofactor. Here, the asymmetry is rationalized by *trans* ligand influences and/or the effect of a highly conserved hydrogen bonded arginine residue.[55,56] The longer Fe–O bond, which is found *trans* to a tyrosine residue, is in this case weakened further by the involvement of the same catecholato oxygen in a hydrogen bond with an arginine. Our results show that it is indeed important to take both effects arising from the *trans* disposition of ligands and the hydrogen bonding interactions into account.

The geometry of **6** can best be described as a severely distorted octahedron with the catecholate oxygens (O12 and O22), imidazole N11 and carboxylato O11 occupying the equatorial plane. The Fe1 atom is essentially in the equatorial plane. The axial positions are occupied by imidazole N41 and the water molecule. The strongly deviating *transoid* O1–Fe1–N41 angle of 165.65(9)° is caused by inherent geometrical restrictions imposed by the tripodal ligand and the involvement of the water molecule in two moderately strong hydrogen bonds.

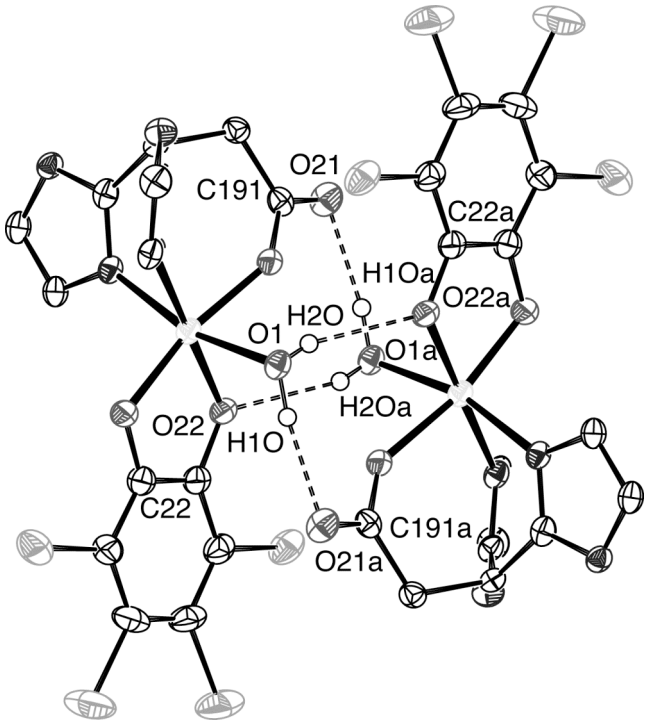

Figure 7. Hydrogen bonding pattern in [Fe(**L3**)(tcc)(H_2O)] (**6**); C–H hydrogen atoms, and the ethyl and isopropyl groups have been omitted for clarity. Symmetry operation a: 1 – x, – y, – z.

Table 4. Selected hydrogen bond lengths (Å) and angles (°) for [Fe(**L3**)(tcc)(H_2O)] (**6**). Symmetry operation a: 1 – x, – y, – z

Donor–H ··· Acceptor	D–H	H ··· A	D ··· A	D–H ··· A	C–O ··· H
O1–H1O ··· O21a	0.92(4)	1.99(4)	2.902(3)	172(3)	97.9(11)
O1–H2O ··· O22a	0.69(4)	2.19(4)	2.843(3)	161(4)	127.6(11)

Structural comparison with the extradiol cleaving enzymes. High-resolution X-ray crystal structures of several of the extradiol cleaving catechol dioxygenases with bound substrate are known.[37,57-61] Structural data for 2,3-dihydroxybiphenyl 1,2-dioxygenase (BphC) from the *Burkholderia cepacia* strain LB400[60,61] and the *Pseudomonas sp.* strain KKS102[57-59] with different catechols has for instance been reported. Recently, the structure of the iron-dependent homoprotocatechuate 2,3-dioxygenase (2,3-HPCD) also became available.[37] The geometry around the iron center of these enzyme-substrate complexes can best be described

as square pyramidal, leaving one coordination site open. The iron(II) metal center is coordinated by the three endogenous ligands and a bidentate, asymmetrically bound catecholato ligand. This asymmetry in Fe–O_{cat} distances (0.2 – 0.4 Å) is the result of the binding of the substrate as a monoanion.[15,60] In the structure of BphC (LB400),[60,61] an additional water molecule occupies the sixth coordination site and in this case the geometry can be best described as distorted octahedral with one of the histidine-N and the protonated catechol oxygen donor atoms as the axial ligands. It should be noted, however, that the position of the water molecule is only partly occupied at a relatively long bond length. In Figure 8 the active site structure of BphC (LB400) is compared the structure of complex **6**.

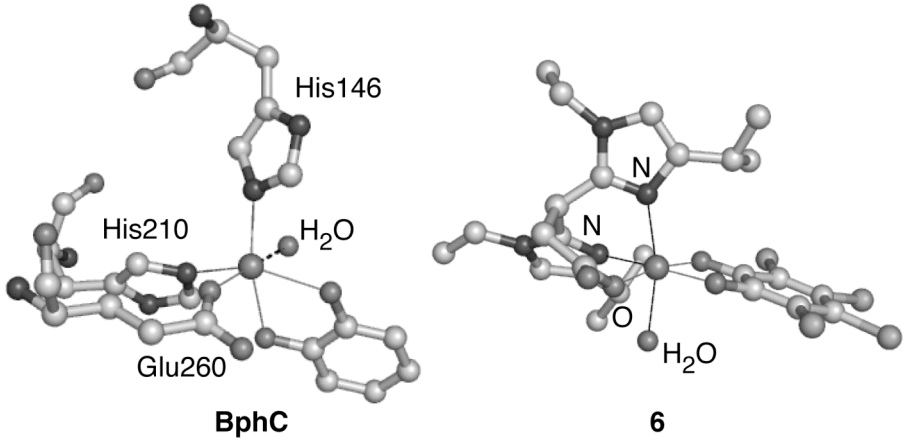

Figure 8. First coordination sphere of the iron(II) metal center of the 2,3-dihydroxybiphenyl 1,2 dioxygenase E–S complex[60,61] (1KND.pdb) (left) and that of complex [Fe(**L3**)(tcc)(H_2O)] (**6**) (right).

From this comparison, complex **6** can be regarded as a rather close structural mimic of the enzyme-substrate complex of the extradiol cleaving catechol dioxygenases. For the first time, a mononuclear iron-catecholato complex has been synthesized, which is facially capped by a ligand offering a tridentate N_{im},N_{im},O_{carb} donor set. Furthermore, the triangular face of the octahedron built by the facial triad is oriented in the same way as found in the enzyme, *i.e.* one of the imidazole groups occupies an axial position. The relative orientation of the catechol is, however different. In the enzyme, both catechol oxygens are positioned *trans* to a histidine-*N* donor atom and, as a result, the vacant site (or coordinated water molecule) in the octahedron is located in the equatorial plane, *trans* to the carboxylato *O* donor. In model complex **6**, the positions of the water and one of the catechol oxygens are interchanged, and now the sixth available coordination site is found at the axial position *trans* to one of the imidazole *N* donor atoms. Interestingly, the *trans*-disposition of the vacant site has been invoked as a possible decisive factor in the regioselectivity of the oxidative catechol cleavage.[37] In addition, the coordinated water molecule nicely illustrates the availability of the vacant coordination site in **6**. Although the complex is constructed with the sterically most demanding ligand **L3**, the metal center is still accessible and the vacant site can either be occupied by a solvent molecule, as in the enzyme resting state, or by dioxygen during catalytic turnover (*vide infra*). The model complex is imperfect in the sense that it contains an

Fe(III) metal center. The higher oxidation state of the metal is reflected in the overall shorter bond lengths when compared to the enzyme crystal structures. The enzyme furthermore provides the *N,N,O* donor set with more flexible X-Fe-Y angles because the donor groups are part of the larger enzyme backbone, whereas in **6** the angles are fixed by the ring strain of the three fused 6, 7, 7-membered chelate rings.

Dioxygen reactivity. In order to determine whether these new iron-catecholato complexes exhibit extradiol catechol cleaving activity, we studied the dtbc complexes for their dioxygen reactivity.[62] The same observations were made for the complexes from all three ligands. Yellow-brown solutions of the [Fe^{II}(**L**)(Hdtbc)] complexes all converted within seconds to intensely colored blue-purple solutions upon exposure to air at ambient temperature. This fast and drastic color change was monitored by UV-Vis absorption spectroscopy. New bands emerged at around 324, 490 and 800 nm (Figure 9), which are identical to those of the independently synthesized [Fe^{III}(**L**)(dtbc)] complexes. The latter two bands can be assigned as catecholato-to-iron(III) charge transfer transitions.[48] Of the few characterized mononuclear iron(II)-catecholato complexes, the systems of Que et al. and Moro-oka et al. showed the same rapid Fe^{II} to Fe^{III}-catecholato oxidation reaction with O_2.[15,18,27] In the $FeCl_2$/tacn/cat system reported by Bugg et al. only slow conversion to an iron(III) species has been observed. In their system the actual catechol cleavage step mediated by an Fe(II)-species is the faster reaction.[22,63]

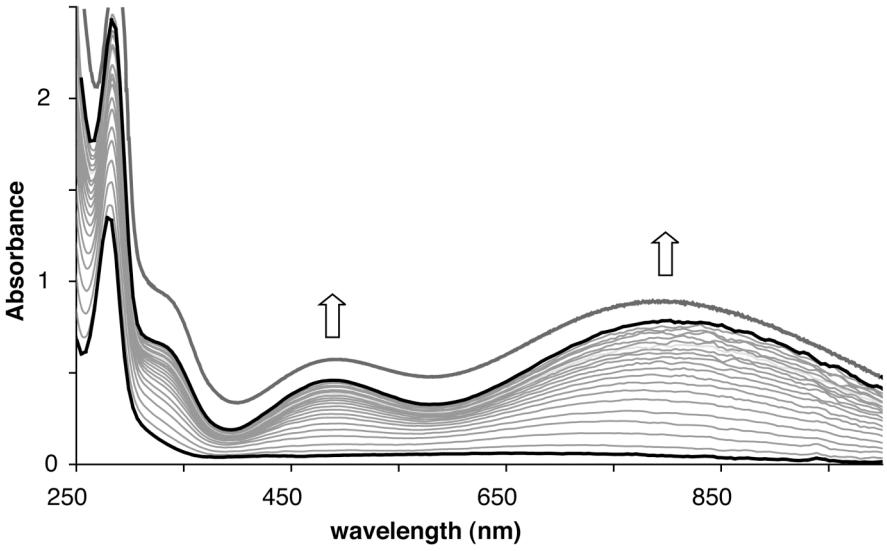

Figure 9. UV-Vis spectral changes upon exposure of [Fe^{II}(**L1**)(Hdtbc)] in methanol to air, showing the formation of [Fe^{III}(**L1**)(dtbc)]. A spectrum was recorded every 6 seconds. The UV-Vis spectrum of anaerobically synthesized [Fe^{III}(**L1**)(dtbc)] is included as the top line. Arrows indicate the increase in absorption over time.

The initial very fast formation of the blue-purple [Fe^{III}(**L**)(dtbc)] species is followed by a second, much slower color change, *i.e.* the intense blue-purple color fades and a green solution is obtained. The rate of disappearance of the characteristic catecholato-iron(III)

LMCT bands in the UV-Vis absorption spectra (Figure 10) depends strongly on the nature of the solvent and takes from a few hours in polar solvents (e.g. methanol) up to several days in more apolar solvents (e.g. dichloromethane).

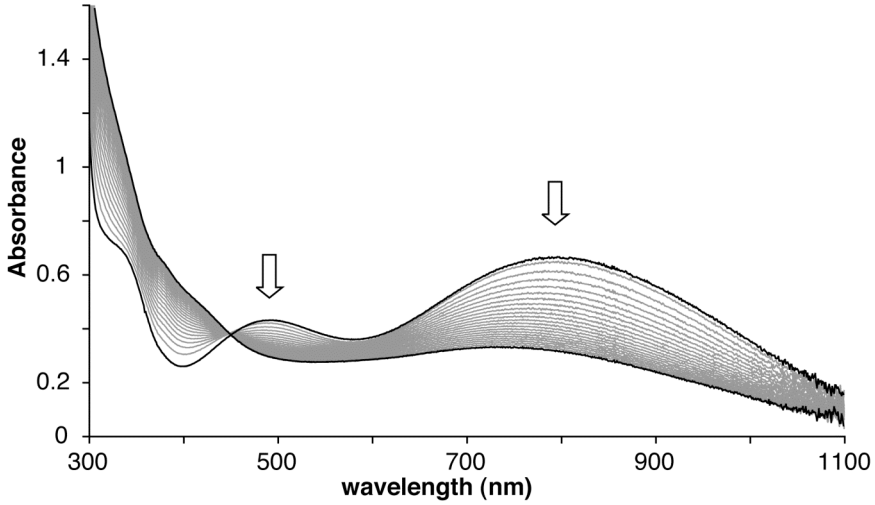

Figure 10. UV-Vis spectral changes upon exposure of anaerobically synthesized [Fe^{III}(**L1**)(dtbc)] in methanol at ambient conditions. A spectrum was recorded every 20 min. Arrows indicate the decrease in absorption over time.

The anaerobically synthesized and isolated [Fe^{III}(**L**)(dtbc)] complexes showed identical behavior upon exposure to air as the *in situ* formed [Fe^{III}(**L**)(dtbc)] complexes did. Therefore, further experiments were carried out with independently synthesized and isolated Fe^{III}-complexes. In order to establish the identity of the products as well as the regioselectivity of the reaction, the products were isolated from the reaction mixture, characterized by ^{1}H NMR spectroscopy and GC-MS and compared to authentic samples.[42,64]

The product distribution was found to be very solvent-dependent (Table 5). When the reactions were performed in a strongly coordinating solvent like acetonitrile, full conversion to the auto-oxidation product 3,5-di-*tert*-butylbenzoquinone was observed (Scheme 2). Changing the solvent to methanol resulted in the formation of some of the intradiol cleavage product 3,5-di-*tert*-butyl-5-carboxymethyl-2-furanone methyl ester (around 10%), in addition to the quinone, which was obtained in 90% yield. Since the availability of a vacant site has been argued to be an essential factor for the occurrence of extradiol type catechol cleavage,[3,42] we also studied the oxygenation in non-coordinating solvents. Indeed, when dichloromethane was employed as the solvent, the product distribution changed completely. Although still about 45% of the 3,5-di-*tert*-butylcatechol was converted into the quinone, a considerable amount of the extradiol type cleavage products 4,6-di-*tert*-butyl-2-pyrone and 3,5-di-*tert*-butyl-2-pyrone was now formed in about 30%. Interestingly, intradiol type products were again observed in the product mixture, accounting for the remaining 30% of organic products and providing a mass balance in product formation.

Table 5. Organic products obtained upon reaction of complexes [Fe(**L**)(dtbc)] with O_2. Selected dtbc cleavage data from related iron complexes with tridentate ligands have been included for comparison

Complex	Additive	Solvent	Conv. (%)	Extradiol (%)[a]	Intradiol (%)	Quinone (%)	Ref
[Fe(**L1**)(dtbc)]		CH_2Cl_2	92	30 (69/31)	27	43	
[Fe(**L2**)(dtbc)]		CH_2Cl_2	90	27 (64/36)	29	44	
[Fe(**L3**)(dtbc)]		CH_2Cl_2	93	18 (42/58)	22	60	
[Fe(**L2**)(dtbc)]	Pyridine (20 eq)	CH_2Cl_2	100	21 (69/31)	20	59	
[Fe(**L2**)(dtbc)]	$[Et_3NH]BF_4$ (1 eq)	CH_2Cl_2	83	38 (63/37)	21	41	
[Fe(**L2**)(dtbc)]		MeCN	100	--	--	100	
[Fe(**L2**)(dtbc)]		MeOH	100	--	11	89	
[FeCl(dtbc)(tacn)]		CH_2Cl_2		3	--	82	21
[FeCl(dtbc)(tacn)]		MeCN		35	--	65	40
[FeCl(dtbc)(Me_3-tacn)]	AgOTf (1eq)	CH_2Cl_2		98	--	--	42
[FeCl(dtbc)(terpy)]		CH_2Cl_2		--	20	78	42
[Fe(dtbc)(Tp^{iPr2})]		toluene		67	33	--	27

[a] Ratio in parentheses: (4,6-di-*tert*-butyl-2-pyrone/3,5-di-*tert*-butyl-2-pyrone)

Similar results were obtained for the reaction of all three [Fe(**L**)(dtbc)] complexes and in each case an extradiol/intradiol molar ratio close to 1 was observed. Reactions of complex [Fe(**L3**)(dtbc)] in dichloromethane showed a lower yield of ring cleavage products, which probably reflects the more limited accessibility of the vacant site due to the use of a more sterically demanding ligand. This is the first time that extradiol type cleavage has been observed with a mixed donor set (*N,N,O*) ligand.

Que et al. showed that for $[Fe(dtbc)(tacn)]^+$ the formation of the quinone auto-oxidation product, originally accounting for 82%, could be completely surprised by the addition of 20 eq of an additional Lewis base, such as pyridine.[21] For our system the addition of pyridine (20 eq) to the complex in dichloromethane, did markedly increase the reaction rate, but ultimately resulted in an increase in the amount of quinone product formed (59% vs. 44%). On the other hand, the addition of a proton donor, such as $[Et_3NH]BF_4$, resulted in a significant increase in

the selectivity towards extradiol cleavage. Almost twice as much of extradiol products than intradiol products are obtained now. The dioxygen reactivity of the iron-catecholato complexes is summarized in Scheme 2.

Scheme 2.

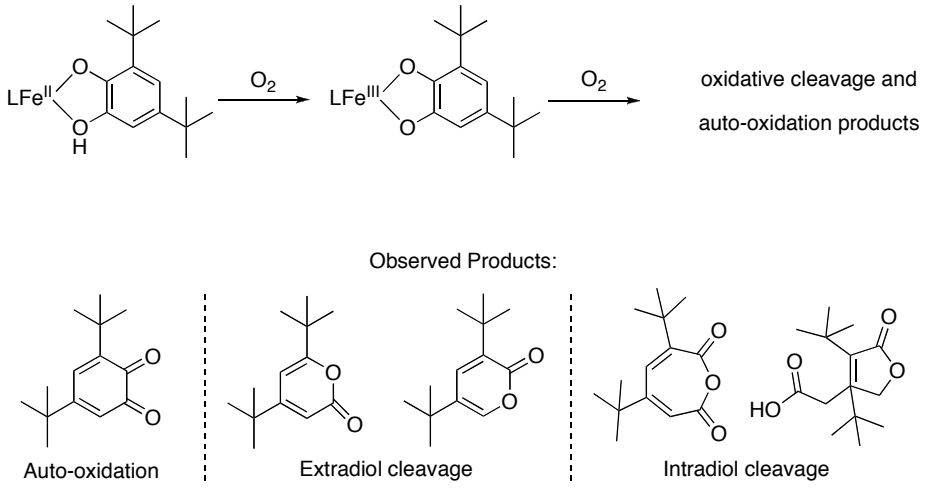

3.3 Discussion

Crystallographic data on a wide variety of enzymes has firmly established the 2-His-1-carboxylate facial triad as one of Nature's recurring structural motifs.[1,7] In this paper, we have presented accurate structural models of this facial triad. The ligand family of substituted bis(1-alkylimidazol-2-yl)propionates provides the metal center with a tripodal, tridentate monoanionic framework and incorporates the biologically relevant imidazole *N* and carboxylate *O* donor atoms. The crystal structure of [Fe(**L3**)(tcc)(H_2O)] (**6**) nicely illustrates the facial capping of the ligand and shows their general potential as models for the 2-His-1-carboxylate facial triad enzyme superfamily. The iron-catecholato complexes containing these ligands are initially isolated as coordinatively unsaturated, five-coordinate iron complexes. The monoanionic nature of the *N,N,O* ligand, together with the binding of the substrate, excludes the need for further ligands to obtain charge neutrality. The complexes therefore have a specifically designed vacant site available for the coordination of a solvent molecule, additional donor groups (e.g. pyridine) or dioxygen. The necessity of this vacant site for the desired reactivity is illustrated clearly by the observed solvent dependency of the oxidative chemistry of the [Fe(**L**)(dtbc)] complexes.

Regarding the displayed reactivity, several points should be considered. First of all, the initial rapid oxidation of the ferrous complex to the ferric complex seems to be an inherent property of the few ferrous active site analogues reported so far and can probably be attributed to insufficient site isolation provided by the model ligand set. The resulting iron(III)-catecholato complexes are, however, still reactive towards dioxygen and oxidative

catechol cleavage products are obtained when the reactions are performed in non-coordinating solvents. The formation of extradiol cleavage products upon oxygenation of the dtbc complexes shows their combined structural and functional modeling potential. Actually, these complexes are the first *N,N,O* mixed-donor complexes that display extradiol type catechol cleavage. Interestingly, we observe both extradiol and intradiol type catechol cleavage in comparable amounts. The few complexes reported thus far that are able to elicit extradiol cleavage also mediate concomitant intradiol cleavage, at least to some extent. The only synthetic complex that exclusively affords extradiol products is [Fe(Cl)(dtbc)(Me_3-tacn)], which required one equivalent of $AgBF_4$ to generate an empty coordination site.[42] This system seems to be quite exceptional, as in most cases both products types are found. This suggests quite similar mechanisms for the two reactions and points at subtle influences on the ultimate product selectivity.

Several mechanisms have been proposed to account for the observed selectivity of the different catechol cleaving enzymes. In all cases, the mechanisms converge on a similar proximal alkylperoxo species, which is implicated as the productive intermediate (Figure 11).

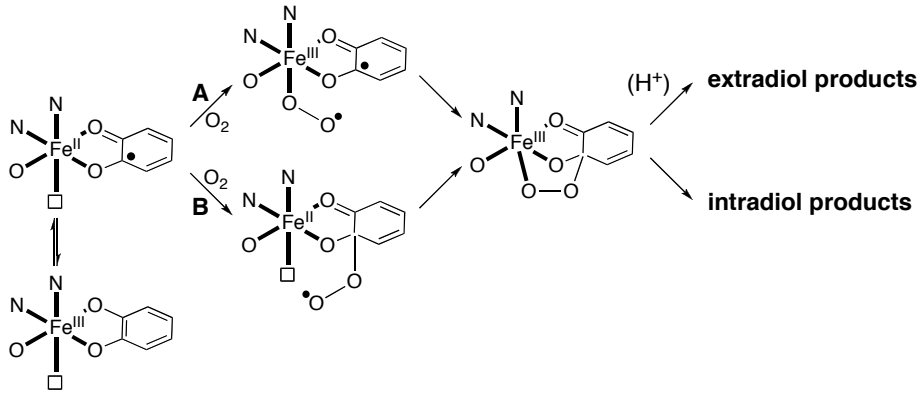

Figure 11. Proposed oxidative cleavage mechanism.

Starting from this common intermediate different explanations have been offered to explain how the enzymes catalyze the regiospecific ring cleavage. Bugg et al. argued that stereoelectronic factors determine the fate of the alkylperoxo species.[2,3] (Pseudo)-axial orientation of the peroxide with respect to the cyclohexadiene ring would lead to alkenyl migration and extradiol type cleavage, whereas a (pseudo)-equatorial orientation would lead to an acyl migration resulting in intradiol type cleavage. These different orientations could be the consequence of the different ligation number of the metals in the intra- and extradiol dioxygenases. The fourfold coordination (His_2Tyr_2) in the intradiol dioxygenases could, in this view, only lead to a (pseudo)-equatorial orientation, whereas the threefold coordination (His_2Glu) in the extradiol dioxygenases results in an axial vacant site and subsequent (pseudo)-axial orientation. However, crystal structural data on protocatechuate 3,4-dioxygenase, an intradiol cleaving enzyme, shows that upon catechol binding the axial tyrosine residue dissociates from the metal center.[56] Therefore, in both enzymes an *N,N,O* coordinated metal center with an axially oriented alkylperoxo intermediate can be implicated. This geometrical situation is very similar to the model complexes presented in this study. The

facial capping of the *N,N,O* ligand ensures that the vacant site is always oriented axially relative to the catechol plane and the overall geometry is therefore most suited for the formation of a pseudo-axial peroxo intermediate. There are two possible routes to this intermediate. As indicated by the spectroscopic data, the catecholato-to-Fe(III) charge transfer transitions confer some iron(II)-semiquinonato character on the complexes.[42] The available vacant site now allows direct attack of the metal center by dioxygen and subsequent attack of the semiquinone by a superoxide species (Figure 11, A) or the direct attack of the substrate by dioxygen and recombination with the metal center (Figure 11, B). Both pathways would lead to the same intermediate.

It has been argued that second-sphere active-site residues may participate in catalysis and that they are one of the decisive factors for regiospecific cleavage.[36,37,65-67] A recent DFT study proposed that the actual selectivity is determined by the character of the products of the O–O cleavage of the alkylperoxo intermediate.[36] These calculations showed that two transitions states could be found upon cleavage of the alkylperoxide intermediate, the one leading to extradiol type cleavage being the one with the lowest barrier. A critical parameter in the calculation was the inclusion of a (fully conserved) second sphere protonated histidine residue. Without this proton donor, the intradiol cleavage pathway became the one with the lowest energy barrier. Recent experiments by Groce and Lipscomb support the suggested critical role of the conserved histidine, since a mutation of this residue to a phenylalanine in homoprotocatechuate 2,3-dioxygenase changed its product selectivity from extradiol to intradiol cleavage.[65] An increase in extradiol type cleavage by the addition of a proton donor was also found in one biomimetic study.[22] The similar yields for the extra- and intradiol type products suggests that our complexes are not selective for one of the two competing pathways, resulting in a nonselective cleavage of the O–O bond. The addition of a proton donor to the reaction mixture did result in an increase of extradiol type cleavage, supporting the hypothesis that the presence of a proton donor enhances extradiol type cleavage.

We have shown that the bis(1-alkylimidazol-2-yl)propionates accurately model the first coordination sphere of the 2-His-1-carboxylate facial triad and that a ferric ion coordinated by this triad is capable of both intra- and extradiol type cleavage of 3,5-di-*tert*-butylcatechol. Previous studies showed that intradiol cleaving enzymes can be turned into extradiol ones while retaining the ferric oxidation state by site-directed mutagenesis,[68] and that extradiol cleaving enzymes can display intradiol type cleavage by site-directed modification, which illustrates the ability of a ferrous ion coordinated by the 2-His-1-carboxylate facial triad to mediate both reactivities.[65] All together this demonstrates that neither the metal valency nor the exact ligand donor set are the decisive factors for regioselectivity. The selectivity of ring cleavage seems to be determined by the acid-base chemistry of conserved second sphere residues that interact with an isostructural Fe-peroxo catecholato complex.

3.4 Summary and Perspective

As part of our efforts to model the 2-His-1-carboxylate facial triad, we have studied the iron coordination chemistry of the new family of the substituted 3,3-bis(1-alkylimidazol-2-yl)propionate ligands. The synthesized iron-catecholato complexes demonstrate the general potential of these ligands to mimic this facial triad. Mononuclear iron complexes were obtained that are facially capped by an *N,N,O* ligand including the biologically relevant imidazole and carboxylate donor groups. The complexes provide good models for the enzyme-substrate complex of the extradiol cleaving catechol dioxygenases and give more insight into the factors governing the reactivity of these enzymes. Similar five-coordinate metal-cofactor/substrate complexes are also found in the biggest subgroup of the enzyme superfamily, the α-ketoglutarate dependent enzymes and are, therefore, quite characteristic for the activated enzyme structures. Further efforts can now be extended to the modeling of other members of the 2-His-1-carboxylate enzyme superfamily and the applicability of iron complexes of these ligands as catalysts for oxidative transformations in organic synthesis.

3.5 Experimental Section

Air-sensitive organic reactions were carried out under an atmosphere of dry, oxygen-free N_2 using standard Schlenk techniques. THF was dried over sodium benzophenone ketyl and distilled under N_2 prior to use. Methanol was dried over magnesium methoxide and distilled under N_2 prior to use. All iron complexes were synthesized and handled under an argon atmosphere using standard Schlenk techniques. Solvents were thoroughly deoxygenated with argon before use. ^{1}H and ^{13}C{^{1}H} NMR spectra were recorded on Varian AS400 or Varian Inova 300 spectrometers, operating at 25 °C. Elemental microanalyses were carried out by the Microanalytisches Laboratorium Dornis & Kolbe, Mulheim a.d. Ruhr, Germany. ESI-MS spectra were recorded on a Micromass LC-TOF mass spectrometer at the Biomolecular Mass Spectrometry group, Utrecht University. Electrospray mass spectra under anaerobic conditions were recorded at the University of Groningen on an API 3+ triple quadrupole mass spectrometer (Sciex, Concord, Ont.,Canada) equipped with a modified pneumatically assisted electrospray (IonSpray) interface.[69] The homemade frontcover and IonSpray interface ensure a gas-tight ion source. The atmospheric pressure ion source was first evacuated and then filled with dry nitrogen. Nitrogen was used as nebulizing gas and curtain gas. Sample preparation took place in a nitrogen-filled glove box. The syringe pump used for sample introduction was also placed inside the glove box, and a 1.6 mm o.d. 0.3 mm i.d. teflon tube was connected between the syringe pump and the IonSpray interface. Mass spectra were recorded as Q1 scans with step size 0.1 and a dwell time of 1 ms. EPR spectra were recorded on a Bruker ER 200 D spectrometer with an ER 4116 DM resonator and a home built helium flow cooling system. UV-Vis spectra were recorded on a Cary 50 Varian spectrometer equipped with a Helma emersion probe for air sensitive experiments. Solution magnetic moments were determined by Evans' NMR method in acetone-d_6/cyclohexane (95/5 *v*/*v*) at 25 °C.[45,46] The ligands K[**L1**] (**14**) and K[**L2**] (**15**),[32] $Fe(OTf)_2 \cdot 2MeCN$[70], and 1-ethyl-4-isopropylimidazole[71] were prepared according to previously published procedures. Tetrachlorocatechol was recrystallized from anhydrous toluene before use. All other chemicals were commercially obtained and used as received.

[Fe^{II}(L1)(Htcc)] (1): To a solution of K[**L1**] (**14**) (175 mg, 0.64 mmol) in hot methanol (10 mL) was added a colorless solution of $Fe(OTf)_2 \cdot 2MeCN$ (279 mg, 0.64 mmol) in methanol (10 mL) upon which the solution turned slightly yellow. The solution was then stirred for 30 min at 50 °C. A solution of H_2tcc (159 mg, 0.79 mmol) and 1.1 eq of Et_3N (100 μL) in methanol (8 mL) was added to the hot reaction mixture and immediately a color change to very deep purple was observed. The reaction mixture was then stirred for 10 min at elevated temperature and gradually a purple precipitate formed. The solution was concentrated *in vacuo* and the solid purple residue was washed with demineralized water (2 × 20 mL) and dried *in vacuo* to yield a purple powder (206 mg, 60%). Anal. for $C_{17}H_{14}Cl_4FeN_4O_4$ (535.97): calc. C 38.10, H 2.63, N 10.45; found C 37.87, H 2.60, N 10.29. UV-Vis (methanol, ε [M^{-1} cm^{-1}]): λ_{max} = 597 (3300) nm. ESI-MS: *m/z* = 535.96 {$[M]^+$, calc. 535.91}. Solution magnetic moment (Evans' method): μ_{eff} = 5.2 μ_B.

[Fe^{II}(L2)(Htcc)] (2): To a solution of K[**L2**] (**15**) (138 mg, 0.37 mmol) in hot methanol (10 mL) was added a colorless solution of $Fe(OTf)_2 \cdot 2MeCN$ (161 mg, 0.37 mmol) in methanol (10 mL) upon which the solution turned yellow. The solution was then stirred for 30 min at 50 °C. A solution of H_2tcc (92 mg, 0.37 mmol) and 1.1 eq of Et_3N (57 μL) in methanol (8 mL) was added to the hot reaction mixture and immediately a color change to very deep purple was observed. The reaction mixture was then stirred for 10 min at elevated temperature and gradually a purple precipitate formed. The solution was concentrated *in vacuo* and the solid purple residue was washed with demineralized water (3 × 20 mL) and dried *in vacuo* to yield a purple powder (101 mg, 39%). Anal. for $C_{25}H_{18}Cl_4FeN_4O_4$ (636.09): calc. C 47.21, H 2.85, N 8.81; found C 47.02, H 2.74, N 8.64. UV-Vis (methanol, ε [M^{-1} cm^{-1}]): λ_{max} = 603 (2400) nm. ESI-MS: *m/z* = 636.13 {$[M]^+$, calc. 635.94}, 658.14 {$[M-H+Na]^+$, calc. 657.92}, 674.07 {$[M-H+K]^+$, calc. 673.90}. Solution magnetic moment (Evans' method): μ_{eff} = 5.3 μ_B.

[Fe^{II}(L3)(Htcc)] (3): To a colorless solution of K[**L3**] (**13**) (88 mg, 0.23 mmol) in hot methanol (10 mL) was added a colorless solution of $Fe(OTf)_2 \cdot 2MeCN$ (100 mg, 0.23 mmol) in methanol (10 mL) upon which the solution turned yellow. The solution was then stirred for 30 min at 50 °C. A solution of H_2tcc (56 mg, 0.23 mmol) and 1.1 eq of Et_3N (35 μL) in methanol (8 mL) was added to the hot reaction mixture and immediately a color change to very deep burgundy red was observed. The clear reaction mixture was then stirred for 10 min at elevated temperature, cooled to room temperature and concentrated *in vacuo*. The solid purple-red residue was washed with demineralized water (2 × 20 mL) and dried under reduced pressure to yield a purple-red powder (107 mg, 72%). Anal. for $C_{25}H_{30}Cl_4FeN_4O_4$ (648.19): calc. C 46.32, H 4.67, N 8.64; found C 46.18, H 4.57, N 8.48. UV-Vis (methanol, ε [M^{-1} cm^{-1}]): λ_{max} = 606 (5000) nm. ESI-MS: *m/z* = 347.34 {$[L+2H]^+$, calc. 347.17} 648.24 {$[M]^+$, calc. 648.03}, 670.25 {$[M-H+Na]^+$, calc. 670.02}. Solution magnetic moment (Evans' method): μ_{eff} = 5.2 μ_B.

[Fe^{III}(L1)(tcc)] (4): To a solution of K[**L1**] (**14**) (128 mg, 0.47 mmol) in hot methanol (10 mL) was added an orange solution of $Fe(NO_3)_3 \cdot 9H_2O$ (190 mg, 0.47 mmol) in methanol (10 mL) and immediately a color change to red-brown was observed. This solution was stirred for 10 min at 50 °C. A solution of H_2tcc (117 mg, 0.47 mmol) and 2.5 eq of Et_3N (170 μL) in methanol (8 mL) was added to the hot reaction mixture and immediately the color of the solution turned intensely deep dark blue. The clear reaction mixture was then stirred for 10 min at elevated temperature, cooled to room temperature and concentrated *in vacuo*. The solid black residue was washed with demineralized water (3 × 20 mL) and dried under reduced pressure to yield a blue-black powder

(240 mg, 95%). Anal. for $C_{17}H_{13}Cl_4FeN_4O_4$ (534.97): calc. C 38.17, H 2.45, N 10.47; found C 38.08, H 2.41, N 10.41. UV-Vis (methanol, ε [M^{-1} cm^{-1}]): λ_{max} = 490 (1600), 626 (2300) nm. ESI-MS: *m/z* = 536.00 {$[M+H]^+$, calc. 535.91}.

[Fe^{III}(L2)(tcc)] (5): To a solution of K[**L2**] (**15**) (163 mg, 0.44 mmol) in hot methanol (10 mL) was added an orange solution of $Fe(NO_3)_3 \cdot 9H_2O$ (177 mg, 0.44 mmol) in methanol (10 mL) and immediately a color change to dark red was observed. This solution was stirred for 10 min at 50 °C. A solution of H_2tcc (109 mg, 0.44 mmol) and 2.5 eq of Et_3N (154 μL) in methanol (8 mL) was added to the hot reaction mixture and immediately the color of the solution turned intensely deep blue. The reaction mixture was then stirred for 10 min at elevated temperature and cooled to room temperature upon which a blue precipitate formed. The solution was concentrated *in vacuo*. The solid blue-black residue was washed with demineralized water (3 × 20 mL) and dried under reduced pressure to yield a blue-black powder (200 mg, 72%). Anal. for $C_{25}H_{17}Cl_4FeN_4O_4$ (635.08): calc. C 47.28, H 2.70, N 8.82; found C 47.31, H 2.84, N 8.73. UV-Vis (methanol, ε [M^{-1} cm^{-1}]): λ_{max} = 480 (1400), 663 (2100) nm. ESI-MS: *m/z* = 636.04 {$[M+H]^+$, calc. 635.94}, 658.02 {$[M+Na]^+$, calc. 657.92}, 673.98 {$[M+K]^+$, calc. 674.19}.

[Fe^{III}(L3)(tcc)] (6): To a colorless solution of K[**L3**] (**13**) (124 mg, 0.32 mmol) in hot methanol (10 mL) was added an orange solution of $Fe(NO_3)_3 \cdot 9H_2O$ (131 mg, 0.32 mmol) in methanol (10 mL) and immediately a color change to yellow was observed. This solution was stirred for 10 min at 50 °C. A solution of H_2tcc (80 mg, 0.32 mmol) and 2.5 eq of Et_3N (113 μL) in methanol (8 mL) was added to the hot reaction mixture and immediately the color of the solution turned intensely deep dark blue. The clear reaction mixture was then stirred for 10 min at elevated temperature, cooled to room temperature and concentrated *in vacuo*. The solid blue-black residue was washed with demineralized water (3 × 20 mL) and dried under reduced pressure to yield a blue-black powder (145 mg, 70%). Crystals suitable for X-ray crystallography were grown by slow evaporation of a solution of **6** in CH_2Cl_2/hexanes. Anal. for $C_{25}H_{29}Cl_4FeN_4O_4$ (647.18): calc. C 46.40, H 4.52, N 8.66; found C 46.24, H 4.41, N 8.73. UV-Vis (methanol, ε [M^{-1} cm^{-1}]): λ_{max} = 492 (1600), 667 (2400) nm. ESI-MS: *m/z* = 648.15 {$[M+H]^+$, calc. 648.03}, 670.16 {$[M+Na]^+$, calc. 670.02}, 686.10 {$[M+K]^+$, calc. 685.99}.

[Fe^{III}(L1)(dtbc)] (7): To a solution of K[**L1**] (**14**) (147 mg, 0.54 mmol) in hot, methanol (10 mL) was added an orange solution of $Fe(NO_3)_3 \cdot 9H_2O$ (218 mg, 0.54 mmol) in methanol (10 mL) and immediately a color change to red-brown was observed. This solution was stirred for 10 min at 50 °C. A solution of H_2dtbc (120 mg, 0.54 mmol) and 2.5 eq of Et_3N (190 μL) in methanol (5 mL) was added to the hot reaction mixture and immediately the color of the solution turned intensely deep purplish-blue. The clear reaction mixture was then stirred for 10 min at elevated temperature and concentrated *in vacuo*. The solid residue was washed with demineralized water (3 × 20 mL) and dried under reduced pressure to yield a purplish-blue powder (195 mg, 71%). Anal. for $C_{25}H_{33}FeN_4O_4$ (509.40): calc. C 58.95, H 6.53, N 11.00; found C 58.72, H 6.64, N 10.87. UV-Vis (methanol, ε [M^{-1} cm^{-1}]): λ_{max} = 490 (2000), 790 (3000) nm. ESI-MS: *m/z* = 510.34 {$[M+H]^+$, calc. 510.19}, 532.36 {$[M+Na]^+$, calc. 532.17}, 548.34 {$[M+K]^+$, calc. 548.15}.

[Fe^{III}(L2)(dtbc)] (8): To a solution of K[**L2**] (**15**) (102 mg, 0.27 mmol) in hot methanol (15 mL) was added an orange solution of $Fe(NO_3)_3 \cdot 9H_2O$ (111 mg, 0.27 mmol) in methanol (5 mL) and immediately a color change to dark red was observed. This solution was stirred for 10 min at 50 °C. A solution of H_2dtbc (61 mg, 0.27 mmol)

and 2.5 eq of Et_3N (96 μL) in methanol (5 mL) was added to the hot reaction mixture and immediately the color of the solution turned intensely deep purplish-blue. The clear reaction mixture was then stirred for 10 min at elevated temperature and concentrated *in vacuo*. The solid residue was washed with demineralized water (3 × 20 mL) and dried under reduced pressure to yield a purplish-blue powder (160 mg, 96%). Anal. for $C_{33}H_{37}FeN_4O_4$ (609.52): calc. C 65.03, H 6.12, N 9.19; found C 64.87, H 6.21, N 9.04. UV-Vis (methanol, ε [M^{-1} cm^{-1}]): λ_{max} = 504 (2900), 822 (4200) nm. ESI-MS: *m/z* = 610.33 {$[M+H]^+$, calc. 610.22}.

[Fe^{III}(L3)(dtbc)] (9): To a colorless solution of K[**L3**] (**13**) (101 mg, 0.26 mmol) in hot methanol (10 mL) was added an orange solution of $Fe(NO_3)_3 \cdot 9H_2O$ (106 mg, 0.26 mmol) in methanol (10 mL) and immediately a color change to yellow was observed. This solution was stirred for 10 min at 50 °C. A solution of H_2dtbc (59 mg, 0.26 mmol) and 2.5 eq of Et_3N (92 μL) in methanol (8 mL) was added to the hot reaction mixture and immediately the color of the solution turned intensely deep dark purple-blue. The clear reaction mixture was then stirred for 10 min at elevated temperature, cooled to room temperature and concentrated *in vacuo*. The solid residue was washed with demineralized water (2 × 20 mL) and dried under reduced pressure to yield a dark purple-blue powder (102 mg, 63%). UV-Vis (methanol, ε [M^{-1} cm^{-1}]): λ_{max} = (521 (2400), 807 (3200) nm. ESI-MS: *m/z* = 622.49 {$[M+H]^+$, calc. 622.32}, 644.49 {$[M+Na]^+$, calc. 644.30}.

Bis(1-ethyl-4-isopropylimidazol-2-yl)ketone (10): A solution of *n*-butyl lithium (31 mL, 50 mmol, 1.6 M solution in hexanes) was added dropwise to a solution of 1-ethyl-4-isopropylimidazole (6.3 g, 46 mmol) and tmeda (6.9 mL, 46 mmol) in THF (60 mL) at 0 °C. The clear solution was stirred for 1.5 h at 0 °C and subsequently cooled to – 55 °C. Dimethylcarbamylchloride (2.0 mL, 22 mmol) was added dropwise to the stirred solution and the reaction mixture was allowed to warm to room temperature overnight. The clear dark solution was quenched by addition of 20 mL of a saturated aqueous NH_4Cl-solution. All volatiles were evaporated *in vacuo* and the aqueous layer was extracted with dichloromethane (4 × 50 mL). The combined organic extracts were dried over Na_2SO_4, filtered, and concentrated to dryness. The product was obtained as an off-white powder (6.5 g, 95%). This product can be further purified using column chromatography (silica, eluent ethyl acetate:hexanes = 1:1), although the crude product is pure enough for further use. ^{1}H NMR (300 MHz, $CDCl_3$, 25 °C): δ = 1.27 (d, 12H, *J* = 6.9 Hz, (C*H*$_3$)CH), 1.45 (t, 6H, *J* = 6.9 Hz, C*H*$_3$CH$_2$), 2.97 (hept., 2H, *J* = 6.9 Hz, (CH$_3$)$_2$C*H*), 4.30 (q, 4H, *J* = 6.9 Hz, C*H*$_2$CH$_3$), 6.86 (s, 2H, H_{im}) ppm. ^{13}C {^{1}H} NMR (75 MHz, $CDCl_3$, 25 °C): δ = 16.4, 22.3, 27.9, 43.0, 119.7, 141.8, 150.1, 174.4 ppm. Anal. for $C_{17}H_{26}N_4O$ (302.41): calc. C 67.52, H 8.67, N 18.53; found C 67.36, H 8.61, N 18.38.

Bis(1-ethyl-4-isopropylimidazol-2-yl)methane (11): Compound **10** (6.5 g, 22 mmol) and ground KOH (7.0 g, 125 mmol) were dissolved in 40 mL hydrazine mono-hydrate and this yellow-brown solution was heated under N_2 to 120 °C upon which the solution became almost colorless. The reaction mixture was kept at 120 °C for 2 h and then heated to 160 °C and stirred for an additional 3 h. Subsequently, the reaction mixture was allowed to cool to ambient temperature, during which an off-white waxy solid precipitated. At this point all following operations were carried out in air. CH_2Cl_2 (40 mL) was added and the solution was transferred into a separation funnel. The CH_2Cl_2 layer was separated and the remaining light brown liquid extracted with CH_2Cl_2 (3 × 40 mL). The combined CH_2Cl_2 extracts were washed with H_2O (2 × 15 mL) to remove excess hydrazine. The combined H_2O extracts were then extracted with CH_2Cl_2 (6 × 30 mL). The combined CH_2Cl_2 extracts were dried over Na_2SO_4, filtered, and evaporated to dryness. The crude product contained some 1-ethyl-4-

isopropylimidazole as impurity, which could be removed by Kugelrohr destillation (75 °C). The desired compound then was obtained as a yellow-brown oil that solidified upon standing (4.65 g, 75%). Due to the limited stability of **11**, it was used immediately in the subsequent reaction without further purification. ^{1}H NMR (300 MHz, $CDCl_3$, 25 °C): δ = 0.99 (t, 6H, *J* = 7.2 Hz, C*H*$_3$CH$_2$), 1.21 (d, 12H, *J* = 6.9 Hz, (C*H*$_3$)$_2$CH), 2.82 (hept, 2H, *J* = 6.9 Hz, (CH$_3$)$_2$C*H*), 3.94 (q, 4H, *J* = 7.2 Hz, CH$_3$C*H*$_2$), 4.25 (s, 2H, C*H*$_2$), 6.48 (s, 2H, H$_{im}$) ppm. ^{13}C {^{1}H} NMR (100 MHz, $CDCl_3$, 25 °C): 16.2, 22.7, 28.0, 28.1, 41.1, 113.5, 142.1, 148.0 ppm.

Propyl 3,3-bis(1-ethyl-4-isopropylimidazol-2-yl)propionate (12): A solution of *n*-butyl lithium (3.1 mL, 5.0 mmol, 1.6 M in hexanes) was added dropwise to a stirred solution of **11** (1.3 g, 4.5 mmol) in THF (40 mL) at – 78 °C. The resulting dark red solution was stirred for 1 h at – 78 °C, followed by the dropwise addition of propyl bromoacetate (0.6 mL, 4.7 mmol). The temperature was allowed to rise to room temperature overnight, the resulting clear red reaction mixture was quenched with H_2O (25 mL) and all volatiles were evaporated *in vacuo*. The water layer was extracted with diethyl ether (4 × 30 mL) and the combined organic layers were dried over $MgSO_4$, filtered, and evaporated to dryness. The crude product was purified by column chromatography (silica, eluent ethyl acetate:hexanes = 1:3, after collection of impurities changed to ethyl acetate) to yield the product as a yellow-brown oil (1.12 g, 64%). ^{1}H NMR (300 MHz, $CDCl_3$, 25 °C): δ = 0.79 (t, 3H, *J* = 7.2 Hz, C*H*$_3$CH$_2$CH$_2$O), 0.90 (t, 6H, *J* = 7.5 Hz, C*H*$_3$CH$_2$N), 1.15 (d, 12H, *J* = 6.6 Hz, (C*H*$_3$)$_2$CH), 1.51 (m, 2H, CH$_3$C*H*$_2$CH$_2$O), 2.78 (hept, 2H, *J* = 6.6 Hz, (CH$_3$)$_2$C*H*), 3.23 (d, 2H, *J* = 7.8 Hz, C*H*$_2$CH), 3.83 (ABX$_3$, 2H, *J* = 6.9 Hz, CH$_3$C(*H*)(H)N), 3.86 (ABX$_3$, 2H, *J* = 7.2 Hz, CH$_3$C(H)(*H*)N), 3.93 (t, 2H, *J* = 6.9 Hz, CH$_3$CH$_2$C*H*$_2$O), 4.97 (t, 1H, *J* = 7.8 Hz, CH$_2$C*H*), 6.44 (s, 2H, H$_{im}$) ppm. ^{13}C {^{1}H} NMR (75 MHz, $CDCl_3$, 25 °C): δ = 10.2, 16.1, 21.9, 22.5, 27.7, 35.2, 36.6, 40.5, 66.1, 113.5, 143.6, 147.7, 171.1 ppm. Anal. for $C_{22}H_{36}N_4O_2$ (388.55): calc. C 68.01, H 9.34, N 14.42; found C 67.88, H 9.26, N 14.42.

Potassium 3,3-bis(1-ethyl-4-isopropylimidazol-2-yl)propionate K[L3] (13): To a solution of ester **12** (1.73 g, 4.5 mmol) in THF (20 mL) was added a KOH solution (4.72 g, 0.989 M solution in H_2O, 4.5 mmol) and the reaction mixture was refluxed overnight. Evaporation of the solvents resulted in an oil and repeated azeotropic drying with toluene and diethyl ether, gave the desired product as an off-white powder in quantitative yield (1.71 g). ^{1}H NMR (300 MHz, CD_3OD, 25 °C): δ = 0.90 (t, 3H, *J* = 6.9 Hz, C*H*$_3$CH$_2$N), 1.19 (d, 12H, *J* = 6.9 Hz, (C*H*$_3$)$_2$CH), 2.80 (hept, 2H, *J* = 6.9 Hz, (CH$_3$)$_2$C*H*), 3.09 (d, 2H, *J* = 7.2 Hz, C*H*$_2$CH), 3.87 (ABX$_3$, 2H, *J* = 6.9 Hz, CH$_3$C(*H*)(H)N), 3.90 (ABX$_3$, 2H, *J* = 7.2 Hz, CH$_3$C(H)(*H*)N), 4.97 (t, 1H, *J* = 6.9 Hz, CH$_2$C*H*), 6.62 (s, 2H, H$_{im}$) ppm. ^{13}C {^{1}H} NMR (75 MHz, CD_3OD, 25 °C): δ = 15.3, 21.9, 22.0, 27.7, 39.3, 40.6, 114.0, 145.4, 147.4, 177.4 ppm. ESI-MS: *m/z* = 385.17 {[M+H]$^+$, calc. 385.20}, 347.17 {[M–K+2H]$^+$, calc. 347.17}. Anal. for $C_{19}H_{29}KN_4O_2$ (384.56): calc. C 59.34, H 7.60, N 14.57; found C 59.26, H 7.54, N 14.46.

Oxygenation Reactions and Characterization of Oxygenation Products. In a typical reaction 25 mg of the [Fe^{III}(**L**)(dtbc)] complexes was dissolved in 40 mL of solvent and the blue-purple solution was exposed to air and stirred until the blue-purple color had completely faded and the solution had turned green after which one equivalent of internal standard was added to the solution. The solvent was then removed *in vacuo* and the residue was redissolved in 20 mL of 1M HCl to decompose the metal complexes. The aqueous solution was extracted with diethyl ether (3 × 20 mL) and the combined organic layers were dried over $MgSO_4$, filtered, and evaporated *in vacuo*. The products were analyzed by GC-MS and ^{1}H NMR. The combined intradiol, extradiol and quinone products accounted for > 90% of the dtbc reactant. The products were quantified by ^{1}H NMR (1,3,5-

tribromobenzene as internal standard), since the quinone auto-oxidation product could not be accurately detected by GS-MS. Authentic samples of the intradiol products 3,5-di-*tert*-butyl-1-oxacyclohepta-3,5-diene-2,7-dione and 3,5-di-*tert*-butyl-5-carboxymethyl-2-furanone methyl ester were prepared according to a published procedure.[64] Authentic samples of the extradiol product isomers 3,5-di-*tert*-butyl-2-pyrone and 4,6-di-*tert*-butyl-2-pyrone were prepared by reacting [FeCl(dtbc)(Me_3-tacn)] with air as described by Que et al.[42] In the experiments with added proton donor one equivalent of $[Et_3NH]BF_4$ in dichloromethane (1 mL) was added to the [Fe(**L**)(dtbc)] solution. $[Et_3NH]BF_4$ was added both before and after exposing the solution to air and no difference in product distribution was observed.

X-ray crystal structure determination of 6. $C_{25}H_{31}Cl_4FeN_4O_5$, Fw = 665.19, black plate, 0.15 × 0.15 × 0.03 mm^3, monoclinic, $P2_1/c$ (no. 14), a = 13.5894(3), b = 12.7606(4), c = 18.8030(5) Å, β = 117.8399(17)°, V = 2883.21(13) $Å^3$, Z = 4, D_x = 1.532 g/cm^3, μ = 0.94 mm^{-1}. 28540 Reflections were measured on a Nonius Kappa CCD diffractometer with rotating anode (graphite monochromator, λ = 0.71073 Å) up to a resolution of $(\sin\theta/\lambda)_{max}$ = 0.60 $Å^{-1}$ at a temperature of 150 K. An absorption correction based on multiple measured reflections was applied (0.92-0.97 correction range). 5255 Reflections were unique (R_{int} = 0.0584). The structure was solved with Direct Methods[72] and refined with SHELXL-97[73] against F^2 of all reflections. Non hydrogen atoms were refined with anisotropic displacement parameters. All hydrogen atoms were located in the difference Fourier map. Water hydrogen atoms were refined freely with isotropic displacement parameters; all other hydrogen atoms were refined with a riding model. 366 parameters were refined with no restraints. R1/wR2 [I>2σ(I)]: 0.0375/0.0832. R1/wR2 [all refl.]: 0.0637/0.0947. S = 1.088. Residual electron density between – 0.32 and 0.32 e/$Å^3$. Geometry calculations and checking for higher symmetry was performed with the PLATON program.[74]

3.6 References & Notes

1. Costas, M.; Mehn, M. P.; Jensen, M. P.; Que, L., Jr. *Chem. Rev.* **2004**, *104*, 939-986.
2. Bugg, T. D. H. *Tetrahedron* **2003**, *59*, 7075-7101.
3. Bugg, T. D. H.; Lin, G. *Chem. Commun.* **2001**, 941-952.
4. Hegg, E. L.; Que, L., Jr. *Eur. J. Biochem.* **1997**, *250*, 625-629.
5. Que, L., Jr. *Nature Struct. Biol.* **2000**, *7*, 625-629.
6. Solomon, E. I.; Brunold, T. C.; Davis, M. I.; Kernsley, J. N.; Lee, S-K.; Lehnert, N.; Neese, F.; Skulan, A. J.; Yang, Y-S.; Zhou, J. *Chem. Rev.* **2000**, *100*, 235-349.
7. Koehntop, K. D.; Emerson, J. P.; Que, L., Jr. *J. Biol. Inorg. Chem.* **2005**, *10*, 87-93.
8. Higgins, L. J.; Yan, F.; Liu, P.; Liu, H-W.; Drennan, C. L. *Nature* **2005**, *437*, 838-844.
9. Burzlaff, N.; Rutledge, P. J.; Clifton, I. J.; Hensgens, C. M. H.; Pickford, M.; Adlington, R. M.; Roach, P. L.; Baldwin, J. E. *Nature* **1999**, *401*, 721-724.
10. Roach, P. L.; Clifton, I. J.; Hensgens, C. M. H.; Shibata, N.; Schofield, C. J.; Hajdu, J.; Baldwin, J. E. *Nature* **1997**, *387*, 827-830.
11. Carredona, E.; Karlsson, A.; Kauppi, B.; Choudhury, D.; Parales, R. E.; Parales, J. V.; Lee, K.; Gibson, D. T.; Eklund, H.; Ramaswamy, S. *J. Mol. Biol.* **2000**, *296*, 701-712.
12. Karlsson, A.; Parales, J. V.; Parales, R. E.; Gibson, D. T.; Eklund, H.; Ramaswamy, S. *Science* **2003**, *299*, 1039-1041.
13. Chen, K.; Costas, M.; Kim, J.; Tipton, A. K.; Que, L., Jr. *J. Am. Chem. Soc.* **2002**, *124*, 3026-3035.
14. Chen, K.; Costas, M.; Que, L., Jr. *J. Chem. Soc., Dalton Trans.* **2002**, 672-679.

15. Chiou, Y-M.; Que, L., Jr. *Inorg. Chem.* **1995**, *34*, 3577-3578.
16. Chiou, Y-M.; Que, L., Jr. *J. Am. Chem. Soc.* **1995**, *117*, 3999-4013.
17. Costas, M.; Que, L., Jr. *Angew. Chem. Int. Ed.* **2002**, *41*, 2179-2181.
18. Jo, D-H.; Chiou, Y-M.; Que, L., Jr. *Inorg. Chem.* **2001**, *40*, 3181-3190.
19. Oh, N. Y.; Suh, Y.; Park, M. J.; Seo, M. S.; Kim, J.; Nam, W. *Angew. Chem. Int. Ed.* **2005**, *44*, 4235-4239.
20. Park, M. J.; Lee, J; Suh, Y.; Kim, J.; Nam, W. *J. Am. Chem. Soc.* **2006**, *128*, 2630-2634.
21. Ito, M.; Que, L., Jr. *Angew. Chem. Int. Ed. Engl.* **1997**, *36*, 1342-1344.
22. Lin, G.; Reid, G; Bugg, T. D. H. *J. Am. Chem. Soc.* **2001**, *123*, 5030-5039.
23. Hegg, E. L.; Ho, R. Y. N.; Que, L., Jr. *J. Am. Chem. Soc.* **1999**, *121*, 1972-1973.
24. Kitajima, N.; Tamura, N.; Amagai, H.; Fukui, H.; Moro-oka, Y.; Mizutani, Y.; Kitagawa, T.; Mathur, R.; Heerwegh, K.; Reed, C. A.; Randall, C. R.; Que, L., Jr.; Tatsumi, K. *J. Am. Chem. Soc.* **1994**, *116*, 9071-9085.
25. Kitajima, N.; Tolman, W. B. *Prog. Inorg. Chem.* **1995**, *43*, 419-531.
26. Mehn, M. P.; Fujisawa, K.; Hegg, E. L.; Que, L., Jr. *J. Am. Chem. Soc.* **2003**, *125*, 7828-7842.
27. Ogihara, T.; Hikichi, S.; Akita, M.; Moro-oka, Y. *Inorg. Chem.* **1998**, *37*, 2614-2615.
28. Abbreviations used in this paper: tpa (tris(2-pyridylmethyl)amine), bpmcn (*N*,*N*-bis-(2-pyridylmethyl)-*N*',*N*'-dimethyl-1,2-cyclohexanediamine), $Tp^{R,R'}$ (hydrotris(3,5-R,R'-pyrazol)borato), tacn (1,4,7-triazacyclononane), Me_3-tacn (*N*,*N*',*N*''-trimethyl-1,4,7-triazacyclononane), bpg (bis(picolyl)glycine), bpia (((1-methylimidazol-2-yl)methyl)(bis-(2-pyridyl)methyl)amine), bpba ((benzimidazol-2-yl)methyl)(bis-(2-pyridyl)methyl)amine)
29. Beck, A.; Barth, A.; Hubner, E.; Burzlaff, N. *Inorg. Chem.* **2003**, *42*, 7182-7188.
30. Beck, A.; Weibert, B.; Burzlaff, N. *Eur. J. Inorg. Chem.* **2001**, 521-527.
31. Oldenburg, P. D.; Shteinman, A. A.; Que, L., Jr. *J. Am. Chem. Soc.* **2005**, *127*, 15673-15674.
32. Bruijnincx, P. C. A.; Lutz, M.; Spek, A. L.; van Faassen, E. L.; Weckhuysen, B. M.; van Koten, G.; Klein Gebbink, R. J. M. *Eur. J. Inorg. Chem.* **2005**, 779-787 (Chapter 2 of this thesis).
33. Kervinen, K.; Bruijnincx, P. C. A.; Beale, A. M.; Mesu, J. G.; van Koten, G.; Klein Gebbink, R. J. M.; Weckhuysen, B. M. *J. Am. Chem. Soc.* **2006**, *128*, 3208-3217.
34. The synthesis of **L1** was independently reported by Burzlaff et al.: Peters, L.; Hübner, E.; Burzlaff, N. *J. Organomet. Chem.* **2005**, *690*, 2009-2016.
35. Ohlendorf, D. H.; Lipscomb, J. D; Weber, P. C. *Nature* **1988**, *336*, 403-405.
36. Siegbahn, P. E. M.; Haeffner, F. *J. Am. Chem. Soc.* **2004**, *126*, 8919-8932.
37. Vetting, M. W.; Wackett, L. P.; Que, L., Jr.; Lipscomb, J. D.; Ohlendorf, D. H. *J. Bact.* **2004**, *186*, 1945-1958.
38. Lipscomb, J. D.; Orville, A., *Metal Ions in Biological Systems*. Marcel Dekker: New York, 1992; Vol. 28, p 243-298.
39. Yamahara, R.; Ogo, S.; Masuda, H.; Watanabe, Y. *J. Inorg. Biochem.* **2002**, *88*, 284-294.
40. Dei, A.; Gatteschi, D.; Pardi, L. *Inorg. Chem.* **1993**, *32*, 1389-1395.
41. Funabiki, T.; Mizoguchi, A.; Sugimoto, T.; Tada, S.; Tsugi, M.; Sakamoto, H.; Yoshida, S. *J. Am. Chem. Soc.* **1986**, *108*, 2921-2932.
42. Jo, D-H.; Que, L., Jr. *Angew. Chem. Int. Ed.* **2000**, *39*, 4284-4287.
43. Raffard, N.; Carina, R.; Simaan, A. J.; Sainton, J.; Rivière, E.; Tchertanov, L.; Bourcier, S.; Bouchoux, G.; Delroisse, M.; Banse, F.; Girerd, J-J. *Eur. J. Inorg. Chem.* **2001**, 2249-2254.
44. Funabiki, T.; Mizoguchi, A.; Sugimoto, T.; Tada, S.; Tsuji, M.; Sakamoto, H.; Yoshida, S. *J. Am. Chem. Soc.* **1986**, *108*, 2921-2932.
45. Britovsek, G. J. P.; Gibson, V. C.; Spitzmesser, S. K.; Tellmann, K. P.; White, A. J. P.; Williams, D. J. *J. Chem. Soc., Dalton Trans.* **2002**, 1159-1171.
46. Evans, D. F. *J. Chem. Soc.* **1959**, 2003-2005.

47. Hagen, W. R. *Adv. Inorg. Chem.* **1992**, *38*, 165-222.
48. Cox, D. D.; Benkovic, S. J.; Bloom, L. M.; Bradley, F. C.; Nelson, M. J.; Que, L., Jr.; Wallick, D. E. *J. Am. Chem. Soc.* **1988**, *110*, 2026-2032.
49. Pascaly, M.; Duda, M.; Schweppe, F.; Zurlinden, K.; Müller, F. K.; Krebs, B. *J. Chem. Soc., Dalton Trans.* **2001**, 828-837.
50. A coordinated water molecule was present in three independent crystal structure determinations, of which the crystals were obtained from three different solvent combinations.
51. Cox, D. D.; Que, L., Jr. *J. Am. Chem. Soc.* **1988**, *110*, 8085-8092.
52. Merkel, M.; Pascaly, M.; Krebs, B.; Astner, J.; Foxon, S. P.; Schindler, S. *Inorg. Chem.* **2005**, *44*, 7582-7589.
53. Merkel, M.; Schnieders, D.; Baldeau, S. M.; Krebs, B. *Eur. J. Inorg. Chem.* **2004**, 783-790.
54. Que, L., Jr.; Kolanczyk, R. C.; White, L. S. *J. Am. Chem. Soc.* **1987**, *109*, 5373-5380.
55. Horsman, G. P.; Jirasek, A.; Vaillancourt, F. D. ; Barbosa, C. J.; Jarzecki, A. A.; Xu, C.; Mekmouche, Y.; Spiro, T. G.; Lipscomb, J. D; Blades, M. W.; Turner, R. F. B.; Eltis, L. D. *J. Am. Chem. Soc.* **2005**, *127*, 16882-16891.
56. Orville, A. M.; Lipscomb, J. D; Ohlendorf, D. H. *Biochemistry* **1997**, *36*, 10052-10066.
57. Sato, M.; Uragami, Y.; Nishizaki, T.; Takahashi, Y.; Sazaki, G.; Sugimoto, K.; Nonaka, T.; Masai, E.; Fukuda, M.; Senda, T. *J. Mol. Biol.* **2002**, *321*, 621-636.
58. Senda, T.; Sugiyama, K.; Narita, H.; Yamamoto, T.; Kimbura, K.; Fukuda, M.; Sato, M.; Yano, K.; Mitsui, Y. *J. Mol. Biol.* **1996**, *255*, 735-752.
59. Uragami, Y.; Senda, T.; Sugimoto, K.; Sato, N.; Nagarajan, V.; Masai, E.; Fukuda, M.; Mitsui, Y. *J. Inorg. Biochem.* **2001**, *83*, 269-279.
60. Vaillancourt, F. H.; Barbosa, C. J.; Spiro, T. G.; Bolin, J. T.; Blades, M. W.; Turner, R. F. B.; Eltis, L. D. *J. Am. Chem. Soc.* **2002**, *124*, 2485-2496.
61. Vaillancourt, F. H.; Han, S.; Fortin, P. D.; Bolin, J. T.; Eltis, L. D. *J. Biol. Chem.* **1998**, *273*, 34887-34895.
62. Initial experiments with ferrous and ferric complexes of the ligand with pyrocatechol did not show any oxidative cleavage at an appreciable rate.
63. Lin, G.; Reid, G; Bugg, T. D. H. *Chem. Commun.* **2000**, 1119-1120.
64. Demmin, T. R.; Rogic, M. M. *J. Org. Chem.* **1980**, *45*, 1153-1156.
65. Groce, S. L.; Lipscomb, J. D. *J. Am. Chem. Soc.* **2003**, *125*, 11780-11781.
66. Groce, S. L.; Lipscomb, J. D. *Biochemistry* **2005**, *44*, 7175-7188.
67. Mendel, S.; Arndt, A.; Bugg, T. D. H. *Biochemistry* **2004**, *43*, 13390-13396.
68. Fujiwara, M.; Golovleva, L. A.; Saeki, Y.; Nozaki, M.; Hayaishi, O. *J. Biol. Chem.* **1975**, *250*, 4848-4855.
69. Bruins, A. P.; Covey, T. R.; Henion, J. D. *Anal. Chem.* **1987**, *59*, 2642-2646.
70. Hagen, K. S. *Inorg. Chem.* **2000**, *39*, 5867-5869.
71. Lynch, W. E.; Kurtz, D. M., Jr.; Wang, S.; Scott, R. A. *J. Am. Chem. Soc.* **1994**, *116*, 11030-11038.
72. Sheldrick, G. M. *SHELXS-97. Program for crystal structure solution*, University of Göttingen, Germany: 1997.
73. Sheldrick, G. M. *SHELXL-97. Program for crystal structure refinement*, University of Göttingen, Germany: 1997.
74. Spek, A. L. *J. Appl. Cryst.* **2003**, *36*, 7-13.

CHAPTER 4

Iron(III)-Catecholato Complexes as Structural and Functional Models of the Intradiol Cleaving Catechol Dioxygenases

Abstract

The synthesis, structural and spectroscopic characterization of mononuclear iron(III)-catecholato complexes of **L4** (H**L4**, methyl bis(1-methylimidazol-2-yl)(2-hydroxyphenyl)methyl ether) are described, which closely mimic the enzyme-substrate complex of the intradiol cleaving enzymes. The structural features of [Fe^{III}(**L4**)(tcc)(H_2O)] in the solid state render it the closest structural model reported to date. Complex [Fe^{III}(**L4**)(dtbc)(H_2O)] was studied with respect to its dioxygen reactivity and oxidative cleavage of the substrate was observed. Intradiol and extradiol type cleavage products were found in roughly equal amounts.

P. C. A. Bruijnincx, M. Lutz, A. L. Spek, W. R. Hagen, G. van Koten, R. J. M. Klein Gebbink, *J. Am. Chem. Soc.*, submitted for publication

4.1 Introduction

The oxidative cleavage of catechols is a key step in the biodegradation of aromatic compounds. In general, the responsible catechol dioxygenases can be divided in two classes, based on the position of the catechol ring cleavage (Figure 1).[1-4] The extradiol dioxygenases represent the more common metabolic pathway in which the C–C bond adjacent to the catechol oxygens is cleaved, whereas the intradiol dioxygenases cleave the C–C bond of the enediol functionality.

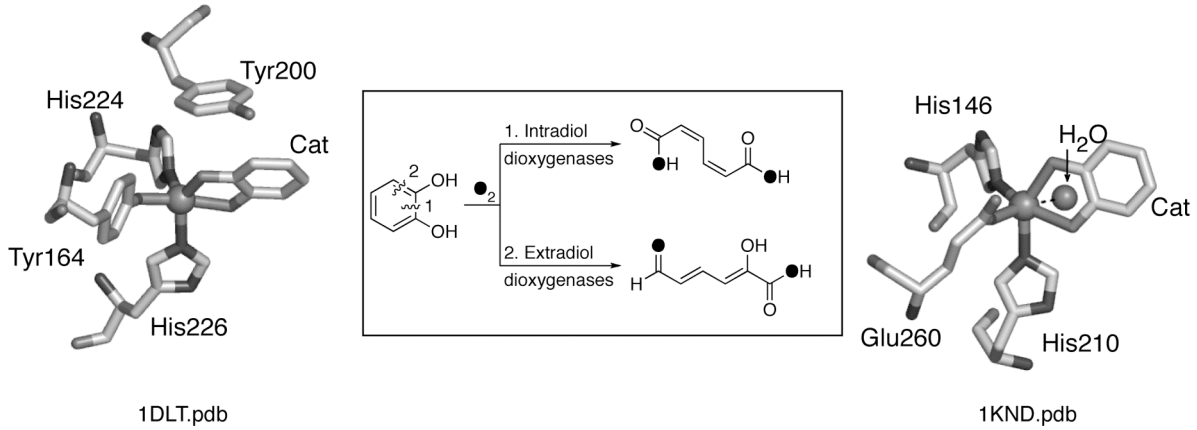

Figure 1. Catechol cleavage by the intradiol and extradiol cleaving catechol dioxygenases (center). Left: active site structure of the enzyme-substrate complex of the intradiol cleaving enzyme catechol 1,2-dioxygenase (1DLT.pdb). Right: active site structure of the enzyme-substrate complex of the extradiol cleaving enzyme 2,3-dihydroxybiphenyl 1,2-dioxygenase (1KND.pdb).

The as-isolated state of the extradiol cleaving enzymes is characterized by a non-heme iron(II) active site coordinated by the so-called 2-His-1-carboxylate facial triad, consisting of two histidines and one glutamate/aspartate residue.[5] The as-isolated intradiol dioxygenases on the other hand show a non-heme iron(III) cofactor coordinated by two histidines, two tyrosines and a hydroxide.[6,7] The active sites of the two types of enzymes are therefore quite distinct at first sight. However, upon substrate binding to the intradiol dioxygenases the axially coordinated tyrosine and the hydroxide ligand dissociate from the metal center.[8,9] The enzyme-substrate (E–S) complexes of both types of catechol dioxygenases, therefore, show an iron metal center coordinated by an *N,N,O* endogenous donor set (Figure 1), which differ in the type of the anionic donor (carboxylato vs. phenolato) and the formal oxidation state of the metal. In the extradiol cleaving enzymes, substrate binding activates the ferrous center for the binding of dioxygen, whereas in the intradiol cleaving enzymes binding of the substrate to the ferric center is generally believed to activate the substrate itself towards direct reaction with dioxygen.[3,4] As an alternative for the latter mechanism, direct dioxygen binding to the metal has also been suggested recently on the basis of modeling[10,11] and theoretical studies[12,13] for the intradiol cleaving enzymes. From this point on the respective mechanisms, however, all proceed through a similar bridged iron-alkylperoxo species. The different fates of this

iron-alkylperoxo species then ultimately determine the outcome of the catechol cleavage for each class of enzymes.

Although much is known about each class of enzymes, the factors that determine the respective regioselectivities are yet to be fully understood. To better understand these underlying mechanisms accurate biomimetic models can provide valuable insights. Many studies have been devoted to the modeling of the extra- and intradiol cleaving enzymes and impressive results have been obtained.[2,3,14] Since the enzymes utilize an ordered mechanism with substrate binding before dioxygen binding, isolated iron-catecholato complexes serve as a good starting point for these modeling studies. Many of the reported mimics of the catechol dioxygenases make use of tetradentate all-nitrogen donor ligands,[15-19] with probably the most well-studied system being the tris(2-pyridylmethyl)amine (tpa) complexes by Que et al.[20-22] Complexes with (several) phenolato groups in the ligand set have also been reported by various groups.[23-30] The ligands employed so far, however, do not accurately reflect the $N_{im}N_{im}O_{phen}$ ligand environment found at the active site of the enzymes (see Figure 1).

In Chapter 3, we described structural mimics of the E–S complex of the extradiol cleaving dioxygenases.[31] The employed substituted bis(1-alkylimidazol-2-yl)propionate ligands **L1**-**L3**[32] accurately mimicked the 2-His-1-carboxylate facial triad found at the active site of these enzymes (Chart 1). Prompted by these results and the intriguing subtleties between the intra- and extradiol cleaving enzymes, we set out to study the iron(III) coordination chemistry of **L4**[33] in order to mimic the active site of the intradiol cleaving dioxygenases (Chart 1). Ligand **L4** includes the biologically relevant imidazole and phenolato donor groups in a tridentate, tripodal framework and is therefore an attractive candidate for the construction of an accurate model of the E–S complex. Although the ligand was first reported in the late '80s by Jameson et al.,[33] to the best of our knowledge no metal complexes have been reported with **L4** to date.

In this Chapter, we report on iron(III)-catecholato complexes of **L4**, representing the most accurate structural models of the E–S complexes of the intradiol enzymes to date. The synthesis and structural characterization of these complexes, as well as their dioxygen reactivity and product selectivity is discussed.

Chart 1. Ligands **L1**-**L4**

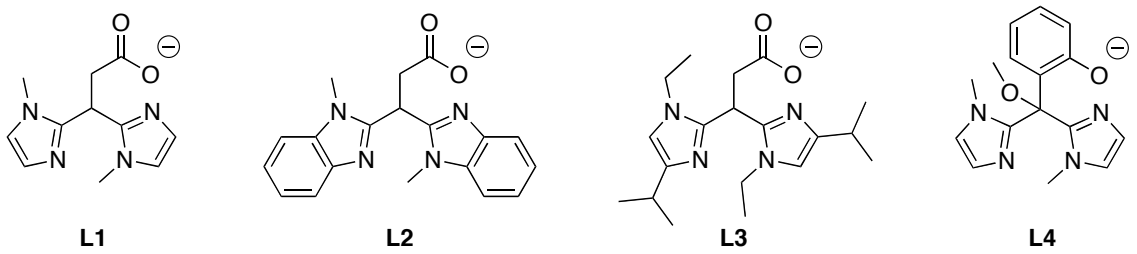

4.2 Results

Synthesis of ligand HL4. Ligand H**L4** was synthesized through an adapted literature procedure.[33] H**L4** can be conveniently synthesized on a multi-gram scale from methyl salicylate in four steps (Scheme 1). The hydroxyl group of methyl salicylate was protected with an ethoxymethyl ether (7% yield) and the resulting ester **1** was reacted with 2 eq of 2-lithio-1-methylimidazole in THF at – 78 °C to yield **2** in 79% yield after column chromatography. The hydroxyl group of **2** was then converted into the methoxy ether **3** with NaH and iodomethane (69%) to prevent any ambiguity in the potential donor set of the ligand.[33] In the last step the ethoxymethyl ether protecting group of **3** was cleaved and H**L4** was obtained as a white powder after column chromatography in 70% yield.

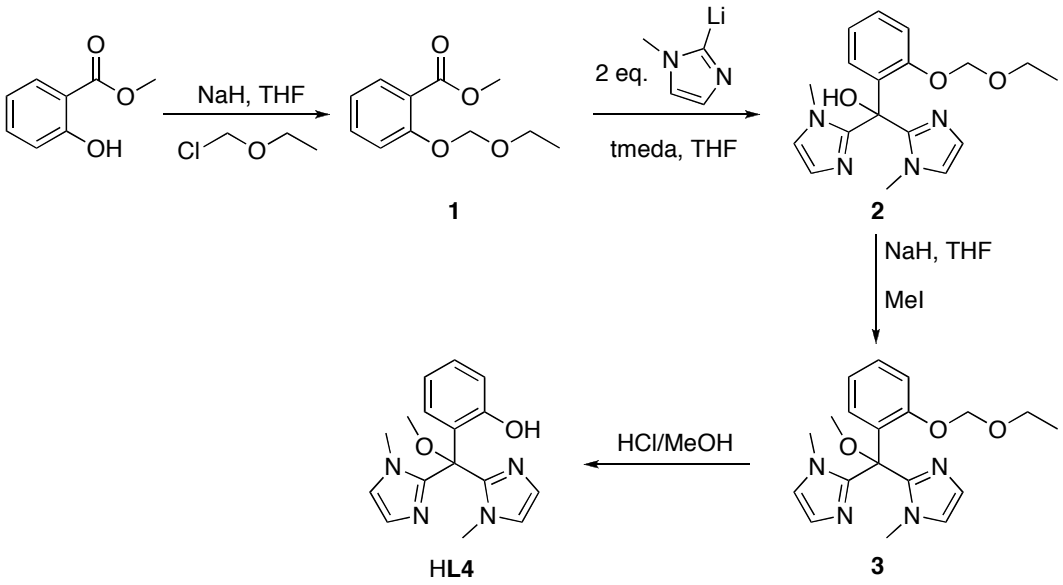

Scheme 1. Synthesis of H**L4**.

The molecular structure of H**L4** was confirmed by single crystal X-ray diffraction (Figure 2). Suitable crystals of H**L4** grew upon standing from a saturated acetone solution at – 30 °C. Interestingly, the phenolic OH group is *intra*molecularly hydrogen bonded to the methoxy oxygen atom O1. This hydrogen bond effectively locks the phenol donor group in a fixed position, at least in the solid state. The resulting limited rotation around the C1–C11 bond influences the ease with which the ligand can coordinate facially to a metal center (*vide infra*).

The hydrogen bonded hydroxyl group is readily observed in the IR absorption spectrum of solid H**L4** as a sharp and intense absorption band at 3351 cm^{-1}. It is also manifested in solution, since a sharp singlet at 9.51 ppm is observed for the hydroxyl proton in the ^1H NMR of H**L4** recorded in acetone-d_6.

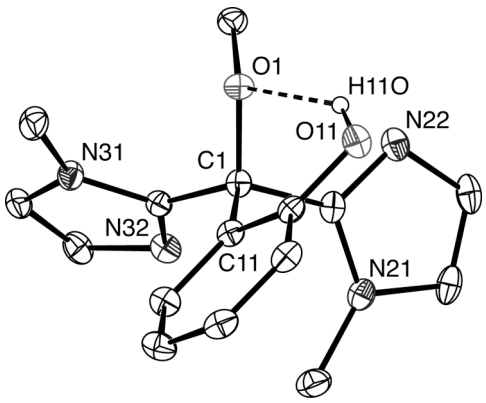

Figure 2. Molecular structure of H**L4** in the crystal with the intramolecular hydrogen bond between H11O and O1. All C–H hydrogen atoms have been omitted for clarity. Displacement ellipsoids are drawn at the 30% probability level. Hydrogen bond lengths and angles for H**L4**: O11–H11O ··· O1: D–H 0.91(4) Å, H···A 1.94(4) Å, D···A 2.704(3) Å, D–H···A 141(3)°.

Synthesis of iron(III) complexes. To investigate the facial capping potential of **L4**, we first synthesized the 2:1 complex of **L4** with an Fe^{III} metal center (Chart 2). The addition of a methanolic solution of half an equivalent of $Fe(NO_3)_3{\cdot}9H_2O$ to a solution containing equimolar amounts of H**L4** and Et_3N in methanol resulted in the immediate formation of the deep purple product which was identified as $[Fe^{III}(\mathbf{L4})_2](NO_3)$ (**4**).

Chart 2. Iron(III) complexes of **L4**.

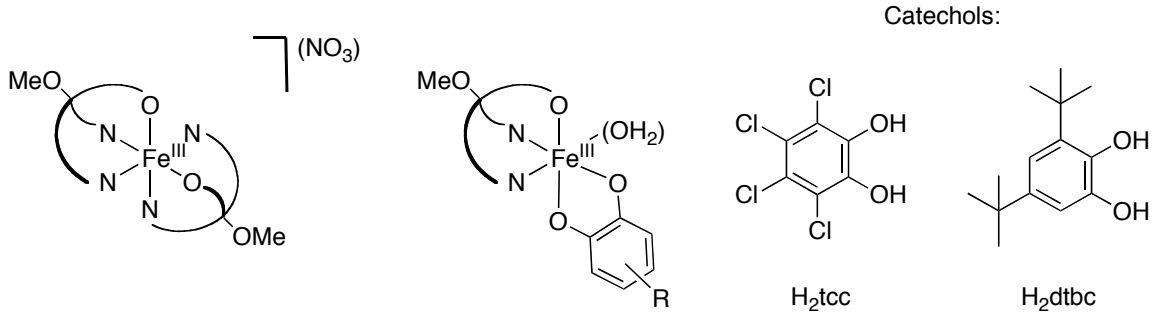

4

5 and **5·H$_2$O** (cat = tcc)
6 (cat = dtbc)

Iron(III)-catecholato complexes of ligand **L4** with two different catechols, i.e. tetrachlorocatechol (H_2tcc) and 3,5-di-*tert*-butylcatechol (H_2dtbc), were also prepared. The complexes $[Fe^{III}(\mathbf{L4})(tcc)]$ (**5**) and $[Fe^{III}(\mathbf{L4})(dtbc)]$ (**6**) were synthesized by the addition of a methanolic solution of $Fe(NO_3)_3{\cdot}9H_2O$ to a methanolic solution containing equimolar amounts of H**L4** and Et_3N. The reaction mixture immediately turned deep blue and was stirred at elevated temperatures to ensure full chelation of the ligand through all donor atoms (*vide infra*). Subsequent addition of a solution of the appropriate catechol and two equivalents of Et_3N resulted in a direct color change to deep purple. Both the air-stable complex $[Fe^{III}(\mathbf{L4})(tcc)]$ (**5**) and the air-sensitive complex $[Fe^{III}(\mathbf{L4})(dtbc)]$ (**6**) were isolated in good yields as purple powders. The iron(III) complexes **5** and **6** were obtained as neutral, five-

coordinate complexes, in which the monoanionic, tridentate ligand and a dianionic, chelated catecholato ligand carry the negative charges. It is important to note at this point, that the complexes **5** and **6** are obtained solvent-free, according to elemental analysis. The five-coordinate iron(III) complexes can bind an additional ligand such as for instance water (*vide infra*) or other coordinating solvents. The structures of **4** and **5·H$_2$O** were established by X-ray crystal structure determination.

Crystal structure of [Fe(L4)$_2$](NO$_3$) (4). Purple crystals suitable for X-ray diffraction were obtained by slow evaporation of a methanolic solution of **4** at 4 °C. The molecular structure of **4** is shown in Figure 3, with selected bond lengths and angles presented in Table 1.

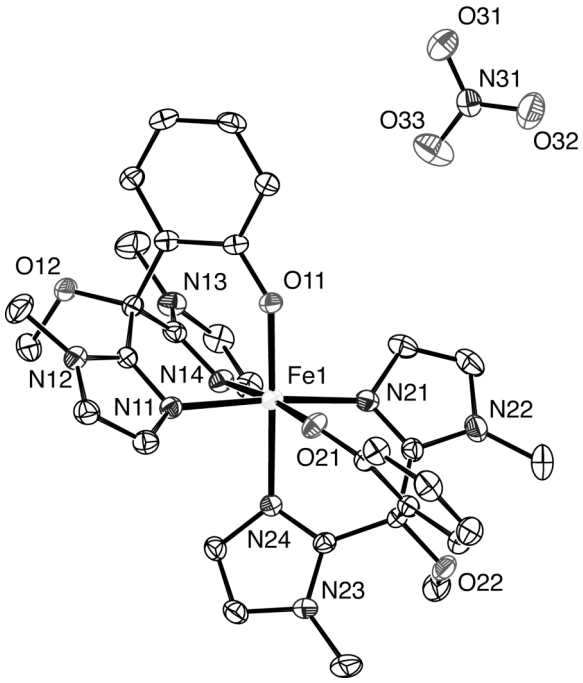

Figure 3. Molecular structure of [Fe^{III}(**L4**)$_2$](NO$_3$) (**4**) in the crystal. All hydrogen atoms have been omitted for clarity. Displacement ellipsoids are drawn at the 50% probability level.

Two monoanionic **L4** ligands facially cap the iron(III) center in **4** through both 1-methylimidazole groups and the phenolato group, resulting in a six-coordinate iron(III) metal center with a N_4O_2 donor set. The two ligands are not arranged centrosymmetrically around the iron ion, but rather are rotated by 120 ° relative to each other. This results in a *cis*-dispositioning of the phenolato *O* donor atoms, each located *trans* to a 1-methylimidazole group. This *cis*-disposition of the phenolato groups has also been observed in related complexes,[34-38] e.g. in [Fe^{III}(L)$_2$](ClO$_4$)·MeCN with the facially coordinated (2-hydroxyphenol)bis(pyrazolyl)methane ligand.[36] The Fe–N bond lengths *trans* to the phenolate (2.1323 and 2.1378 Å for Fe1–N14 and Fe1–N24, respectively) are longer than the other two Fe–N bond lengths, reflecting the stronger *trans* donor ligands of the latter. The average Fe–O and Fe–N bond lengths are in accordance with the values for related Fe(III) complexes with an

N_4O_2 donor set.[34-38] The geometry of **4** is distorted octahedral with the phenolato oxygens (O11 and O21) and imidazole nitrogens N14 and N24 occupying the equatorial plane. The diminished angles found for N14–Fe1–N11 and N24–Fe1–N21 (82.15(6) and 83.24(6)°) deviate quite strongly from ideal octahedral geometry and are dictated by the inherent geometrical restrictions imposed by the tripodal ligand.

Table 1. Selected bond lengths (Å) and angles (°) for $[Fe^{III}(\mathbf{L4})_2](NO_3)$ (**4**)

	Bond length		Angle		Angle
Fe1–N11	2.1014(15)	O11–Fe1–N24	174.08(6)	O11–Fe1–N14	87.74(6)
Fe1–N14	2.1323(16)	O21–Fe1–N14	174.12(6)	N14–Fe1–N24	86.58(6)
Fe1–N21	2.0812(16)	N11–Fe1–N21	171.08(6)	N24–Fe1–O21	87.86(6)
Fe1–N24	2.1378(15)			O21–Fe1–O11	97.87(6)
Fe1–O11	1.9104(13)	N14–Fe1–N11	82.15(6)	N11–Fe1–N24	90.15(6)
Fe1–O21	1.9077(12)	N11–Fe1–O21	95.95(6)	N24–Fe1–N21	83.24(6)
		O21–Fe1–N21	89.80(6)	N21–Fe1–O11	95.22(6)
		N21–Fe1–N14	91.46(6)	O11–Fe1–N11	90.75(6)

Crystal structure of [Fe(L4)(tcc)(H_2O)] (5·H_2O). Blue-purple crystals of **5·H_2O** suitable for X-ray diffraction were obtained by slow evaporation of a methanolic solution of **5** under ambient conditions. Upon crystallization the complex picked up a water molecule from the (wet) solvent and a six-coordinate iron complex is obtained. The molecular structure of **5·H_2O** is depicted in Figure 4, with selected bond lengths and angles presented in Table 2.

The iron(III) metal center in **5·H_2O** is facially capped by the three donor atoms of the *N,N,O* coordinated ligand. A chelated tetrachlorocatecholato ligand and a water molecule complete the distorted octahedral coordination sphere. The crystal structure of [Fe(**L4**)(tcc)(H_2O)] (**5·H_2O**) very closely resembles the structure found for [Fe(**L3**)(tcc)(H_2O)] (**L3**, 3,3-bis(1-ethyl-4-isopropylimidazol-2-yl)propionate), which we reported in Chapter 3 as a close structural mimic of the extradiol cleaving catechol dioxygenases.[31] The two complexes differ in the oxygen donor atom of the *N,N,O* donor set offered by the ligand, i.e. a phenolato *O* in **L4** vs. a carboxylato *O* in **L3**. The tetrachlorocatecholato ligand in **5·H_2O** is coordinated *trans* to the phenolato group and one of the imidazoles. The Fe1–O21 phenolato bond length (2.006(2) Å) is significantly longer than the Fe–O phenolato bond length found in **4** (average Fe–O 1.909 Å). This is probably caused by both the different *trans* influences exerted by an imidazole *N* and a catecholato *O*, respectively, and the involvement of the phenolato oxygen in a hydrogen bonding interaction in **5·H_2O** (*vide infra*).

Only a few crystal structures of iron(III)-catecholato complexes with a phenolate-containing ligand system have been reported to date, of which only one contains a tridentate ligand with an N,N,O_{phen} donor set.[23-25,30] The $Fe–O_{phen}$ bond length found in **5·H_2O** is

comparable to those reported for the complexes [Fe(L)(tbc)][24] (L, substituted bis(2-hydroxybenzyl)(2-pyridylmethyl)amines) (average Fe–O_{phen} 2.001 Å) and [Fe(salen)(cat)] (1.989 Å),[23] but longer than those observed in [Fe(L)Cl(dtbc)][25] (L, *N*-(2-hydroxyphenyl)-*N*-(2-pyridylmethyl)benzylamine) (1.957 Å) and [Fe(L)(dtbc)][30] (L, (2-hydroxyphenyl)-bis(pyridylmethyl)amine) (1.953 Å). The Fe1–N21 and Fe1–N23 bond lengths differ slightly (2.089(3) Å vs. 2.119(3) Å) and are somewhat shorter than the Fe–N bond lengths in [Fe(**L3**)(tcc)(H_2O)].[31]

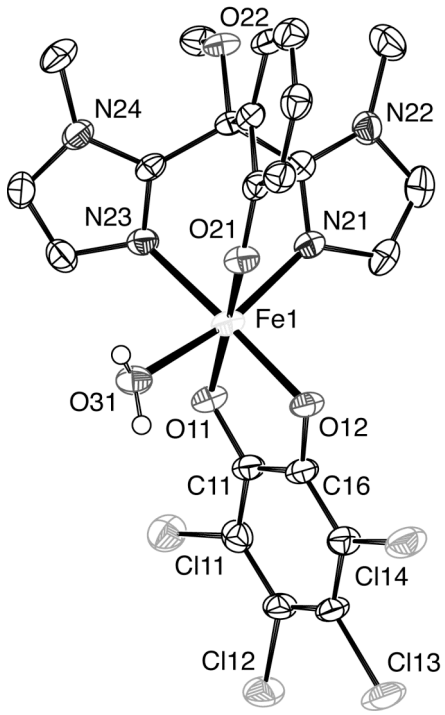

Figure 4. Molecular structure of [Fe(**L4**)(tcc)(H_2O)] (**5·H_2O**) in the crystal. All C–H hydrogen atoms have been omitted for clarity. Displacement ellipsoids are drawn at the 50% probability level.

The catecholato ligand is bound symmetrically to the iron center with essentially equal Fe–O bond lengths (Fe1–O11 1.967(2) Å and Fe1–O12 1.973(2) Å). This is rather unexpected, given the different donor groups located *trans* to each of the catechol oxygens. The binding of dianionic catecholates *trans* to different donor groups has been reported to lead to asymmetric chelation with the strongest interaction *trans* to the weaker donor group.[18,21,39] The symmetric binding of the catechol in **5·H_2O** can be the consequence of the involvement of both phenolato oxygen O21 and catecholato oxygen O12 in hydrogen bonding interactions. In fact, the water molecule is engaged in two hydrogen bonds with a second complex, resulting in the formation of centrosymmetric dimers of **5·H_2O** in the solid state (Figure 5, Table 3); hydrogen atom H31A is bonded intermolecularly to phenolato O21, while hydrogen atom H31B is bonded intermolecularly to catecholato oxygen O12. The first interaction weakens the donor strength of O21, while the second weakens the interaction of catecholato oxygen O12 with the metal center. This results, in this particular case, in equal Fe–O_{cat} bond lengths.

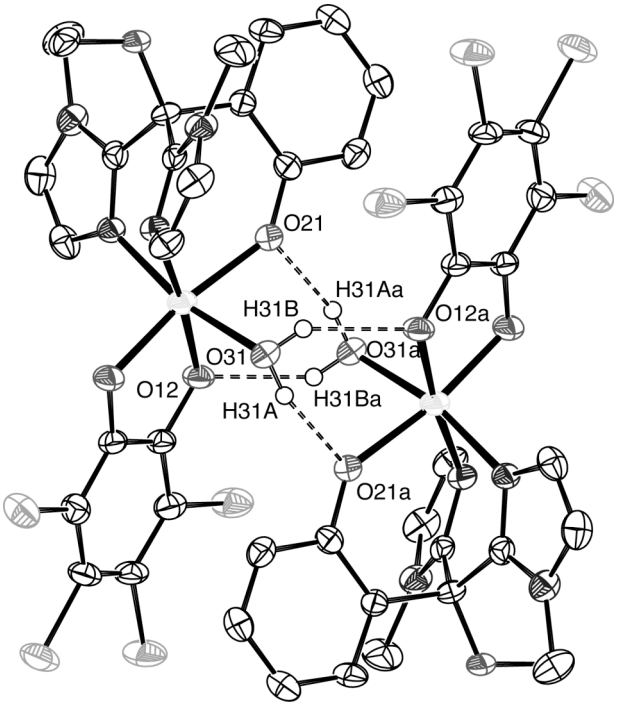

Figure 5. Hydrogen bonding pattern in [Fe(**L4**)(tcc)(H_2O)] (**5·H_2O**). All C–H hydrogen atoms have been omitted for clarity. Symmetry operation a: 1 – x, 1 – y, 1 – z.

Table 2. Selected bond lengths (Å) and angles (°) for **5·H_2O**

Bond length		Angle			Angle
Fe1–N21	2.089(3)	O12–Fe1–N23	174.23(10)	O31–Fe1–N23	89.12(10)
Fe1–N23	2.119(3)	O21–Fe1–O11	171.20(9)	N23–Fe1–N21	82.75(10)
Fe1–O21	2.006(2)	O31–Fe1–N21	167.74(11)	N21–Fe1–O12	96.92(10)
Fe1–O11	1.967(2)			O12–Fe1–O31	92.08(10)
Fe1–O12	1.973(2)				
Fe1–O31	2.127(3)	O21–Fe1–O31	83.91(10)	N23–Fe1–O21	92.94(10)
C11–O11	1.331(4)	O31–Fe1–O11	88.64(10)	O21–Fe1–O12	92.79(9)
C16–O12	1.344(4)	O11–Fe1–N21	100.71(10)	O12–Fe1–O11	82.79(9)
		N21–Fe1–O21	87.34(9)	O11–Fe1–N23	91.61(10)

Table 3. Selected hydrogen bond lengths (Å) and angles (°) for [Fe(**L4**)(tcc)(H_2O)] (**5·H_2O**). Symmetry operation a: 1 – x, 1 – y, 1 – z

Donor–H ··· Acceptor	D–H	H ··· A	D ··· A	D–H ··· A
O31–H31A ··· O21a	0.83(5)	1.95(5)	2.748(3)	160(5)
O31–H31B ··· O12a	0.81(4)	2.07(4)	2.759(3)	143(3)

A similar hydrogen bonding pattern and formation of dimers in the solid state was observed for the closely related [Fe(**L3**)(tcc)(H_2O)].[31] Here, the effects of the hydrogen bonding on the iron-catecholato bond lengths are more pronounced, resulting in an asymmetric binding mode of the catechol. The C11–O11 and C16–O12 bond lengths in the tcc moiety in **5·H_2O** are similar (1.331(4) and 1.344(4) Å, respectively) and are comparable to those found in the other Fe(III)-tetrachlorocatecholato complexes.[16,18,40] Together with the regular C–C bond lengths of the aromatic ring, it is clear that the catecholato ligand is bound as a *O,O*-dianion. No structural evidence for the manifestation of partial semiquinone character of the catecholato ligand is found.[41]

The geometry of **5·H_2O** can be best described as a severely distorted octahedron with the catecholato oxygens (O11 and O12), imidazole N23 and phenolato O21 occupying the equatorial plane. The axial positions are occupied by imidazole N21 and the water molecule. The angular deviation from ideal octahedral geometry is caused by inherent geometrical restrictions imposed by the tripodal ligand and the involvement of the water molecule in two moderately strong hydrogen bonds.

Structural comparison with the intradiol cleaving enzymes. Crystal structure information is available for several intradiol cleaving catechol dioxygenases. The structures of the as-isolated states of four different intradiol cleaving enzymes have been reported.[6,42-45] In addition, the crystal structures of enzyme-substrate complexes of the enzymes protocatechuate 3,4-dioxygenase from *Pseudonomas putida* (3,4-PCD) and catechol 1,2-dioxygenase from *Acinetobacter calcoaceticus* ADP1 (1,2-CTD) with different catechols are known.[8,9,46] Prior to substrate binding the ferric ion at the active site is coordinated by four endogenous ligands, i.e. two tyrosines and two histidines, and a hydroxide resulting in a trigonal bipyrimidal geometry. Substrate binding results in displacement of both the hydroxide ligand and the axial tyrosine residue. The active-site geometry of the enzyme-substrates complexes can, therefore, best be described as octahedral with one open coordination site.[9] At this stage the penta-coordinate ferric metal center is coordinated by only three endogenous ligands (His_2Tyr) and an asymmetrically bound catecholato dianion.[47] A comparison of the active site structure of 1,2-CTD and the structure of complex **5·H_2O** is shown in Figure 6.

From this comparison, **5·H_2O** can be regarded as a close structural mimic of the enzyme-substrate (E–S) complex of the intradiol cleaving catechol dioxygenases. Ligand **L4** accurately models the endogenous donor groups of the enzyme. The *trans*-disposition of the ligands is the same in the E–S complex and in the model compound. In both cases, the catechol is coordinated *trans* to one of the imidazoles and the phenolato moiety. The sixth coordination site is located in both structures *trans* to an imidazole group and is open in the E–S complex and occupied by a water molecule in **5·H_2O**. The availability of this vacant site is important for the formation of an implicated bridged alkylperoxo intermediate (*vide infra*). In the crystal structure of 3,4-PCD·INO, with the substrate analogue 2-hydroxyisonicotinic acid *N*-oxide (INO), the sixth coordination site is also occupied by a water molecule.[8] The

Fe–O_{cat} bond lengths differ significantly (~ 0.3 Å) in the enzyme, but are almost equal in the model complex. The asymmetric chelation in the enzyme-substrate complex is attributed to the different *trans* influences exerted by the histidine and tyrosine residues and the involvement of one of the catecholato oxygens in a hydrogen bond.[3,47] Both factors also play a role in complex **5·H$_2$O**, but now the hydrogen bonding interactions counterbalance the effect of the different *trans* ligands. All these features are illustrated by a quaternion fit[48] of the donor atoms and the metal center of both the E–S complex and the model compound (Figure 6, right).

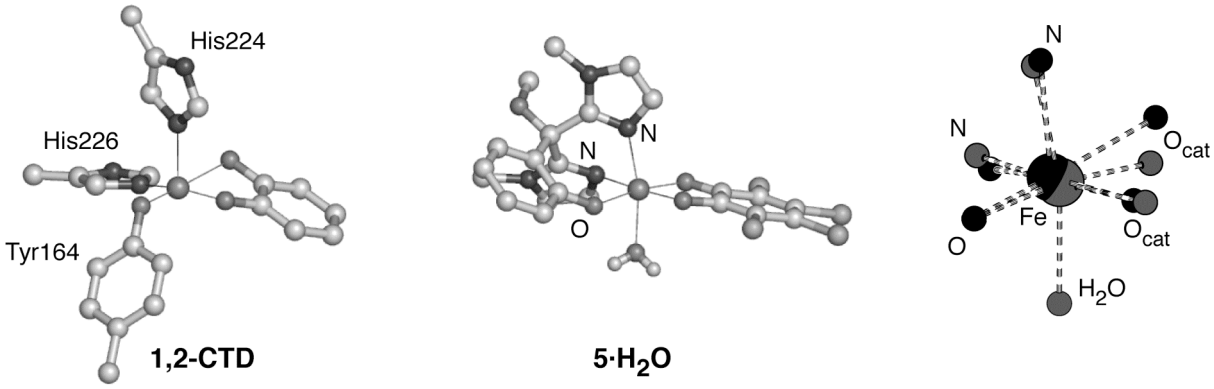

Figure 6. First coordination sphere of the iron(III) metal center of the catechol 1,2-dioxygenase E–S complex (1,2-CTD, 1DLT.pdb) (left) and that of complex [Fe(**L4**)(tcc)(H_2O)] (**5·H$_2$O**) (middle). On the right a quaternion fit[48] of the iron(III) metal center and the donor atoms in the enzyme-substrate complex (black) and the donor atoms in **5·H$_2$O** (grey) (The grey sphere of the phenolato donor atom of the model complex is obscured due to exact overlap).

Electronic absorption and EPR spectra. Two important features of the UV-Vis absorption spectrum of **4** in methanol are the absorption bands at 318 (ε = 6400 M^{-1} cm^{-1}) and 540 nm (ε = 6400 M^{-1} cm^{-1}), of which the latter gives rise to the typical purple color of the complex (Figure 7). These bands can both be assigned to phenolato-to-iron(III) charge transfer transitions from the p_π to the d_σ^* and d_π^* orbitals of the Fe(III) ion, respectively.[38,49] The absorptions are slightly blue-shifted compared to the related [$Fe^{III}(L)_2$](ClO_4) (L, (2-hydroxyphenol)bis(pyrazolyl) methane; λ_{max} = 324 and 570 nm).[36] This shift to higher energy is correlated to the longer iron-phenolato distance (1.91 Å vs. 1.88 Å) and consequently, the weaker phenolato-to-iron overlap. The absorption feature at 285 nm, which is observed for all complexes, is ligand-based and can probably be assigned to a $\pi \rightarrow \pi^*$ transition involving the phenolato moiety.

The electronic spectra of **5** and **6** both show a much broader absorption feature in the visible region. [Fe^{III}(**L4**)(dtbc)] (**6**) exhibits bands at 316, 524 and 720(sh) nm. The additional catecholato ligand in **6** is expected to give rise to two new catecholato-to-iron LMCT transitions, the position of which is very dependent on the Lewis-acidity of the ferric metal center.[20] The catecholato-to-iron LMCT bands in **6** overlap with the ligand LMCT transition, which results in the observed broad absorption feature.[50]

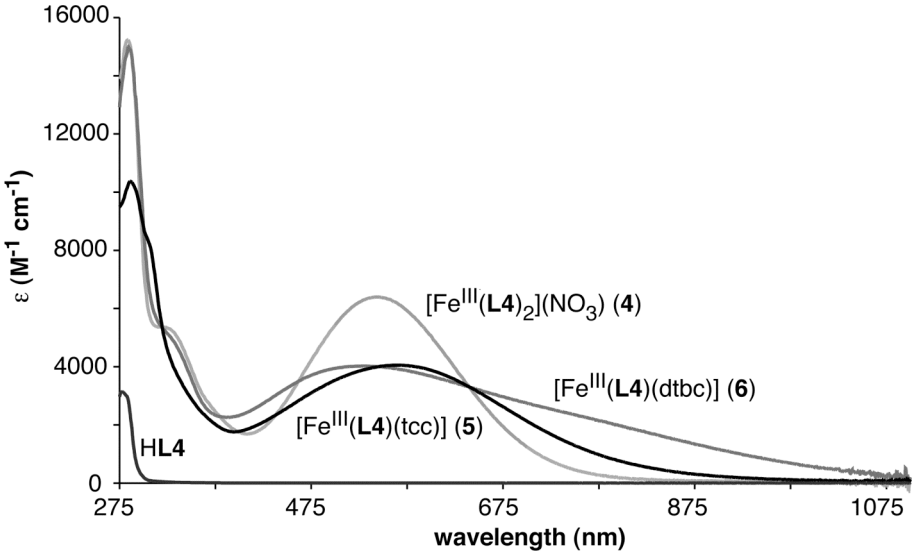

Figure 7. UV-Vis absorption spectra of $[Fe^{III}(\mathbf{L4})_2](NO_3)$ (**4**), $[Fe^{III}(\mathbf{L4})(tcc)]$ (**5**), and $[Fe^{III}(\mathbf{L4})(dtbc)]$ (**6**) and H**L4**. All spectra were recorded in methanol solution.

This overlap of LMCT bands can be nicely illustrated by monitoring the formation of the complex in time by UV-Vis spectroscopy. When $Fe(NO_3)_3 \cdot 9H_2O$, H**L4**, H_2dtbc and three equivalents of Et_3N are mixed together at room temperature under anaerobic conditions, first a greenish solution is obtained which gradually turns purple. The changes in the UV-Vis absorption spectra are displayed in Figure 8.

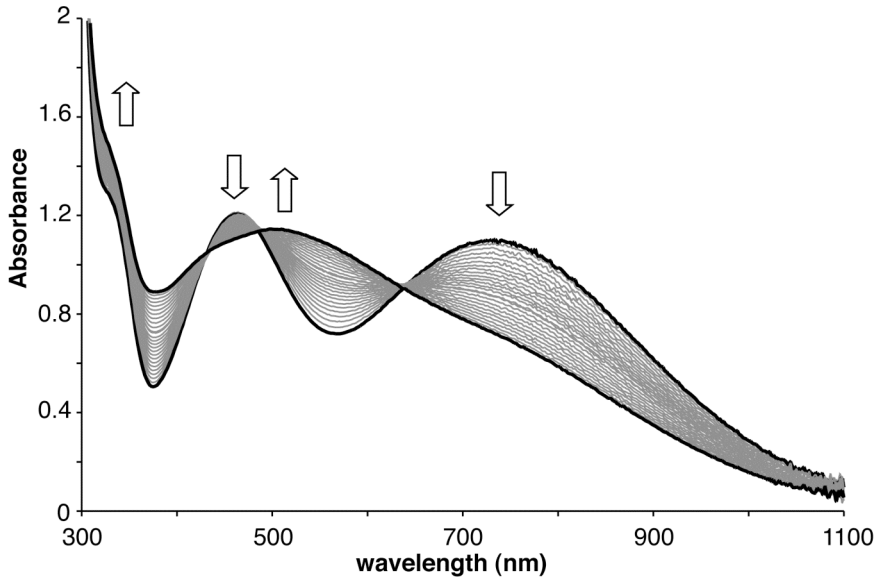

Figure 8. UV-Vis spectral changes upon mixing $Fe(NO_3)_3 \cdot 9H_2O$, H**L4**, H_2dtbc and 3 eq of Et_3N in deoxygenated methanol. Arrows indicate the decrease or increase in absorption over time.

Initially, two bands are observed at 460 and 730 nm. These bands can be assigned to catecholato-to-iron(III) charge transfer transitions. The characteristic phenolato-to-iron charge transfer band is not yet present. In time, the intensity of the two original LMCT bands

decreases and a new absorption around 510 nm grows in, signifying the slow coordination of the phenolato *O* donor to the metal center. Finally, after two hours, the solution turns purple and the absorption spectrum of independently synthesized [Fe^{III}(**L4**)(dtbc)] (**6**) is obtained. This indicates that, although the greenish species might already have the *N* donor atoms of the ligand coordinated to the metal center, the coordination of the ligand through all donor atoms is rather slow. The slow coordination might be related to a limited rotation of the phenol group in H**L4**. This rotation is hindered by the intramolecular hydrogen bond as observed in the crystal structure of H**L4**. One has to note, that when H**L4** and the iron(III)-salt are premixed, as in the actual synthesis of **5** and **6**, the formation of this greenish species is not observed after addition of the catechol. The blue solution immediately turns purple in this case.

Overall, the absorption spectrum of **6** shows a striking similarity with the absorption spectrum reported for the enzyme-substrate complex of protocatechuate 3,4-dioxygenase.[51] The E–S complex also features the broad tail on the phenolato-to-iron LMCT absorption with comparable extinction coefficients.

The dominant feature in the absorption spectra of **5** and **6** is the phenolato-to-iron charge transfer band at 560 and 524 nm, respectively (Table 4). Que et al. showed that the phenolato-to-iron charge transfer band reflects the strength of the other ligands coordinated to the iron. A weaker ligand would result in a stronger phenolato-iron interaction and a red shift in the absorption maximum. The relative blue shift of the absorption maximum upon going from a tetrachlorocatecholato ligand to the 3,5-di-*tert*-butylcatecholato ligand thus reflects the stronger interaction of the metal with the latter ligand. Furthermore, the lower energy catecholato-to-iron LMCT transition is known to shift to higher energy as the substituents on the catechol ring are varied from electron donating to electron withdrawing, since electron withdrawing groups would be expected to lower the energy of the catecholate frontier orbitals and thus increase the ligand-to-metal energy gap. This blue-shift of the catecholato-to-iron LMCT transitions and the red-shift of the ligand-to-iron LMCT transition could account for the less broad absorption spectrum that is observed for [Fe^{III}(**L4**)(tcc)] (**5**).

Table 4. Absorption maxima in the UV-Vis spectra [λ_{max}, (ε [M^{-1} cm^{-1}])] and EPR data[a] of the complexes [Fe^{III}(**L4**)$_2$](NO_3) (**4**), [Fe^{III}(**L4**)(tcc)] (**5**), and [Fe^{III}(**L4**)(dtbc)] (**6**)

Complex	λ_{max} (nm)	ε (M^{-1} cm^{-1})	$\eta = E/D$	$\Delta\eta$ (%)	*g*
[Fe^{III}(**L4**)$_2$](NO_3)] (**4**)	318, 540	5400, 6400	0.12	15.5	8.3, 5.6
[Fe^{III}(**L4**)(tcc)] (**5**)	303, 560	8500, 4000	0.15	20	8.7, 5.4
[Fe^{III}(**L4**)(dtbc)] (**6**)[b]	316, 524, 720(sh)	5400, 4000, 2500	0.11	18	8.2, 5.6

[a] EPR spectra were recorded on 2 mM complex solution in frozen methanol at 15 K. [b] a minor low spin Fe(III) species is also observed accounting for < 1% of the total spin concentration.

Complexes **4-6** exhibit EPR spectra that show that these complexes are all high-spin ferric complexes (data given in Table 4). The EPR spectra of **4-6** are depicted in Figure 9; simulations are also included based on the standard spin Hamiltonian:

$$H_S = D[S_z^2 - S(S+1)/3] + E(S_x^2 - S_y^2) + g\,\beta \boldsymbol{B}\cdot\boldsymbol{S},$$

and on the assumption of the weak-field limit, $D >> h\upsilon$. In general, the spectra of distributed high-spin transition ion complexes are frequently found to be rather broad presumably reflecting a distribution in electronic structure as a consequence of relative geometrical flexibility of the complex. This leads to a distribution in the zero-field splitting (ZFS) parameters, which has been named *D*-strain.[52] The resulting EPR spectra can be simulated by summing a large number of spectra calculated for different ZFS-values.[53] However, multi-frequency EPR studies of $S = 5/2$ models and metalloproteins have pointed to the difficulty of establishing the quantitative nature of their ZFS distributions.[53-55] Recently, Weisser et al. have presented an analysis of EPR spectra of iron-catecholato complexes by simulation as ZFS distributed $S = 5/2$ systems.[56] An unexpected result of this study was the conclusion that a $g = 4.3$ signal commonly present in the spectra is not an $S = 5/2$ contaminant of high rhombicity ($E/D \approx 1/3$), but rather is an intrinsic part of the iron catecholato spectrum whose ZFS distribution is very broad to the extent that even extreme values of rhombicity are sampled with finite intensity by the distribution.[56] This is an attractive proposal because it resolves the apparent problem of a contaminating spectral component in chemically pure compounds. On the other hand, the analysis of Weisser et al. used a detailed distribution model with seven adjustable parameters including the absolute value of the axial ZFS parameter, *D*, while it has thus far been generally taken to be impossible to determine the value of *D* from data recorded at a single X-band frequency and a single temperature for systems near the weak-field limit (cf. ref. 57).

We have, therefore, attempted to fit the present data with a drastically simplified model of only three parameters: the absolute values of *D* and *E* are undetermined; only the rhombicity $\eta = E/D$ is a fitting parameter (i.e. the weak-field limit[57]). Also, the Gaussian distributions in *D* and *E* are assumed to be fully (negatively) correlated, and their standard deviations are identical when expressed as percentage of the ZFS values; this gives a second fitting parameter, $\Delta\eta$ (cf. Table 4). Because the high-spin Fe^{III} d^5 system is subject to quenching of orbital angular momentum, it is assumed that the real *g*-value does not significantly deviate from the free electron value, $g = 2.00$. Finally, a third parameter is introduced: the residual width W_0, namely, an isotropic line width (Gaussian standard deviation) of the line shape of individual spectra, which should phenomenologically account for any additional, less significant, broadening mechanism, e.g. *g*-strain and intermolecular dipolar interactions. In Figure 9 it can be seen that this simple model affords semi-quantitative fits to the data, and, notably, corroborates the proposal[56] that the $g = 4.3$ line is an intrinsic part of the EPR spectra of iron compounds of intermediate rhombicity subject to a broad distribution in rhombicity. The residual line width W_0 is found to be constant over the three complexes at circa 35 Gauss. Clearly, the development of a more sophisticated model for the

ZFS distribution(s) than the one employed here, would require testing against a much more extended EPR data set encompassing high quality data at several (higher) frequencies.

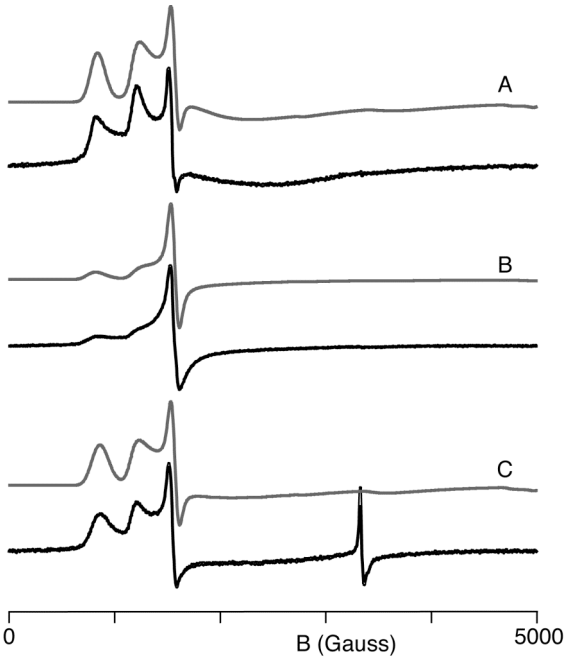

Figure 9. Simulated (grey) and experimental (black) X-band EPR spectra of 2mM $[Fe^{III}(\mathbf{L4})_2](NO_3)$ (**4**) (A), $[Fe^{III}(\mathbf{L4})(tcc)]$ (**5**) (B) and $[Fe^{III}(\mathbf{L4})(dtbc)]$ (**6**) (C) recorded in frozen methanol solution at 15 K. Typical EPR measuring conditions: microwave frequency 9.41 GHz, microwave power 0.5 mW, modulation amplitude 12.5 G, modulation frequency 100 kHz, and sweep width 5000 G. See Table 4 and the text for simulation parameters.

The EPR powder spectrum of **4** shows features at $g = 8.3$, 5.6 and a broad feature at $g \approx 3$. The fitted rhombicity, $\eta = 0.12$ defines the effective g_{zyx}-values of the three transitions within the Kramers doublets to be (1.60, 8.32, 3.25), (5.57, 2.41, 2.65), (9.97, 0.09, 0.10) for the lowest, middle, and highest doublet respectively. Thus, one observes the g_y of the lowest doublet, the g_z of the middle doublet, and a broad feature from a combination of the g_x of the lowest doublet and the g_y and g_x of the middle doublet. The other effective g-values are associated with features that are beyond detection due to low intensity, broadening, or magnetic field limitation. And the $g = 4.3$ feature is from a small subset of molecules with maximally rhombic coordination sites that happen to be subject to extensive D-strain.

In the spectrum of **6** a minor feature is observed around $g \approx 2$, which is not accounted for by the distributed $S = 5/2$ simulation. The signal is possibly attributable to a minority low-spin Fe(III) species; its integrated intensity accounts for < 1% of the total spin concentration.

There is a marked similarity between the EPR spectra of **4**-**6** amongst themselves and also compared with other reported EPR spectra of iron(III)-catecholato complexes.[20,31,56] Especially, a comparison of the spectral data of the six-coordinated iron(III)-catecholato complexes **4** and $[Fe^{III}(hda)(dtbc)]^{2-}$ (E/D 0.15) (hda, *N*-(2-hydroxybenzyl)-*N*-(carboxymethyl)glycine)[20] and **6**, suggest that the latter is probably also six-coordinate in

solution. A solvent molecule is then assumed to occupy the sixth available site, as also observed in the crystal structure of **5·H$_2$O** (*vide supra*).

Dioxygen reactivity. Upon exposure of [Fe^{III}(**L4**)(dtbc)] (**6**) to air a slow and subtle color change was observed. This process was monitored by UV-Vis absorption spectroscopy and in time the broad absorption feature disappeared and concomitantly a new feature appeared with an absorption maximum at 536 nm (Figure 10). No changes were observed in the absorption spectra of **4** or **5** upon exposure to air.

The loss in absorption intensity at longer wavelengths, originally attributed to the lower energy catecholato-to-iron LMCT transition, suggested oxidative transformation of the catechol in the case of **6**. The new band that emerged at 550 nm can be ascribed to a [Fe^{III}(**L4**)$_2$]$^+$ species, given the similarity with the absorption spectrum of [Fe^{III}(**L4**)$_2$](NO$_3$)] (**4**). Only two out of the three isosbestic points observed in Figure 10 are well-defined, suggesting more than two principal species and the involvement of an intermediate species in the oxygenation.

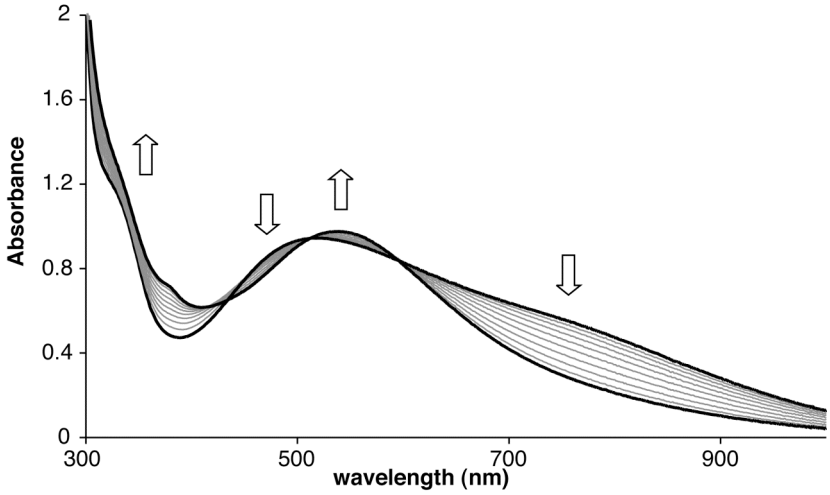

Figure 10. UV-Vis spectral changes upon exposure of [Fe^{III}(**L4**)(dtbc)] (**6**) in methanol to air. Arrows indicate the increase or decrease in absorption over time.

In order to identify the products and the regioselectivity of the reaction, the products were isolated from the reaction mixture, characterized by ^{1}H NMR spectroscopy and GC-MS and compared to authentic samples. The oxygenation reactions were performed in both a coordinating and non-coordinating solvent, i.e. acetonitrile and dichloromethane. A similar product distribution was found for the oxygenation reactions in the two different solvents (Table 5). In general, the reactions proceeded slowly and after two weeks only about 60% of the catechol was converted. Both intradiol *and* extradiol type cleavage products were observed in a roughly equal ratio for both solvents, with a slight preference for the extradiol type cleavage product. The amount of detected quinone auto-oxidation product is rather low. The addition of one equivalent of a proton donor to the solution resulted in a drop in conversion and an increase of the quinone auto-oxidation product.

Table 5. Organic products obtained upon reaction of complex [Fe(**L4**)(dtbc)] (**6**) with air

Solvent	Additive	Conv. (%)	Extradiol (%)	Intradiol (%)	Quinone (%)
MeCN	--	62	49 (61/39)[a]	40	11
CH_2Cl_2	--	58	51 (61/39)	41	8
MeCN	$[Et_3NH]BF_4$ (1 eq)	46	45 (70/30)	26	29
CH_2Cl_2	$[Et_3NH]BF_4$ (1 eq)	47	32 (58/42)	27	41

[a] Ratio in parentheses: (4,6-di-*tert*-butyl-2-pyrone/3,5-di-*tert*-butyl-2-pyrone)

4.3 Discussion

The intricacies of the respective regioselectivities of the intra- and extradiol cleaving catechol dioxygenases are not yet completely understood and subject of ongoing research.[2-4] A vast amount of *functional* models of the intradiol cleaving dioxygenases have been reported,[3,10,14,17-19,21,24,25,27,58] amongst which the tpa derived complexes feature prominently.[15,16,22,59] Small synthetic analogues that accurately mimic the *structural* features of the active site of the intradiol cleaving enzymes are, however, more limited in number. The best structural and spectroscopic model for the as-isolated His_2Tyr_2FeOH state of the intradiol cleaving enzymes is the $[Fe(Mes_6\text{-salen})(H_2O)](ClO_4)$ complex reported by Fujii et al.[60,61] We anticipated that **L4**[33] could be an attractive candidate for obtaining a close structural mimic of the $His_2TyrFe^{III}Cat$ state of the enzyme-substrate complex. Since no metal complexes of **L4** were reported to date, the facial capping potential of **L4** was first explored by the synthesis of the 2:1 ligand to metal complex **4**. The crystal structure of **4** shows that the ligand can indeed act as a tridentate, facially coordinating ligand, rendering it a good mimic of the His_2Tyr facial triad.

The iron(III)-catecholato complexes **5** and **6** of ligand H**L4** are originally isolated as five-coordinate complexes. The structural and spectroscopic data show that a sixth coordination site is available and readily accessible for the coordination of small molecules such as for instance water. The availability of an empty coordination site is important, since it is one of the essential features of the E–S complex. Complexes **5** and **6** are directly related to the previously reported $[Fe^{III}(\mathbf{L1\text{-}3})(tcc)]$ and $[Fe^{III}(\mathbf{L1\text{-}3})(dtbc)]$ complexes[31] and differ only in the type of oxygen donor offered by the ligand (Chart 1). The influence of the ligand donor set on the dioxygenase reactivity of a ferric metal center can now be directly probed by comparison of the two types of complexes.

The X-ray structure of **5·H_2O** and the spectroscopic data of **5** and **6** show that the iron-catecholato complexes do not only duplicate the structural features of the active site of the E–S complex of the intradiol cleaving catechol dioxygenases, but also closely resemble its spectral characteristics.[4,51] $[Fe^{III}(\mathbf{L4})(tcc)(H_2O)]$ (**5·H_2O**) is actually the closest, crystallographically characterized structural model of the E–S complex of the intradiol cleaving enzymes reported to date. The oxidative cleavage of the catechol upon exposure of

complex **6** to air was found to proceed slowly and with only moderate conversions (around 60%). The slow reactivity can be ascribed to the low Lewis acidity of the iron(III) metal center[21,22] compared to complexes with neutral, all-*N* ligands and was observed before for complexes with phenolato groups in the ligand set.[29,50]

The low Lewis acidity can, however, be only part of the answer, since the enzyme manages to show good turnover (≈ 36 s^{-1} for 3,4-PCD with product release as rate limiting step)[4] with the same donor set. In the enzyme, the combination of hydrogen bonding interactions with second sphere residues and the precise positioning of the substrate in the binding pocket, results in an enhanced asymmetric binding of the substrate. The asymmetric binding of the ligand enhances the iron(II)-semiquinonato character. This (increased) radical character is thought to be essential for dioxygen reactivity[3,12] and is further stabilized by the local dielectric properties of the enzyme active site. The combination of these factors lead to a lower activation barrier and comparably high catalytic activity of the natural systems.

Despite the rather low reactivity, important observations can be made regarding the selectivity of the oxygenation reaction. The product distribution is remarkably less solvent dependent than previously observed for the extradiol model complexes [Fe^{III}(**L1-3**)(tcc)]. Oxygenation of **6** in acetonitrile results in 90% oxidative cleavage products with only 10% quinone formation, whereas quinone was the only product observed for the oxygenation of [Fe^{III}(**L1-3**)(tcc)] in acetonitrile. Interestingly, both intradiol *and* extradiol cleavage products are formed in more or less equal amounts. The product distribution for oxygenative cleavage of [Fe(**L4**)(dtbc)] (**6**) thus shows that there is no inherent preference for intra- or extradiol type cleavage by an iron(III) metal center coordinated by a N_{im},N_{im},O_{phen} donor set. The same conclusion was drawn for the oxygenative cleavage in [Fe^{III}(**L1-3**)(dtbc)]. This illustrates that in both cases the endogenous ligand donor set in the enzyme is not a decisive factor for the regioselectivity of the cleavage. These results support the hypothesis that both the intradiol and extradiol cleaving enzymes proceed through a common intermediate, i.e. a bridged alkylperoxo species (Figure 11).

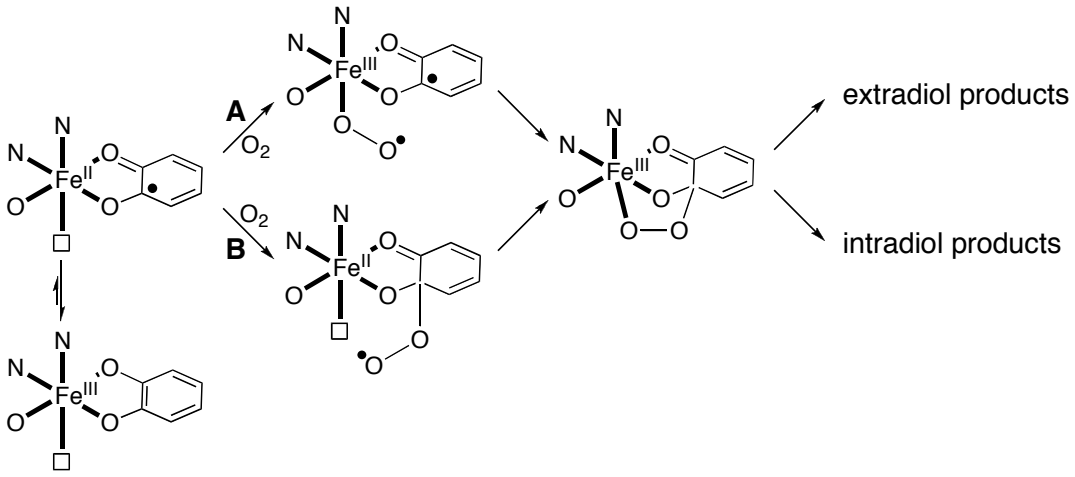

Figure 11. Proposed oxidative cleavage mechanism for [Fe(**L4**)(dtbc)] (**6**).

Such an intermediate is accessible in both complexes reported here and in our previous study. The oxygenative cleavage of **6** is initiated by the introduction of some iron(II)-semiquinonato character on the complex by the catecholato-to-iron(III) charge transfer transitions.[10] As a consequence of the tripodal, tridentate nature of the ligand, an empty coordination site is available *trans* to the 1-methylimidazole donor groups that mimics His224 in the active site of the enzyme. The bridged alkylperoxo species can then be formed by either binding of dioxygen to the metal center at the vacant site and subsequent attack of the semiquinone by a superoxide species (Figure 11, A), or alternatively by direct attack on the substrate and subsequent recombination with the metal center at the vacant site (Figure 11, B).[3,12] The latter pathway has been preferred based on the available spectroscopic data,[3] but recent hybrid DFT calculations suggest that this is unlikely and rather point to pathway A.[12] The available data does not allow us to distinguish between the two possible pathways in the case of **6**. Finally, the non-selective cleavage of the O–O bond of the alkylperoxo species leads to roughly equal amounts of intra- and extradiol type cleavage for complex **6**.

4.4 Conclusions

In addition to our reported mimics of the extradiol cleaving catechol dioxygenases, we have studied the iron(III) coordination chemistry of the tripodal, tridentate ligand H**L4**, as a potential mimic of the endogenous ligands of the intradiol cleaving catechol dioxygenases. The structurally characterized iron-catecholato complex [Fe^{III}(**L4**)(tcc)(H_2O)] can be regarded as the closest structural model of the enzyme-substrate complex reported to date. As part of its spectroscopic characterization, the EPR spectra were successfully simulated using a simplified model that accounts for *D*-strain. The simulation procedure showed that the $g = 4.3$ line is an intrinsic part of the EPR envelope of the studied complexes and should not necessarily be attributed to a highly rhombic impurity. Oxygenation studies of the complexes revealed that equal amounts of intradiol and extradiol type cleavage products are formed. This suggests that the first coordination sphere of the metal center at the enzyme active site is not decisive for regioselective intradiol cleavage. The complexes thus provide more insight into the factors governing the reactivity of this intriguing class of enzymes.

4.5 Experimental Section

Air-sensitive organic reactions were carried out under an atmosphere of dry, oxygen-free N_2 using standard Schlenk techniques. Tetrachlorocatechol was recrystallized from anhydrous toluene before use. THF and hexanes were dried over sodium benzophenone ketyl and distilled under N_2 prior to use. Methanol was dried over magnesium methoxide and distilled under N_2 prior to use. All other chemicals were commercially obtained and used as received. The air-sensitive iron complex **6** was synthesized and handled under an argon atmosphere using standard Schlenk techniques. Solvents were thoroughly deoxygenated with argon before use. ^1H and ^{13}C NMR spectra were recorded on a Varian AS400 or Varian Inova 300 spectrometer, operating at 25 °C. Elemental

microanalyses were carried out by the Microanalytisches Laboratorium Dornis & Kolbe, Mulheim a.d. Ruhr, Germany. ESI-MS spectra were recorded on a Micromass LC-TOF mass spectrometer by the Biomolecular Mass Spectrometry group, Utrecht University. EPR spectra were recorded on a Bruker ER 200 D spectrometer with an ER 4116 DM resonator and a home built helium flow cooling system. UV-Vis spectra were recorded on a Varian Cary 50 spectrometer equipped with a Helma emersion probe for air-sensitive experiments.

Methyl 2-ethoxymethoxybenzoate (1). A solution of methyl salicylate (8.3 g, 54 mmol) in THF (30 mL) was added dropwise to a stirred suspension of NaH (8.6 g, 215 mmol, 60 weight% dispersion in mineral oil) in THF (500 mL). After stirring the resulting suspension for 1 h at room temperature, chloromethyl ethyl ether (10.2 g, 108 mmol) was added at once. The reaction mixture was then stirred overnight, filtered to remove the residual solid, and evaporated to dryness. The crude product was redissolved in hexanes (100 mL), dried over $MgSO_4$, filtered and again evaporated to dryness. The resulting turbid oil was purified by flame distillation to yield the product as a colorless, clear oil (9.0 g, 79%). ^{1}H NMR (300 MHz, $CDCl_3$, 25 °C): δ = 1.17 (t, 3H, *J* = 6.9 Hz, OCH_2CH_3), 3.73 (q, 2H, *J* = 6.9 Hz OCH_2CH_3), 3.85 (s, 3H, OCH_3), 5.28 (s, 2H, OCH_2O), 6.99 (t, 1H, *J* = 6.0 Hz, H_{Ph}), 7.19 (d, 1H, *J* = 8.7 Hz, H_{Ph}), 7.40 (t, 1H, *J* = 6.6 Hz, H_{Ph}), 7.74 (d, 1H, *J* = 7.8 Hz, H_{Ph}) ppm. ^{13}C{^{1}H} (100 MHz, acetone-d_6 , 25 °C): δ = 15.4, 52.1, 65.0, 94.5, 117.4, 122.1, 123.1, 131.6, 133.7, 157.3, 167.1 ppm.

Bis(1-methylimidazol-2-yl)(2-ethoxymethoxyphenyl)methanol (2). A solution of *n*-butyl lithium (24 mL, 38.4 mmol, 1.6 M solution in hexanes) was added dropwise to a solution of 1-methylimidazole (2.9 g, 35 mmol) and tmeda (5 mL, 35 mmol) in THF (100 mL) at 0 °C. The solution was stirred for 1 h at 0 °C and subsequently cooled to – 78 °C. A solution of methyl 2-ethoxymethoxybenzoate (**1**) (3.5 g, 16.7 mmol) in THF (20 mL) was added dropwise to the stirred solution and the reaction mixture was allowed to warm to room temperature overnight. The reaction mixture was quenched by addition of 30 mL of a saturated aqueous NH_4Cl solution. All volatiles were evaporated *in vacuo* and the aqueous layer was extracted with dichloromethane (4 × 50 mL). The combined organic extracts were dried over Na_2SO_4, filtered, and concentrated to dryness. The crude product was obtained as a brown oil and purified by column chromatography (silica, eluent ethyl acetate:triethylamine = 10:1). The product was obtained as a foamy, white solid (4.5 g, 79%). ^{1}H NMR (300 MHz, $CDCl_3$, 25 °C): δ = 1.13 (t, 3H, *J* = 7.2 Hz, OCH_2CH_3), 3.46 (q, 2H, *J* = 6.9 Hz, OCH_2CH_3), 3.53 (s, 6H, NCH_3), 5.09 (s, 2H, OCH_2O), 5.93 (s, 1H, O*H*), 6.43 (d, 1H, *J* = 7.7 Hz, H_{Ph}), 6.89 (s, 2H, H_{im}), 6.92 (t, 1H, *J* = 7.2 Hz, H_{Ph}), 6.96 (s, 2H, H_{im}), 7.20 (d, 1H, *J* = 8.4 Hz, H_{Ph}), 7.31 (t, 1H, *J* = 7.4 Hz, H_{Ph}) ppm. ^{13}C{^{1}H} (75 MHz, $CDCl_3$, 25 °C): δ = 15.2, 35.1, 64.6, 76.4, 93.9, 116.0, 122.1, 123.2, 126.5, 128.4, 130.3, 130.8, 148.1, 155.7 ppm.

Methyl bis(1-methylimidazol-2-yl)(2-ethoxymethoxyphenyl)methyl ether (3). A solution of bis(1-methylimidazol-2-yl)(2-ethoxymethoxyphenyl)methanol (**2**) (4.0 g, 11.7 mmol) in THF (30 mL) was added to a stirred suspension of NaH (1 g, 25 mmol, 60% weight dispersion in mineral oil) in THF (100 mL). The suspension was stirred for 1 h, after which MeI (2.0 g, 14 mmol) was added. The reaction mixture was stirred overnight at room temperature, quenched with a saturated, aqueous NH_4Cl solution (20 mL), diluted with H_2O (20 mL) and extracted with dichloromethane (3 × 50 mL). The combined organic extracts were dried over Na_2SO_4, filtered, and concentrated to dryness. The crude product was obtained as a yellowish-brown oil, which solidified upon standing. After purification by flash column chromatography (silica, first hexanes:Et_3N 10:1 *v*/*v*, then EtOAc:Et_3N 10:1 *v*/*v*) compound **3** was obtained as a white powder (2.9 g, 69%). ^{1}H NMR (300 MHz, $CDCl_3$, 25 °C): δ = 1.08 (t, 3H, *J* = 6.9 Hz, OCH_2CH_3), 3.29 (s, 3H, OCH_3), 3.42 (s, 6H, NCH_3), 3.43 (q, 2H, *J* =

6.3 Hz, OCH_2CH$_3$), 4.89 (s, 2H, OCH_2O), 6.82 (s, 2H, H_{im}), 6.96 (s, 2H, H_{im}), 6.99 (t, 1H, J = 7.7 Hz, H_{Ph}), 6.92 (t, 1H, J = 7.4 Hz, H_{Ph}), 7.27 (m, 2H, H_{Ph}) ppm. $^{13}C\{^1H\}$ (75 MHz, $CDCl_3$, 25 °C): δ = 15.2, 15.4, 34.7, 53.9, 64.0, 93.6, 116.0, 121.1, 123.0, 126.1, 126.8, 128.8, 130.4, 145.9, 156.5 ppm.

Methyl bis(1-methylimidazol-2-yl)(2-hydroxyphenyl)methyl ether (HL4). Methyl bis(1-methylimidazol-2-yl)(2-ethoxymethoxyphenyl)methyl ether (**3**) (2.4 g, 6.7 mmol) was dissolved in a mixture of methanol/hydrochloric acid (30%) (50 mL, 4:1 *v*/*v*) and the solution was refluxed for 1.5 h under N_2. The solution was allowed to cool to room temperature and the methanol was evaporated *in vacuo*. The resulting aqueous solution was diluted (20 mL) and washed twice with pentane (2 × 20 mL). The pH of the aqueous solution was then adjusted to 8.2 by the addition of aqueous NaOH (1M) and the solution was extracted with dichloromethane (3 × 40 mL). The organic layers were dried over Na_2SO_4, filtered, and evaporated *in vacuo*. The crude product was purified by column chromatography (silica, first EtOAc, then EtOAc:MeOH 5:1 *v*/*v*) and H**L4** was obtained as a white powder (1.4 g, 70%). Colorless, single crystals suitable for X-ray diffraction were obtained from an acetone solution cooled to – 30 °C. ^1H NMR (400 MHz, acetone-d_6, 25 °C): δ = 3.22 (s, 3H, OCH_3), 3.49 (s, 6H, NCH_3), 6.79 (d, 1H, J = 8.0 Hz, H_{Ph}), 6.85 (t, 1H, J = 7.4 Hz, H_{Ph}), 6.88 (s, 2H, H_{im}), 7.10 (s, 2H, H_{im}), 7.21 (m, 2H, H_{Ph}), 9.51 (s, 1H, OH) ppm. $^{13}C\{^1H\}$ (100 MHz, $CDCl_3$, 25 °C): δ = 34.7, 53.5, 81.5, 119.2, 119.8, 123.8, 124.2, 126.3, 127.0, 130.3, 145.3, 156.0 ppm. Anal. for $C_{16}H_{18}N_4O_2$ (298.34): calc. C 64.41, H 6.08, N 18.78; found C 64.57, H 6.12, N 18.89. ESI-MS: *m/z* = 299.13 {$[M+H]^+$, calc. 299.15}, 321.08 {$[M+Na]^+$, calc 321.13}.

[Fe(L4)$_2$](NO$_3$) (4). To a solution of H**L4** (159 mg, 0.53 mmol) and 1 eq Et_3N (75 μL) in methanol (6 mL) was added an orange solution of $Fe(NO_3)_3{\cdot}9H_2O$ (107 mg, 0.26 mmol) in methanol (6 mL) and immediately a color change to purple was observed. The solution was stirred for 20 min at 50 ºC and concentrated *in vacuo*. The crude purple solid was redissolved in water (50 mL) and product was extracted with dichloromethane (3 × 25 mL). The organic solution was washed twice with water (2 × 15 mL) and concentrated *in vacuo*. The crude product was then recrystallized from methanol/diethyl ether (1:2 *v*/*v*) at – 30 °C to give the purple title compound (62 mg, 33% yield). Crystals suitable for X-ray diffraction were obtained by slow evaporation of a methanolic solution of **4** at 4 °C. Anal. for $C_{32}H_{35}FeN_9O_7$ (712.51): calc. C 53.94, H 4.81, N 17.69; found C 53.52, H 4.65, N 17.60. UV-Vis (MeOH, ε [M^{-1} cm^{-1}]): λ_{max} = 318 (5400), 540 (6400) nm. ESI-MS: *m/z* = 650.22 {$[M-NO_3]^+$, calc. 650.20}.

[Fe(L4)(tcc)] (5). To an orange solution of $Fe(NO_3)_3{\cdot}9H_2O$ (220 mg, 0.54 mmol) in methanol (10 mL) was added a solution of H**L4** (162 mg, 0.54 mmol) and 1 eq Et_3N (77 μL) in methanol (10 mL) and immediately a color change to dark blue was observed. The reaction mixture was stirred for 30 min at 50 ºC. A solution of H_2tcc (135 mg, 0.54 mmol) and 2.2 eq of Et_3N (170 μL) in methanol (10 mL) was added to the reaction mixture. The now purple reaction mixture was then stirred for 30 min at elevated temperature, cooled to room temperature and concentrated to 3 mL *in vacuo*. The crude product was precipitated with water, separated off and washed with water (3 × 50 mL) and diethyl ether (2 × 50 mL). The product was obtained as a purple powder (245 mg, 76%) Crystals suitable for X-ray diffraction were obtained by slow evaporation of a methanolic solution of **5** at room temperature. Anal. for $C_{22}H_{17}Cl_4FeN_4O_4$ (599.05): calc. C 44.11, H 2.86, N 9.35; found C 43.88, H 3.00, N 9.67. UV-Vis (MeOH, ε [M^{-1} cm^{-1}]): λ_{max} = 303 (8500), 560 (4000) nm. ESI-MS: *m/z* = 597.92 {$[M+H]^+$, calc 597.94}.

[Fe(L4)(dtbc)] (6). To an orange solution of $Fe(NO_3)_3 \cdot 9H_2O$ (304 mg, 0.75 mmol) in methanol (15 mL) was added a solution of H**L4** (224 mg, 0.75 mmol) and 1 eq Et_3N (110 μL) in methanol (20 mL) and immediately a color change was observed to dark blue. The reaction mixture was stirred for 20 min at elevated temperature. A solution of H_2dtbc (168 mg, 0.75 mmol) and 2.2 eq of Et_3N (230 μL) in methanol (10 mL) was added to the reaction mixture. The purple reaction mixture was then stirred for 20 min at elevated temperature, cooled to room temperature and concentrated to 2 mL *in vacuo*. The crude product was precipitated with water, separated off and washed with water (3 × 50 mL) and hexanes (2 × 50 mL). The product was obtained as a purple-black powder (410 mg, 95%). Anal. for $C_{30}H_{37}FeN_4O_4$ (573.48): calc. C 62.83, H 6.50, N 9.77; found C 62.75, H 6.71, N 9.58. UV-Vis (MeOH, ε [M^{-1} cm^{-1}]): λ_{max} = 316 (5400), 524(4000), 720 (sh, 2500) nm. ESI-MS: *m/z* = 573.14 {$[M]^+$, calc. 573.22}.

Oxygenation Reactions and Characterization of Oxygenation Products. In a typical reaction 25 mg of [Fe^{III}(**L4**)(dtbc)] (**6**) was dissolved in 40 mL of solvent and the purple solution was exposed to air and stirred for two weeks after which one equivalent of internal standard (1,3,5-tribromobenzene) was added to the solution. In the experiments with added proton donor one equivalent of $[Et_3NH]BF_4$ in dichloromethane (1 mL) was added to the purple solution. The solvent was then removed *in vacuo* and the residue was redissolved in 10 mL of DMF and 25 mL of 4M HCl was added to decompose the metal complexes. The resulting solution was extracted with chloroform (3 × 20 mL). The combined organic layers were washed with 1M HCl (20 mL) and water (20 mL), dried over $MgSO_4$, filtered, and evaporated *in vacuo*. The products were analyzed by GC-MS and ^{1}H NMR. The combined intradiol, extradiol and quinone products accounted for at least > 85% of the converted dtbc reactant. The quinone auto-oxidation product could not be accurately detected by GS-MS and the products were therefore quantified by ^{1}H NMR. Authentic samples of the intradiol products 3,5-di-*tert*-butyl-1-oxacyclohepta-3,5-diene-2,7-dione and 3,5-di-*tert*-butyl-5-carboxymethyl-2-furanone methyl ester were prepared according to a published procedure.[62] Authentic samples of the extradiol product isomers 3,5-di-*tert*-butyl-2-pyrone and 4,6-di-*tert*-butyl-2-pyrone were prepared by reacting [FeCl(dtbc)(Me_3-tacn)] with air as described by Que et al.[10]

X-ray crystal structure determinations of HL4, 4 and 5·H_2O. X-ray intensities were measured on a Nonius KappaCCD diffractometer with rotating anode and graphite monochromator (λ = 0.71073 Å) at a temperature of 150 K. The structures were solved with Direct Methods (SHELXS-97[63] for H**L4**, SIR2004[64] for **4**, and SIR97[65] for **5·H_2O**) and refined with SHELXL-97[66] against F^2 of all reflections. Geometry calculations and checking for higher symmetry were performed with the PLATON[48] program. H**L4** consisted of two crystal fragments, of which the intensities were integrated separately with the program EvalCCD.[67] Refinement was performed using a HKLF5 file.[68] All hydrogen atoms were located in the difference Fourier map. The OH hydrogen atom was refined freely with isotropic displacement parameters. All other hydrogen atoms were refined with a riding model. In **4**, all hydrogen atoms were located in the difference Fourier map and were refined with a riding model. In **5·H_2O**, all hydrogen atoms were located in the difference Fourier map. The OH hydrogen atoms were refined freely with isotropic displacement parameters. All other hydrogen atoms were refined with a riding model. Further crystallographic details are given in Table 6.

Table 6. Crystallographic data for compounds H**L4**, **4**, and **5·H_2O**

	H**L4**	**4**	**5·H_2O**
Formula	$C_{16}H_{18}N_4O_2$	$[C_{32}H_{34}FeN_8O_4](NO_3)$	$C_{22}H_{19}Cl_4FeN_4O_5$
Fw	298.34	712.53	617.06
crystal color	colorless	dark purple	black
crystal size [mm^3]	0.09 × 0.09 × 0.09	0.33 × 0.10 × 0.06	0.12 × 0.12 × 0.06
crystal system	Triclinic	monoclinic	triclinic
space group	$P\overline{1}$ (no. 2)	$P2_1/c$ (no. 14)	$P\overline{1}$ (no. 2)
a [Å]	8.6380(4)	13.9987(1)	9.4907(3)
b [Å]	8.8289(5)	12.2216(1)	10.8082(4)
c [Å]	10.9157(8)	19.6864(2)	13.2111(5)
α [°]	80.941(2)	–	106.1042(13)
β [°]	72.880(3)	101.9129(4)	102.8529(12)
γ [°]	67.299(3)	–	101.8027(13)
V [$Å^3$]	733.05(8)	3295.54(5)	1217.00(8)
Z	2	4	2
D_x [g/cm^3]	1.352	1.436	1.684
μ [mm^{-1}]	0.092	0.520	1.102
abs. corr. method	–	multiscan	multiscan
abs. corr. range	–	0.91-0.97	0.83-0.94
$(\sin\theta/\lambda)_{max}$ [$Å^{-1}$]	0.61	0.65	0.60
refl. (meas./unique)	7642 / 2722	73042 / 7533	15576 / 4292
param./restraints	207 / 0	448 / 0	336 / 0
R1/wR2 [$I>2\sigma(I)$]	0.0629 / 0.1409	0.0372 / 0.0905	0.0414 / 0.1026
R1/wR2 [all refl.]	0.1008 / 0.1646	0.0616 / 0.1007	0.0657 / 0.1163
S	1.081	1.091	1.068
$\rho_{min/max}$ [$e/Å^3$]	– 0.32 / 0.31	– 0.53 / 0.38	– 0.38 / 0.40

4.6 References

1. Bugg, T. D. H. *Tetrahedron* **2003**, *59*, 7075-7101.
2. Bugg, T. D. H.; Lin, G. *Chem. Commun.* **2001**, 941-952.
3. Costas, M.; Mehn, M. P.; Jensen, M. P.; Que, L., Jr. *Chem. Rev.* **2004**, *104*, 939-986.
4. Solomon, E. I.; Brunold, T. C.; Davis, M. I.; Kernsley, J. N.; Lee, S-K.; Lehnert, N.; Neese, F.; Skulan, A. J.; Yang, Y-S.; Zhou, J. *Chem. Rev.* **2000**, *100*, 235-349.
5. Koehntop, K. D.; Emerson, J. P.; Que, L., Jr. *J. Biol. Inorg. Chem.* **2005**, *10*, 87-93.
6. Ohlendorf, D. H.; Lipscomb, J. D; Weber, P. C. *Nature* **1988**, *336*, 403-405.
7. True, A. E.; Orville, A. M.; Pearce, L. L.; Lipscomb, J. D; Que, L., Jr. *Biochemistry* **1990**, *29*, 10847-10854.
8. Orville, A. M.; Lipscomb, J. D.; Ohlendorf, D. H. *Biochemistry* **1997**, *36*, 10052-10066.
9. Vetting, M. W.; Ohlendorf, D. H. *Structure* **2000**, *8*, 429-440.

10. Jo, D-H.; Que, L., Jr. *Angew. Chem. Int. Ed.* **2000**, *39*, 4284-4287.
11. Hitomi, Y.; Tase, Y.; Higuchi, M.; Tanaka, T.; Funabiki, T. *Chem. Lett.* **2004**, *33*, 316-317.
12. Borowski, T.; Siegbahn, P. E. M. *J. Am. Chem. Soc.* **2006**, *128*, 12941-12953.
13. Funabiki, T.; Yamazaki, T. *J. Mol. Cat. A* **1999**, *150*, 37-47.
14. Yamahara, R.; Ogo, S.; Masuda, H.; Watanabe, Y. *J. Inorg. Biochem.* **2002**, *88*, 284-294.
15. Hitomi, Y.; Yoshida, M.; Higuchi, M.; Minami, H.; Tanaka, T.; Funabiki, T. *J. Inorg. Biochem.* **2005**, *99*, 755-763.
16. Merkel, M.; Pascaly, M.; Krebs, B.; Astner, J.; Foxon, S. P.; Schindler, S. *Inorg. Chem.* **2005**, *44*, 7582-7589.
17. Mialane, P.; Tchertanov, L.; Banse, F.; Sainton, J.; Girerd, J.-J. *Inorg. Chem.* **2000**, *39*, 2440-2444.
18. Pascaly, M.; Duda, M.; Schweppe, F.; Zurlinden, K.; Müller, F. K.; Krebs, B. *J. Chem. Soc., Dalton Trans.* **2001**, 828-837.
19. Velusamy, M.; Mayilmurugan, R.; Palaniandavar, M. *J. Inorg. Biochem.* **2005**, *99*, 1032-1042.
20. Cox, D. D.; Benkovic, S. J.; Bloom, L. M.; Bradley, F. C.; Nelson, M. J.; Que, L., Jr. *J. Am. Chem. Soc.* **1988**, *110*, 2026-2032.
21. Cox, D. D.; Que, L., Jr. *J. Am. Chem. Soc.* **1988**, *110*, 8085-8092.
22. Jang, H. G.; Cox, D. D.; Que, L., Jr. *J. Am. Chem. Soc.* **1991**, *113*, 9200-9204.
23. Lauffer, R. B.; Heistand, R. H.; Que, L., Jr. *Inorg. Chem.* **1983**, *22*, 50-55.
24. Merkel, M.; Müller, F. K.; Krebs, B. *Inorg. Chim. Acta* **2002**, *337*, 308-316.
25. Ogo, S.; Yamahara, R.; Funabiki, T.; Masuda, H.; Watanabe, Y. *Chem. Lett.* **2001**, 1062-1063.
26. Shongwe, M. S.; Kaschula, C. H.; Adsetts, M. S.; Ainscough, E. W.; Brodie, A. M.; Morris, M. J. *Inorg. Chem.* **2005**, *44*, 3070-3079.
27. Velusamy, M.; Mayilmurugan, R.; Palaniandavar, M. *Inorg. Chem.* **2004**, *43*, 6284-6293.
28. Velusamy, M.; Palaniandavar, M.; Gopalan, R. S.; Kulkarni, G. U. *Inorg. Chem.* **2003**, *42*, 8283-8293.
29. Viswanathan, R.; Palaniandavar, M.; Balasubramanian, T.; Muthiah, T. P. *Inorg. Chem.* **1998**, *37*, 2943-2951.
30. Yamahara, R.; Ogo, S.; Watanabe, Y.; Funabiki, T.; Jitsukawa, K.; Masuda, H.; Einaga, H. *Inorg. Chim. Acta* **2000**, *300-302*, 587-596.
31. Bruijnincx, P. C. A.; Lutz, M.; Spek, A. L.; Hagen, W. R.; Weckhuysen, B. M.; van Koten, G.; Klein Gebbink, R. J. M. *J. Am. Chem. Soc.*, accepted for publication (Chapter 3 of this thesis).
32. Bruijnincx, P. C. A.; Lutz, M.; Spek, A. L. ; van Faassen, E. L.; Weckhuysen, B. M.; van Koten, G.; Klein Gebbink, R. J. M. *Eur. J. Inorg. Chem.* **2005**, 779-787 (Chapter 2 of this thesis).
33. Jameson, D. L.; Hilgen, S. E.; Hummel, C. E.; Pichla, S. L. *Tetrahedron Lett.* **1989**, *30*, 1609-1612.
34. Davis, J. C.; W.-J., Kung; Averill, B. A. *Inorg. Chem.* **1986**, *25*, 394-396.
35. Hayami, S.; Gu, Z.-Z.; Shiro, M.; Einaga, Y.; Fujishima, A.; Sato, O. *J. Am. Chem. Soc.* **2000**, *122*, 7126-7127.
36. Higgs, T. C.; Ji, D.; Czernuscewicz, R. S.; Carrano, C. J. *Inorg. Chim. Acta* **1999**, *286*, 80-92.
37. Lubben, M.; Meetsma, A.; van Bolhuis, F.; Feringa, B. L.; Hage, R. *Inorg. Chim. Acta* **1994**, *215*, 123-129.
38. Imbert, C.; Hratchian, H. P.; Lanznaster, M.; Heeg, M. J.; Hryhorczuk, L. M.; McGarvey, B. R.; Schlegel, H. B.; Verani, C. N. *Inorg. Chem.* **2005**, *44*, 7414-7422.
39. Jo, D-H.; Chiou, Y-M.; Que, L., Jr. *Inorg. Chem.* **2001**, *40*, 3181-3190.
40. Merkel, M.; Schnieders, D.; Baldeau, S. M.; Krebs, B. *Eur. J. Inorg. Chem.* **2004**, 783-790.
41. Mialane, P.; Anxolabéhère-Mallart, E.; Blondin, G.; Nivorojkine, A.; Guilhem, J.; Tchertanova, L.; Cesario, M.; Ravi, N.; Bominaar, E.; Girerd, J.-J.; Münck, E. *Inorg. Chim. Acta* **1997**, *263*, 367-378.
42. Ferraroni, M.; Seifert, J.; Travkin, V. M.; Thiel, M.; Kaschabek, S.; Scozzafava, A.; Golovleva, L.; Schlömann, M.; Briganti, F. *J. Biol. Chem.* **2005**, *280*, 21133-21154.
43. Ferraroni, M.; Solyanikova, I. P.; Kolomytseva, M. P.; Scozzafava, A.; Golovleva, L.; Briganti, F. *J. Biol. Chem.* **2004**, *279*, 27646-27655.

44. Ohlendorf, D. H.; Orville, A. M.; Lipscomb, J. D. *J. Mol. Biol.* **1994**, *244*, 586-608.
45. Vetting, M. W.; D'Argenio, D. A.; Ornston, L. N.; Ohlendorf, D. H. *Biochemistry* **2000**, *39*, 7943-7955.
46. Elgren, T. E.; Orville, A. M.; Kelly, K. A.; Lipscomb, J. D.; Ohlendorf, D. H.; Que, L., Jr. *Biochemistry* **1997**, *36*, 11504-11513.
47. Horsman, G. P.; Jirasek, A.; Vaillancourt, F. H.; Barbosa, C. J.; Jarzecki, A. A.; Xu, C.; Mekmouche, Y.; Spiro, T. G.; Lipscomb, J. D.; Blades, M. W.; Turner, R. F. B.; Eltis, L. D. *J. Am. Chem. Soc.* **2005**, *127*, 16882-16891.
48. Spek, A. L. *J. Appl. Cryst.* **2003**, *36*, 7-13.
49. Gaber, B. P.; Miskowski, V.; Spiro, T. G. *J. Am. Chem. Soc.* **1974**, *96*, 6868-6873.
50. Que, L., Jr.; Kolanczyk, R. C.; White, L. S. *J. Am. Chem. Soc.* **1987**, *109*, 5373-5380.
51. Bull, C.; Ballou, D. P.; Otsuka, S. *J. Biol. Chem.* **1981**, *256*, 12681-12686.
52. Hagen, W. R. *J. Magn. Reson.* **1981**, *44*, 447-469.
53. Hagen, W. R.; Dunham, W. R.; Sands, R. H.; Shaw, R. W.; Beinert, H. *Biochim. Biophys. Acta* **1984**, *765*, 399-402.
54. Priem, A. Explorations in high frequency EPR, PhD Thesis. Nijmegen University, The Netherlands, 2002. http://webdoc.ubn.kun.nl/mono/p/priem_a/explinhif.pdf
55. Priem, A.; van Bentum, P. J. M.; Hagen, W. R.; Reijerse, E. J. *Appl. Magn. Reson.* **2001**, *21*, 535-548.
56. Weissner, J. T.; Nilges, M. J.; Sever, M. J.; Wilker, J. J. *Inorg. Chem.* **2006**, *45*, 7736-7747.
57. Hagen, W. R. *Dalton Trans.* **2006**, 4415-4434.
58. Koch, W. O.; Krüger, H.-J. *Angew. Chem. Int. Ed.* **1995**, *34*, 2671-2674.
59. Higuchi, M.; Hitomi, Y.; Minami, H.; Tanaka, T.; Funabiki, T. *Inorg. Chem.* **2005**, *44*, 8810-8821.
60. Fujii, H.; Funahashi, Y. *Angew. Chem. Int. Ed.* **2002**, *41*, 3638-3641.
61. Kurahashi, T.; Oda, K.; Sugimoto, M.; Ogura, T.; Fujii, H. *Inorg. Chem.* **2006**, *45*, 7709-7721.
62. Demmin, T. R.; Rogic, M. M. *J. Org. Chem.* **1980**, *45*, 1153-1156.
63. Sheldrick, G. M. *SHELXS-97. Program for crystal structure solution*, University of Göttingen: Germany, 1997.
64. Burla, M. C.; Caliandro, R.; Camalli, M.; Carrozzini, B.; Cascarano, G. L.; De Caro, L.; Giacovazzo, C.; Polidori, G.; Spagna, R. *J. Appl. Cryst.* **2005**, *38*, 381-388.
65. Altomare, A.; Burla, M. C.; Camalli, M.; Cascarano, G. L.; Giacovazzo, C.; Guagliardi, A.; Moliterni, A. G. G.; Polidori, G.; Spagna, R. *J. Appl. Cryst.* **1999**, *32*, 115-119.
66. Sheldrick, G. M. *SHELXL-97. Program for crystal structure refinement*, University of Göttingen: Germany, 1997.
67. Duisenberg, A. J. M.; Kroon-Batenburg, L. M. J.; Schreurs, A. M. M. *J. Appl. Cryst.* **2003**, *36*, 220-229.
68. Herbst-Irmer, R.; Sheldrick, G. M. *Acta Cryst.* **1998**, *B54*, 443-449.

CHAPTER 5

Iron(II) Complexes with Bio-Inspired *N,N,O* Ligands as Oxidation Catalysts: Olefin Epoxidation and *Cis*-Dihydroxylation

Abstract

Ferrous complexes of the type $[FeL_2]$ have been synthesized with the ligands 3,3-bis(1-methylimidazol-2-yl)propionate (**L1**) and its neutral ester analogue propyl 3,3-bis(1-methylimidazol-2-yl)propionate (**PrL1**). Different coordination modes of the ester ligand were found depending on the crystallization conditions. In the complex $[Fe(\mathbf{PrL1})_2](X)_2$ (X = OTf, BPh_4) the ligand coordinates as a tridentate *N,N,O* tripod, whereas in $[Fe(\mathbf{PrL1})_2(MeOH)_2](OTf)_2$ a bidentate *N,N* coordination mode is found. The complexes were tested in the oxidation of olefins and found to be active catalysts, capable of both epoxidation and *cis*-dihydroxylation of several different substrates.

P. C. A. Bruijnincx, I. L. C. Buurmans, S. Gosiewska, M. Lutz, A. L. Spek, G. van Koten, R. J. M. Klein Gebbink, to be submitted for publication

5.1 Introduction

The selective and catalytic oxidation of organic substrates is an important area of research in both academia and industry.[1] Nature has developed several strategies for dioxygen activation and uses metalloenzymes to selectively oxidize and functionalize hydrocarbons. An important group of these metalloenzymes are the non-heme iron oxygenases.[2,3] A specific subset that utilizes a mononuclear, non-heme iron(II) center coordinated by the so-called 2-His-1-carboxylate facial triad has recently emerged as a common, versatile platform for these oxidative transformations.[4] The Rieske dioxygenases belong to this class of enzymes and catalyze the stereospecific *cis*-dihydroxylation of arenes as the first step in the biodegradation of these compounds. Naphthalene 1,2-dioxygenase (NDO) was the first Rieske dioxygenase that has been characterized crystallographically.[5] The active site of NDO with bound substrate and the *cis*-dihydroxylation reaction are shown in Figure 1. It features a mononuclear iron center coordinated by two histidines and a bidentate aspartate in a variation on the 2-His-1-carboxylate facial triad.[5] This bidentate binding mode is found in some but not all crystallographically characterized Rieske dioxygenases.[6]

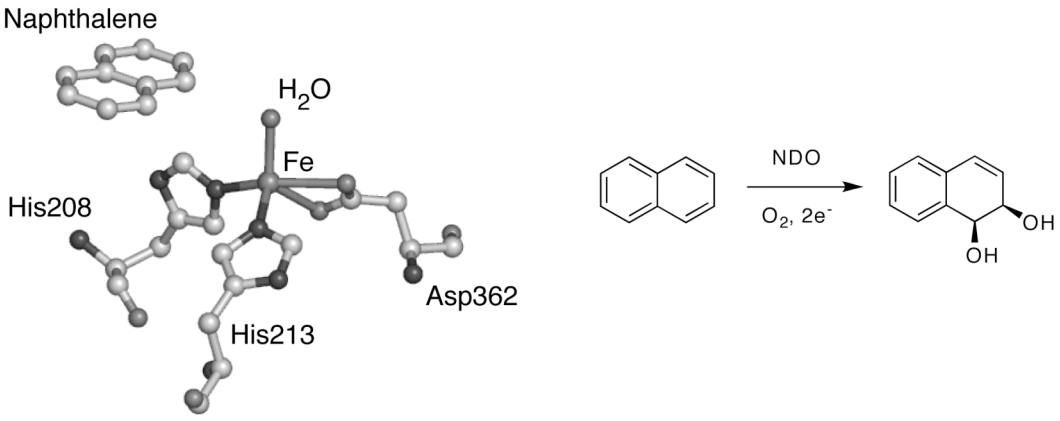

Figure 1. Active site of naphthalene 1,2-dioxygenase (NDO), a Rieske dioxygenase, with bound substrate (1O7G.pdb). The catalyzed *cis*-dihydroxylation reaction is shown on the right.

The unique reactivity of non-heme iron enzymes has inspired the development of synthetic non-heme iron complexes as potential oxidation catalysts.[1,2] The family of tpa- and bpmen-based catalysts developed by Que *et al.*, for instance, catalyzes the epoxidation and/or *cis*-dihydroxylation of olefins with H_2O_2 as oxidant.[7-9] These catalysts therefore serve as excellent functional models of the non-heme iron oxygenases. Other mononuclear iron systems capable of olefin epoxidation have also been reported.[10-14] All ligands employed in these studies provide the metal center with an all-*N* donor set, that does not accurately reflect the N_{im},N_{im},O_{carb} ligand environment found at the active site of the enzymes. For this reason, attention has been recently devoted to the development of iron complexes with mixed donor ligands.[15-19] Burzlaff *et al.* have, for example reported on the iron coordination chemistry of the bispyrazolylacetate *N*,*N*,*O* ligand system,[15,16] and Que *et al.* recently communicated a very

effective olefin cis-dihydroxylation catalyst based on the (bis-(2-pyridyl)methyl)benzamide ligand.[18] A different approach to the isolation of mononuclear iron(II) complexes with a $N,N,O_{carboxylato}$ donor set has also been recently reported and involves the use of sterically hindered bidentate *N* and monodentate *O* donor ligands.[20]

As part of our efforts to build suitable models that mimic the active site of non-heme iron(II) enzymes which exhibit the so-called 2-His-1-carboxylate facial triad,[2,4] we have been studying the coordination chemistry of the substituted bis(1-alkylimidazol-2-yl)propionate ligand family[21,22] and have synthesized mononuclear iron complexes that accurately mimic the coordination environment of the 2-His-1-carboxylate facial triad.[23] Here, we describe the synthesis and structural characterization of bio-inspired iron(II) complexes with the ligand 3,3-bis(1-methylimidazol-2-yl)propionate (**L1**) and its neutral ester analogue propyl 3,3-bis(1-methylimidazol-2-yl)propionate (**PrL1**) (Chart 1). The latter complexes were found to be active catalysts in the epoxidation and *cis*-dihydroxylation of olefinic substrates.

Chart 1. Ligands **L1** and **PrL1**

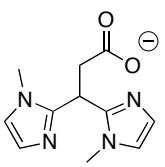

L1

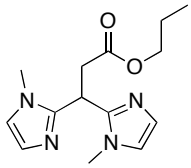

PrL1

5.2 Results

Synthesis and Characterization of the iron(II) complexes 1-4. In Chapter 2 we reported the synthesis and copper(II) coordination chemistry of the new bis(1-alkylimidazol-2-yl)propionate ligand family.[21,22] In analogy to the $[CuL_2]$ complexes, we synthesized the 2:1 ferrous complex with ligand **L1** (Figure 2). The addition of half an equivalent of $Fe^{II}(OTf)_2 \cdot 2MeCN$ to a solution containing the tetrabutylammonium salt of **L1** (3,3-bis(1-methylimidazol-2-yl)propionate) in methanol, resulted in the formation of neutral $[Fe^{II}(\mathbf{L1})_2]$ (**1**). The white product was analyzed by ESI-MS, IR spectroscopy, and elemental analysis. The ESI-MS and elemental analysis data point to the formation of a mononuclear, neutral species with a 2:1 ligand to metal ratio. The major peaks at *m*/*z* 523.00 and 261.98 in the ESI-MS spectrum correspond to the $[Fe(\mathbf{L1})_2+H]^+$ and $[Fe(\mathbf{L1})_2+2H]^{2+}$ ions, respectively. The IR absorption spectrum obtained for the iron(II) complex is similar to that of the copper(II) complex[22] and, most importantly, the asymmetric stretching vibration of the carboxylato group is found at the same frequency (ν_{as} = 1580 cm^{-1}). This indicates that the carboxylato group is bound to the metal in the same fashion. The symmetric stretch of the carboxylato group is assigned to the absorption at 1392 cm^{-1}, which results in a $\Delta(\nu_{as}-\nu_s)$ of 188 cm^{-1}. It has been recently shown, that this Δ value is determined by the coordination mode symmetry and thus provides a useful structural probe.[24] The $\Delta(\nu_{as}-\nu_s)$ value is identical to $\Delta(\nu_{as}-\nu_s)_{ionic}$ obtained for the corresponding free carboxylate $K[\mathbf{L1}]$[22] and thus indicative of a monodentate

binding mode of the carboxylate.[24] Based on this data, the structure of $[Fe^{II}(\mathbf{L1})_2]$ (**1**) is proposed to be isostructural to the corresponding copper(II) complex $[Cu^{II}(\mathbf{L1})_2]$[22] (Figure 2). Two **L1** ligands facially cap the iron(II) metal center in **1** through both imidazole *N* and the carboxylato *O* donor atoms, very similar to the coordination observed for the 2-His-1-carboxylate facial triad.[2,4] The solution magnetic moment of **1** in D_2O as determined by Evans' NMR method[25,26] amounts to 5.2 μ_B, which is consistent with a high-spin configuration (S = 2) at ambient temperature. Unfortunately, attempts at obtaining single crystals of complex **1** for X-ray analysis failed.

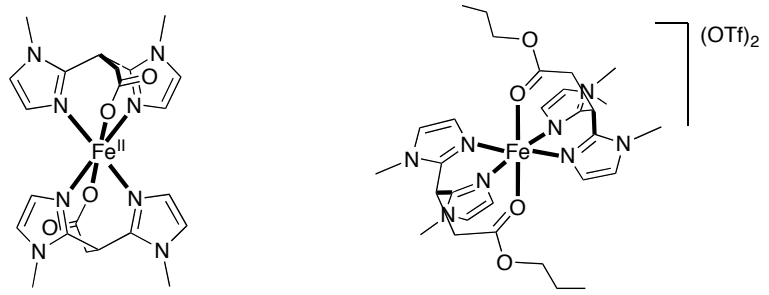

$[Fe^{II}(\mathbf{L1})_2]$ (**1**) $[Fe^{II}(\mathbf{PrL1})_2](OTf)_2$ (**2**)

Figure 2. Iron(II) complexes $[Fe^{II}(\mathbf{L1})_2]$ (**1**) and $[Fe^{II}(\mathbf{PrL1})_2](OTf)_2$ (**2**).

Preliminary catalytic results in alkane and alkene oxidations with H_2O_2 showed that **1** is not an active catalyst for these kinds of transformations (*vide infra*). We, therefore, also synthesized ferrous complexes with the neutral ligand **PrL1** (propyl 3,3-bis(1-methylimidazol-2-yl)propionate), the propyl ester precursor of **L1**. The mononuclear complex $[Fe^{II}(\mathbf{PrL1})_2](OTf)_2$ (**2**) was synthesized by reacting two equivalents of **PrL1** with $Fe^{II}(OTf)_2 \cdot MeCN$ in methanol affording an off-white solid that could be recrystallized from acetonitrile/diethyl ether. In the IR absorption spectrum of **2** the ν(C=O) absorption frequency appears at 1689 cm^{-1}, a shift of 35 cm^{-1} to lower wavenumbers compared to the free ligand (ν(C=O): 1724 cm^{-1}). A similar shift has been observed before upon coordination of an ester carbonyl functionality to an iron(II) metal center.[17] Furthermore, the four sharp single vibrations at 1259 ($\nu_{as}SO_3$), 1216 (ν_sCF_3), 1153 ($\nu_{as}CF_3$), 1030 (ν_sSO_3) cm^{-1} are indicative of the presence of non-coordinated triflate anions.[17,27,28] This implies that both ligands **PrL1** are coordinated as a tridentate *N,N,O* ligand (Figure 2). This notion is further corroborated by the X-ray crystal structure determination of the complex $[Fe^{II}(\mathbf{PrL1})_2](BPh_4)_2$ (**3**) (*vide infra*), which features two facially coordinated **PrL1** ligands. The solution magnetic moment of $[Fe^{II}(\mathbf{PrL1})_2](OTf)_2$ (**2**) in acetone-d_6 was found to be 5.1 μ_B, consistent with a high spin iron(II) metal center.

In order to exclude any possible coordination of the anion to the metal in solution and/or participation of the anion in hydrogen bonding, such as observed in **4** (*vide infra*), we exchanged the triflates in **2** for the non-coordinating tetraphenylborate anions. $[Fe(\mathbf{PrL1})_2](BPh_4)_2$ (**3**) was synthesized by the addition of a methanolic solution of $NaBPh_4$ to a solution of **2** in methanol followed by the addition of water, which resulted in immediate precipitation of the crude product. The product was recrystallized from an acetonitrile/diethyl

ether mixture and characterized by IR spectroscopy, ESI-MS, elemental analysis, and X-ray crystal structure determination. The observed sharp carbonyl stretch vibration at 1677 cm^{-1} again reflects the coordination of the carbonyl group of the ester functionality to the ferrous metal center. [Fe(**PrL1**)$_2$](BPh$_4$)$_2$ (**3**) is a high spin iron(II) complex (μ_{eff} = 5.0 μ_B). From the data given above it can be concluded that both complexes **2** and **3** have isostructural cations in the solid state.

Crystal structure of [Fe(PrL1)$_2$](BPh$_4$)$_2$ (3). Colorless crystals of **3** suitable for X-ray diffraction were obtained by slow evaporation of a dichloromethane solution of **3**. The molecular structure of **3** is depicted in Figure 3, with selected bond lengths and angles presented in Table 1.

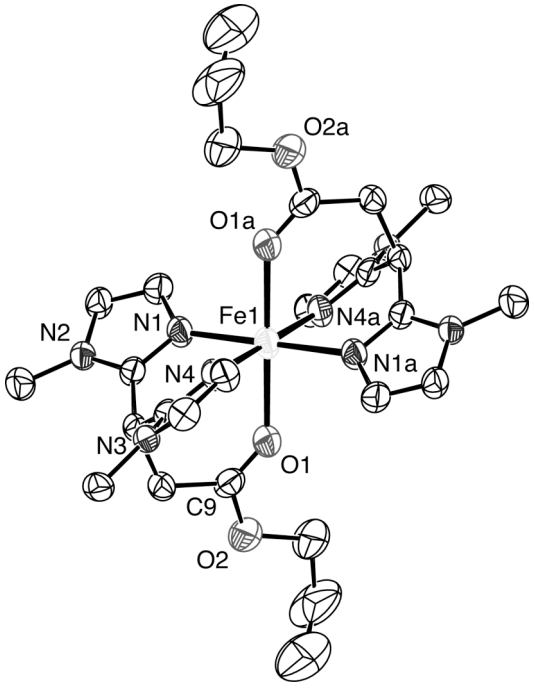

Figure 3. Molecular structure of the [Fe^{II}(**PrL1**)$_2$]$^{2+}$ cation of **3** in the crystal. All hydrogen atoms, the tetraphenylborate anion and disordered solvent molecules have been omitted for clarity. Displacement ellipsoids are drawn at the 50% probability level. Symmetry operation a: 1 – x, 1 – y, 1 – z.

The crystal structure of **3** consists of discrete mononuclear molecules. The iron(II) metal ion is situated on a crystallographic inversion center and two neutral **PrL1** ligands are centrosymmetrically arranged around the metal. The ligands facially cap the metal center through all three donor groups, i.e. two 1-methylimidazole nitrogens and the carbonyl oxygen of the ester functionality, resulting in a six coordinate iron(II) metal center with a N_4O_2 donor set and nearly ideal octahedral geometry. The deviation from ideal octahedral geometry is reflected in the (diminished) angles, which are mainly dictated by the inherent geometrical restrictions imposed by the tripodal ligand. The Fe–N distances (Fe1–N1 2.122(2) Å, Fe1–N4 2.100(2) Å) are characteristic of a high-spin iron(II) metal center and are comparable to those found in high-spin iron(II) complexes with poly-imidazole ligands.[29,30] The structure is similar

to the iron(II) complex $[Fe^{II}(Ph\text{-}dpah)_2](OTf)_2$ (Ph-dpah, (di-2-(pyridyl)methyl)benzamide) recently reported by Que et al.,[18] featuring an N_4O_2 donor set of four pyridines and two amide carbonyl oxygens. Although the average Fe–N bond lengths in **3** are shorter than those in $[Fe^{II}(Ph\text{-}dpah)_2](OTf)_2$ (2.11 Å vs. 2.18 Å), the Fe–O distance of 2.228(2) Å in **3** is considerably longer than the amide carbonyl oxygen to iron distance of 2.043 Å. This difference in the coordination strength of an amide carbonyl and an ester carbonyl to an iron(II) metal center has been observed before.[31] The coordination of an ester group to a ferrous metal center is rather rare and only few structurally characterized examples have been reported.[17,31-33]

Table 1. Selected bond lengths (Å) and angles (°) for $[Fe(\mathbf{PrL1})_2](BPh_4)_2$ (**3**)

Bond length		Angle	
Fe1–N1	2.122(2)	N1–Fe1–N4	86.35(9)
Fe1–N4	2.100(2)	N4–Fe1–O1	87.94(8)
Fe1–O1	2.228(2)	N1–Fe1–O1	86.60(9)
		N1–Fe1–N4a	93.66(9)
C9–O1	1.216(4)	N1–Fe1–O1a	93.41(9)
C9–O2	1.332(4)	N4–Fe1–O1a	92.06(8)

Crystal structure of $[Fe(PrL1)_2(MeOH)_2](OTf)_2$ (4). Recrystallization of $[Fe(\mathbf{PrL1})_2](OTf)_2$ (**2**) from methanol and diethyl ether, resulted in the formation of complex **4**, whose structure was determined by X-ray diffraction. In $[Fe(\mathbf{PrL1})_2(MeOH)_2](OTf)_2$ (**4**), the ester carbonyl functionalities of both ligands are *not* coordinated to the ferrous metal center. IR analysis of the crystals showed that the carbonyl stretch vibration ν(C=O) is split in two signals at 1732 and 1724 cm^{-1} of almost equal intensity close to the value of the free ligand. The two signals are probably the result of the slightly different orientations of the ligands around the metal ion, as seen in the crystal structure of **4**. The solution magnetic moment of $[Fe(\mathbf{PrL1})_2(MeOH)_2](OTf)_2$ (**4**) in acetone-d_6 is 5.2 μ_B, consistent with a high-spin iron(II) complex. Colorless crystals of **4** suitable for X-ray diffraction were obtained by slow diffusion of diethyl ether into a solution of **2** in methanol. The molecular structure of **4** is given in Figure 4, with selected bond lengths and angles presented in Table 2.

The crystal structure of **4** consists of discrete mononuclear molecules. In the complex cation of **4**, two ligands **PrL1** bind to the metal center in an N_2-bidentate fashion through the *N* donor atoms of the 1-methylimidazole groups. The propoxy group of one of the non-coordinated ester groups is disordered over two positions with occupancies of 62.1% and 37.9% for the major and minor component, respectively. The orientation of the ligands resembles the one found in $[Fe^{II}(L)_2(OH)]BF_4$ (L, bis(1-methylimidazol-2-yl)-3-methylthiopropanol), in which the thioether tail is similarly pointing away from the metal center.[29] The fifth and sixth coordination sites are occupied by two *cis*-positioned methanol molecules, completing the distorted octahedral N_4O_2 coordination sphere around the Fe(II)

ion. The Fe–N distances are rather different, ranging from 2.135(2) Å for Fe1–N31 to 2.170(2) Å for Fe1–N32. Both the imidazole groups at the longest and shortest distance are located *trans* to a methanol molecule. The average Fe–N distance is 2.16 Å, characteristic of a high-spin iron(II) species. The Fe–N distances are longer than those observed in $[Fe(\mathbf{PrL1})_2](BPh_4)_2$ (**3**). The Fe–O bond lengths of both methanol molecules are similar and on average amount to 2.20 Å, a value that compares well to the Fe–O distance found for the methanol molecule located *trans* to a pyridine donor group (Fe–O = 2.195 Å) in $[Fe^{II}(tpa)(MeOH)_2](BPh_4)_2 \cdot MeOH$ (tpa, tris(2-pyridylmethyl)amine).[34]

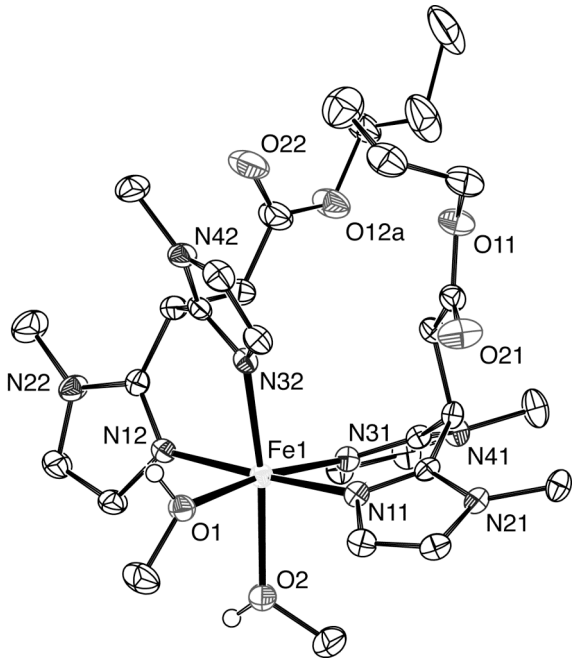

Figure 4. Molecular structure of the $[Fe^{II}(\mathbf{PrL1})_2(MeOH)_2]^{2+}$ cation of **4** in the crystal. C–H hydrogen atoms and triflate anions have been omitted for clarity. Only the major disorder component (62.1% occupancy) of the disordered propoxy group is depicted. Displacement ellipsoids are drawn at the 50% probability level.

Table 2. Selected bond lengths (Å) and angles (°) for $[Fe(\mathbf{PrL1})_2(MeOH)_2](OTf)_2$ (**4**)

	Bond length		Angle		Angle
Fe1–N11	2.161(2)	N32–Fe1–O2	171.23(8)	N31–Fe1–N32	101.75(8)
Fe1–N12	2.154(2)	N11–Fe1–N12	175.78(8)	N32–Fe1–O1	84.80(8)
Fe1–N31	2.135(2)	N31–Fe1–O1	171.65(8)	O1–Fe1–O2	86.62(8)
Fe1–N32	2.170(2)			O2–Fe1–N31	86.96(8)
Fe1–O1	2.1941(19)	N11–Fe1–N31	84.58(8)	N12–Fe1–N32	84.63(8)
Fe1–O2	2.209(2)	N31–Fe1–N12	97.79(8)	N32–Fe1–N11	91.48(8)
		N12–Fe1–O1	87.89(8)	N11–Fe1–O2	90.33(8)
		O1–Fe1–N11	90.13(8)	O2–Fe1–N12	93.27(8)

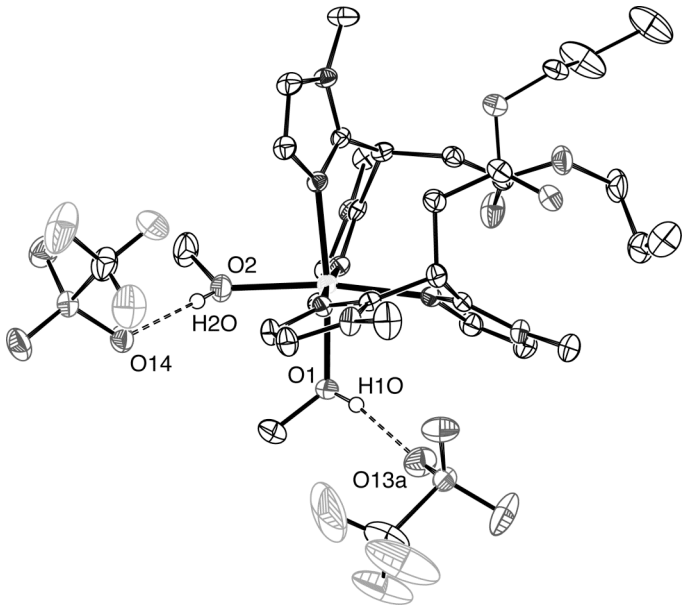

Figure 5. Hydrogen bonding pattern in $[Fe^{II}(\mathbf{PrL1})_2(MeOH)_2](OTf)_2$ (**4**). C–H Hydrogen atoms have been omitted for clarity. Only the major disorder component of the disordered propoxy group is depicted. Symmetry operation a: x – 1, y, z.

Each methanol ligand is involved in a hydrogen bond, acting as a hydrogen bond donor with a triflate oxygen as acceptor. The hydrogen bonding pattern is shown in Figure 5 and relevant angles and distances are given in Table 3.

Table 3. Selected hydrogen bond lengths (Å) and angles (°) for $[Fe^{II}(\mathbf{PrL1})_2(MeOH)_2](OTf)_2$ (**4**). Symmetry operation a: x – 1, y, z

Donor–H ··· Acceptor	D–H	H ··· A	D ··· A	D–H ··· A
O1–H1O ··· O13a	0.79(3)	1.93(3)	2.705(3)	166(3)
O2–H2O ··· O14	0.75(3)	2.07(3)	2.812(3)	172(3)

Solution structures of 2-4 (ESI-MS and solution IR spectra). The crystal structures of **3** and **4** illustrate the possibility of different binding modes of the ligand **PrL1** to a ferrous ion. To determine the structure of the complexes in solution, the ESI-MS and solution IR spectra of complexes **2-4** were recorded. The position of the carbonyl stretch vibration was found to be indicative of the coordination mode of the ligand. Vibrations at distinct wavenumbers were observed for the coordinated and non-coordinated ester carbonyl group vibrations in the solid state (Table 4). The energies of these vibrations corroborate the structural information provided by the crystal structures. The solution IR spectra were found to be very solvent dependent. Unfortunately, due to the limited solubility of $[Fe(\mathbf{PrL1})_2](BPh_4)_2$ (**3**) in methanol and dichloromethane, data could only be obtained for an acetonitrile solution of this compound. Interestingly, the IR spectra of **2** and **3** in acetonitrile

are identical in the carbonyl absorption region (Figure 6). Two absorptions at 1737 and 1702 cm^{-1} were observed, corresponding to non-coordinated and coordinated ester carbonyl groups, respectively. Furthermore, four sharp vibrations at 1272, 1227, 1156 and 1035 cm^{-1} were found for the triflate anions of **2**. The data suggests that dissociation of the ester groups and subsequent replacement with acetonitrile solvent molecules happens to the same extent for both **2** and **3**. This is important since vacant sites on the metal center are a necessary requirement for metal-based catalysis (*vide infra*). Identical spectra were also obtained for methanolic solutions of [Fe(**PrL1**)$_2$](OTf)$_2$ (**2**) and [Fe(**PrL1**)$_2$(MeOH)$_2$](OTf)$_2$ (**4**), with the major carbonyl stretch at 1740 cm^{-1}. This suggests a quite facile ligand rearrangement process in methanol solution and the structure of the cation of **2** and **4** in solution might actually resemble more the structure of the cation observed in the crystal structure of **4**. The vibrations associated with the triflate anions are rather broad and several shoulders were observed. This indicates that not all triflate anions are non-coordinated, but part of them are either directly bound to the metal center or involved in hydrogen bonds with coordinated solvent molecules. Finally, spectra recorded in the non-coordinating solvent dichloromethane showed the carbonyl vibration around 1695 cm^{-1} for both **2** and **4**, indicating coordination of the ester carbonyl functionalities.

Table 4. Solid state and solution IR vibrations of the carbonyl groups in complexes **2**-**4**[a]

ν(C=O)[b] (cm^{-1})	[Fe(**PrL1**)$_2$](OTf)$_2$ (**2**)	[Fe(**PrL1**)$_2$](BPh$_4$)$_2$ (**3**)	[Fe(**PrL1**)$_2$(MeOH)$_2$](OTf)$_2$ (**4**)
Solid	1689	1677	1732, 1724
MeCN	**1737**, 1702	**1737**, 1702	n.d.[d]
MeOH	**1740**, 1704 (sh)	i.s.[c]	**1740**, 1707 (sh)
CH_2Cl_2	1727 (sh), **1694**	i.s.	1732, **1697**

[a] The signal with the strongest absorption is reported in bold. [b] Free ligand **PrL1**: 1724 and 1735 cm^{-1} for solid state and MeCN solution, resp. [c] i.s. insufficiently soluble [d] n.d. not determined

ESI-MS measurements indicate the presence of mononuclear species in solution for all complexes (Figure 6), with the {[Fe(**PrL1**)$_2$]}$^{2+}$ and {[Fe(**PrL1**)$_2$](X)}$^{+}$ (X=OTf, BPh$_4$) ions as the major species. Interestingly, the 1:1 ligand to iron complex and free ligand are also observed in the ESI-MS spectrum (*m*/*z* 481.021). This feature is not observed in dichloromethane solution (data not shown), which indicates that a ligand dissociation-association equilibrium only takes place in coordinating solvents.

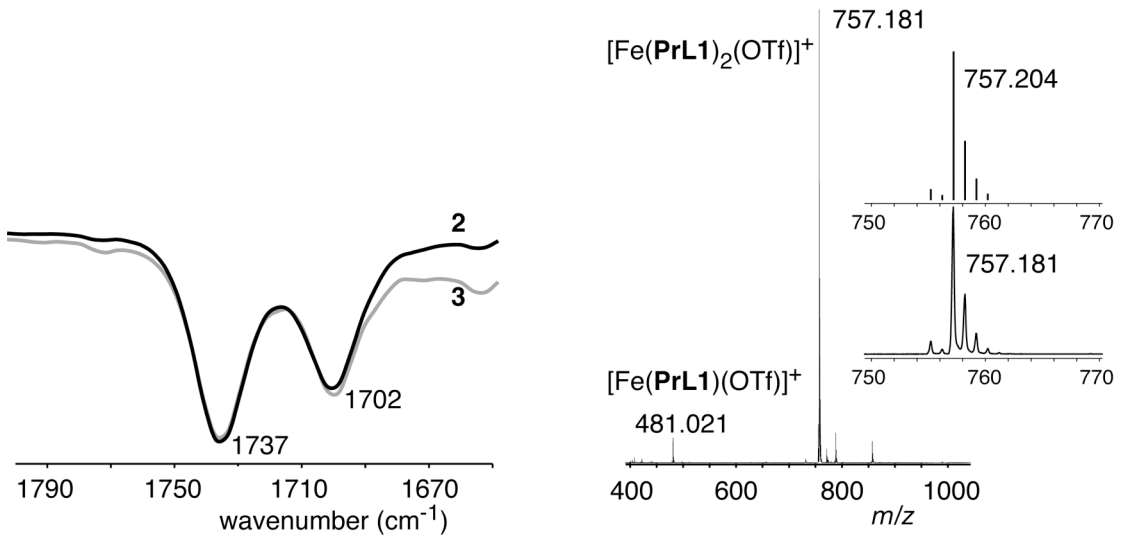

Figure 6. Left: solution IR spectra of [Fe(**PrL1**)$_2$](OTf)$_2$ (**2**) (black) and [Fe(**PrL1**)$_2$](BPh$_4$)$_2$ (**3**) (grey) in acetonitrile. Right: electrospray ionization mass spectrum for [Fe^{II}(**PrL1**)$_2$](OTf)$_2$ (**2**) in methanol. The inset shows the measured and calculated isotope distribution pattern for the {[Fe^{II}(**PrL1**)$_2$](OTf)}$^+$ cation.

Oxidation catalysis. Complexes **1**, **2** and **3** were tested in the oxidation of several different alkenes in acetonitrile solution with H_2O_2 as the oxidant. The catalytic reactions were performed at ambient conditions by slow, dropwise addition of 10 equivalents of H_2O_2 over 20 min, in order to minimize peroxide disproportionation. The oxidations of styrene and cyclohexene were run under N_2 atmosphere to suppress autoxidation of the substrate. [Fe^{II}(**L1**)$_2$] (**1**) was found to be incapable of catalyzing the oxidation of olefins with H_2O_2 as oxidant. The coordination of two monoanionic ligands in **1** probably results in relatively slow ligand exchange and hence coordinative saturation at the metal center. This in turn hampers the interaction of the metal with either peroxide or substrate and makes **1** ineffective in catalysis.

Table 5 summarizes the results obtained in the olefin oxidation experiments with **2** and **3**. [Fe(**PrL1**)$_2$](OTf)$_2$ (**2**) catalyzes the epoxidation and *cis*-1,2-dihydroxylation of various olefins with the conversion of H_2O_2 ranging from 39-51%. The oxidation of cyclooctene with 10 eq of peroxide afforded a clean reaction with 1,2-epoxycyclooctane and *cis*-1,2-cyclooctanediol as the only products with 39% efficiency and an epoxide/diol ratio of 2.5 : 1. A slight preference for epoxidation is also observed for the substrates styrene and cyclohexene. For 1-octene, the formation of the *cis*-diol product was favored over the epoxide by a factor of almost two. A small amount of benzaldehyde was found in the oxidation of styrene (0.6 and 1.1 TON for **2** and **3**, resp.) A considerable amount of the allylic oxidation product 2-cyclohexen-1-ol (7.9 turnovers), but no 2-cyclohexen-1-one, was observed with cyclohexene as a substrate. The addition of more equivalents of peroxide resulted in a gradual drop in efficiency of the catalytic conversion. Control experiments showed that the diol product did not result from the hydrolysis of the epoxide under the experimental conditions.

The stereoselectivity of the reactions was studied by the oxidation of the *cis*- and *trans*-2-heptene isomers. The epoxidation of *cis*-2-heptene and *trans*-2-heptene occurs with high stereoselectivity to the corresponding *cis*- and *trans*-epoxides, i.e. with retention of configuration of 93 and 84%, respectively. In addition, the *cis*-dihydroxylation of both substrates also shows a high retention of configuration. The high stereoselectivity characterizes this oxidation as a true *cis*-dihydroxylation.

Table 5. Oxidation of alkenes catalyzed by [Fe(**PrL1**)$_2$](OTf)$_2$ (**2**) and [Fe(**PrL1**)$_2$](BPh$_4$)$_2$ (**3**) with H_2O_2

Substrate	eq H_2O_2	epoxide[a]		diol[a]		conversion (%)[b]		epoxide:diol ratio
		2	**3**	**2**	**3**	**2**	**3**	**2**
cyclooctene	10	2.8	0.8	1.1	0	39	8	2.5 : 1
	20	3.8	1.5	1.5	0	27	8	2.5 : 1
styrene[c,d]	10	2.3	1.2	1.7	0	40	12	1.4 : 1
	20	4.9	2.2	3.4	0	41	11	1.4 : 1
		2		**2**		**2**		**2**
1-octene	10	1.6		2.7		43		1 : 1.7
	20	2.4		4.5		35		1 : 1.9
	40	3.3		7.0		26		1 : 2.1
cyclohexene[c,e]	10	3.0		2.1		51		1.4 : 1
	20	5.0		3.9		45		1.3 : 1
trans-2-heptene	20	3.2 [93][f]		2.3 [91][f]		28		1.4 : 1
cis-2-heptene	20	6.2 [84][f]		6.3 [92][f]		63		1 : 1

[a] Yields expressed as turnover numbers (TON = mol product/mol catalyst). [b] Percent conversion of H_2O_2 into epoxide and *cis*-diol. [c] Reaction performed under N_2 atmosphere with deoxygenated solutions. [d] Some benzaldehyde formation was observed with TON = 0.6 and 1.1 for **2** and **3**, resp. [e] The allylic oxidation product 2-cyclohexen-1-ol was observed with TON = 7.9. [f] [%RC]: retention of configuration = 100 × (A – B)/(A + B), where A is the *cis*-dihydroxylation product with retention and B is the epimer.

Interestingly, [Fe(**PrL1**)$_2$](BPh$_4$)$_2$ (**3**) is a rather poor catalyst under the tested reaction conditions. Low turnovers numbers to epoxide are obtained in the oxidation of cyclooctene (0.8), styrene (1.2), 1-octene (0.2), and cyclohexene (0.6). No formation of diol is observed in these reactions. The difference in activity is remarkable, given the similar structure of the cations of **2** and **3** in solution (Figure 6). The influence of the anion on the accessible reaction pathways is therefore substantial and might be related to the possibility of hydrogen bonding

interactions with the reactive iron-based oxidant and the chemical stability of the anion under the reaction conditions. Instead, significant amounts of biphenyl were observed in the GC traces of reaction mixtures with **3** pointing to the degradation of the BPh_4 anion.

5.3 Discussion

The reaction of two equivalents of ligands **L1** or **PrL1** with a ferrous metal source resulted in the formation of the 2:1 ligand to metal complexes **1**, **2**, and **3**. In $[Fe^{II}(\mathbf{L1})_2]$ (**1**), the ligand facially caps the metal center with an *N,N,O* donor set, similar to the coordination observed at the active site of the mononuclear non-heme iron(II) enzymes featuring the 2-His-1-carboxylate facial triad.[2,4] In this respect, **1** is related to, but yet distinct from the iron(II)-bispyrazolylacetate complexes developed by Burzlaff *et al.*[15,16] Both ligand systems offer an monoanionic *N,N,O* donor set, but differ in the actual *N* donor groups. The X-ray crystal structure of $[Fe(\mathbf{PrL1})_2](BPh_4)_2$ (**3**) shows that **PrL1** is also able to facially cap a metal center through all donor atoms. However, the structure of **4** illustrates that the tridentate, facial capping mode of **PrL1** is not the only possible coordination mode of the ligand. In fact, solution IR measurements indicate the presence of both coordinated and non-coordinated carbonyl groups. It is interesting to note, that the weakly bound carbonyl donor groups are located *trans* to each other in the solid state structure of **3**, whereas the two solvent molecules in **4** occupy positions *cis* relative to each other. This requires a rearrangement of the ligands with respect to each other. The availability of two labile sites located *cis* to each other is important, since this is a necessary requirement for *cis*-dihydroxylation.[7,8] The combination of (step-wise) ligand dissociation and/or rearrangement leads to many possible isomers in solution (Figure 7). The combination of (solution) IR data and ESI-MS measurements suggests that all isomers are present in solution to a certain extent. The fact that **2** catalyzes the *cis*-dihydroxylation of alkenes implies that either species G or F contributes significantly to the catalytic reactions.

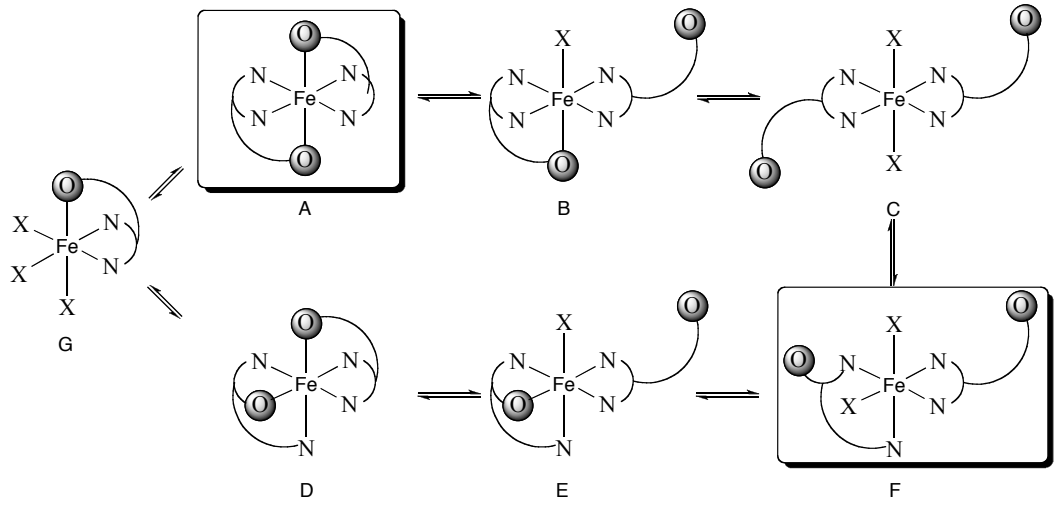

Figure 7. Possible solution structures of **2** and **3**. X denotes solvent or OTf, depending on the compound and conditions. The boxed species correspond to the crystal structures of **3** and **4**.

Only a few mononuclear iron complexes capable of epoxidation *and cis*-dihydroxylation have been reported to date.[8,9,13,35] The most well-studied examples of catalysts that elicit this type of reactivity are the prototypical tpa- and bpmen-based catalysts,[7,8] which both feature tetradentate N4 ligands. Related to these complexes are the N3py catalysts reported by Feringa *et al.*[13] Only very recently the first example of an iron complex with a facially coordinated *N*,*N*,*O* ligand capable of olefin *cis*-dihydroxylation was reported ([Fe(Ph-dpah)$_2$](OTf)$_2$).[18] [Fe(**PrL1**)$_2$](OTf)$_2$ (**2**) adds a new example to this rather exclusive set of iron-catalysts. Given the overall structural resemblance between [Fe(Ph-dpah)$_2$](OTf)$_2$ and [Fe(**PrL1**)$_2$](OTf)$_2$ (**2**), the difference in selectivity for epoxide or *cis*-diol formation is remarkable. Whereas [Fe(Ph-dpah)$_2$](OTf)$_2$ yields predominantly *cis*-diol product (it is actually the most efficient *cis*-dihydroxylation catalyst reported to date), **2** seems to slightly favor epoxidation.

The epoxide:diol product ratio has been correlated to the spin-state of iron(III)-hydroperoxide intermediates, with high-spin complexes leading to increased selectivity for the *cis*-diol product.[7] **2** features a high-spin metal center and is expected to yield a putative high-spin hydroperoxide intermediate upon reaction with H_2O_2, given the weak field exerted by the tridentate ligand. Yet, **2** is more selective for epoxide formation. The formation of a purple species was observed in the reaction of both **2** and **3** with *tert*-butyl hydroperoxide at low temperature, which indicates the formation of an Fe^{III}–OOtBu species[36-38] similar to the hydroperoxide intermediate invoked above. Interestingly, the purple species slowly converts into a second green intermediate. Further investigations of these intermediates and, e.g., their spin state are currently under way.

The influence of the anion on the observed catalytic activity of **2** and **3** is remarkable. The exchange of triflate for tetraphenylborates anions results in a complete loss of *cis*-dihydroxylation activity and a greatly diminished epoxidation efficiency. Solution IR studies and ESI-MS measurements, however, suggest that the structures of the cations of **2** and **3** in acetonitrile are similar and the influence of the anions should, therefore, be attributed either to second-sphere interactions or to BPh_4 anion degradation under the catalytic conditions (cf. biphenyl formation). Precedent for the role of second-sphere noncovalent interactions, e.g. hydrogen bonds, is found both in Nature and in biomimetic model systems.[39,40] The interesting catalytic properties of **2** might therefore be correlated with the ability of triflate anions to accept hydrogen bonds and in this way stabilize reactive intermediates of the catalytic cycle.

Finally, the molecular structure of [Fe(**PrL1**)$_2$(MeOH)$_2$](OTf)$_2$ (**4**) is of interest because of its resemblance to the active site of apocarotenoid-15-15'-oxygenase (ACO), a retinal-forming carotenoid oxygenase.[41] Carotenoids are precursors for retinal and its derivatives, which are crucial for vision and for the immune system.[42] ACO catalyzes the oxidative cleavage of the 15-15' double bond of its substrate. The crystal structure of the enzyme-substrate complex reveals a non-heme iron(II) active site, in which the metal center is coordinated by four histidine residues (Figure 8).[41]

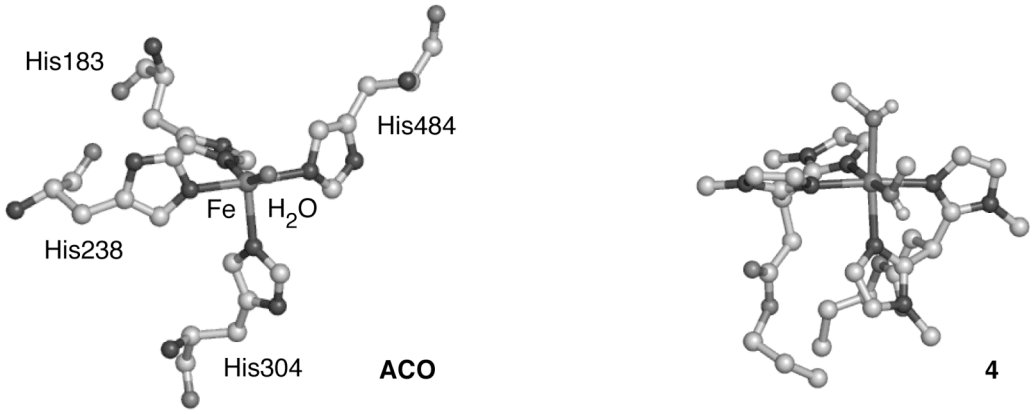

Figure 8. First coordination sphere of the mononuclear iron(II) enzyme apocarotenoid-15-15'-oxygenase (ACO, 2BIW.pdb) and that of complex $[Fe(\mathbf{PrL1})_2(MeOH)_2](OTf)_2$ (**4**).

This structural motif is relatively rare and has been reported in only four other enzymes.[43-46] The coordination geometry around the iron in ACO is octahedral with an average $Fe–N_{Im}$ distance of 2.17 Å and two *cis*-positioned coordination sites available for the binding of dioxygen. A water molecule occupies one of these sites, the other one being vacant in the reported crystal structure. $[Fe^{II}(\mathbf{PrL1})_2(MeOH)_2](OTf)_2$ (**4**) closely resembles the active site of apocarotenoid-15-15'-oxygenase (Figure 8). The biologically relevant 1-methylimidazole donor groups of **PrL1** accurately mimic the fourfold histidine coordination. The average Fe–N bond lengths (2.16 Å) agree well with the reported values. The second key structural feature is the availability of two *cis*-positioned vacant sites, which can be occupied by solvent molecules. The two coordinated methanol solvent molecules in **4** mimic this structural feature of the active site. The ester tails furthermore provide an entry into peptide chemistry to mimic the protein backbone and thus allow the inclusion of the second coordination sphere in modeling studies.

The oxidative cleavage of carotenoids was recently established as a dioxygenative process[47] and a side-on binding of dioxygen to the metal center has been suggested.[41] These mechanistic features are reminiscent of the Rieske dioxygenases,[5] which served as the inspiration for the biomimetic *cis*-dihydroxylation catalysts reported here. Further studies into the reactivity of the complexes presented here, might shed light on possible mechanistic similarities between these two classes of non-heme iron enzymes.

5.4 Concluding remarks

As part of our recent efforts on the structural and functional modeling of non-heme iron enzymes featuring the 2-His-1-carboxylate facial triad, we studied the ferrous coordination chemistry of the potentially tridentate, tripodal *N,N,O* ligands **L1** and **PrL1**. The molecular structures of **3** and **4** revealed two different binding modes of the new ligand **PrL1**, i.e. tridentate *N,N,O* and bidentate *N,N* coordination, respectively. Solution studies, however,

revealed the facile interconversion between the two different geometries. Complex $[Fe^{II}(\mathbf{PrL1})_2](OTf)_2$ (**2**), but not complex $[Fe^{II}(\mathbf{PrL1})_2](BPh_4)_2$ (**3**), was found to be an active catalyst in olefin oxidation reactions, which illustrates the importance of the anion. Complex **2** constitutes a new example of the rather exclusive class of non-heme iron catalysts that are capable of catalyzing both the epoxidation and *cis*-dihydroxylation of substrates.

5.5 Experimental Section

Air-sensitive organic reactions were carried out under an atmosphere of dry, oxygen-free N_2 using standard Schlenk techniques. THF and diethyl ether were dried over sodium benzophenone ketyl and distilled under N_2 prior to use. Methanol was dried over magnesium methoxide and distilled under N_2 prior to use. The air-sensitive iron complexes **1**-**4** were synthesized and handled under an N_2 atmosphere using standard Schlenk techniques. Solvents were thoroughly deoxygenated with N_2 before use. ^1H and $^{13}C\{^1H\}$ NMR spectra were recorded on a Varian AS400 or Varian Inova 300 spectrometer, operating at 25 °C. Infrared spectra were recorded with a Perkin-Elmer Spectrum One FT-IR instrument. Solution IR measurements were recorded with a Mettler Toledo ReactIR™ 1000 spectrometer with a SiComp™ probe which was fitted in a reaction vessel under N_2 atmosphere. GC analyses were performed on a Perkin Elmer Autosystem XL GC (30 m, PE-17 capillary column) and a Perkin Elmer Clarus 500 GC (30m, Econo-Cap EC-5) both with FID detector. Elemental microanalyses were carried out by the Microanalytisches Laboratorium Dornis & Kolbe, Mulheim a.d. Ruhr, Germany. ESI-MS spectra were recorded on a Micromass LC-TOF mass spectrometer at the Biomolecular Mass Spectrometry group, Utrecht University. UV-Vis spectra were recorded on a Varian Cary 50. Solution magnetic moments were determined by the Evans' NMR method in D_2O/1,4-dioxane (95/5 *v/v*) (**1**) or acetone-d_6/cyclohexane (95/5 *v*/*v*) (**2**-**4**) at 25 °C.[25,26] Tetrabutylammonium 3,3-bis(1-methylimidazol-2-yl)propionate ($[Bu_4N][\mathbf{L1}]$),[22] propyl 3,3-bis(1-methylimidazol-2-yl)propionate (**PrL1**),[22] and $Fe(OTf)_2{\cdot}2MeCN$[48] were prepared according to published procedures. The epoxides of *cis*- and *trans*-2-heptenes were synthesized by stereoselective epoxidation of the olefins with *m*CPBA. Hydrolysis of these epoxides by $HClO_4$ in H_2O/THF yielded the corresponding diols. All other chemicals were commercially obtained and used as received.

$[Fe(L1)_2]$ (1): To a solution of $[Bu_4N][\mathbf{L1}]$ (300 mg, 0.63 mmol) in methanol (20 mL) was added a solution of $Fe(OTf)_2{\cdot}2MeCN$ (275 mg, 0.31 mmol) in methanol (10 mL) and gradually a white precipitate formed. The reaction mixture was stirred for 1 h at 50 °C, after which diethyl ether was added to precipitate the product. The crude product was separated by centrifugation and washed twice with diethyl ether (2 × 40 mL). The product was obtained as a white powder (161 mg, 98%). Anal. for $C_{22}H_{26}FeN_8O_4$ (522.34): calc. C 50.59, H 5.02, N 21.45; found C 50.28, H 4.92, N 21.30. IR (solid): ν = 3120.2, 2946.8, 2906.3, 2815.2, 1580.2, 1506.7, 1426.0, 1392.4, 1310.1, 1286.9, 1230.4, 1163.0, 1140.4, 1045.2, 953.3, 771.9, 753.3 cm^{-1}. ESI-MS: *m/z* = 261.97 $\{[M+2H]^{2+}$, calc. 262.08$\}$, 523.00 $\{[M+H]^{+}$, calc. 523.15$\}$. Solution magnetic moment (Evans' method): μ_{eff} = 5.2 μ_B.

$[Fe(PrL1)_2](OTf)_2$ (2): To a solution of **PrL1** (506 mg, 1.83 mmol) in methanol (15 mL) was added a solution of $Fe(OTf)_2{\cdot}2MeCN$ (399 mg, 0.91 mmol) in methanol (10 mL) and the reaction mixture was stirred for 30 min. The solvent was evaporated *in vacuo* and the remaining off-white solid was recrystallized from an acetonitrile/diethyl ether mixture at – 30 °C overnight. The product was obtained as a slightly greenish

crystalline solid (430 mg, 52%). Anal. for $C_{30}H_{40}F_6FeN_8O_{10}S_2$ (906.65): calc. C 39.34, H 4.45, N 12.36; found C 39.75, H 4.64, N 12.48. IR (solid): ν = 3126.5, 2973.5, 1689.1, 1506.7, 1404.4, 1258.9, 1215.6, 1152.4, 1029.9, 948.7, 782.1, 755.3 cm^{-1}. ESI-MS: *m/z* = 277.12 {$[PrL1+H]^+$, calc 277.17}, 304.00 {$[M-2OTf]^{2+}$, calc. 304.13}, 481.02 {$[M-PrL1-OTf]^+$, calc. 481.05}, 757.20 {$[M-OTf]^+$, calc. 757.18}. Solution magnetic moment (Evans' method): μ_{eff} = 5.1 μ_B.

$[Fe(PrL1)_2](BPh_4)_2$ (3): To a solution of **PrL1** (312 mg, 1.13 mmol) in methanol (10 mL) was added a solution of $Fe(OTf)_2 \cdot 2MeCN$ (246 mg, 0.56 mmol) in methanol (10 mL) and the reaction mixture was stirred for 30 min. Subsequently, a solution of $NaBPh_4$ (1.1 g, 3.2 mmol) in methanol (10 mL) was added at once to the reaction mixture and immediately some white precipitate formed. The addition of water (50 mL) to the suspension caused further precipitation of the product. The suspension was stirred for 20 min, after which the solid was filtered off and washed three times with H_2O (3 × 20 mL) to yield an off-white powder. The crude product was recrystallized from acetonitrile/diethyl ether at – 30 ºC to give the product as a slightly greenish crystalline solid (401 mg, 57% yield). Single crystals of **3** suitable for X-ray diffraction were obtained by slow evaporation of a dichloromethane solution. Anal. for $C_{76}H_{80}B_2FeN_8O_4$ (1246.97): calc. C 73.20, H 6.47, N 8.99; found C 73.28, H 6.40, N 8.86. IR (solid): ν = 3139.2, 3122.5, 3052.5, 2972.1, 2860.8, 1677.3, 1579.5, 1507.7, 1479.4, 1426.5, 1388.2, 1287.1, 1268.0, 1214.6, 1178.4, 1118.6, 1064.6, 1029.2, 946.3, 850.0, 732.7, 704.0 cm^{-1}. ESI-MS: *m/z* = 303.99 {$[M-2(BPh_4)]^{2+}$, calc. 304.13}, 927.33 {$[M-BPh_4]^+$, calc. 927.42}. Solution magnetic moment (Evans' method): μ_{eff} = 5.0 μ_B.

$[Fe(PrL1)_2(MeOH)_2](OTf)_2$ (4): Recrystallization of **2** (100 mg, 0.11 mmol) from a methanol/diethyl ether mixture at – 30 °C resulted in the formation of **$[Fe(PrL1)_2(MeOH)_2](OTf)_2$ (4)** as a white, microcrystalline solid after several days (54 mg, 50%). Slow vapor diffusion of diethyl ether into a solution of **$[Fe(PrL1)_2](OTf)_2$** (**2**) in methanol at room temperature yielded colorless crystals suitable for X-ray diffraction. Anal. for $C_{32}H_{48}F_6FeN_8O_{12}S_2$ (970.74): calc. C 39.59, H 4.98, N 11.54; found C 39.40, H 5.02, N 11.59. IR (solid): ν = 3371.8, 2969.5, 1732.0, 1723.7, 1503.6, 1421.6, 1360.4, 1281.1, 1247.0, 1222.7, 1194.7, 1150.8, 1031.6, 1011.84, 977.3, 731.6 cm^{-1}. ESI-MS: *m/z* = 303.96 {$[M-2OTf]^{2+}$, calc. 304.13}, 757.05 {$[M-OTf]^+$, calc. 757.18}. Solution magnetic moment (Evans' method): μ_{eff} = 5.2 μ_B.

Catalysis protocol. To a solution of catalyst (3 μmol) in acetonitrile (2 mL) was added substrate (1000 eq, 3 mmol) and acetonitrile (to bring the total volume to 2.5 mL). Subsequently, 0.5 mL of oxidant solution (10 eq, 60 mM solution in acetonitrile diluted from 35% aqueous H_2O_2) was added dropwise in 20 min. The reaction mixture was stirred at room temperature and after 1 h (from start of oxidant addition) internal standard (10 μL, cyclooctene: 1,2-dibromobenzene, all other substrates: bromobenzene) was added and the first sample was taken. An aliquot of the reaction mixture was filtered over a short silica plug, after which the short column was flushed twice with diethyl ether. The sample was concentrated by a stream of N_2 and analyzed by GC. The products were identified and quantified by comparison with authentic compounds.

X-ray crystal structure determinations. X-ray intensities were measured on a Nonius Kappa CCD diffractometer with rotating anode (graphite monochromator, λ = 0.71073 Å) at a temperature of 150 K. The structures were solved with automated Patterson Methods[49] (compound **3**) or Direct Methods[50] (compound **4**) and refined with SHELXL-97[51] against F^2 of all reflections. Geometry calculations and checking for higher symmetry was performed with the PLATON program.[52]

X-ray crystal structure determination of 3. $[C_{28}H_{40}FeN_8O_4](C_{24}H_{20}B)_2$, Fw = 1246.95 [*], colorless block, 0.15 × 0.15 × 0.10 mm^3, monoclinic, $P2_1/c$ (no. 14), a = 14.9857(2), b = 11.0234(2), c = 24.7254(4) Å, β = 119.7779(5)°, V = 3545.14(10) $Å^3$, Z = 2, D_x = 1.168 g/cm^3[*], μ = 0.27 mm^{-1}[*]. 40742 Reflections were measured up to a resolution of $(\sin\theta/\lambda)_{max}$ = 0.52 $Å^{-1}$. The reflections were corrected for absorption on the basis of multiple measured reflections (0.86-0.97 correction range). 4189 Reflections were unique (R_{int} = 0.0845). Non hydrogen atoms were refined with anisotropic displacement parameters. All hydrogen atoms were introduced in calculated positions and refined with a riding model. The crystal structure contains large voids, filled with disordered solvent molecules (300.1 $Å^3$/unit cell). Their contribution to the structure factors was secured by back Fourier transformation with the SQUEEZE routine of the PLATON package[52] (56 electrons/unit cell). 415 Parameters were refined with no restraints. R1/wR2 [I>2σ(I)]: 0.0441/0.1095. R1/wR2 [all refl.]: 0.0652/0.1197. S = 1.047. Residual electron density between – 0.27 and 0.49 e/$Å^3$.

X-ray crystal structure determination of 4. $[C_{30}H_{48}FeN_8O_6](CF_3SO_3)_2$, Fw = 970.75, yellow needle, 0.85 × 0.09 × 0.06 mm^3, triclinic, $P\bar{1}$ (no. 2), a = 8.9674(8), b = 12.7224(16), c = 19.9574(16) Å, α = 106.688(3), β = 101.274(5), γ = 91.638(4)°, V = 2130.2(4) $Å^3$, Z = 2, D_x = 1.513 g/cm^3, μ = 0.55 mm^{-1}. 37349 Reflections were measured up to a resolution of $(\sin\theta/\lambda)_{max}$ = 0.61 $Å^{-1}$. The reflections were corrected for absorption on the basis of multiple measured reflections (0.80-0.97 correction range). 7945 Reflections were unique (R_{int} = 0.0436). Non hydrogen atoms were refined with anisotropic displacement parameters. All hydrogen atoms were located in the difference Fourier map. The O-H hydrogen atom was refined freely with isotropic displacement parameters; all other hydrogen atoms were refined with a riding model. The propoxy group was refined with a disorder model. 604 Parameters were refined with 55 restraints. R1/wR2 [I > 2σ(I)]: 0.0416/0.0844. R1/wR2 [all refl.]: 0.0691/0.0945. S = 1.050. Residual electron density between – 0.39 and 0.31 e/$Å^3$.

[*] derived parameters do not contain the contribution of the disordered solvent.

5.6 References

1. Tanase, S.; Bouwman, E. *Adv. Inorg. Chem.* **2006**, *58*, 29-75.
2. Costas, M.; Mehn, M. P.; Jensen, M. P.; Que, L., Jr. *Chem. Rev.* **2004**, *104*, 939-986.
3. Solomon, E. I.; Brunold, T. C.; Davis, M. I.; Kernsley, J. N.; Lee, S-K.; Lehnert, N.; Neese, F.; Skulan, A. J.; Yang, Y-S.; Zhou, J. *Chem. Rev.* **2000**, *100*, 235-349.
4. Koehntop, K. D.; Emerson, J. P.; Que, L., Jr. *J. Biol. Inorg. Chem.* **2005**, *10*, 87-93.
5. Karlsson, A.; Parales, J. V.; Parales, R. E.; Gibson, D. T.; Eklund, H.; Ramaswamy, S. *Science* **2003**, *299*, 1039-1042.
6. Ferraro, D. J.; Gakhar, L.; Ramaswamy, S. *Biochem. Biophys. Res. Commun.* **2005**, *338*, 175-190.
7. Chen, K.; Costas, M.; Kim, J.; Tipton, A. K.; Que, L., Jr. *J. Am. Chem. Soc.* **2002**, *124*, 3026-3035.

8. Chen, K.; Costas, M.; Que, L., Jr. *J. Chem. Soc., Dalton Trans.* **2002**, 672-679.
9. Mas-Ballesté, R.; Costas, M.; van den Berg, T.; Que, L., Jr. *Chem. Eur. J.* **2006**, *12*, 3026-3035.
10. Guajardo, R. J.; Hudson, S. E.; Brown, S. J.; Mascharak, P. K. *J. Am. Chem. Soc.* **1993**, *115*, 7971-7977.
11. Nam, W.; Ho, R.; Valentine, J. S. *J. Am. Chem. Soc.* **1991**, *113*, 7052-7054.
12. White, M. C.; Doyle, A. G.; Jacobsen, E. N. *J. Am. Chem. Soc.* **2001**, *123*, 7194-7195.
13. Klopstra, M.; Roelfes, G.; Hage, R.; Kellogg, R. M.; Feringa, B. L. *Eur. J. Inorg. Chem.* **2004**, 846-856.
14. Rotthaus, O.; Le Roy, S.; Tomas, A.; Barkigia, K. M.; Artaud, I. *Inorg. Chim. Acta* **2004**, *357*, 2211-2217.
15. Beck, A.; Barth, A.; Hubner, E.; Burzlaff, N. *Inorg. Chem.* **2003**, *42*, 7182-7188.
16. Beck, A.; Weibert, B.; Burzlaff, N. *Eur. J. Inorg. Chem.* **2001**, 521-527.
17. Gosiewska, S.; Cornelissen, J. L. M.; Lutz, M.; Spek, A. L.; van Koten, G.; Klein Gebbink, R. J. M. *Inorg. Chem.* **2006**, *45*, 4214-4227.
18. Oldenburg, P. D.; Shteinman, A. A.; Que, L., Jr. *J. Am. Chem. Soc.* **2005**, *127*, 15673-15674.
19. Otero, A.; Fernández-Baeza, J.; Antiñolo, A.; Tejeda, J.; Lara-Sánchez, A. *Dalton Trans.* **2004**, 1499-1510.
20. Friese, S. J.; Kucera, B. E.; Que, L., Jr.; Tolman, W. B. *Inorg. Chem* **2006**, *45*, 8003-8005.
21. Kervinen, K. ; Bruijnincx, P. C. A.; Beale, A. M.; Mesu, J. G.; van Koten, G.; Klein Gebbink, R. J. M.; Weckhuysen, B. M. *J. Am. Chem. Soc.* **2006**, *128*, 3208-3217.
22. Bruijnincx, P. C. A.; Lutz, M.; Spek, A. L.; van Faassen, E. L.; Weckhuysen, B. M.; van Koten, G.; Klein Gebbink, R. J. M. *Eur. J. Inorg. Chem.* **2005**, 779-787 (Chapter 2 of this thesis).
23. Bruijnincx, P. C. A.; Lutz, M.; Spek, A. L.; Hagen, W. R.; Weckhuysen, B. M.; van Koten, G.; Klein Gebbink, R. J. M. *J. Am. Chem. Soc.*, accepted for publication (Chapter 3 of this thesis).
24. Robert, V.; Lemercier, G. *J. Am. Chem. Soc.* **2006**, *128*, 1183-1187.
25. Britovsek, G. J. P.; Gibson, V. C.; Spitzmesser, S. K.; Tellmann, K. P.; White, A. J. P.; Williams, D. J. *J. Chem. Soc., Dalton Trans.* **2002**.
26. Evans, D. F. J. *J. Chem. Soc.* **1959**, 2003-2005.
27. Gejji, S. P.; Hermansson, K.; Lindgren, J. *J. Phys. Chem.* **1993**, *97*, 3712-3715.
28. Johnston, D. H.; Shriver, D. F. *Inorg. Chem* **1993**, *32*, 1045-1047.
29. Bénisvy, L.; Halut, S.; Donnadieu, B.; Tuchagues, J.-P.; Chottard, J.-C.; Li, Y. *Inorg. Chem.* **2006**, *45*, 2403-2405.
30. Lemercier, G.; Mulliez, E.; Brouca-Cabarrecq, C.; Dahan, F.; Tuchagues, J.-P. *Inorg. Chem.* **2004**, *43*, 2105-2113.
31. Ion, A.; Moutet, J.-C.; Saint-Aman, E.; Royal, G.; Tingry, S.; Pecaut, J.; Ménage, S.; Ziessel, R. *Inorg. Chem.* **2001**, *40*, 3632-3636.
32. Szafert, S.; Lis, T.; Drabent, K.; Sobota, P. *J. Chem. Cryst.* **1994**, *24*, 197-.
33. Weber, B.; Görls, H.; Rudolph, M.; Jäger, E.-G. *Inorg. Chim. Acta* **2002**, *337*, 247-265.
34. Diebold, A.; Hagen, K. S. *Inorg. Chem.* **1998**, *37*, 215-223.
35. Oldenburg, P. D.; Que, L., Jr. *J. Mol. Cat. A.* **2006**, *117*, 15-21.
36. Gosiewska, S.; Permentier, H. P.; Bruins, A. P.; van Koten, G.; Klein Gebbink, R. J. M. *submitted*.
37. Jensen, M. P.; Costas, M.; Ho, R. Y. N.; Kaizer, J.; Mairata i Payeras, A.; Münck, E.; Que, L., Jr.; Rohde, J.-U.; Stubna, A. *J. Am. Chem. Soc.* **2005**, *127*, 9117-9128.
38. Bukowski, M. R.; Halfen, H. L.; van den Berg, T.; Halfen, J. A.; Que, L., Jr. *Angew. Chem. Int. Ed.* **2005**, *44*, 584-587.
39. Borovik, A. S. *Acc. Chem. Res.* **2005**, *38*, 54-61.
40. Lu, Y.; Valentine, J. S. *Curr. Opin. Struct. Biol.* **1997**, *7*, 495-500.
41. Kloer, D. P.; Ruch, S.; Al-Babili, S.; Beyer, P.; Schultz, G. E. *Science* **2005**, *308*, 267-269.
42. Giuliano, G.; Al-Babili, S.; von Lintig, J. *Trends Plant Sci.* **2003**, *8*, 145-149.
43. Ferreira, K. N.; Iverson, T. M.; Maghlaoui, K.; Barber, J.; Iwata, S. *Science* **2004**, *303*, 1831-1838.

44. Katona, G.; Andréasson, U.; Landau, E. M.; Andréasson, L.-E.; Neutze, R. *J. Mol. Biol.* **2003**, *331*, 681-692.
45. Lancaster, C. R. D.; Michel, H. *J. Mol. Biol.* **1999**, *286*, 883-898.
46. Gillmor, S. A.; Villasenor, A.; Fletterick, R.; Sigal, E.; Browner, M. F. *Nat. Struct. Biol.* **1997**, *4*, 1003-1008.
47. Schmidt, H.; Kurtzer, R.; Eisenreich, W.; Schwab, W. *J. Biol. Chem.* **2006**, *281*, 9845-9851.
48. Hagen, K. S. *Inorg. Chem.* **2000**, *39*, 5867-5869.
49. Beurskens, P. T.; Admiraal, G.; Beurskens, G.; Bosman, W. P.; Garcia-Granda, S.; Gould, R. O.; Smits, J. M. M.; Smykalla, C. *The DIRDIF99 program system*, Technical Report of the Crystallography Laboratory; University of Nijmegen: The Netherlands, 1999.
50. Altomare, A.; Burla, M. C.; Camalli, M.; Cascarano, G. L.; Giacovazzo, C.; Guagliardi, A.; Moliterni, A. G. G.; Polidori, G.; Spagna, R. *J. Appl. Cryst.* **1999**, *32*, 115-119.
51. Sheldrick, G. M. *SHELXL-97. Program for crystal structure refinement*, University of Göttingen: Germany, 1997.
52. Spek, A. L. *J. Appl. Cryst.* **2003**, *36*, 7-13.

CHAPTER 6

Mono- and Dinuclear Iron Complexes of Bis(1-methylimidazol-2-yl)ketone (bik): Structural Characterization and Catalytic Oxidation Studies

Abstract

The new dinuclear complex $[Fe^{III}_2(\mu\text{-}OH)_2(\mathbf{bik})_4](NO_3)_4$ with the bidentate bis(1-methylimidazol-2-yl)ketone ligand (**bik**) has been synthesized and characterized crystallographically. Variable temperature magnetic susceptibility studies revealed that the metal ions of the diamond core in this complex are antiferromagnetically coupled. Spontaneous reduction of the complex was observed in methanol resulting in the isolation of a blue $[Fe^{II}(bik)_3]^{2+}$ species. The mononuclear complex $[Fe^{II}(bik)_3](OTf)_2$ was structurally characterized and found to display spin crossover behavior. $[Fe^{II}(bik)_3](OTf)_2$ catalyzed the oxidation of alkanes with *t*-BuOOH and a high 3°/2° value of 29.6 was obtained in the oxidation of adamantane. Stereoselective oxidation of olefins with hydrogen peroxide yielding epoxides was also observed under various conditions.

P. C. A. Bruijnincx, I. L. C. Buurmans, M. Quesada, M. Viciano, S. Tanase, M. Lutz, D. M. Tooke, A. L. Spek, J. Reedijk, G. van Koten, R. J. M. Klein Gebbink, manuscript in preparation

6.1 Introduction

The development of environmentally friendly catalytic oxidation processes for the selective conversion of hydrocarbons is a topic of continuing interest.[1] In particular, inspiration for the design of new catalytic systems has been drawn from Nature, where metalloenzymes are often involved in highly selective oxidative transformations under mild conditions. The non-heme iron oxygenases[2-4] constitute an important and versatile subgroup of these metalloenzymes capable of oxidative transformations. Non-heme iron oxygenases generally feature either a mononuclear or a dinuclear active site. Amongst the mononuclear non-heme iron enzymes, the 2-His-1-carboxylate facial triad has recently emerged as a common structural motif.[2] The oxidative transformations that these enzymes catalyze are very diverse, ranging from the *cis*-dihydroxylation of arenes by the Rieske dioxygenases to, for example the dioxygenative cleavage of aromatic substrates by the extradiol cleaving dioxygenases. A particularly impressive example of a dinuclear non-heme iron enzyme is methane monooxygenase, which selectively catalyzes the unique conversion of methane to methanol.[4]

Many biomimetic modeling studies have been devoted to these two classes of non-heme iron enzymes. These studies have not only contributed to our understanding of the enzymes under scrutiny, but the properties of synthetic mono- and dinuclear iron complexes as potential synthetic oxidation catalysts have been widely investigated as well. Promising examples of catalysts capable of alkane hydroxylation, olefin epoxidation, and *cis*-dihydroxylation have been reported.[1,2,4-6] Ligand systems that are widely used for the construction of both mono- and dinuclear iron complexes include the polydentate tris(2-pyridylmethyl)amine (tpa) and *N*,*N*'-bis(2-pyridylmethyl)-*N*,*N*'-dimethyl-1,2-ethylenediamine ligand family (bpmen),[7,8] and the *N*,*N*-bis(2-pyridylmethyl)-*N*-bis(2-pyridyl)methylamine (N4py),[9,10] 2-(2',5'-diazapentyl)-5-bromopyrimidine-6-carboxylic acid N-[2,(4'-imidazolyl)ethyl]amide (Hpma)[11], and tris((1-methylimidazol-2-yl)methyl)amine (tmima) ligands,[12] amongst many others (Figure 1). Efficient dinuclear iron oxidation catalysts were also reported with the simple bidentate bipyridine (bipy) and phenanthroline (phen) ligands.[13,14]

As part of our recent efforts to develop biomimetic models of the 2-His-1-carboxylate facial triad, we have reported on the new ligand family of the substituted 3,3-bis(1-alkylimidazol-2-yl)propionates, with **L1** being the parent ligand, and their iron complexes.[15-17] $[Fe^{II}(\mathbf{PrL1})_2](OTf)_2$ (**PrL1**, propyl 3,3-bis(1-methylimidazol-2-yl)propionate) was for instance found to be an active bio-inspired catalyst for the epoxidation and *cis*-dihydroxylation of olefins.[15]

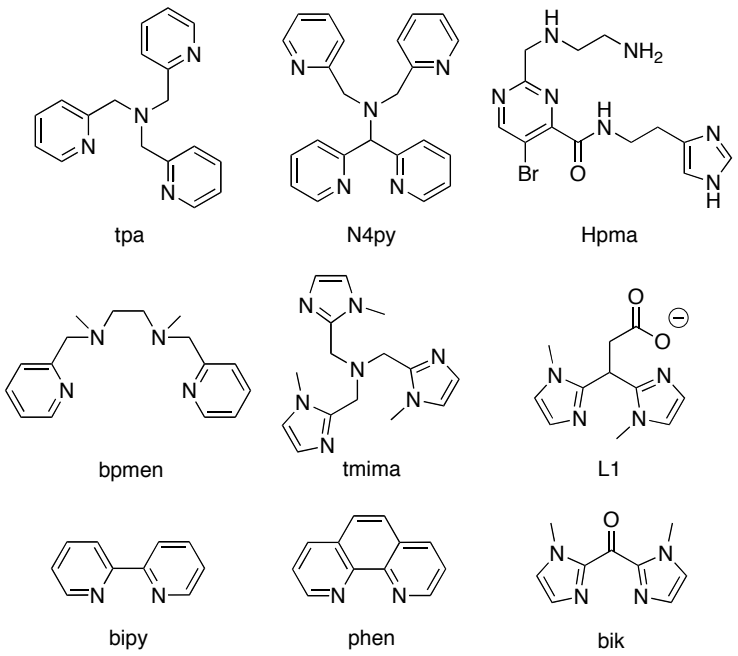

Figure 1. Some selected ligands used in mono- and dinuclear non-heme iron oxidation catalysis, including the **bik** ligand used in this study.

Encouraged by the results obtained with the dinuclear ferric catalysts containing the simple bidentate bipy and phen ligands, we decided to explore the structure and catalytic properties of iron complexes of the ligand bis(1-methylimidazol-2-yl)ketone (**bik**). This bidentate ligand is used as a building block for the synthesis of **L1** and can be synthesized in one step on a multigram scale.[18] Here, we report the synthesis and structural, spectroscopic and magnetic characterization of the bis(μ-hydroxy)diiron(III) complex $[Fe^{III}_2(\mu\text{-}OH)_2(\mathbf{bik})_4](NO_3)_4$ (**1**) and the mononuclear complex $[Fe^{II}(\mathbf{bik})_3](OTf)_2$ (**2**). Complex **2** was found to be active in the oxidation of alkanes and alkenes with *t*-BuOOH or H_2O_2 as the oxidant.

6.2 Results

Synthesis and structural characterization of a dinuclear bis(μ-hydroxy)diiron(III) complex. In an effort to construct dinuclear iron(III) complexes with the *N*,*N*-bidentate bis(1-methylimidazol-2-yl)ketone (**bik**) ligand, we adopted the synthetic route reported for the $[((phen)_2(H_2O)Fe^{III})_2(\mu\text{-}O)](X)_4$ complexes (X = NO_3, ClO_4).[13,14] The addition of two equivalents of **bik** to a solution of ferric nitrate in ethanol/water resulted in the gradual formation of a yellowish-orange precipitate. Recrystallization of the precipitate from aqueous solution yielded red-orange crystals. The product was identified as a C_2 symmetric dinuclear iron complex of the composition $[Fe^{III}_2(\mu\text{-}OH)_2(\mathbf{bik})_4](NO_3)_4{\cdot}2H_2O$ (**1**) by X-ray crystal structure determination, elemental analysis, and IR spectroscopy. Complex **1** features an $Fe^{III}_2(\mu\text{-}OH)_2$ diamond core (*vide infra*), which is spontaneously formed by self assembly (no base was added to the reaction mixture).[19] Some of the structural features of **1** are reflected in

its infrared absorption spectrum. The IR spectra of the isolated yellow-orange colored powder and the red-orange crystals are identical except for the presence of a broad absorption centered around 3100 cm^{-1} for the red-orange crystals. This broad absorption can be attributed to the OH stretching mode of co-crystallized water molecules. The binding of the **bik** ligand to a ferric metal center results in a strong shift of the carbonyl stretching vibration to higher wavenumbers by 32 cm^{-1} and is now found at 1662 cm^{-1}. Two absorptions of equal intensity are observed at 3438 and 3549 cm^{-1}, of which the latter is tentatively assigned as the OH stretch vibration of the bridging OH groups.

It is important to note that the reaction of **bik** with ferric nitrate in the presence of water does not lead to the formation of the hydrated bis(1-methylimidazol-2-yl)methanediol ligand. It is well known that the similar bis(2-pyridyl)ketone ligand (bpk) easily hydrates upon coordination to several different transition metals,[20-22] including iron(III). For instance, the reaction of $Fe(NO_3)_3{\cdot}9H_2O$ with two equivalents of bpk under identical conditions as employed here leads to the formation of the geminal diol of bpk. Two hydrated ligands then coordinate in a terdentate fashion to the metal center, resulting in mononuclear bis-ligand complex.[23] Apparently, the carbonyl carbon atom of **bik** is less susceptible for nucleophilic attack of water after coordination to a ferric metal center.

Crystal Structure of $[Fe^{III}_2(\mu\text{-}OH)_2(bik)_4](NO_3)_4{\cdot}2H_2O$. Red-orange crystals of **1** suitable for X-ray diffraction were obtained by slow evaporation of an aqueous solution of **1**. The molecular structure of the dinuclear cation of **1** is depicted in Figure 2, with selected bond lengths and angles presented in Table 1.

The crystal structure of the cation of **1** consists of a dinuclear unit with two crystallographically equivalent iron(III) metal centers that are bridged by two hydroxyl groups. The two equivalent ferric ions are related by a twofold rotation axis parallel to the monoclinic *b*-axis. Two **bik** ligands are coordinated in a bidentate fashion to each of the iron atoms, resulting in an N_4O_2 donor set and a distorted octahedral coordination geometry around the metal center. The $Fe_2(\mu\text{-}OH)_2$ core is planar, with the Fe1–O3 and Fe1–O3a bond lengths equal within error (1.941(2) and 1.949(2) Å, resp.). The distance between the metal centers is 3.0723(6) Å and the Fe1–O3–Fe1(a) bridging angle of the planar unit is 104.32(9)°. Only a limited number of structures with an unsupported[24-29] or supported[30-32] $Fe^{III}_2(\mu\text{-}OH)_2$ core have been reported. The metal-metal distance in **1** is on the short side of the range reported for structures with a doubly bridged, unsupported $Fe^{III}_2(\mu\text{-}OH)_2$ core (3.078-3.161 Å).[24-29] The relatively short Fe···Fe distance is probably due to the assembly of the core with neutral **bik** ligands only. All other complexes were constructed with anionic ligands, which lead to longer Fe–OH bond lengths *trans* to the anionic donor groups and an increase in intermetallic separation. Consequently, the Fe–OH bond lengths in **1** are relatively short (1.941(2)/1.949(2) Å for Fe1–O3/Fe–O3a). The distortion from ideal octahedral geometry is evidenced by the diminished *transoid* (164.75(9)-171.44(10) Å) and N–Fe–N angles, the latter caused by the limited 'bite' of the **bik** ligand.

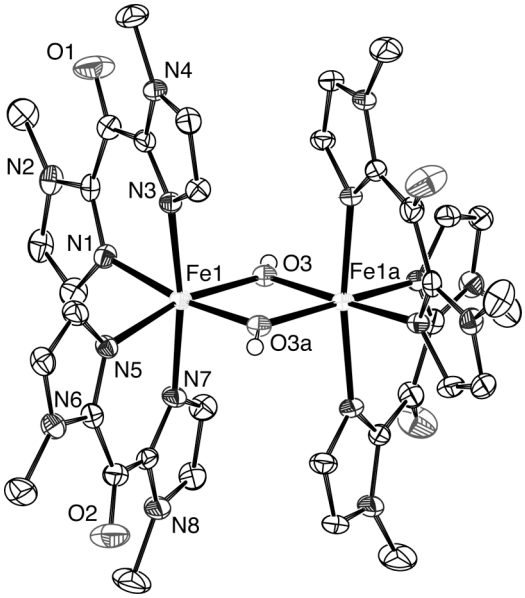

Figure 2. Molecular structure of the dinuclear $[Fe^{III}_2(\mu\text{-}OH)_2(\mathbf{bik})_4]^{4+}$ cation of **1** in the crystal. All C–H hydrogen atoms, nitrate anions and co-crystallized water molecules have been omitted for clarity. Displacement ellipsoids are drawn at the 50% probability level. Symmetry operation a: 1–x, y, 1/2–z.

The $Fe^{III}_2(\mu\text{-}OH)_2$ core of the dinuclear cation is further stabilized by hydrogen bonds, since the hydroxyl group is involved in an intermolecular, bifurcated hydrogen bond (Σ_{angles} = 360°) with O7 and O8 of a nitrate anion as acceptors (Figure 3 (left), Table 2). This hydrogen bond is asymmetric, as reflected by the different H···O bond lengths of 1.82(2) Å (O8) and 2.43(3) Å (O7). The co-crystallized water molecules and the two other nitrate anions are also involved in hydrogen bonding interactions with each other. This leads to the formation of an infinite linear chain in the direction of the crystallographic *b*-axis. Sheets of the infinite linear chains run in between layers of the dinuclear cations, which are also oriented in the direction of the crystallographic *b*-axis (Figure 3 (right), Table 2).

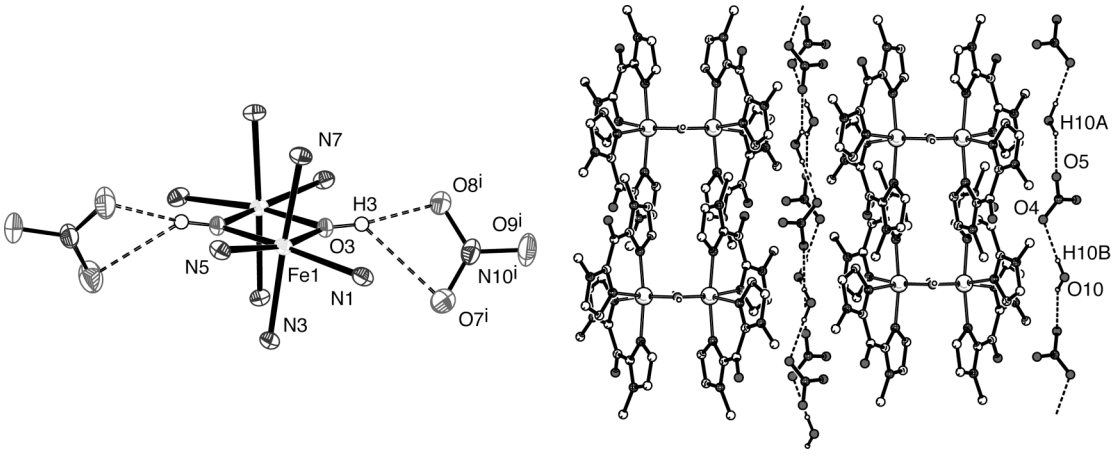

Figure 3. Hydrogen bonding interactions in $[Fe^{III}_2(\mu\text{-}OH)_2(\mathbf{bik})_4](NO_3)_4{\cdot}2H_2O$ (**1**). Left: Hydrogen bonds between two nitrate anions and the $[Fe^{III}_2(\mu\text{-}OH)_2(\mathbf{bik})_4]^{4+}$ cation of **1**. The $Fe^{III}_2(\mu\text{-}OH)_2$ core with donor atoms and the two hydrogen bonded nitrate anions are shown. Right: Hydrogen bonds resulting in infinite linear chains. Symmetry operation i: 1/2 – x, 1/2 – y, 1 – z.

Table 1. Selected bond lengths (Å) and angles (°) for $[Fe^{III}_2(\mu\text{-}OH)_2(\mathbf{bik})_4](NO_3)_4{\cdot}2H_2O$ (**1**). Symmetry operation a: 1 – x, y, 1/2 – z

Bond length		Angle		Angle	
Fe1–N1	2.136(2)	O3–Fe1–O3a	75.68(9)	O3–Fe1–N7	89.46(9)
Fe1–N3	2.096(2)	O3a–Fe1–N5	90.93(9)	N7–Fe1–N5	84.82(10)
Fe1–N5	2.133(2)	N5–Fe1–N1	97.20(10)	N5–Fe1–N3	90.42(9)
Fe1–N7	2.112(2)	N1–Fe1–O3	96.82(9)	N3–Fe1–O3	96.86(9)
Fe1–O3	1.941(2)	Fe1–O3–Fe1a	104.32(9)	O3a–Fe1–N7	96.70(9)
Fe1–O3a	1.949(2)	N7–Fe1–N3	171.44(10)	N7–Fe1–N1	88.95(10)
		O3–Fe1–N5	164.75(9)	N1–Fe1–N3	84.59(10)
		O3a–Fe1–N1	170.50(9)	N3–Fe1–O3a	90.46(9)

Table 2. Hydrogen bond lengths (Å) and angles (°) for $[Fe^{III}_2(\mu\text{-}OH)_2(\mathbf{bik})_4](NO_3)_4{\cdot}2H_2O$ (**1**). Symmetry operation i: 1/2 – x, 1/2 – y, 1 – z, ii: 1/2 – x, 1/2 + y, 1/2 – z

Donor–H ··· Acceptor	D–H	H ··· A	D ··· A	D–H ··· A
O3–H3A ··· $O7^{i}$	0.81(2)	2.43(3)	3.022(3)	130(4)
O3–H3A ··· $O8^{i}$	0.81(2)	1.82(2)	2.623(3)	171(4)
O10–H10A ··· O5	0.87(4)	2.22(4)	3.024(6)	154(4)
O10–H10B ··· $O\,4^{ii}$	0.85(3)	2.05(3)	2.903(6)	176(3)

Magnetic properties of 1. The temperature-dependent magnetic susceptibility of **1**, measured on a powdered sample from 2 to 300 K, is shown in Figure 4 in the form a χ_M versus T and χ_MT versus T plot. The χ_MT product of $[Fe_2(\mu\text{-}OH)_2(\mathbf{bik})_4](NO_3)_4{\cdot}2H_2O$ at 300 K is 4.71 $cm^3\ mol^{-1}$ K, which is significantly lower than the spin-only value for two non-interacting iron(III) ions with $S = 5/2$ (8.75 $cm^3\ mol^{-1}$ K). The χ_MT value decreases down to 0.012 $cm^3\ mol^{-1}$ K at 10 K, which arises from antiferromagnetic coupling of the two iron(III) centers. The experimental data were fitted to the equation derived from the Hamiltonian $H = J(\mathbf{S}_1 \cdot \mathbf{S}_2)$ given as follows:[33]

$$\chi_M = \frac{2N_A g^2 \beta^2}{kT} \cdot \frac{e^x + 5e^{3x} + 14e^{6x} + 30e^{10x} + 55e^{15x}}{1 + 3e^x + 5e^{3x} + 7e^{6x} + 9e^{10x} + 11e^{15x}}$$

where $x = J/kT$. The best fit to the χ_MT versus T curve gave $g = 2$ and the exchange parameter $J = -35.86\ cm^{-1}$ ($R = 8.9 \times 10^{-4}$).

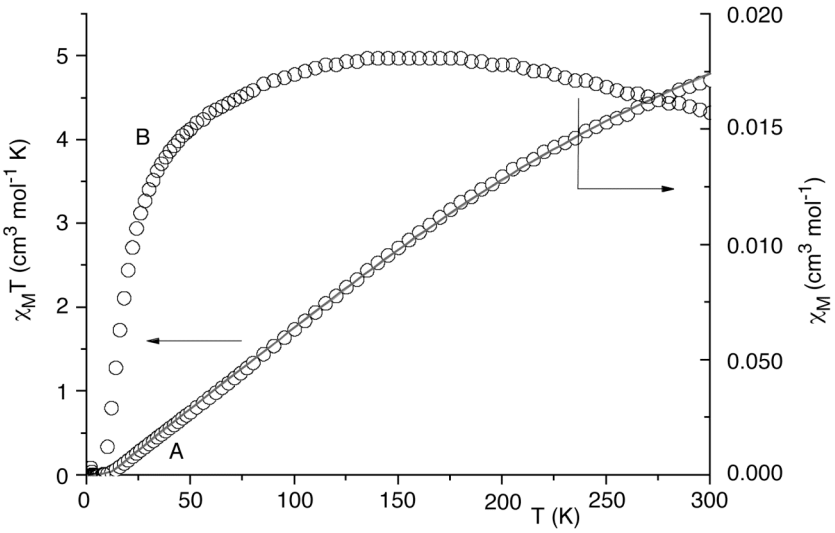

Figure 4. Plots of $\chi_M T$ versus T (A) and χ_M versus T (B) for **1** from 2 to 300 K in 0.08 T field.

The *J* value is larger than the reported *J* values for other bis(μ-hydroxo) dinuclear iron(III) compounds ($6 < J < 22$ cm^{-1}).[24-27,29] The magnitude of the exchange parameter *J* has been correlated to the length of the Fe–O distance, i.e. half of the shortest superexchange pathway between the two metal centers.[34,35] Indeed, **1** has the shortest average Fe–O bond length of crystallographically characterized [Fe^{III}(μ-OH)$_2$] complexes to date. Interestingly, the observed *J* value for **1** is rather similar to the exchange parameter that was recently reported for the first crystallographically characterized diiron(III) complex with a *single* hydroxo bridge ($J = 42$ cm^{-1}).[35]

Formation of an [Fe^{II}(bik)$_3$]$^{2+}$ complex. Complex **1** was found to be unstable in methanolic solution. Yellow-orange solutions of **1** in methanol slowly turned dark blue in time under ambient conditions (Figure 5).

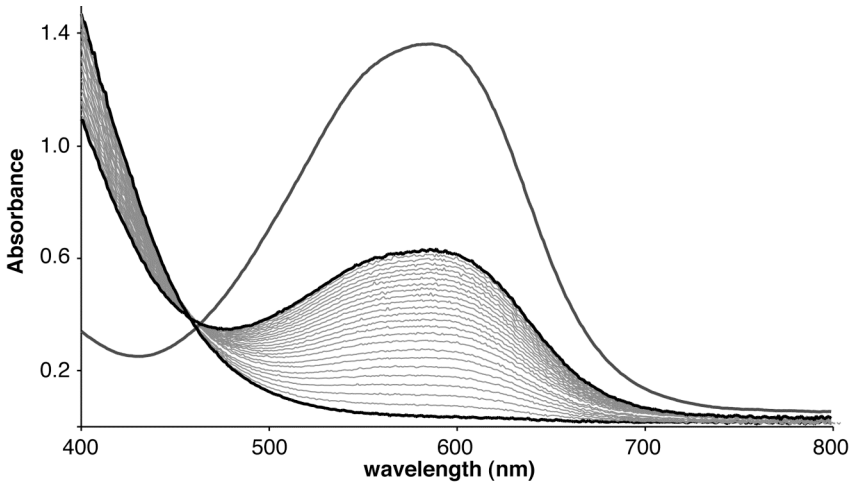

Figure 5. UV-Vis spectral changes observed for **1** in methanol at room temperature showing the formation of an [Fe^{II}(**bik**)$_3$]$^{2+}$ species (t = 120 min). The UV-Vis spectrum of independently synthesized [Fe^{II}(**bik**)$_3$](OTf)$_2$ (**2**) is included for comparison.

The color change was monitored by UV-Vis absorption spectroscopy as a new band emerged at 583 nm. The conversion of **1** to this blue species is accelerated by the addition of Et_3N. The blue chromophore was identified as the $[Fe^{II}(\mathbf{bik})_3]^{2+}$ cation, by comparison with the UV-Vis and IR data of independently synthesized $[Fe^{II}(\mathbf{bik})_3](OTf)_2$ (**2**) (*vide infra*). ESI-MS measurements on the blue solution showed two prominent ions, corresponding to the $[Fe^{II}(\mathbf{bik})_3]^{2+}$ (*m*/*z* 313.19) and $[Fe^{II}(\mathbf{bik})_3NO_3]^{+}$ (*m*/*z* 498.18) cations.

The ferric centers in **1** were therefore *in situ* reduced to give an air-stable, tris-chelated ferrous complex. The formation of $[Fe^{II}(\mathbf{bik})_3]^{2+}$ has been observed before with ligand systems based on the related bis(1-methylimidazol-2-yl)methane backbone.[36-38] $[Fe^{II}(\mathbf{bik})_3]^{2+}$ has been identified in the iron catalyzed oxidations of the ligands bis(1-methylimidazol-2-yl)methanol,[37] bis(1-methylimidazol-2-yl)-2-methylthioethanol,[36] and bis(1-methylimidazol-2-yl)methane[38] to give **bik**. The latter oxidation was also accelerated by the addition of a nitrogenous base. Note that in the reported examples the starting ligand itself is oxidized to **bik**.

We also observed the formation of the $[Fe^{II}(\mathbf{bik})_3]$ cation in an attempt to synthesize the analogous ferrous complex of $[Fe^{III}_2(\mu\text{-}OH)_2(\mathbf{bik})_4](NO_3)_4$ (**1**), i.e. a complex with an $Fe^{II}_2(\mu\text{-}OH)_2$ core. According to published procedures for the construction of such cores,[39-41] equimolar amounts of $Fe(OTf)_2{\cdot}2MeCN$ and sodium hydroxide were reacted with 2 eq of **bik** in methanol. Immediately upon mixing of the reagents the solution turned dark blue. The blue product was isolated and identified as $[Fe^{II}(\mathbf{bik})_3](OTf)_2$ (**2**) by X-ray diffraction (*vide infra*). The formation of the $[Fe^{II}(\mathbf{bik})_3]^{2+}$ cation therefore seems to be inevitable and can be regarded as a thermodynamic sink in the coordination chemistry of iron and **bik**. Our further studies on the structure and reactivity of **bik** complexes of iron were therefore focused on the ferrous complex $[Fe^{II}(\mathbf{bik})_3](OTf)_2$ (**2**).

Synthesis and characterization of $[Fe^{II}(\mathbf{bik})_3](OTf)_2$ (2). $[Fe^{II}(\mathbf{bik})_3](OTf)_2$ (**2**) was synthesized by the simple addition of 3 eq of **bik** to a solution of $Fe(OTf)_2{\cdot}2MeCN$ in methanol. Recrystallization from methanol/diethyl ether at – 30 °C yielded **2** as a dark blue microcrystalline powder. $[Fe^{II}(\mathbf{bik})_3](OTf)_2$ (**2**) is stable under ambient conditions. In contrast to the observed shift of the carbonyl stretch vibration in the IR spectrum upon coordination of **bik** to a ferric center (as in **1**), no shift is observed for $[Fe^{II}(\mathbf{bik})_3](OTf)_2$ (**2**). The carbonyl stretch vibration is found at 1629 cm^{-1}, identical to that in the free ligand. Four sharp vibrations at 1254, 1223, 1144, and 1028 cm^{-1} are observed for the triflate anions, which is indicative of the presence of non-coordinated triflate anions.[42,43] In the ESI-MS spectrum of an acetonitrile solution of **2**, next to the $[Fe^{II}(\mathbf{bik})_3(OTf)_2{+}H]^{+}$ molecular ion (*m*/*z* 925.14) and the $[Fe^{II}(\mathbf{bik})_3]^{2+}$ dication (*m*/*z* 313.07), a prominent ion is observed that corresponds to the $[Fe^{II}(\mathbf{bik})_2OTf]^{+}$ cation (*m*/*z* 584.97). This shows that ligand dissociation from the ferrous center is rather facile in acetonitrile. Ligand dissociation from the coordinatively saturated complex leads to two *cis*-positioned vacant sites at the metal center. This makes the readily accessible and easily synthesized **2** an attractive candidate for exploring its potential in oxidation catalysis.

Crystal structure and spectroscopic properties of $[Fe^{II}(bik)_3](OTf)_2 \cdot MeOH$. Blue crystals of **2·MeOH** suitable for X-ray diffraction were obtained by slow vapor diffusion of diethyl ether into a solution of **2** in methanol. The crystal structure of the cation of **2·MeOH** is depicted in Figure 6 with selected bond lengths and angles in Table 3. The iron(II) metal center in **2·MeOH** is coordinated by three *N,N*-chelate bonded **bik** ligands, resulting in a slightly distorted octahedral coordination geometry. The Fe–N distances range from 1.9942(16) to 1.9735(16) Å and are characteristic of a low-spin iron(II) metal center ($S = 0$). The co-crystallized methanol solvent molecule is hydrogen bonded to one of the triflate anions. Although the complex is inherently chiral, the crystal overall is racemic.

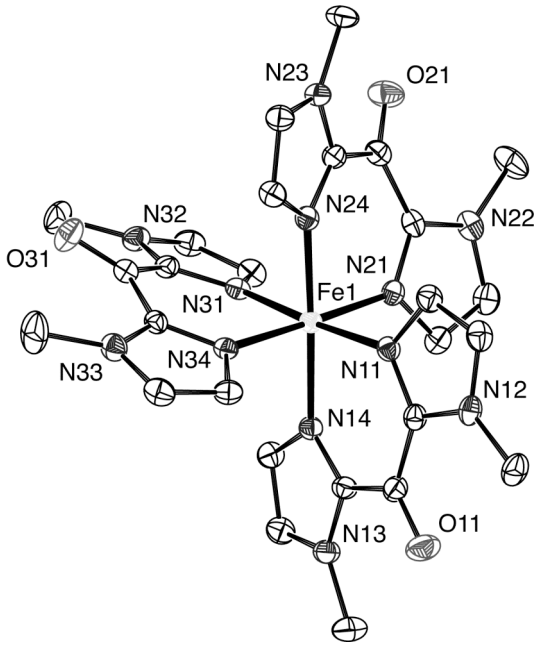

Figure 6. Molecular structure of the $[Fe^{II}(\mathbf{bik})_3]^{2+}$ cation of **2** in the crystal. All hydrogen atoms, triflate anions and the co-crystallized methanol molecule have been omitted for clarity. Displacement ellipsoids are drawn at the 50% probability level.

Two other crystal structures with the same $[Fe^{II}(\mathbf{bik})_3]^{2+}$ cation have been very recently reported.[36,44] Remarkably, the crystal structure of $[Fe^{II}(\mathbf{bik})_3](ClO_4)_2$[36] reveals a high spin iron(II) complex with an average Fe–N distance of 2.14 Å, whereas in $[Fe^{II}(\mathbf{bik})_3]Cl_2$[44] a low spin Fe(II) is found with an average Fe–N distance of 1.98 Å comparable to the Fe–N bond lengths found for **2·MeOH**. Since the structure of $[Fe^{II}(\mathbf{bik})_3](ClO_4)_2$ was determined at 298 K and the structures of $[Fe^{II}(\mathbf{bik})_3]Cl_2$ and **2·MeOH** at around 150 K, these differences in bond length indicate the presence of a temperature induced spin-state conversion.

Table 3. Selected bond lengths (Å) and angles (°) for $[Fe^{II}(\mathbf{bik})_3](OTf)_2 \cdot MeOH$

	Bond length		Angle		Angle
Fe1–N11	1.9942(16)	N11–Fe1–N21	88.02(6)	N21–Fe1–N24	89.48(6)
Fe1–N14	1.9871(16)	N21–Fe1–N31	89.12(6)	N24–Fe1–N34	88.74(6)
Fe1–N21	1.9837(15)	N31–Fe1–N34	89.97(6)	N34–Fe1–N14	87.76(6)
Fe1–N24	1.9891(16)	N34–Fe1–N11	92.91(6)	N14–Fe1–N21	93.98(6)
Fe1–N31	1.9735(16)			N11–Fe1–N24	93.38(6)
Fe1–N34	1.9741(15)	N14–Fe1–N24	175.77(7)	N24–Fe1–N31	87.08(6)
		N21–Fe1–N34	178.04(6)	N31–Fe1–N14	90.54(6)
		N11–Fe1–N31	177.10(7)	N14–Fe1–N11	89.17(6)

Spin-crossover is not uncommon for iron(II)-d^6 metal complexes with an N_6 donor set[45] and a spin-crossover has been reported for $[Fe^{II}(\mathbf{bik})_3](BF_4)_2$.[46] The paramagnetism of $[Fe^{II}(\mathbf{bik})_3](OTf)_2$ (**2**) at room temperature and the spin-state change to a diamagnetic low-spin species is also readily apparent in solution from the variable temperature ^{1}H NMR spectra of **2**. At 298 K three signals at chemical shifts of 4.18 (H_{im}), 7.58 (NCH_3) and 18.04 (H_{im}) ppm are observed, indicative of a solution consisting of a mixture of both high and low spin species. The signals gradually shift to the diamagnetic region upon cooling the sample and are found close to the values of the free ligand at 193 K. Heating of the sample results in an increased population of the high spin state and subsequent further paramagnetic shifting of the signals. At 333 K for instance, the imidazole proton signal at the highest frequency is found at 27.49 ppm.

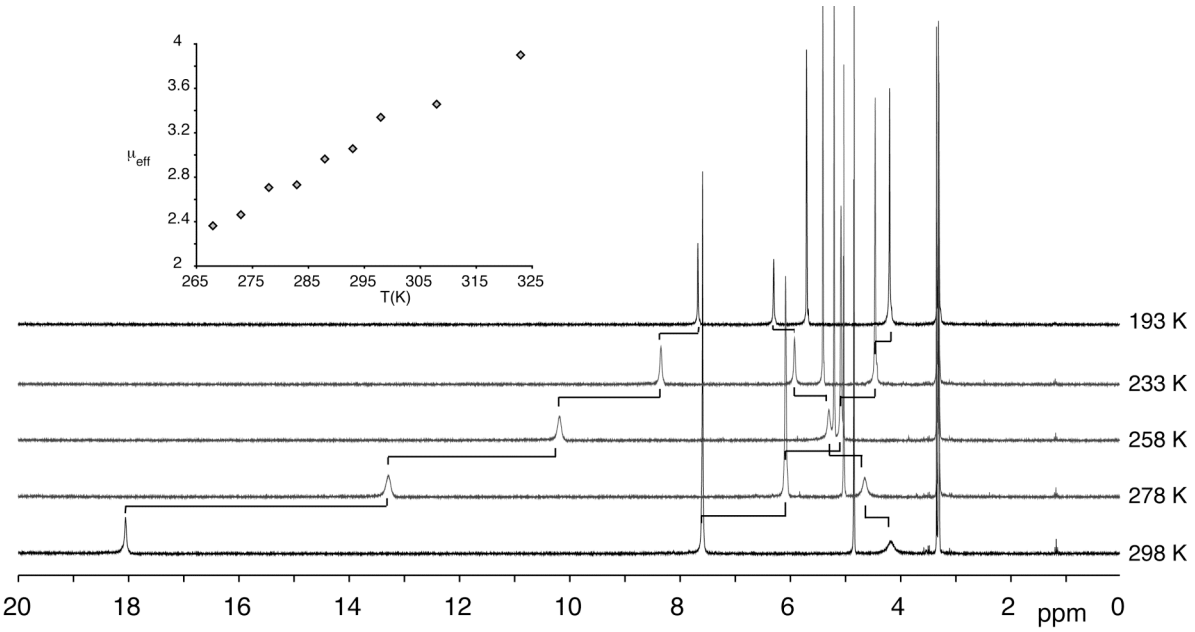

Figure 7. ^{1}H NMR spectral changes upon cooling a solution of $[Fe^{II}(\mathbf{bik})_3](OTf)_2$ (**2**) in methanol-d_4. The inset shows the changes in the solution magnetic moment at various temperatures.

These observations are further substantiated by the change of solution magnetic moments of **2** determined at various temperatures by Evans' NMR method (Figure 7).[47,48] At room temperature (298 K) the solution magnetic moment amounts to 3.3 μ_B, which corresponds to a mixture of high-spin and low-spin iron(II) configurations. Upon heating the sample to 323 K the magnetic moment increased to 3.9 μ_B. A gradual decrease of the solution magnetic moment to 2.4 μ_B at 268 K was observed upon cooling. This method did not allow the determination of the magnetic moment at temperatures lower than 268 K, since coalescence of the two probe signals was observed below this temperature. The magnetic properties of solid **2·MeOH** were further studied by a variable temperature magnetic susceptibility determination (*vide infra*).

The visible region of the absorption spectra of $[Fe^{II}(\mathbf{bik})_3](OTf)_2$ (**2**) is dominated by a LMCT absorption around 590 nm at room temperature, which causes the blue color of the complex. Upon cooling of a solution of **2** in methanol the LMCT band increases in intensity (ε_{298K} 4500, ε_{203K} 7500 M^{-1} cm^{-1}) and is slightly red shifted (λ_{298K} 583, λ_{203K} 592 nm). This intensification upon cooling suggests that the blue color is associated with an electronic transition of the low-spin species.

Magnetic properties of 2. The thermal variation of the magnetic susceptibility measured for compound $[Fe^{II}(\mathbf{bik})_3](OTf)_2$·MeOH (**2·MeOH)** under an applied magnetic field of 1000 G in the temperature range of 6 to 400 K in shown in Figure 8A. In the first heating mode, the compound shows a diamagnetic response to the magnetic field from 0 to 200 K (Figure 8A, ◇) until it reaches temperatures around 250 K where the $\chi_M T$ value gradually increases. At 400 K $\chi_M T$ = 2.79 cm^3 mol^{-1} K, indicating that a fraction of the spin crossover centers are still in the low spin state and thus, the transition is not complete (Fe^{II}(HS), S = 2, $\chi_M T \approx 3$ cm^3 mol^{-1} K). In the cooling mode (Figure 8A, ○) the transition follows a different path than that of the heating mode, and gradually reaches its diamagnetic low spin state at low temperatures (Fe^{II}(LS), S = 0, $\chi_M T$ = 0 cm^3 mol^{-1} K). As the temperature is increased for a second time, the compound follows the exact same path of the cooling mode, reaching at 400 K a similar value as previously observed (Figure 8A, △). The material thus shows an irreversible change that alters the magnetic properties of the material during the first heating mode.

To verify this, a thermogravimetric (TGA) measurement was performed in the temperature range of 293 to 573 K. The compound loses 3.2% of its total mass between 303 and 373 K and then stays stable until a temperature of 523 K, above which a second decrease is observed (data not shown). This last decrease is probably due to decomposition of the compound. As noted previously, compound $[Fe^{II}(\mathbf{bik})_3](OTf)_2$·MeOH (**2·MeOH**) crystallizes in the presence of methanol lattice solvent molecules. Their presence corresponds to 3.4% of the total mass, which nicely corresponds to the observed weight loss upon heating. That the loss of solvent is responsible for the change in magnetic response is further confirmed by measuring the magnetic susceptibility on cooling from room temperature to 6 K first and then

up again. As shown in Figure 8B, **2·MeOH** shows the same path both for the cooling and the heating mode.

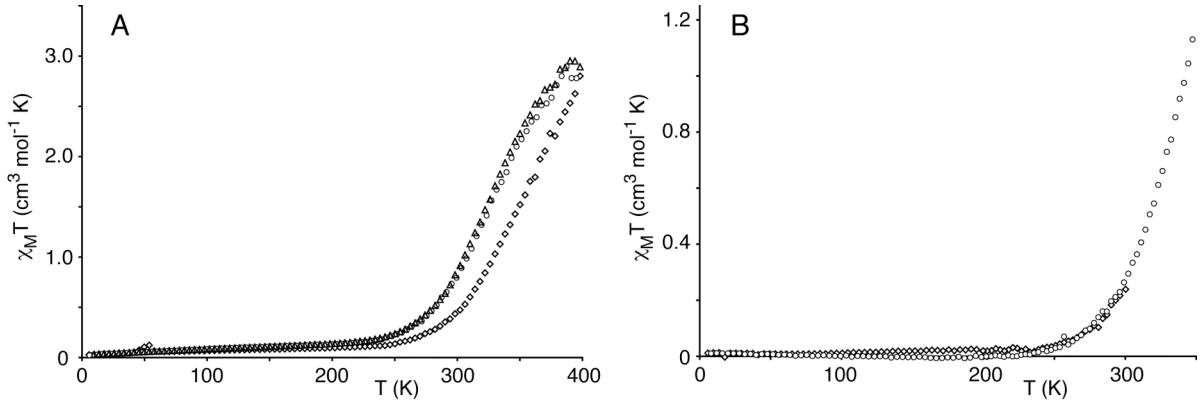

Figure 8. Thermal variation of the $\chi_M T$ product of $[Fe^{II}(\mathbf{bik})_3](OTf)_2 \cdot MeOH$ (**2·MeOH**). A: $\chi_M T$ versus T plot upon heating from 6K to 400 K (◇), first cooling (△), second heating (○). B: $\chi_M T$ versus T plot when cooling first from room temperature to 6 K (◇) and back up again (○).

The effect of solvent molecules on the spin crossover property has attracted much attention.[49-51] In some cases, the inherent property of some solvent molecules to form hydrogen bonds is responsible for its influences on the spin crossover properties. In **2·MeOH**, the methanol molecule is hydrogen bonded to a triflate anion and weakly to the methyl group of one imidazole rings. Although the effect could be due to this hydrogen bonding, it seems unlikely, as the interactions should not affect the electron donation of the ligand. Thus, the relative stabilization of the HS state upon loss of solvent has to be related to a structural rearrangement of the compound, maybe due to a closer packing of the complexes.

The cooperative behavior for $[Fe^{II}(\mathbf{bik})_3](OTf)_2$ (**2**) does not change from that of $[Fe^{II}(\mathbf{bik})_3](OTf)_2 \cdot MeOH$ (**2·MeOH**). Cooperativity in a spin-transition compound accelerates the transition, i.e. increases the observed slope.[52] This effect is known to be enhanced by intermolecular interactions as they increase the "communication" between the metal centers.[53] The low temperature at which the solvent molecules are lost is probably due to the lack of strong interactions in the structure, which would correlate with the unchanged cooperativity after de-solvation. In fact, the compound is quite cooperative, which must be due to the interactions of the counterions with the complex cations.

Oxidation catalysis. The instability of **1** in solution and its subsequent transformation into **2**, prompted us to study the latter rather than the former compound as a potential oxidation catalyst. The facile dissociation of (at least) one **bik** ligand from the metal center in acetonitrile, as evidenced by the ESI-MS measurements, results in the availability of two vacant sites at the metal center and would render the coordinatively saturated non-heme iron(II) complex **2** a suitable precatalyst for mediating oxidation reactions. The catalytic activity of **2** in the oxidation of alkanes and alkenes was tested with H_2O_2 and *t*-BuOOH as the terminal oxidants.

Alkane functionalization experiments were typically carried out in acetonitrile at room temperature. The oxidant was added drop wise to the reaction mixture with a final 1:100:1000 ratio of **2**:oxidant:substrate. Samples were taken three hours after the start of the addition of oxidant. No significant amounts of product were observed in the oxidation of alkanes with hydrogen peroxide as oxidant. The use of *tert*-butylhydrogen peroxide, however, did result in product formation in reactions of **2** with adamantane, cyclohexane and ethylbenzene. The product distribution for the oxidation of adamantane under various conditions is given in Table 4.

Table 4. Oxidation of adamantane catalyzed by [Fe(**bik**)$_3$](OTf)$_2$ (**2**) with *t*-BuOOH[a]

Conditions	adamant-1-ol[b]	adamant-2-ol[b]	adamant-2-one[b]	3°/2°[c]
acetonitrile, air	20.6	0.3	2.8	19.9
acetonitrile, N_2	15.0	n.d.[d]	2.0	22.5
acetone, air	23.7	n.d.	2.4	29.6

[a] For reaction conditions: see experimental section reaction. [b] Yields expressed as turnover numbers (TON = mol product/mol catalyst). [c] 3°/2° = 3*(TON adamant-1-ol)/(TON adamant-2-ol + TON adamant-2-one).[d] not detected.

2 oxidizes adamantane with up to 26% efficiency based on the oxidant. A high 3°/2° value of 19.9 is observed under standard conditions (acetonitrile, air). This value further increases when the reaction is carried out under N_2 atmosphere (22.5) or when using acetone as the solvent (29.6). Adamantane is commonly employed as a mechanistic probe for alkane oxidation and a high selectivity for oxidation at the tertiary position, i.e. a high 3°/2° value, is indicative for involvement of a more discriminating oxidant than freely diffusing hydroxyl or *tert*-butoxyl radicals.[5] The latter would result in a 3°/2° value of up to around 10.[5] Reported regioselectivities of adamantane oxidation for different non-heme iron/*t*-BuOOH systems[12,54-59] vary from 2.7 to 15.4, with the Gif-type systems on the lower end of the scale[54] and values of 12.6 and 15.4, for instance, reported for [Fe(Py(ProMe)$_2$(OTf)$_2$][55] (Py(ProMe)$_2$, 2,6-bis[[(*S*)-2-(methyloxycarbonyl)-1-pyrrolidinyl]methyl]pyridine) and [Fe$_2$OL$_2$(NO$_3$)$_2$(MeOH)$_2$][59] (L, 2,6-bis(*N*-methylbenzimidazol-2-yl)pyridine), respectively. The 3°/2° values observed for **2** seem to be the highest reported thus far for a non-heme iron/*t*-BuOOH system and thus suggest the involvement of an active oxidant more selective than free alkyloxy radicals.

Under standard reaction conditions, cyclohexane was converted with 27% efficiency to cyclohexanol and cyclohexanone with an alcohol to ketone ratio (A/K) of 0.6. A sharp drop in conversion to around 10% is observed when the reaction is carried out either in acetone, a known scavenger of oxygen-centered radicals, or under an N_2 atmosphere. Similar observations were made for ethylbenzene. The catalytic oxidation of ethylbenzene yielded both acetophenone and 1-phenylethanol with high turnovers and 79% conversion of the oxidant. Acetophenone was the major product (A/K = 0.4). Performing the reaction under a

nitrogen atmosphere had a dramatic effect for this substrate. Conversion dropped to less than 2% and almost no acetophenone or 1-phenylethanol was formed. Finally, the oxidation of the probe substrate *cis*-1,2-dimethylcyclohexane proceeded only to a limited extent. Both *cis*- and *trans*-1,2-dimethylcyclohexanol were formed and many side products, such as secondary alcohols and ketones were detected as well. The stereoselectivity of the reaction was very limited with only 27% retention of configuration. Data on these observations are combined in Table 5.

Table 5. Oxidation of alkanes by $[Fe^{II}(\mathbf{bik})_3](OTf)_2$ (**2**) with *t*-BuOOH[a]

Substrate	Product	TON[b]	Remarks
cyclohexane	cyclohexanol (A)	10.4	acetonitrile, air
	cyclohexanone (K)	16.9	A/K = 0.6
cyclohexane	cyclohexanol	4.0	acetone, air
	cyclohexanone	6.4	A/K = 0.6
cyclohexane	cyclohexanol	4.0	acetonitrile, N_2
	cyclohexanone	5.7	A/K = 0.7
ethylbenzene	1-phenylethanol	21.5	acetonitrile, air
	acetophenone	57.9	A/K = 0.4
ethylbenzene	1-phenylethanol	0.2	acetonitrile, N_2
	acetophenone	1.7	
cis-1,2-dimethylcyclohexane[d]	*cis*-1,2-ol	2.2	acetonitrile, air
	trans-1,2-ol	1.3	RC = 27%[c]

[a] For reaction conditions: see experimental section. [b] Yields expressed as turnover numbers (TON = mol product/mol catalyst). [c] Retention of configuration, [%RC] = 100 × (cis-1,2-ol – trans-1,2-ol)/(cis-1,2-ol + trans-1,2-ol). [d] Secondary alcohols and ketones not quantified.

Despite the promisingly high 3°/2° values obtained in the oxidation of adamantane, the results obtained in the oxidation of cyclohexane, ethylbenzene and *cis*-1,2-dimethylcyclohexane point to the operation of a free-radical based rather than a metal-based oxidation mechanism under the conditions described here. The low A/K value, the (strong) dioxygen dependence, and the low retention of configuration all point to the formation of long-lived free radicals.[60,61] Alkyloxy radicals could be the result of homolytic cleavage of a tentative iron(III)-*tert*-butylperoxo, as has been evidenced in a few cases.[55,62] The rather powerful *tert*-butoxy radical then abstracts a hydrogen atom from the alkane to give a long-lived alkyl radical. The free alkyl radicals combine with dioxygen and yield the products in Russel-type termination steps. Although the alkane oxidations of **2**/*t*-BuOOH seem to be dominated by free radical chemistry, the high 3°/2° value of 29.6 in the oxidation of adamantane in acetone suggest that other chemically competent oxidants are present in

solution as well. The possibility of other mechanisms with different oxidizing species than the alkyloxy radicals can therefore not be excluded.

The reactivity of **2**/H_2O_2 towards several different alkenes was also investigated. The alkene functionalizations were studied under similar experimental conditions as used for the alkane oxidations (acetonitrile, **2**:H_2O_2:substrate, 1:100:1000). The **2**/H_2O_2 combination was found to be active in olefin oxidation with conversions up to 17% and the results are listed in Table 6.

Table 6. Oxidation of alkenes catalyzed by [Fe(**bik**)$_3$](OTf)$_2$ (**2**) with H_2O_2[a]

Substrate	Epoxide (TON)[b] (drop wise addition of H_2O_2)		Epoxide (TON)[b] (addition of H_2O_2 at once)	
	1 hour	**7 hours**	**1 hour**	**7 hours**
cyclooctene	6.8	14.7	6.9	14.1
styrene[c,d]	7.7 (5.7)	14.5 (6.1)	7.3 (5.9)	12.8 (5.9)
1-octene	3.4	7.0	3.2	6.5
cyclohexene[d,e]	2.0 (15.6/13.8)	2.8 (24.2/17.6)	1.8 (17.2/14.7)	2.6 (22.3/15.3)
trans-2-heptene[f]	5.6 [93]	13.5 [91]	5.8 [88]	12.7 [94]
cis-2-heptene[f]	6.7 [62]	16.9 [77]	7.1 [64]	17.1 [77]

[a] See experimental section for reaction conditions. [b] Yields expressed as turnover numbers (TON = mol product/mol catalyst). [c] Value in brackets is the observed TON for benzaldehyde formation. [d] Reactions done under N_2 atmosphere. [e] Values in brackets are the observed TONs for 2-cyclohexen-1-ol and 2-cyclohexen-2-one, respectively. [f] Values in square brackets are the retention of configuration values, [%RC] = 100 × (A – B)/(A + B), where A is the epoxide with retention and B is the epimer.

Whereas in the alkane oxidations the reactions were completed after three hours, we found that the olefin oxidation proceeded more slowly. Monitoring the reaction in time showed an increase in product formation up to seven hours after the start of the drop wise addition of oxidant. The slow consumption of oxidant suggested that the slow, drop wise addition of oxidation was unnecessary under these conditions. Indeed, when all oxidant was added at once, similar results were obtained. The slow, drop wise addition is usually employed to minimize hydrogen peroxide disproportionation (catalase side reaction). Here, this non-productive consumption of H_2O_2 apparently proceeds at a comparably slow rate. Cyclooctene as substrate afforded the epoxide as the sole product with up to 15% conversion of the oxidant.

We tested the influence of acetic acid as an additive in the oxidation of cyclooctene by **2**/H_2O_2 (Table 7), since it has been reported to result in an increase in catalytic activity[63] or change in product selectivity.[64] In this case, the addition of 30 or 100 eq of acetic acid had a detrimental effect on the catalytic activity, which dropped to 4% with 100 eq of additive.

Styrene was epoxidized with a efficiency of about 15%, with concomitant formation of some benzaldehyde. 1-Octene and cyclohexene proved to be poorer substrates for the combination **2**/H_2O_2 with only 7 and 3% conversion and the predominant formation of allylic oxidation products for the latter substrate. The stereoselectivity of the oxidations was studied by the oxidation of the isomeric *cis*- and *trans*-2-heptenes. The epoxidation of *trans*-2-heptene occurs with high stereoselectivity, i.e. 94% retention of configuration (RC). The stereoretention in the oxidation of *cis*-2-heptene is somewhat lower (RC = 77%), which means that some isomerization of an oxidized olefin species to the more stable *trans* isomer happens prior to epoxide ring formation. The observed stereoselectivity suggests the involvement of a metal-based oxidant and the formation of a substrate radical type intermediate.[65] This substrate radical species would allow the partial isomerization observed for *cis*-2-heptene before epoxide ring formation and would account for the observed benzaldehyde formation in the styrene oxidation.[66]

Table 7. Oxidation of cyclooctene by [Fe(**bik**)$_3$](OTf)$_2$ (**2**) with H_2O_2 with acetic acid as additive and under limiting substrate conditions[a]

Ratio cat.:H_2O_2:substrate	Epoxide[b] (TON) (drop wise addition)		Epoxide[b] (TON) (addition at once)		Conversion[c] (%)	
1 : 100 : 1000	**1 hour**	**7 hours**	**1 hour**	**7 hours**	**drop wise**	**at once**
0 eq CH_3COOH[d]	6.8	14.7	6.9	14.1	14.7	14.1
30 eq CH_3COOH[d]	2.2	7.0	--	--	7.0	--
100 eq CH_3COOH[d]	2.0	4.3	--	--	4.3	--
limiting substrate						
1 : 300 : 30	2.8	3.6	2.3	3.0	12.0	10.0
1 : 150 : 30	3.0	5.4	2.9	5.5	18.0	18.3
1 : 60 : 30	2.8	7.0	2.3	6.6	**23.3**	**22.0**
1 : 45 : 30	2.0	4.3	1.8	3.6	14.3	12.0
1 : 35 : 30	1.3	2.3	1.3	2.1	7.7	7.0

[a] Reaction conditions: see footnote a, Table 6. [b] Yields expressed as turnover numbers (TON = mol product/mol catalyst). [c] Percent conversion of H_2O_2 into epoxide (acetic acid entries) or substrate into epoxide (limiting substrate entries) after 7 hours. [d] 0, 30, or 100 equivalents of acetic acid added before addition of oxidant.

The olefin oxidations described above were all conducted with excess substrate with respect to the oxidant. From a practical point of view, however, it is desirable to develop a system capable of doing the oxidations under limiting substrate conditions. Jacobsen et al., for instance, reported the selective olefin epoxidation by a non-heme iron complex using 1.5 eq of H_2O_2 with respect to the substrate.[63] Que et al. obtained both epoxide and diol products under limiting substrate conditions with 4 eq of H_2O_2.[67] To investigate if **2** could also mediate

olefin oxidation under limiting substrate conditions, different substrate to oxidant ratios were tested (Table 7). The results were found to vary significantly and maximum conversion of about 23% of the substrate to cyclooctene oxide was found using two equivalents of hydrogen peroxide with respect to the substrate. The use of both more or less than two equivalents resulted in a decrease in observed turnover. Two equivalents of hydrogen peroxide is the apparent optimum for the two competing pathways, i.e. substrate oxidation versus catalase activity.

Remarkably, no *cis*-dihydroxylation products were detected in any of these olefin oxidation reactions. Several examples of non-heme iron complexes capable of olefin epoxidation *and cis*-dihydroxylation have recently been reported,[15,65,67-71] most notably the family of iron catalysts developed by Que et al. The distinguishing feature of these catalysts is the availability of *cis*-positioned labile sites.[65] This structural element has therefore been suggested to be essential for observing both types of reactivities. The final ratio between these epoxide and *cis*-dihydroxylation products then ultimately depends on the ligand structure. Non-heme iron complexes with two vacant sites *trans* with respect to each other, such as for example $[Fe^{II}(cyclam)(OTf)_2]$, were indeed found to be fully selective towards epoxidation.[72,73] The fact that **2** selectively catalyzes epoxide formation and that no *cis*-dihydroxylation products are observed, is therefore somewhat remarkable. The dissociation of one **bik** ligand would initially result in the availability of two *cis*-positioned vacant sites. Rearrangement to a structure with both remaining **bik** ligands in the equatorial plane and thus the formation of a complex with two *trans*-located vacant sites is unlikely for steric reasons, since the hydrogen atoms on the imidazole-rings would collide in such an arrangement. Together with the observed lack of *cis*-dihydroxylation activity, this geometrical argument, therefore, suggests the presence of a structure with an intermediate geometry that does not possess two readily available cis-positioned vacant sites.

6.3 Conclusions

The study of the iron coordination chemistry of the simple **bik** building block resulted in the isolation of a ferric and ferrous complex with interesting properties. The self-assembly of the $[Fe^{III}_2(\mu\text{-}OH)_2]^{4+}$ core of the dinuclear complex **1** with **bik** provides an easy access to this interesting structure. The antiferromagnetic coupling of the metal centers was expected, but the observed coupling constant does not fall in the range reported for this type of structures. This warrants further investigation of the magnetic properties of **1** by Mössbauer spectroscopy and DFT calculations. Unfortunately, the instability of **1** in solution did not allow the study of **1** as a potential oxidation catalyst. The $[Fe^{II}(\mathbf{bik})_3]^{2+}$ decomposition product of **1**, however, proved to be an interesting species as well. It lead to the independent synthesis of $[Fe^{II}(\mathbf{bik})_3](OTf)_2$ (**2**), which showed spin-crossover behavior at a rather high temperature and moderate to good activity in the oxidation of alkanes and alkenes. Taking into consideration that **2** is an air-stable ferrous complex, which can be easily obtained in one step, renders **2** a good candidate for further optimization of its catalytic properties.

6.4 Experimental Section

Air-sensitive reactions were carried out under an atmosphere of dry, oxygen-free N_2 using standard Schlenk techniques. All chemicals were commercially obtained and used as received. THF was dried over sodium benzophenone ketyl and distilled under N_2 prior to use. Methanol was dried over magnesium methoxide and distilled under N_2 prior to use. ^{1}H and ^{13}C NMR spectra were recorded on a Varian AS400 or Varian Inova 300 spectrometer, operating at 25 °C. Elemental microanalyses were carried out by the Microanalytisches Laboratorium Dornis & Kolbe, Mulheim a.d. Ruhr, Germany. Infrared spectra were recorded on a Perkin Elmer Spectrum One FT-IR instrument. ESI-MS spectra were recorded on a Micromass LC-TOF mass spectrometer by the Biomolecular Mass Spectrometry group, Utrecht University. Solution magnetic moments were determined by Evans' NMR method in acetone-d_6/cyclohexane (95/5 *v*/*v*) at a temperature range of – 25 to 50 °C. UV-Vis spectra were recorded on a Varian Cary 50 spectrometer equipped with a Helma emersion probe for in situ measurements. Bulk magnetization measurements were performed with a Quantum Design MPMS-5 5T (**1**, 2-300 K) or MPMS-XL (**2**, 6-400 K) SQUID magnetometer. Data were corrected for magnetization of the sample holder in the case **1**, but not **2**, since its contribution in the latter case was found to be negligible. Diamagnetic contributions were estimated from Pascal's constants. TGA measurements were performed using a Setaram TAG 24 thermoanalyzer. Bis(1-methylimidazol-2-yl)ketone (**bik**)[74] and $Fe(OTf)_2{\cdot}2MeCN$[75] were prepared according to literature procedures. All other chemicals were commercially obtained and used as received.

$[Fe_2(\mu\text{-}OH)_2(bik)_4](NO_3)_4$ (1). To a solution of **bik** (1.85 g, 9.73 mmol) in ethanol/water (32 mL, 15:1 *v*/*v*) was added an orange solution of $Fe(NO_3)_3{\cdot}9H_2O$ (1.96 mg, 4.86 mmol) in ethanol (30 mL). The solution was stirred for 90 min at 60 ºC, during which gradually a yellowish-orange precipitate formed. The precipitate was separated by centrifugation, washed with ethanol (30 mL) and dried *in vacuo*. The product was obtained as a yellowish-orange powder (2.65 g, 94% yield). Orange-red crystals of **1** suitable for X-ray diffraction were obtained by slow evaporation of a water solution. Anal. for $C_{36}H_{42}Fe_2N_{20}O_{18}{\cdot}2H_2O$ (1190.56): calc. C 36.32, H 3.89, N 23.53; found C 36.45, H 3.81, N 23.61. IR (solid) ν = 3549.2, 3437.9, 3105.2, 3068.9, 1661.9, 1490.2, 1463.8, 1424.4, 1401.6, 1357.9, 1309.6, 1166.8, 1037.4, 960.5, 900.7, 827.3, 790.4, 773.4, 726.0 cm^{-1}. UV-Vis (MeOH, ε [M^{-1} cm^{-1}]): λ_{max} = 285 (43000), 327 (71000) nm.

$[Fe(bik)_3](OTf)_2$ (2). To a colorless solution of **bik** (255 mg, 1.35 mmol) in dry methanol (15 mL) was added a colorless solution of $Fe(OTf)_2{\cdot}2MeCN$ (197 mg, 0.45 mmol) in dry methanol (5 mL) and immediately a color change to dark purplish blue was observed. The solution was stirred for 30 min at room temperature, after which diethyl ether (30 mL) was added to precipitate the product. The precipitate was separated by centrifugation, washed with diethyl ether (2 × 20 mL) and dried in *vacuo* to give a dark blue powder. Recrystallization from methanol/diethyl ether at – 30 °C yielded the product as a blue microcrystalline powder (384 mg, 89%) Blue crystals suitable for X-ray diffraction were obtained by slow vapor diffusion of diethyl ether into a methanolic solution of **2**. Anal. for $C_{29}H_{30}F_6FeN_{12}O_9S_2$ (924.59): calc. C 37.67, H 3.27, N 18.18; found C 37.59, H 3.34, N 18.08. ^{1}H NMR (300 MHz, CD_3OD) 25 ºC: δ = 4.18 (s, 2H, H_{im}), 7.59 (s, 6H, CH_3), 18.05 (s, 2H, H_{im}) ppm; -95 ºC: δ = 4.18 (s, 6H, CH_3), 6.34 (s, 2H, H_{im}), 7.65 (s, 2H, H_{im}) ppm. IR (solid) ν = 3561.7 3134.3, 2970.4, 1628.6, 1521.2, 1486.8, 1420.5, 1253.6, 1223.0, 1144.4, 1028.1, 896.3, 788.3, 767.0 cm^{-1}. UV-Vis (MeOH, ε [M^{-1} cm^{-1}]): λ_{max} = 236 (14000), 290 (26000), 324 (51000), 583 (4500) nm. ESI-MS: *m/z* = 313.07 {$[Fe^{II}(bik)_3]^{2+}$,

calc. 313.10}, 584.97 {$[Fe^{II}(bik)_2(OTf)]^+$, calc. 585.06}, 775.18 {$[Fe^{II}(bik)_3(OTf)]^+$, calc. 775.14}, 925.15 {$[Fe^{II}(bik)_3(OTf)_2+H]^{2+}$, calc. 925.10}.

Catalysis protocol. To a stirred solution of catalyst (3 μmol) in acetonitrile (2 mL) was added substrate (1000 eq, 3 mmol) and acetonitrile (to bring the total volume to 2.5 mL). Subsequently, 0.5 mL of oxidant solution (100 eq, 600 mM solution in acetonitrile diluted from 35% aqueous H_2O_2 or 70% aqueous *t*-BuOOH) was added either drop wise in 20 min or at once. The ratio of catalyst:oxidant:substrate was 1:100:1000. The reaction mixture was stirred at room temperature and after 1 hour (from start of oxidant addition) internal standard (10 μL, cyclooctene: 1,2-dibromobenzene, cyclohexane: chlorobenzene, all other substrates: bromobenzene) was added and the first sample was taken. After three (alkanes) or seven hours (alkenes) a second sample was taken from the reaction mixture. The aliquots of the reaction mixture were filtered over a short silica plug, after which the short column was flushed twice with diethyl ether. The samples were concentrated by a stream of N_2 and analyzed by GC. The products were identified and quantified by GC by comparison with authentic compounds. The reported values are the average of at least two independent runs.

X-ray crystal structure determinations of 1 and 2·MeOH. Reflections were measured on a Nonius Kappa CCD diffractometer with rotating anode (graphite monochromator, λ = 0.71073 Å) at a temperature of 150 K. Intensities were integrated with EvalCCD[76] using an accurate description of the experimental setup for the prediction of the reflection contours. The structures were refined with SHELXL-97[77] against F^2 of all reflections. Non hydrogen atoms were refined with anisotropic displacement parameters. Hydrogen atoms were introduced in geometrically optimized positions. The O-H hydrogen atoms were refined freely with isotropic displacement parameters; all other hydrogen atoms were refined with a riding model. Geometry calculations and checking for higher symmetry was performed with the PLATON program.[78]

X-ray crystal structure determination of 1. $[C_{36}H_{42}Fe_2N_{16}O_6](NO_3)_4{\cdot}2H_2O$, Fw = 1190.63, colorless block, 0.22 × 0.13 × 0.05 mm^3, monoclinic, C2/c (no. 15), a = 23.5604(10), b = 14.6757(10), c = 13.9671(10) Å, β = 92.071(1)°, V = 4826.2(5) $Å^3$, Z = 4, D_x = 1.639 g/cm^3, μ = 0.70 mm^{-1}. 88283 Reflections were measured up to a resolution of $(\sin\theta/\lambda)_{max}$ = 0.62 $Å^{-1}$. The crystal appeared to be non-merohedrally twinned with a twofold rotation about the reciprocal *c**-axis as twin operation. This twin operation was taken into account during the integration of the intensities and the refinement as a HKLF5 refinement.[79] The reflections were corrected for absorption and scaled on the basis of multiple measured reflections with the program TWINABS[80] (0.76-0.96 correction range). 4782 Reflections were unique (R_{int} = 0.0547). The structure was solved with the program SHELXS-86[81] using Direct Methods. 369 Parameters were refined with 3 restraints. R1/wR2 [I>2σ(I)]: 0.0473/0.0934. R1/wR2 [all refl.]: 0.0677/0.1029. S = 1.081. The twin fraction refined to 0.1049(16). Residual electron density between – 0.43 and 0.60 e/$Å^3$.

X-ray crystal structure determination of 2·MeOH. $[C_{27}H_{30}FeN_{12}O_3](CF_3O_3S)_2{\cdot}CH_3OH$, Fw = 956.66, dark blue plate, 0.24 × 0.18 × 0.06 mm^3, orthorhombic, Fdd2 (no. 43), a = 25.85847(1), b = 50.00278(10), c = 11.81363(2) Å, V = 15274.97(15) $Å^3$, Z = 16, D_x = 1.664 g/cm^3, μ = 0.61 mm^{-1}. 65769 Reflections were measured up to a resolution of $(\sin\theta/\lambda)_{max}$ = 0.65 $Å^{-1}$. The reflections were corrected for absorption and scaled on the basis of multiple measured reflections with the program SADABS[82] (0.76-0.96 correction range). 8742 Reflections were unique (R_{int} = 0.0418). The structure was solved with the program SIR-97[83] using Direct

Methods. One triflate anion was refined with a disorder model. 594 Parameters were refined with 92 restraints. R1/wR2 [I>2σ(I)]: 0.0278/0.0593. R1/wR2 [all refl.]: 0.0357/0.0624. S = 1.033. Flack parameter x = 0.001(8). [84] Residual electron density between – 0.20 and 0.21 e/Å^3.

6.5 References

1. Tanase, S.; Bouwman, E. *Adv. Inorg. Chem.* **2006**, *58*, 29-75.
2. Costas, M.; Mehn, M. P.; Jensen, M. P.; Que, L., Jr. *Chem. Rev.* **2004**, *104*, 939-986.
3. Solomon, E. I.; Brunold, T. C.; Davis, M. I.; Kernsley, J. N.; Lee, S-K.; Lehnert, N.; Neese, F.; Skulan, A. J.; Yang, Y-S.; Zhou, J. *Chem. Rev.* **2000**, *100*, 235-349.
4. Tshuva, E. Y.; Lippard, S. J. *Chem. Rev.* **2004**, *104*, 987-1012.
5. Costas, M.; Chen, K.; Que, L. Jr. *Coord. Chem. Rev.* **2000**, *200-202*, 517-544.
6. Du Bois, J.; Mizoguchi, T. J.; Lippard, S. J. *Coord. Chem. Rev.* **2000**, *200-202*, 443-485.
7. Chen, K.; Costas, M.; Kim, J.; Tipton, A. K.; Que, L., Jr. *J. Am. Chem. Soc.* **2002**, *124*, 3026-3035.
8. Chen, K.; Que, L. Jr. *J. Am. Chem. Soc.* **2001**, *123*, 6327-6337.
9. Roelfes, G.; Lubben, M.; Hage, R.; Que, L. Jr.; Feringa, B. L. *Chem. Eur. J.* **2000**, *6*, 2152-2159.
10. van den Berg, T. A.; de Boer, J. W.; Browne, W. R.; Roelfes, G.; Feringa, B. L. *Chem. Commun.* **2004**, 2550-2551.
11. Guajardo, R. J.; Hudson, S. E.; Brown, S. J.; Mascharak, P. K. *J. Am. Chem. Soc.* **193**, *115*, 7971-7977.
12. Buchanan, R. M.; Chen, S.; Richardson, J. F.; Bressan, M.; Forti, L.; Morvillo, A.; Fish, R. H. *Inorg. Chem.* **1994**, *33*, 3208-3209.
13. Dubois, G.; Murphy, A.; Stack, T. D. P. *Org. Lett.* **2003**, *5*, 2469-2472.
14. Ménage, S.; Vincent, J. M.; Lambeaux, C.; Chottard, G.; Grand, A.; Fontecave, M. *Inorg. Chem.* **1993**, *32*, 4766-4773.
15. Bruijnincx, P. C. A.; Buurmans, I. L. C.; Gosiewska, S.; Lutz, M.; Spek, A. L.; van Koten, G.; Klein Gebbink, R. J. M. *to be submitted* (Chapter 5 of this thesis).
16. Bruijnincx, P. C. A.; Lutz, M.; Spek, A. L.; Hagen, W. R.; Weckhuysen, B. M.; van Koten, G.; Klein Gebbink, R. J. M., *J. Am. Chem. Soc.*, accepted for publication (Chapter 3 of this thesis).
17. Bruijnincx, P. C. A.; Lutz, M.; Spek, A. L.; van Faassen, E. L.; Weckhuysen, B. M.; van Koten, G.; Klein Gebbink, R. J. M. *Eur. J. Inorg. Chem.* **2005**, 779-787 (Chapter 2 of this thesis).
18. Braussaud, N.; Rüther, T.; Cavell, K. J.; Skelton, B. W.; White, A. H. *Synthesis* **2001**, *4*, 626-632.
19. Ardon, M.; Bino, A.; Michelsen, K. *J. Am. Chem. Soc.* **1987**, *109*, 1986-1990.
20. Yang, G.; Zheng, S.-L.; Chen, X.-M.; Lee, H. K.; Zhou, Z.-Y.; Mak, T. C. W. *Inorg. Chim. Acta* **2000**, *303*, 86-93.
21. Crowder, K. N.; Garcia, S. J.; Burr, R. L.; North, J. M.; Wilson, M. H.; Conley, B. L.; Fanwick, P. E.; White, P. S.; Sienerth, K. D.; Granger II, R. M. *Inorg. Chem.* **2004**, *43*, 72-78.
22. Byers, P. K.; Canty, A. J.; Engelhardt, L. M.; Patrick, J. M.; White, A. H. *J. Chem. Soc., Dalton Trans.* **1985**, 981-986.
23. Woltz, J.; Westcott, B. L.; Crundwell, G.; Zeller, M.; Hunter, A. D.; Sommerer, S. O. *Acta Cryst.* **2002**, *E58*, m609-m610.
24. Borer, L.; Thalken, L.; Ceccarelli, C.; Glick, M.; Zhang, J. H.; Reiff, W. M. *Inorg. Chem.* **1983**, *22*, 1719-1724.
25. Ou, C. C.; Lalancette, R. A.; Potenza, J. A.; Schugar, H. J. *J. Am. Chem. Soc.* **1978**, *100*, 2053-2057.
26. Tanase, S.; Bouwman, E.; Long, G. J.; Shahin, A. M.; Mills, A. M.; Spek, A. L.; Reedijk, J. *Eur. J. Inorg. Chem.* **2004**, 4572-4578.

27. Thich, J. A.; Ou, C. C.; Powers, D.; Vasiliou, B.; Mastropaolo, D.; Potenza, J. A.; Schugar, H. J. *J. Am. Chem. Soc.* **1976**, *98*, 1425-1432.
28. Zhu, S.; Brennessel, W. W.; Harrison, R. G.; Que, L., Jr. *Inorg. Chim. Acta* **2002**, *337*, 32-38.
29. Nanda, K. K.; Dutta, S. K.; Baitalik, S.; Venkatsubramanian, K.; Kamalaksha, N. *J. Chem. Soc., Dalton Trans.* **1995**, 1239-1244.
30. Lee, D.; Du Bois, J.; Petasis, D.; Hendrich, M. P.; Krebs, C.; Huynh, B. H.; Lippard, S. J. *J. Am. Chem. Soc.* **1999**, *121*, 9893-9894.
31. Lee, D.; Lippard, S. J. *J. Am. Chem. Soc.* **1998**, *120*, 12153-12154.
32. Yoon, S.; Lippard, S. J. *J. Am. Chem. Soc.* **2004**, *126*, 2666-2667.
33. Kahn, O., *Molecular Magnetism*. Wiley-VCH: New York, 1993.
34. Gorun, S. M.; Lippard, S. J. *Inorg. Chem.* **1991**, *30*, 1625-1630.
35. Jullien, J.; Juhász, G.; Mialane, P.; Dumas, E.; Mayer, C. R.; Marrot, J.; Rivière, E.; Bominaar, E. L.; Münck, E.; Sécheresse, F. *Inorg. Chem.* **2006**, *45*, 6922-6927.
36. Bénisvy, L.; Chottard, J.-C.; Marrot, J.; Li, Y. *Eur. J. Inorg. Chem.* **2005**, 999-1002.
37. Gorun, S. M.; Lippard, S. J. *Inorg. Chem.* **1988**, *27*, 149-156.
38. Guillot, G.; Mulliez, E.; Leduc, P.; Chottard, J.-C. *Inorg. Chem.* **1990**, *29*, 579-581.
39. Kitajima, N.; Tamura, N.; Tanaka, M.; Moro-oka, Y. *Inorg. Chem.* **1992**, *31*, 3342-3343.
40. Stubna, A.; Jo, D.-H.; Costas, M.; Brenessel, W. W.; Andres, H.; Bominaar, E. L.; Münck, E.; Que, L. Jr. *Inorg. Chem.* **2004**, 3067-3079.
41. Kryatov, S. V.; Taktak, S.; Korendovych, I. V.; Rybak-Akimova, E.; Kaizer, J.; Torelli, S.; Shan, X.; Mandal, S.; MacMurdo, V. L.; Mairata i Payeras, A.; Que, L. Jr. *Inorg. Chem.* **2005**, *44*, 85-99.
42. Gejji, S. P.; Hermansson, K.; Lindgren, J. *J. Phys. Chem.* **1993**, *97*, 3712-3715.
43. Gosiewska, S.; Cornelissen, J. L. M.; Lutz, M.; Spek, A. L.; van Koten, G.; Klein Gebbink, R. J. M. *Inorg. Chem.* **2006**, *45*, 4214-4227.
44. Batten, M. P.; Canty, A. J.; Cavell, K. J.; Rüther, T.; Skelton, B. W.; White, A. H. *Acta Cryst.* **2004**, *C60*, m316-m319.
45. Gütlich, P.; Garcia, Y.; Goodwin, H. A. *Chem. Soc. Rev.* **2000**, *29*, 419-427.
46. Bousseksou, A.; Place, C.; Linares, J.; Varret, F. *J. Magn. Magn. Mat.* **1992**, *104-107*, 225-226.
47. Britovsek, G. J. P.; Gibson, V. C.; Spitzmesser, S. K.; Tellmann, K. P.; White, A. J. P.; Williams, D. J. *J. Chem. Soc., Dalton Trans.* **2002**.
48. Evans, D. F. J. *J. Chem. Soc.* **1959**, 2003-2005.
49. Buchen, T.; Gütlich, P.; Sugiyarto, K. H.; Goodwin, H. A. *Chem. Eur. J.* **1996**, *2*, 1134-1138.
50. Gütlich, P.; Köppen, H.; Steinhäuser, H. G. *Chem. Phys. Lett.* **1980**, *74*, 475-480.
51. Sorai, M.; Ensling, J.; Hasselbach, K. M.; Gütlich, P. *Chem. Phys.* **1977**, *20*.
52. Gütlich, P.; Hauser, A.; Spiering, H. *Angew. Chem. Int. Ed.* **1994**, *33*, 2024-2054.
53. Marchivie, M.; Guionneau, P.; Létard, J. F.; Chasseau, D. *Acta Cryst.* **2005**, *B61*, 25-28.
54. Barton, D. H. R.; Boivin, J.; Motherwell, W. B.; Ozbalik, N.; Schwartzentruber, K. M.; Jankowski, K. *New. J. Chem.* **1987**, *10*, 387-398.
55. Gosiewska, S.; Permentier, H. P.; Bruins, A. P.; van Koten, G.; Klein Gebbink, R. J. M. *submitted*.
56. Kojima, T.; Leising, R. A.; Yan, S.; Que, L. Jr. *J. Am. Chem. Soc.* **1993**, *115*, 11328-11335.
57. Ménage, S.; Vincent, J. M.; Lambeaux, C.; Fontecave, M. *J. Mol. Cat. A* **1996**, *113*, 61-75.
58. Nguyen, C.; Guajardo, R. J.; Mascharak, P. K. *Inorg. Chem.* **1996**, *35*, 6273-6281.
59. Wang, X.; Wang, S.; Li, L.; Sundberg, E. B.; Gacho, G. P. *Inorg. Chem.* **2003**, *42*, 7799-7808.

60. MacFaul, P. A.; Arends, I. W. C. E.; Ingold, K. U.; Wayner, D. D. M. *J. Chem. Soc., Perkin Trans. 2* **1997**, 135-145.
61. MacFaul, P. A.; Arends, I. W. C. E.; Ingold, K. U.; Wayner, D. D. M.; Que, L. Jr. *J. Am. Chem. Soc.* **1997**, *119*, 10594-10598.
62. Jensen, M. P.; Costas, M.; Ho, R. Y. N.; Kaizer, J.; Mairata i Payeras, A.; Münck, E.; Que, L. Jr.; Rohde, J.-U.; Stubna, A. *J. Am. Chem. Soc.* **2005**, *127*, 10512-10525.
63. White, M. C.; Doyle, A. G.; Jacobsen, E. N. *J. Am. Chem. Soc.* **2001**, *123*, 7194-7195.
64. Mas-Ballesté, R.; Fujita, M.; Hemmila, C.; Que, L. Jr. *J. Mol. Cat. A* **2006**, *251*, 49-53.
65. Chen, K.; Costas, M.; Que, L., Jr. *J. Chem. Soc., Dalton Trans.* **2002**, 672-679.
66. Groves, J. T.; Gross, Z.; Stern, M. K. *Inorg. Chem.* **1994**, *33*, 5065-5072.
67. Ryu, J. Y.; Kim, J.; Costas, M.; Chen, K.; Nam, W.; Que, L., Jr. *Chem. Commun.* **2002**, 1288-1289.
68. Chen, K.; Costas, M.; Kim, J.; Tipton, A. K.; Que, L., Jr. *J. Am. Chem. Soc.* **2003**, *124*, 3026-3035.
69. Costas, M.; Tipton, A. K.; Chen, K.; Jo, D.-H.; Que, L., Jr. *J. Am. Chem. Soc.* **2001**, *123*, 6722-6723.
70. Klopstra, M.; Roelfes, G.; Hage, R.; Kellogg, R. M.; Feringa, B. L. *Eur. J. Inorg. Chem.* **2004**, 846-856.
71. Oldenburg, P. D.; Shteinman, A. A.; Que, L., Jr. *J. Am. Chem. Soc.* **2005**, *127*, 15673-15674.
72. Chen, K.; Que, L., Jr. *Angew. Chem. Int. Ed.* **1999**, *38*, 2227-2229.
73. Nam, W.; Ho, R.; Valentine, J. S. *J. Am. Chem. Soc.* **1991**, *113*, 7052-7054.
74. Lucas, P.; El Mehdi, N.; Ang Ho, H.; Bélanger, D.; Breau, L. *Synthesis* **2000**, *9*, 1253-1258.
75. Hagen, K. S. *Inorg. Chem.* **2000**, *39*, 5867-5869.
76. Duisenberg, A. J. M.; Kroon-Batenburg, L. M. J.; Schreurs, A. M. M. *J. Appl. Cryst.* **2003**, *36*, 220-229.
77. Sheldrick, G. M. *SHELXL-97. Program for crystal structure refinement*, University of Göttingen: Germany, 1997.
78. Spek, A. L. *J. Appl. Cryst.* **2003**, *36*, 7-13.
79. Herbst-Irmer, R.; Sheldrick, G. M. *Acta Cryst.* **1998**, *B54*, 443-449.
80. Sheldrick, G. M. *TWINABS: Bruker-Nonius scaling and absorption correction for twinned crystals, V1.05*, University of Göttingen: Germany, 2004.
81. Sheldrick, G. M. *SHELXS-86. Program for crystal structure solution*, University of Göttingen: Germany, 1986.
82. Sheldrick, G. M. *SADABS: Area-Detector Absorption Correction, V2.10*, University of Göttingen: Germany, 1999.
83. Altomare, A.; Burla, M. C.; Camalli, M.; Cascarano, G. L.; Giacovazzo, C.; Guagliardi, A.; Moliterni, A. G. G.; Polidori, G.; Spagna, R. *J. Appl. Cryst.* **1999**, *32*, 115-119.
84. Flack, H. D. *Acta Cryst.* **1983**, *A39*, 876-881.

CHAPTER 7

Zinc Complexes of the Biomimetic *N,N,O* Ligand Family of Substituted 3,3-Bis(1-alkylimidazol-2-yl)propionates: The Formation of Oxalate from Pyruvate

Abstract

The coordination chemistry of the 2-His-1-carboxylate facial triad mimics 3,3-bis(1-methylimidazol-2-yl)propionate (**L1**) and 3,3-bis(1-ethyl-4-isopropylimidazol-2-yl) propionate (**L3**) towards $ZnCl_2$ was studied both in solution and in the solid state. The 1:1 ligand to metal complexes [Zn(**L1**)Cl(H_2O)] (**2·H_2O**) and [Zn(**L3**)Cl] (**3**) were crystallographically characterized and found to be polymeric in nature. A new, bridging coordination mode of the ligands was observed in both structures comprising *N,N*-bidentate coordination of the ligand to one zinc atom and *O*-monodentate to a second. A rather unique transformation of pyruvate into *oxalate* was found with [Zn(**L1**)Cl] (**2**), which resulted in the isolation of the new, oxalato bridged zinc coordination polymer $[Zn_2(\mathbf{L1})_2(ox)]\cdot 6H_2O$ (**7**), which structure was established by X-ray crystal structure determination.

P. C. A. Bruijnincx, M. Lutz, J. P. den Breejen, A. L. Spek, G. van Koten, R. J. M. Klein Gebbink, manuscript in preparation

7.1 Introduction

The 2-His-1-carboxylate facial triad is a structural motif of increasing prominence among structurally characterized metalloenzymes. Next to the rapidly growing subgroup of non-heme iron enzymes,[1,2] several mononuclear zinc enzymes also feature this triad at their active site.[3] The proteases thermolysin, carboxypeptidase, and neutral protease, for example, catalyze the hydrolysis of peptide bonds. The zinc ion in these enzymes is coordinated by three endogenous residues, i.e. one glutamate and two histidine residues (Figure 1). The fourth coordination site of the pseudo-tetrahedral zinc center is occupied by a catalytically important water or hydroxide ligand. This 2-His-1-carboxylate facial triad is a variation of the most commonly observed structural motif for the active sites of zinc-containing enzymes. Typically, the tetrahedral zinc centers in these enzymes are bound by a combination of histidine (*N*), glutamate or aspartate (*O*) and/or cysteine (*S*) residues. The resulting $N_xO_yS_z$ donor set determines its biological function.[3] Accordingly, it is important to understand how a particular combination of donor groups modulates the reactivity of the Zn(II) metal center.

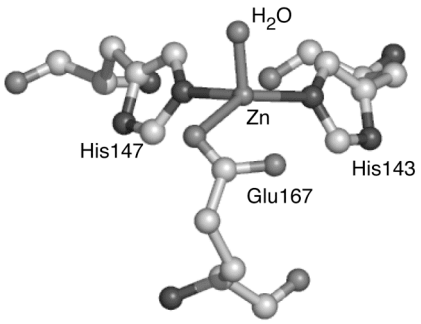

Figure 1. Active site of a zinc containing enzyme that features the 2-His-1-carboxylate facial triad: neutral protease from *Bacillus cereus* (1NPC.pdb).[4]

The study of small synthetic analogues has focused on establishing a basis for such a structure-function relationship for these mononuclear zinc-containing enzymes.[3,5] Initially, pioneering studies by the groups of Vahrenkamp, Parkin, Kitajima, and others employed all-*N* donor ligands such as the trispyrazolylborates.[6-8] In order to obtain close structural models for the 2-His-1-carboxylate facial triad containing zinc enzymes, one would preferentially like to construct small analogues based on a tripodal *N*,*N*,*O* ligand framework that incorporates the biologically relevant donor groups. Of the complexes with a mixed *N*/*O* donor set reported to date,[9-22] only few make use of such tridentate, tripodal $N,N,O_{carboxylato}$ ligands. These tripodal ligands should be particularly well-suited for the structural modeling of tetrahedral metal centers.[23] Parkin reported the first example of an *N*,*N*,*O* model complex with a carboxylato donor group, which resulted from the insertion of carbon dioxide into a borohydride bond.[24,25] More recently, the groups of Burzlaff and Carrano have reported studies on the zinc coordination chemistry of the bispyrazolylacetate ligand family.[9,11,12,18,19] Burzlaff et al., for instance, reported that a 2:1 ligand:zinc complex was obtained with bis(3,5-dimethylpyrazol-

2-yl)acetate (bdmpza), a ligand closely related to **L1** (*vide infra*). These 2:1 complexes were obtained regardless of the ratio of reactants, i.e. even with stoichiometric amounts of ligand and zinc(II).[9] Very recently, Que and Tolman and coworkers constructed mononuclear zinc models via a new approach, i.e. by the use of sterically hindered carboxylato and *N*-donor ligand building blocks.[22]

We have been studying the copper and iron coordination chemistry of the new ligand family of the substituted 3,3-bis(1-alkylimidazol-2-yl)propionates as accurate structural mimics of the 2-His-1-carboxylate facial triad.[26-30] These ligands incorporate the biologically relevant donor groups, i.e. two imidazoles and a carboxylate group, into a monoanionic, tripodal framework. Their general biomimetic potential has been illustrated by the structurally characterized copper[28-30] and iron complexes[26,27] of these ligands. In this Chapter, we expand our studies to the structural modeling of the zinc containing enzymes and describe the zinc coordination chemistry of the ligands 3,3-bis(1-methylimidazol-2-yl)propionate (**L1**) and 3,3-bis(1-ethyl-4-isopropylimidazol-2-yl)propionate (**L3**) (Chart 1). Furthermore, the attempted synthesis of zinc complexes with 3,3-bis(1-methylimidazol-2-yl)acetate (**L5**), a direct analogue of the bispyrazolylacetates, is described. During the course of these studies, we found that zinc complexes of ligand **L1** catalyze the unexpected and unprecedented conversion of pyruvate to oxalate in aqueous solution.

Chart 1. Ligands **L1**, **L3**, and **L5** and the synthesis of the zinc complexes **1**-**3**.

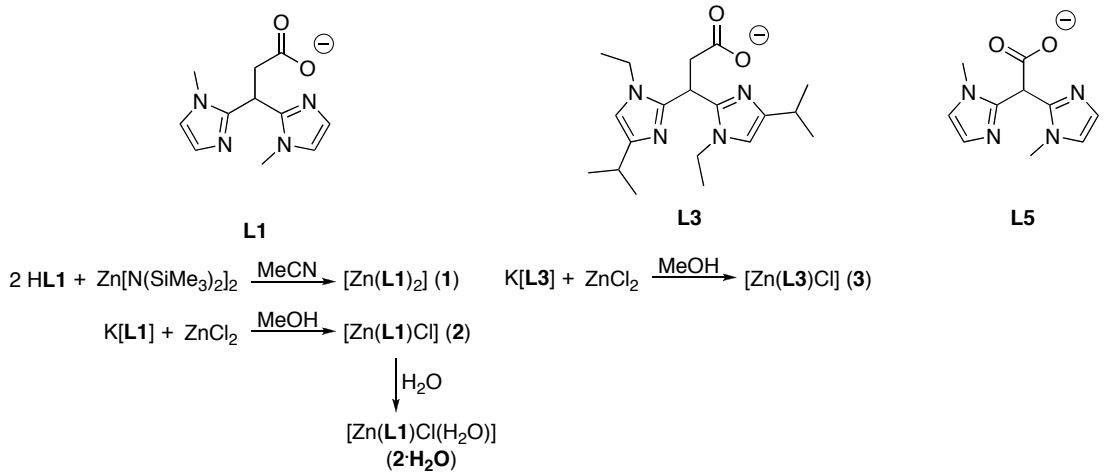

7.2 Results

As part of our efforts to study the coordination chemistry of the substituted 3,3-bis(1-alkylimidazol-2-yl)propionate ligand family, the complexes of **L1** and **L3** with $ZnCl_2$ were synthesized and structurally characterized (Chart 1). **L1** is the parent ligand of the family and **L3** offers the most steric hindrance of the ligands studied so far. The coordination chemistry of **L1** and **L3** with zinc was found to be stoichiometry dependent.

Zinc complexes of L1. The formation of different species upon addition of either 0.5 or 1.0 equivalent of $ZnCl_2$ to a solution of the potassium salt of **L1** in D_2O is evidenced by the respective ^1H NMR spectra in D_2O (Figure 2).

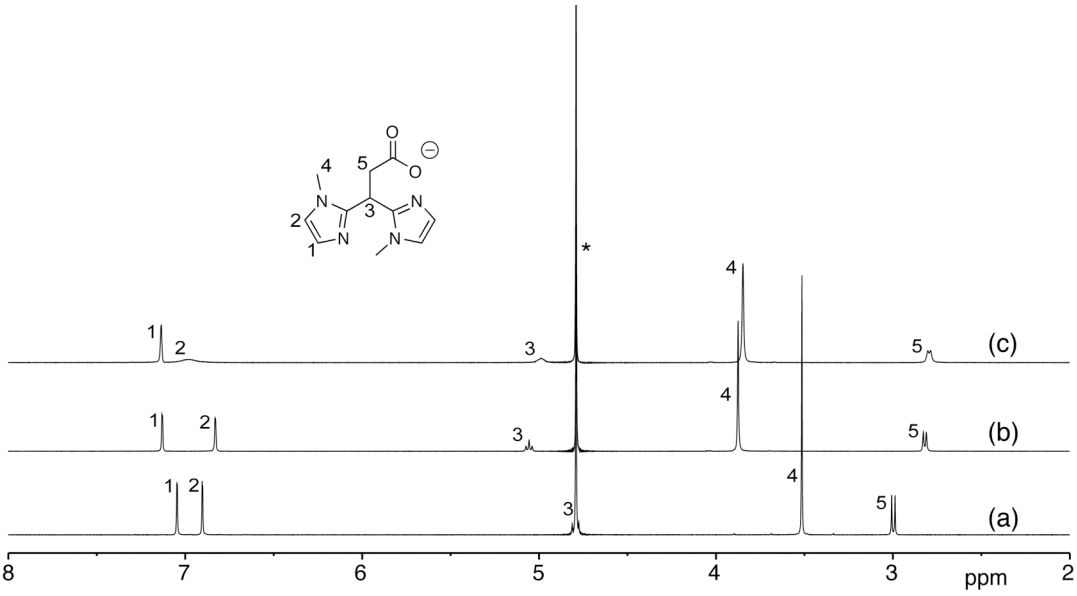

Figure 2. 400 MHz ^1H NMR spectra of the titration of K[**L1**] with $ZnCl_2$ in D_2O at room temperature: a) K[**L1**]; b) K[**L1**]:$ZnCl_2$ 2:1; c) K[**L1**]:$ZnCl_2$ 1:1 (* denotes the residual solvent peak).

All four resonances associated with ligand **L1** (spectrum a) shifted upon addition of 0.5 eq of $ZnCl_2$ (spectrum b). The observation of two sharp signals of equal intensity for the imidazole-protons shows that all four imidazole groups are equivalent. This is indicative of symmetric binding of both ligands to the zinc ion. The resonances of the methyl-groups and the methine proton at the bridging carbon shift downfield relative to the free ligand, whereas the propionate-CH_2 protons shift upfield. Note that the methine proton resonance of the free ligand is hidden under the residual solvent signal in spectrum a. The lack of any other resonances suggests the clean formation of a neutral, 2:1 [Zn(**L1**)$_2$] complex. Upon addition of another half equivalent of $ZnCl_2$ several resonances shift and signal broadening is observed (c). Especially, one of the two imidazole signals is severely broadened. Again, no free ligand is observed in the spectrum. These observations indicate a dynamic system with an overall 1:1 ligand:zinc stoichiometry.

The isolation and purification of the complex formed with 2 eq of **L1** with respect to $ZnCl_2$ proved troublesome. The separation of the inorganic salts formed as a by-product in the synthesis by means of repetitive washing in all cases resulted in partial loss of coordinated ligand (as observed by NMR), regardless of the A[**L1**] salt (A = K^+, $[Bu_4N]^+$) originally employed. We therefore attempted the synthesis of this complex by the reaction of two equivalents of the acid H**L1** with $Zn[N(SiMe_3)_2]_2$. Zinc(bis-trimethylsilyl amide) can be synthesized in sizeable quantities[31] and was found to be a convenient reagent in this case. Indeed, the reaction of $Zn[N(SiMe_3)_2]_2$ with two equivalents of H**L1** in acetonitrile resulted in

the formation of a white precipitate, which was recrystallized from an acetonitrile/water solution and was identified as the 2:1 complex [Zn(**L1**)$_2$] (**1**).

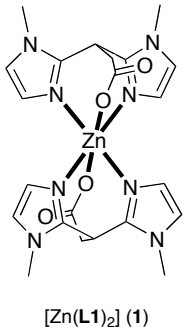

[Zn(**L1**)$_2$] (**1**)

Figure 3. The 2:1 complex [Zn(**L1**)$_2$] (**1**).

Unfortunately, all attempts at obtaining single crystals of **1** failed. Based on ESI-MS, IR, and the previously described NMR analysis, we propose that [Zn(**L1**)$_2$] (**1**) (see Figure 3) is isostructural to the crystallographically characterized, analogues complex [Cu^{II}(**L1**)$_2$].[28] The position of the symmetric and asymmetric carbonyl stretching vibrations proved to be indicative of the binding mode of **L1**.[26,28] The ν_{as}(C=O) and ν_s(C=O) are found at 1581 and 1391 cm^{-1}, respectively, indicative of a monodentate binding mode of the carboxylate ($\Delta(\nu_{as}$-$\nu_s)$ = 190 cm^{-1}, identical to Δ_{ionic}).[32] Furthermore, the clean ESI-MS spectrum of **1** confirmed the structure of a mononuclear, neutral 2:1 species with [M+X]$^+$ (X = H, Na, K) as the prominent ions.

The 1:1 complex [Zn(**L1**)Cl)] (**2**) was synthesized by the reaction of equimolar amounts of $ZnCl_2$ and K[**L1**] in dry methanol. This lead to the precipitation and isolation of [Zn(**L1**)Cl] (**2**) in almost quantitative yield. The broadened signals in the ^{1}H NMR spectrum of **2** in D_2O prompted us to study this complex by variable temperature NMR (Figure 4). As complex **2** is insoluble in organic solvents, the variable temperature NMR studies were limited to aqueous solutions, which restricted the temperature range that could be studied. Spectra were recorded in the range from 2 ºC to 70 ºC.

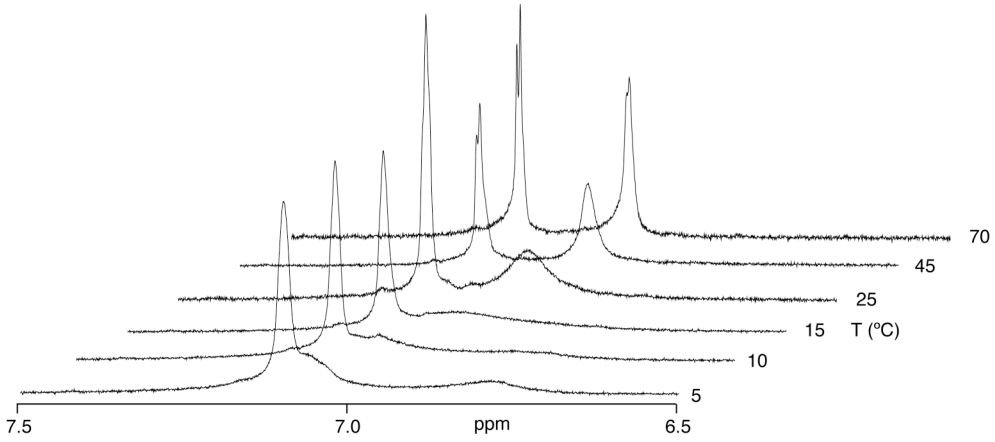

Figure 4. ^{1}H NMR resonances of the imidazole rings of [Zn(**L1**)Cl] (**2**) at variable temperatures in D_2O.

Figure 4 shows that at elevated temperatures two sharp imidazole resonances are observed. In the spectrum recorded at 70 ºC, the (small) coupling between the two imidazole protons H_1 and H_2 can also be discerned. The imidazole signal at higher field broadens upon cooling and ultimately splits into two separate (broad) resonances. This implies that at higher temperature the imidazole-H_1 protons (Figure 2) become magnetically equivalent, whereas at lower temperature exchange slows down to the effect that decoalesence in two broad resonances occurs. This behavior can be tentatively explained by the possibility of two different spatial orientations of the imidazole rings with respect to the carboxylate group of a second ligand upon coordination to zinc (*vide infra*), which would result in nonequivalent imidazole-H_1 protons at lower temperature. At higher temperatures these orientations average on the NMR timescale and only one signal is observed.

The asymmetric and symmetric carbonyl stretch vibrations of isolated [Zn(**L1**)Cl] (**2**) were observed at 1615 cm^{-1} and 1390 cm^{-1} ($\Delta(\nu_{as}-\nu_s)$ = 225 cm^{-1}), respectively. The asymmetric stretch thus shifted to higher wavenumbers compared to the one observed for **1** and a different, but still monodentate coordination mode of the carboxylate must therefore be present in [Zn(**L1**)Cl] (**2**). The ESI-MS spectrum of **2** showed the presence of several different species, with ions corresponding to e.g. $[\mathbf{L1}+Zn]^+$, $[2\mathbf{L1}+Zn+H]^+$, $[2\mathbf{L1}+2Zn+Cl]^+$, $[3\mathbf{L1}+2Zn+H]^{2+}$ and $[3\mathbf{L1}+2Zn]^+$. Based on the NMR, IR and ESI-MS data, the structure of **2** can be described as an oligomeric/polymeric species both in the solid state and in solution. This was confirmed by the single crystal structure determination of [Zn(**L1**)Cl(H_2O)] (**2·H_2O**).

Crystal Structure of [Zn(L1)Cl(H_2O)] (2·H_2O). Colorless single crystals of complex **2·H_2O** suitable for X-ray diffraction were obtained from a solution of **2** in H_2O upon standing. The molecular structure of **2·H_2O** is depicted in Figure 5, with selected bond lengths and angles presented in Table 1.

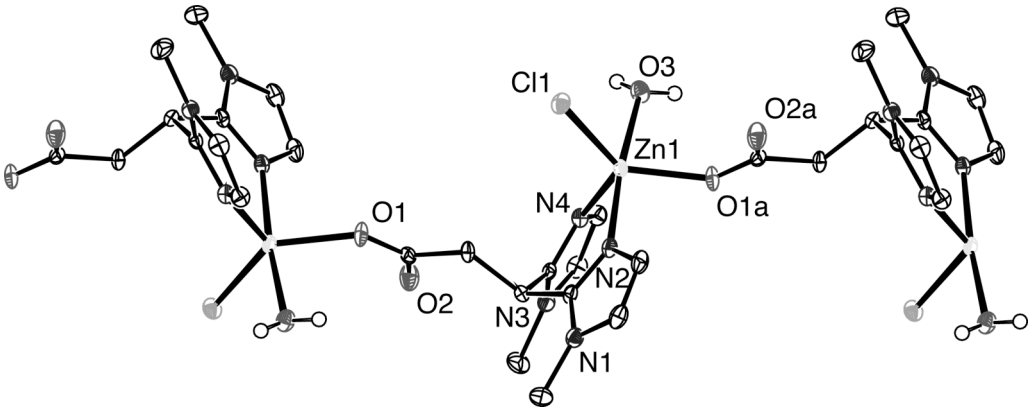

Figure 5. Molecular structure of [Zn(**L1**)Cl(H_2O)] (**2·H_2O**) in the crystal, showing three molecules of the carboxylato-bridged coordination polymer, forming a one-dimensional chain in the crystallographic *c*-direction. C–H hydrogen atoms have been omitted for clarity. Displacement ellipsoids are drawn at the 50% probability level. Symmetry operation a: 3/2 – x, 1 – y, z – 1/2.

Table 1. Selected bond lengths (Å) and angles (°) for [Zn(**L1**)Cl(H_2O)] (**2·H_2O**). Symmetry operation a: 3/2 – x, 1 – y, z – 1/2

	Bond length		Angle		Angle
Zn1–N2	2.1203(15)	N4–Zn1–N2	88.05(6)	N2–Zn1–O1a	92.41(5)
Zn1–N4	2.0517(14)	N2–Zn1–O3	173.58(5)	O1a–Zn1–O3	82.24(5)
Zn1–O1a	1.9975(11)	O3–Zn1–N4	90.38(5)	N4–Zn1–Cl1	119.50(4)
Zn1–Cl1	2.2844(4)	O3–Zn1–Cl1	90.23(4)	Cl1–Zn1–O1a	130.40(4)
Zn1–O3	2.1860(13)	Cl1–Zn1–N2	95.97(4)	O1a–Zn1–N4	109.55(5)

The single crystal structure determination reveals that the structure of the metal complex is that of a coordination polymer. The zinc atom is coordinated by two 1-methylimidazole groups of one **L1** ligand while the carboxylato group of this ligand coordinates to a neighboring zinc atom. In this way an infinite one-dimensional chain parallel to the crystallographic *c*-axis is formed. The chlorido anion and a coordinated water molecule complete the coordination sphere around each zinc center and renders it five-coordinate. Thus, a new, bridging coordination mode of **L1** is observed in the structure of **2·H_2O** comprising *N*,*N*-bidentate coordination to one metal center and *O*-monodentate to a second one. This coordination mode complements the alternative, *N*,*N*,*O*-tridentate facial capping mode of the ligand, which is commonly observed for divalent transition metals.[27,28,33] The coordination geometry around the five-coordinate Zn atom is distorted trigonal bipyrimidal (τ = 0.72).[34] The equatorial positions are occupied by N4 and the monoanionic carboxylato-O1a and chlorido Cl1 ligands with O1a–Zn1–N4, Cl1–Zn1–O1a, and N4–Zn1–Cl1 angles of 109.55(5), 130.40(4), and 109.50(4)°, respectively (Σ_{angles} = 360°). The axial positions are occupied by O3 of the water molecule and imidazole-N2 (O3–Zn1–N2 173.58(5)°). The Zn1–N2 and Zn1–N4 bond lengths are different (2.1203(15) and 2.0517(14) Å), consistent with their respective axial and equatorial positions. The Zn1–O1a distance of 1.9975(11) Å is slightly longer than the Zn–$O_{carboxylato}$ bond length observed in [Zn(bda^{tBu2,Me2})Cl]$_2$ (1.942 Å)[12] (bpa^{tBu2,Me2}, (3,5-di-*tert*-butylpyrazol-1-yl)(3',5'-dimethylpyrazol-1-yl)acetate), in which a carboxylato group is similarly coordinated to the metal center. The zinc-aquo distance of 2.1860(13) Å in **2·H_2O** is rather long compared to most reported Zn–OH_2 distances (mean Zn–OH_2 distance for five-coordinate zinc complexes: 2.046 Å, Cambridge Structural Database version 5.27).[35] In the related coordination polymer [Zn(bpa^{tBu,Me})(H_2O)](ClO_4)[11] (bpa^{tBu,Me}, bis(5-tert-butyl-3-methylpyrazol-2-yl)acetate), where the water molecule occupies a position in the basal plane of the trigonal bipyramid, the zinc-water distance for example amounts to 1.961 Å. **2·H_2O** crystallizes in the non-centrosymmetric space group $P2_12_12_1$ and the determination of the Flack parameter indicates that the crystal is enantiomerically pure.

The one-dimensional linear chains in **2·H_2O** are interconnected via hydrogen bonding interactions into a two-dimensional network (Figure 6, Table 2). The water molecule binds via its two hydrogen atoms by hydrogen bonding to a carbonyl-O and a chlorido anion as H-acceptors of a [Zn(**L1**)Cl(H_2O)] molecule in a neighboring strand.

Table 2. Selected hydrogen bond lengths (Å) and angles (°) for [Zn(**L1**)Cl(H_2O)] (**2·H_2O**). Symmetry operations: i) 1 – x, 1/2 + y, 1/2 – z; ii) – 1/2 + x, 3/2 – y, – z

Donor–H···Acceptor	D–H	H···A	D···A	D–H···A
O3–H1O···O2^{i}	0.78(3)	1.95(3)	2.7307(19)	176(3)
O3–H2O···Cl1^{ii}	0.84(3)	2.31(3)	3.1472(15)	171(3)

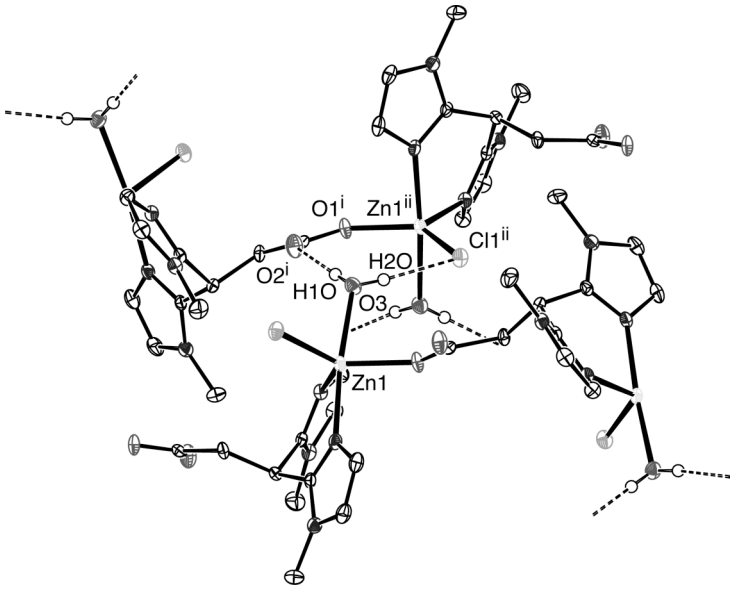

Figure 6. Hydrogen bonding network in [Zn(**L1**)Cl(H_2O)] (**2·H_2O**). Hydrogen bonds connect the infinite one-dimensional chains into a two-dimensional network. C–H hydrogen atoms have been omitted for clarity. Symmetry operations: i) 1 – x, 1/2 + y, 1/2 – z; ii) – 1/2 + x, 3/2 – y, – z.

Zinc complexes of L3. In order to assess the influence of the presence of steric bulk in the ligand framework, we also studied the zinc coordination chemistry of ligand **L3**. The ethyl and isopropyl substituents of this ligand provide significant steric hindrance and, moreover, increase the solubility of its complexes in organic solvents. The 1:1 complex [Zn(**L3**)Cl] (**3**) was synthesized by the reaction of equimolar amounts of $ZnCl_2$ and K[**L3**] in methanol. The complex was isolated in almost quantitative yield. The IR spectrum of [Zn(**L3**)Cl] (**3**) showed the asymmetric and symmetric carbonyl stretch vibrations at 1627 cm^{-1} and 1381 cm^{-1} ($\Delta(\nu_{as}$-$\nu_s)$ = 246 cm^{-1}), respectively. The structure of **3** was determined by X-ray crystal structure determination.

Crystal Structure of [Zn(L3)Cl] (3). Colorless single crystals of complex **3** suitable for X-ray diffraction were obtained from a solution of **3** in methanol. The molecular structure of **3** is depicted in Figure 7, with selected bond lengths and angles presented in Table 3. The crystal structure shows that whereas alike [Zn(**L1**)Cl(H_2O)] (**2·H_2O**), [Zn(**L3**)Cl] (**3**) also crystallizes as a coordination polymer, the molecular structure of **3** is noticeably different. Unlike in the structure of **2·H_2O**, no water molecule is found to coordinate to zinc in complex **3**. Instead of the five-coordinate structure in **2·H_2O**, the zinc atom in **3** is four-coordinate. It

has a pseudo-tetrahedral coordination geometry with two imidazole groups of one **L3** ligand, a chlorido and a carboxylato group of a neighboring ligand coordinated to it. The bridging mode of **L3** observed in **3** is the same as found in [Zn(**L1**)Cl(H_2O)] (**2·H_2O**). The deviation from ideal tetrahedral geometry is reflected in the observed bond angles (91.90(9) Å to 119.66(6) Å). The smallest angle (N2–Zn1–N4) is caused by the inherent geometrical restrictions imposed by the ligand and the largest angle (Cl1–Zn1–O1a) probably reflects the steric influence of the isopropyl groups. The Zn–N, Zn–O and Zn–Cl bond lengths in **3** are shorter than the corresponding distances in **2·H_2O**, which reflects the stronger Lewis acidity of zinc(II) in a four-coordinate versus a five-coordinate geometry. The Zn1–O1a bond length of 1.9628(19) Å is comparable to values reported for other tetrahedral *N,N,O* zinc complexes with a monodentate carboxylate.[9,11,12,18] The different coordination geometry at zinc results in a more folded zigzag polymer chain in **3**, compared to the more stretched zigzag chain observed for **2·H_2O**.

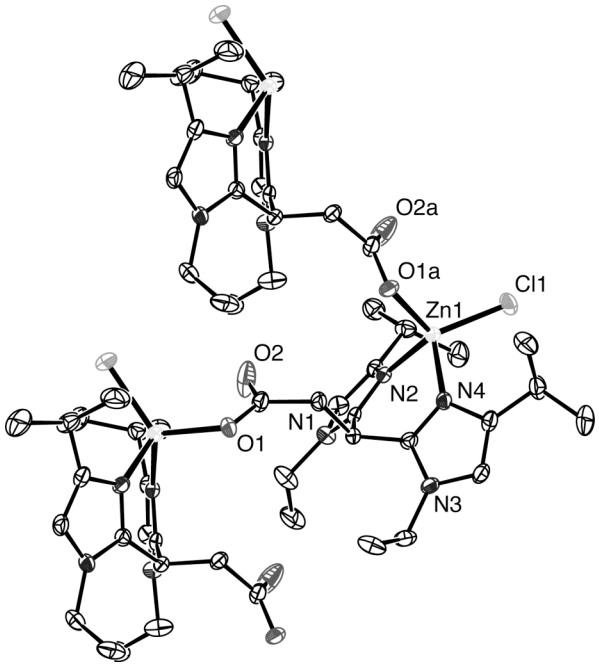

Figure 7. Molecular structure of [Zn(**L3**)Cl] (**3**) in the crystal, showing three molecules of the carboxylato-bridged coordination polymer. C–H hydrogen atoms have been omitted for clarity. Displacement ellipsoids are drawn at the 50% probability level. Symmetry operation a: x, 1–y, z–1/2.

Table 3. Selected bond lengths (Å) and angles (°) for [Zn(**L3**)Cl] (**3**). Symmetry operation a: x, 1 – y, z – 1/2

	Bond length		Angle		Angle
Zn1–N2	2.038(2)	Cl1–Zn1–N2	116.85(7)	N2–Zn1–O1a	108.85(8)
Zn1–N4	2.045(2)	Cl1–Zn1–N4	112.12(7)	N4–Zn1–O1a	103.15(9)
Zn1–O1a	1.9628(19)	Cl1–Zn1–O1a	119.66(6)		
Zn1–Cl1	2.2146(7)	N2–Zn1–N4	91.90(9)		

The structure of **3** and more generally, the coordination chemistry of **L3** with Zn in methanol solution were studied by ^{1}H NMR spectroscopy and ESI-MS. The ^{1}H NMR spectra of a titration experiment comprising the addition of $ZnCl_2$ to the potassium salt of **L3** in methanol solution are shown in Figure 8.

Comparison of the ^{1}H NMR spectra of K[**L3**] (Figure 8, spectrum a) with that of an equimolar K[**L3**]/$ZnCl_2$ mixture shows significant shifts pointing to the formation of a [ZnCl(**L3**)] (**3**) complex (spectrum b). In the ^{1}H NMR spectrum of **3** one sharp resonance is observed for the imidazole protons at 6.99 ppm, which is shifted to lower field compared to that of the free ligand. The two imidazole rings are equivalent on the NMR timescale suggesting that they are symmetrically bound to zinc. Importantly, the CH_2 resonance of the ethyl groups is shifted and split in two signals of equal intensity (4.20 and 4.32 ppm). Similarly, the methyl groups of the isopropyl substituent now appear as two doublets of equal intensity. These splittings confirm that the CH_2(Et) and CH_3(*i*Pr) groupings contain diastereotopic protons and methyl groups, respectively. No splitting or change in multiplicity of the resonances associated with the propionate backbone is observed, which is indicative of mirror symmetry of the complex in solution. Although at first sight the NMR data would allow an assignment of the solution structure for **3** as a mononuclear zinc complex with a facially capped ligand, a bridged oligomeric species (similar as the one discussed before for **2**) is preferred. ESI-MS data support the latter description since trimeric, dimeric, and monomeric species are observed. Prominent ions corresponding to [Zn(**L3**)Cl+H]$^+$, [Zn_2(**L3**)$_2Cl_2$+H]$^+$, and [Zn_3(**L3**)$_3Cl_3$+H]$^+$ are for instance observed. The structure of **3** in solution can therefore best be described as a coordination polymer similar to [Zn(**L1**)Cl] (**2**).

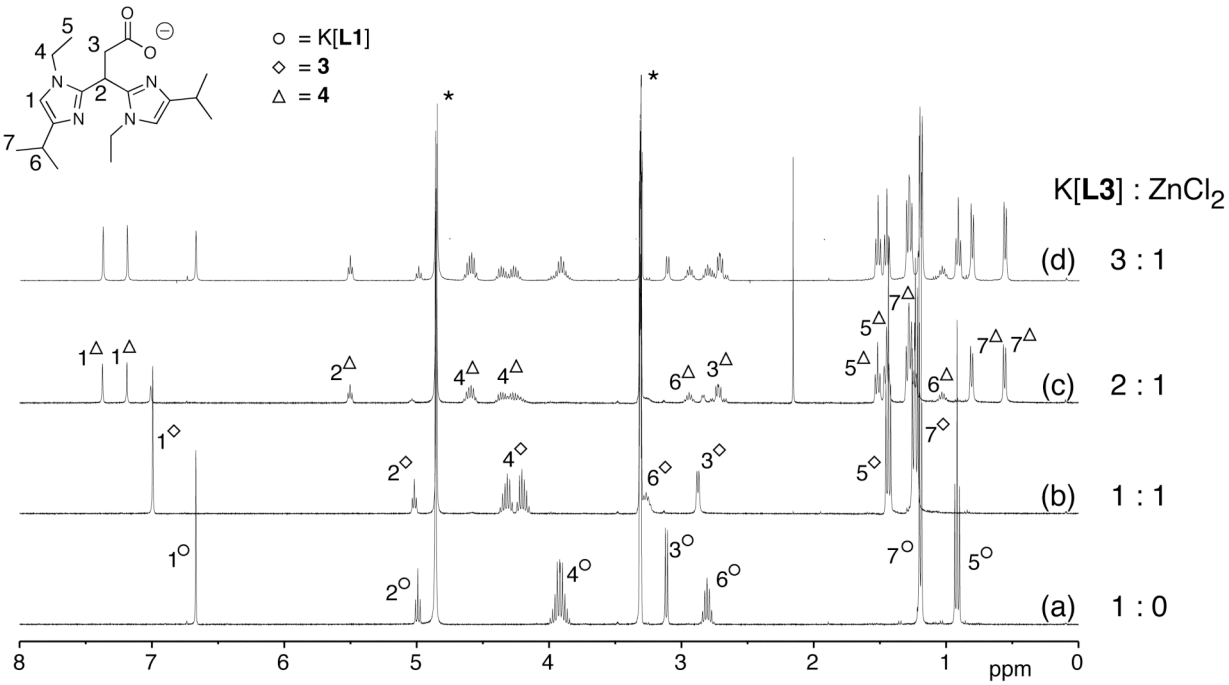

Figure 8. 400 MHz ^{1}H NMR spectra of the titration of K[**L3**] with $ZnCl_2$ in CD_3OD at room temperature: a) K[**L3**]:$ZnCl_2$ 1:0; b) K[**L3**]:$ZnCl_2$ 1:1; c) K[**L3**]:$ZnCl_2$ 2:1; d) K[**L3**]:$ZnCl_2$ 3:1 (* denote the residual solvent peak and H_2O).

Upon addition of two equivalents of K[**L3**] to $ZnCl_2$ in CD_3OD (cf. Figure 8, spectrum c), a second species is formed next to the 1:1 complex **3**. The fact that two species are observed, indicates that an equilibrium is obtained, i.e. the clean formation of a symmetrical 2:1 **L3** to zinc complex, as previously observed for **L1**, does not occur. Further inspection of the ^1H NMR spectrum indicated that all resonances of the 1-ethyl-4-isopropylimidazole groups of the new species are split into two signals of equal intensity, e.g. the imidazole ring protons at 7.37 and 7.19 ppm. This suggests that the two imidazole groups are inequivalent and experience a drastically different magnetic environment. For instance, the two resonances of the CH protons of the two isopropyl groups are found at 2.96 and 1.03 ppm. Furthermore, the methine proton at the bridging carbon is still a single triplet, whereas the CH_2 group of the propionate backbone has become diastereotopic. Variable temperature NMR studies over a temperature range from -40 °C to 60 °C did not show significant spectral changes. The ESI-MS spectrum of a 2:1 K[**L3**]:$ZnCl_2$ solution showed prominent ions corresponding to the $[Zn(\mathbf{L3})_2+H]^+$ and $[Zn(\mathbf{L3})_2+2H]^{2+}$ cations.

Based on this data, the structure of the new species is proposed to be a 2:1 ligand to zinc complex $[Zn(\mathbf{L3})_2]$ (**4**) in which each ligand is coordinated via its carboxylate group and one imidazole-group resulting in a four-coordinated zinc(II) ion (Figure 9). The coordination of two of the three donor atoms in a 2:1 ligand to metal complex has also been observed in the complex $[Zn(L2S)_2]$ (L2SH, 3-*tert*-butyl-5-methyl-2-thiophenyl)-bis-(3,5-dimethyl pyrazolyl) methane).[36] The addition of a third equivalent of K[**L3**] (spectrum d) results in the disappearance of the signals associated with [Zn(**L3**)Cl] and both free ligand K[**L3**] and $[Zn(\mathbf{L3})_2]$ (**4**) are detected. No attempts to isolate **4** were undertaken.

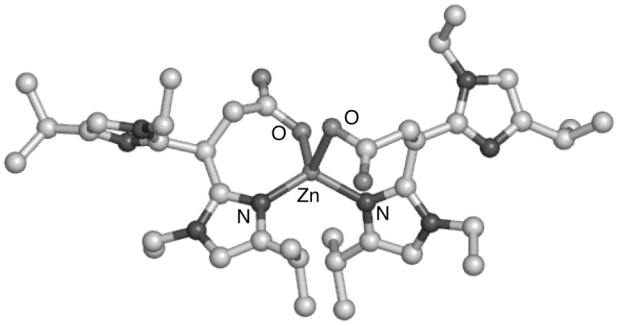

Figure 9. Proposed structure for $[Zn(\mathbf{L3})_2]$ (**4**). The structure was calculated by molecular mechanics geometry optimization (Spartan SGI[37] MMFF94).

Attempted synthesis of a zinc bis(1-methylimidazol-2-yl)acetate complex. Recently, the zinc-coordination chemistry of bis(pyrazolyl)acetates (bpa) has been actively explored to mimic the 2-His-1-carboxylate facial triad found in several different zinc enzymes.[9,11,12,18,19] The backbone of bpa is more rigid than the backbone of the ligands **L1** and **L3** used in the present study. In particular, the bridging *N*,*N*-bidentate-*O*-monodentate coordination mode reported here is less favorable for bpa, for which a strong predisposition to a *N*,*N*,*O* facial capping mode is expected. The synthesis of zinc complexes of bis(1-methylimidazol-2-yl)acetate (**L5**), would therefore be desirable, since it would allow a direct comparison of the respective pyrazole and imidazole donor groups (Chart 2).

Chart 2. Ligands **BnL5**, **L5**, bpa and the synthesis of zinc complexes **5** and **6**.

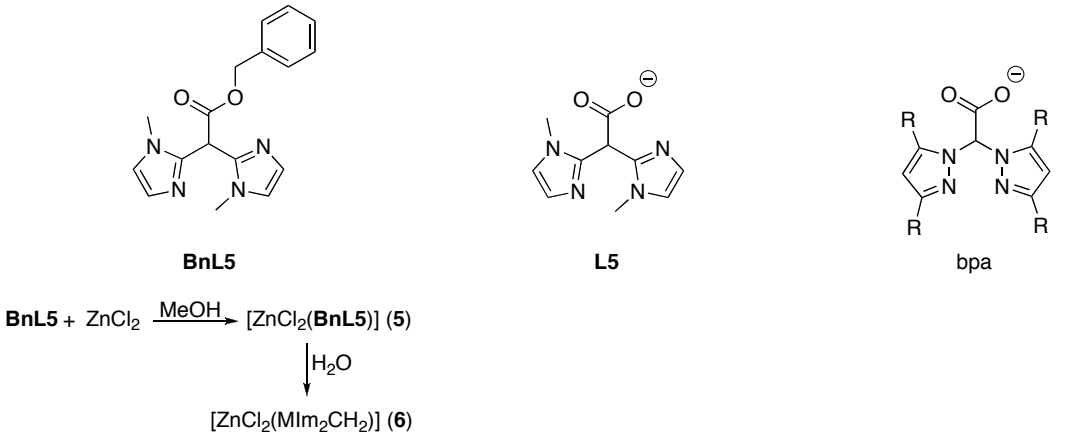

We have attempted the synthesis of ligand **L5**, but found that the common synthetic procedure, i.e. lithiation of bis(1-methylimidazol-2-yl)methane followed by reaction with carbon dioxide,[38] did not result in product formation in acceptable yields. Instead, we found that the ligand or an ester precursor of the ligand decarboxylates rather easily, as was also observed by Burzlaff and coworkers.[33] The benzyl ester of bis(1-methylimidazol-2-yl)acetic acid (**BnL5**), however, was sufficiently stable and could be isolated and purified after reaction of lithio bis(1-methylimidazol-2-yl)methane with benzylchloroformate. Since hydrolysis and hydrogenolysis of the ester moiety resulted in decomposition of the ligand, we synthesized the 1:1 zinc dichloride complex with benzyl bis(1-methylimidazol-2-yl)acetate (**BnL5**) in the hope that autocatalytic ester hydrolysis by the zinc complex would yield the desired zinc bis(1-methylimidazol-2-yl)acetate complex. A similar approach, involving the autocatalytic saponification of a zinc-bis(picolyl)glycine ethyl ester complex, has been reported by Vahrenkamp et al.[39]

The reaction of equimolar amounts of $ZnCl_2$ and **BnL5** gave the complex [$ZnCl_2$(**BnL5**)] (**5**) as a white powder in quantitative yield. The structure of [$ZnCl_2$(**BnL5**)] (**5**) was determined by X-ray diffraction studies and showed the **BnL5** ligand bound to the zinc center in a *N*,*N*-bidentate way (Figure 10, left). However, stirring of [$ZnCl_2$(**BnL5**)] (**5**) in H_2O at room temperature in an attempt to obtain [Zn(**L5**)Cl] resulted in decomposition of the ligand and formation of [$ZnCl_2$(MIm_2CH_2)] (**6**) (MIm_2CH_2, bis(1-methylimidazol-2-yl)methane), which was isolated as one of the decomposition products. Complex **6** was also crystallographically characterized (Figure 10, right). Based on these findings, we concluded that the 3,3-bis(1-methylimidazol-2-yl)acetate monoanion is too unstable for practical studies and abandoned the pursuit of this ligand.

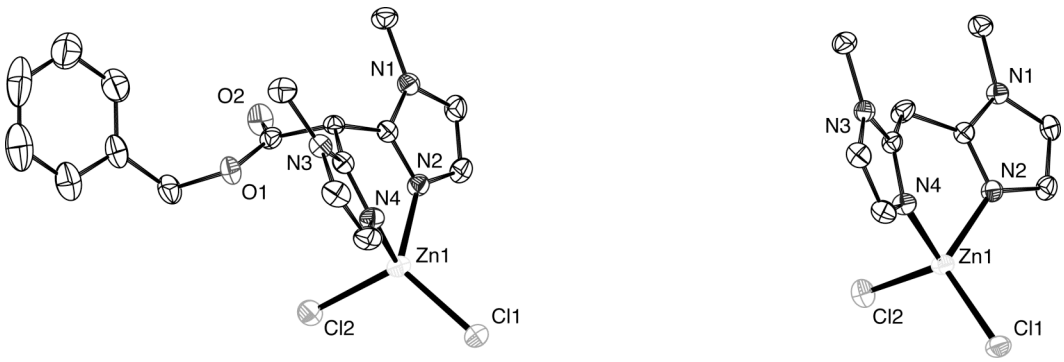

Figure 10. Molecular structures of [$ZnCl_2$(**BnL5**)] (**5**) (left) and [$ZnCl_2(MIm_2CH_2)$] (**6**) (right) in the crystal. Displacement ellipsoids are drawn at the 50% probability level. All hydrogen atoms have been omitted for clarity. Selected bond lengths (Å): **5**: Zn1–N2 2.011(2), Zn1–N4 1.994(2), Zn1–Cl1 2.2242(7), Zn1–Cl2 2.2554(7); **6**: Zn1–N2 2.0247(17), Zn1–N4 2.0222(17), Zn1–Cl1 2.2110(6), Zn1–Cl2 2.2504(6).

Reaction of [Zn(L1)Cl] with sodium pyruvate: oxalate formation. In an attempt to prevent the formation of coordination polymers of **L1** and to obtain mononuclear complexes with the desired *N*,*N*,*O* facial capping mode of the ligand, we used several different monoanionic, bidendate co-ligands. In the course of this study, we also investigated the reaction of [Zn(**L1**)Cl] (**2**) with sodium pyruvate. The addition of 1 eq of sodium pyruvate to a solution of **2** in D_2O resulted in the appearance of a new singlet at 2.38 ppm in the ^{1}H NMR spectrum (Figure 11, top). The signal is not shifted with respect to the signal observed for free sodium pyruvate, which indicates that the interaction between **2** and the pyruvate anion is weak, at best. The ESI-MS spectrum of an aqueous solution of equimolar amounts of **2** and sodium pyruvate, however, did show some major ions corresponding to a mononuclear $\{[Zn(\mathbf{L1})(pyruvate)]+Na\}^+$ and a dinuclear $\{[Zn_2(\mathbf{L1})_2(pyruvate)]\}^+$ cation, in addition to the ions observed in the ESI-MS spectrum of a solution of **2** in water.

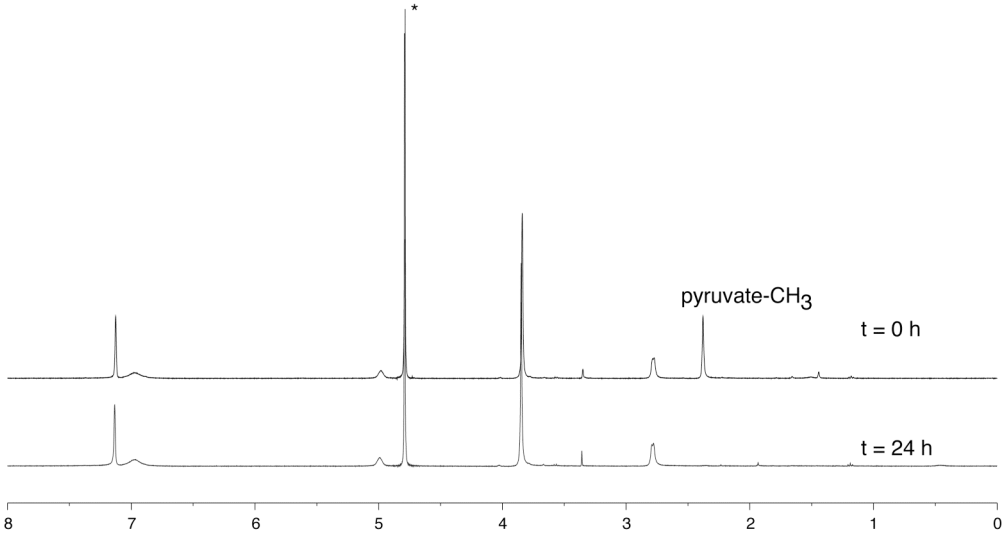

Figure 11. ^{1}H NMR spectra of a solution of [Zn(**L1**)Cl] (**2**) in D_2O (*) after addition of one equivalent of sodium pyruvate and the same solution after 24 hours.

However, when the **2**/pyruvate mixture in D_2O was followed in time by NMR spectroscopy, we noticed the gradual decrease in intensity of the signal of the pyruvate methyl group until it ultimately disappeared (Figure 11, bottom). After several days colorless crystals suitable for X-ray diffraction studies were formed in the NMR tube. To our surprise, the X-ray crystal structure showed the structure of the zinc complex $[Zn_2(\mathbf{L1})_2(ox)]\cdot 6H_2O$ (**7**) (ox, oxalate). Complex **7** has the structure of a coordination polymer involving $[Zn(\mathbf{L1})]^+$ cations bridged by *oxalato* dianions.

To unequivocally prove the relevance of the obtained structure, zinc coordination polymer **7** was also synthesized independently. Indeed, the addition of 0.5 eq of $K_2C_2O_4\cdot H_2O$ to an aqueous solution of [Zn(**L1**)Cl] (**2**) yielded a white, insoluble powder. This powder was identified as $[Zn_2(\mathbf{L1})_2(ox)]$ (**7**) by elemental analysis and IR spectroscopy. Typical features of the IR spectrum of **7** include absorptions at 1674, 1638, 1591 and 1399 cm^{-1}, which can be attributed to the oxalato and carboxylato groups in the polymer. Crystallization of **7** proved difficult given its general insolubility. Single crystals could, however, be obtained via the gel crystallization method.[40] A gel formed from a solution of tetramethoxysilane and potassium oxalate hydrate in water was layered with an aqueous solution of K[**L1**] and $ZnCl_2$. Single crystals were obtained after several days and could be unequivocally identified as **7** by X-ray crystal structure determination.

Crystal structure of $[Zn_2(L1)_2(ox)]\cdot 6H_2O$ (7). The molecular structure of **7** is shown in Figure 12, with selected bond lengths and angles presented in Table 4. The polymeric structure of **7** comprises two crystallographically inequivalent zinc atoms. Both zinc centers are five-coordinate and differ only in the slightly different bond lengths and angles. Each zinc atom is coordinated in an *N*,*N*-bidentate fashion by the 1-methylimidazole groups of one **L1** ligand, two oxygen atoms of a bis-*O*,*O*-bidentate bridging oxalato group, and a carboxylato-*O* donor atom of a neighboring **L1** ligand. The combination of the bridging oxalato and **L1** ligands construct a polymeric structure leading to the formation of two-dimensional sheets.

The coordination geometry around each zinc center is best described as a severely distorted trigonal bipyramid, with τ values of 0.60 and 0.59 for Zn1 and Zn2, respectively.[34] The equatorial positions are occupied by N24b/N14, and the anionic carboxylato-O11/O21 and oxalato-O32/O42 ligands for Zn1/Zn2, respectively. The axial positions are occupied by O31/O41 of the oxalato group and imidazole-N22b/N12 for Zn1/Zn2 (O–Zn–N angles of 161.43(9)/160.51(8)). The planar oxalato moieties are rather asymmetrically bound to the metal centers, with the Zn1–O31 and Zn1–O32 distances amounting to 2.258(2) and 2.018(2) Å for instance. This asymmetry has also been observed in other bis-bidentate bridged zinc-oxalato complexes with five-coordinated metal centers and is consistent with the occupation of one equatorial and one axial site of the trigonal bipyramid.[10,41] The shortest Zn···Zn distances via the bridging oxalato group are 5.5667(7) Å for Zn1···Zn1d and 5.5332(7) Å for Zn2···Zn2c. The distances of the metal centers to the donor atoms of **L1** follow the same trend as observed in **$2\cdot H_2O$**. The crystal structure of **7** is further stabilized by 14 different hydrogen bonding interactions, which involve the co-crystallized water molecules, the oxalato bridges

and the carboxylato groups (Figure 13). The oxalato groups are for instance involved in two chelated, three-centered hydrogen bonds with two water molecules via four O–H···O hydrogen bonds.

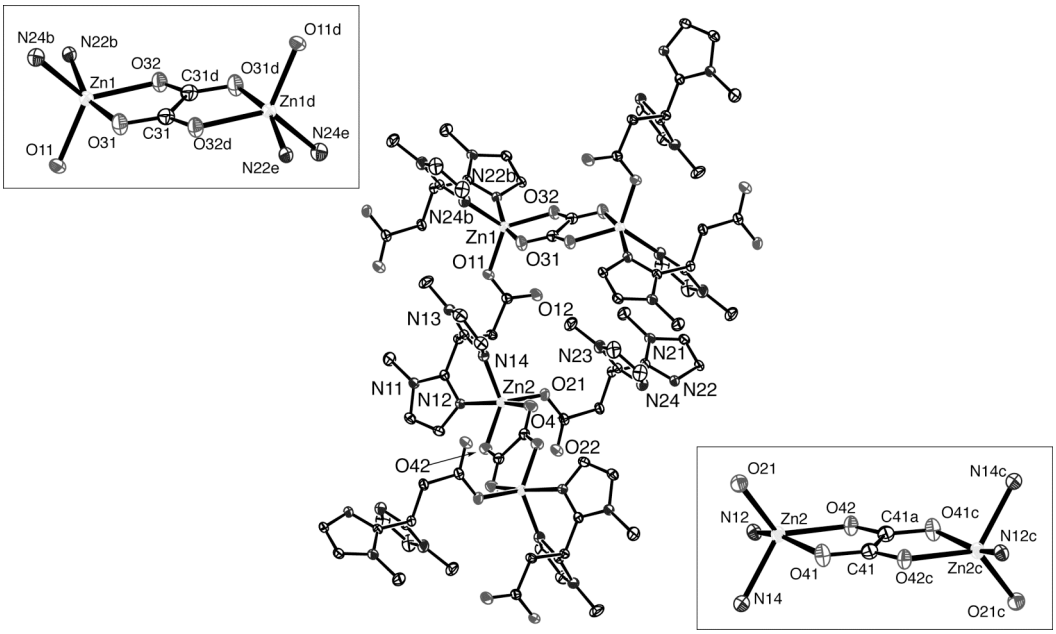

Figure 12. Molecular structure of $[Zn_2(\mathbf{L1})_2(ox)]\cdot 6H_2O$ (**7**) in the crystal. C–H hydrogen atoms and all solvent water molecules have been omitted for clarity. Displacement ellipsoids are drawn at the 50% probability level.

Table 5. Selected bond lengths (Å) and angles (°) for **7**. Symmetry operations b: 1 + x, y, z; c: – x, 1 – y, – z; d: 1 – x, 1 – y, 1 – z

	Bond length		Angle		Angle
Zn1–O31	2.258(2)	O11–Zn1–O31	89.48(8)	O21–Zn2–O41	90.33(8)
Zn1–O32	2.018(2)	O11–Zn1–O32	124.09(9)	O21–Zn2–O42	125.19(8)
Zn1–O11	1.9694(19)	O11–Zn1–N22b	108.91(9)	O21–Zn2–N12	109.08(9)
Zn1–N24b	2.046(2)	O11–Zn1–N24b	107.61(9)	O21–Zn2–N14	107.85(9)
Zn1–N22b	2.088(2)	O31–Zn1–O32	77.16(9)	O41–Zn2–O42	77.84(8)
Zn2–O41	2.233(2)	O31–Zn1–N22b	161.43(9)	O41–Zn2–N12	160.51(8)
Zn2–O42	2.0179(19)	O31–Zn1–N24b	87.69(9)	O41–Zn2–N14	87.24(9)
Zn2–O21	1.9630(19)	O32–Zn1–N22b	89.94(8)	O42–Zn2–N12	89.12(8)
Zn2–N12	2.089(2)	O32–Zn1–N24b	125.38(9)	O42–Zn2–N14	124.42(9)
Zn2–N14	2.052(2)	N22b–Zn1–N24b	89.06(9)	N12–Zn2–N14	88.34(9)
		Oxalato bond lengths			
C31–O31	1.248(4)			C41–O41	1.250(3)
C31d–O32	1.252(4)			C41c–O42	1.254(3)
C31–C31d	1.544(6)			C41–C41c	1.537(6)

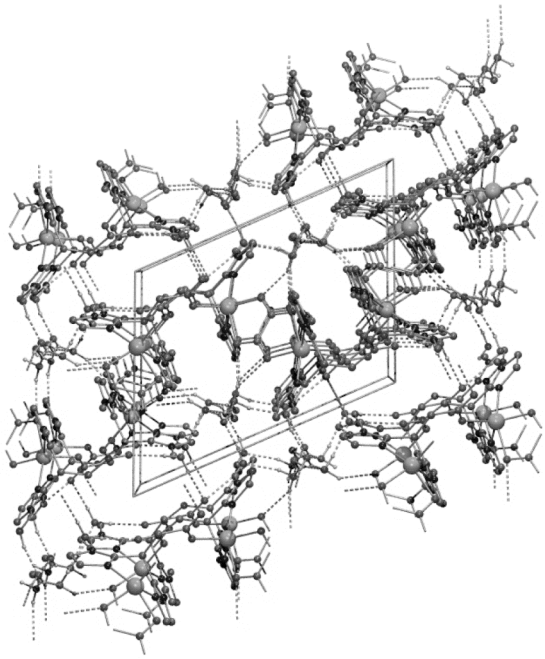

Figure 13. Hydrogen bonding network and crystal packing of **7**.

7.3 Discussion

The aim of this investigation was to explore the biomimetic modeling potential of the 3,3-bis(1-methylimidazol-2-yl)propionate ligand family with respect to mononuclear zinc enzymes featuring the 2-His-1-carboxylate facial triad. Complex [Zn(**L1**)$_2$] (**1**) shows that the facial capping mode of **L1**, as earlier observed with copper[28,30] and iron,[26,27] is also accessible for zinc. The crystal structure of the 1:1 complex [Zn(**L1**)Cl(H_2O)] (**2·H_2O**), however, shows that **L1** can also adopt other coordination modes. The formation of the oligomeric/polymeric structure of **2** both in solution and in the solid state, can be attributed to the flexibility of the ligand due to the CH_2 spacer of the propionate backbone. The formation of polymeric **2·H_2O** is further aided by the insolubility of the resulting coordination polymer. Two strategies were explored to circumvent polymer formation, i.e. increasing the steric bulk of the ligand and elimination of the CH_2 spacer. The latter approach demanded the synthesis of the bis(1-methylimidazol-2-yl)acetate analogue of **L1**, which was found to be rather unstable and its zinc complexes could not be obtained. The effect of more steric bulk was studied with **L3**, which contains the sterically more demanding isopropyl and ethyl substituents. Zinc complexes of **L3** are polymeric in nature as well, albeit with a different coordination geometry at the zinc atom as observed in **2·H_2O**. The first coordination spheres of [Zn(**L1**)Cl(H_2O)] (**2·H_2O**) and [Zn(**L3**)Cl] (**3**) are compared in Figure 14. The added steric bulk in **L3** causes the zinc ion to adopt a pseudo-tetrahedral geometry in **3**, instead of the distorted trigonal bipyramid observed for **2·H_2O**. The coordination around zinc in **3** resembles the first coordination sphere of the active sites of the zinc enzymes thermolysin, carboxypeptidase A, and neutral protease. The polymeric rather than monomeric nature of the complex, however, clearly limits its potential as a biological mimic.

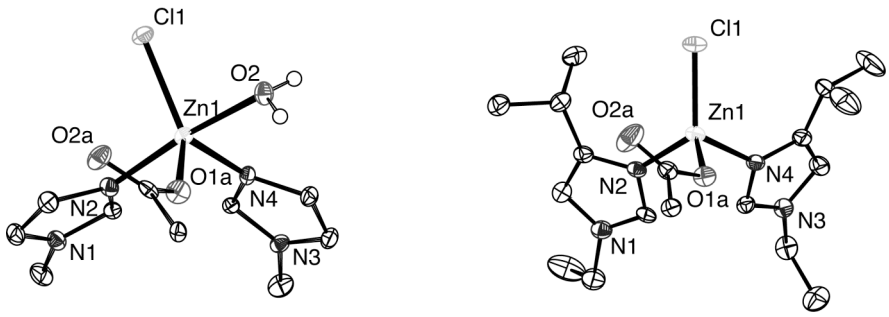

Figure 14. Comparison of the first coordination spheres of the zinc atoms in the coordination polymers **2·H$_2$O** (left) and **3** (right).

The isolation of [Zn$_2$(**L1**)$_2$(ox)] (**7**) from the reaction of [Zn(**L1**)Cl] (**2**) with sodium pyruvate was rather unexpected and is, to the best of our knowledge, the first report of the non-oxidative formation of oxalate from pyruvate (Scheme 1).[42,43,44]

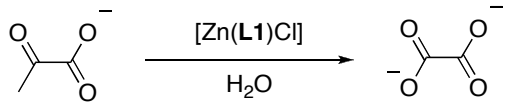

Scheme 1. The observed transformation of pyruvate to oxalate mediated by **2**.

A control experiment showed that an aqueous sodium pyruvate solution is stable under the reaction conditions. Apparently, **2** mediates the conversion of pyruvate to oxalate. The product **7** invariably deposited as crystals in experiments done on NMR scale. On a preparative scale (0.3 mmol), the reaction also takes place, yet the product was isolated as a insoluble white powder. The IR spectrum of this powder was identical to the one obtained for independently synthesized [Zn$_2$(**L1**)$_2$(ox)] (**7**). Most importantly, further experiments revealed that the reaction is catalytic in zinc. For example, addition of 20 eq of sodium pyruvate to a solution of **2** in water under ambient conditions resulted in 10 turnovers after 24 hours. The disappearance of the pyruvate methyl signal was also observed in a solution containing $ZnCl_2$ and sodium pyruvate without any further additives. Concomitantly, a precipitate was observed in the NMR tube. However, the composition of this precipitate, i.e. the formation of oxalate, could not be unambiguously established.

Since it is known that pyruvate keto-enol tautomerization is catalyzed by divalent metal ions such as Zn(II),[45,46] the disappearance of the methyl signal could in principle also be attributed to consecutive H/D-exchange steps. This would yield the deuterated pyruvate-d_3 anion, which is also invisible in ^{1}H NMR spectroscopy. To be able to exclude this possibility, experiments were performed in H_2O and samples were diluted with 2 eq (v) of D_2O just before the measurement. The same observations were made as previously, *i.e.* gradual disappearance of the methyl-signal and slow crystallization of the product in the NMR tube. The presence of appreciable amounts of enolate should also lead to the detection of the dimerization product of pyruvate.[45,46] This pyruvate dimer, which results from an aldol condensation reaction and has characteristic signals at 1.38 (singlet) and 3.35 (AB pattern) ppm,[45-47] was not observed under these conditions.

Phenyl pyruvic acid (and other α-ketoacids) is oxidized by molecular oxygen to give benzaldehyde and oxalate or the carbon oxides (CO and/or CO_2).[48,49] This reaction is catalyzed by several metal ions, such as Mn(II), Fe(II), and Cu(II), but not by Zn(II),[50,51] and has been attributed to the presence of the enol-tautomer, which is capable of reacting with dioxygen.[52] In the absence of dioxygen, i.e. under an Ar atmosphere, pyruvate does react with **2** to form oxalate. The anaerobic reactivity cannot be attributed to any residual dioxygen traces, since phenyl pyruvate (a substrate more prone to the reaction with dioxygen) did not show any reactivity under these conditions.

The observed conversion of pyruvate to oxalate under anaerobic conditions clearly places it outside previously observed formation of oxalate from oxidative transformations of α-keto acids.[48,49,52-56] The observation is important, since pyruvate is a major metabolic junction and it is therefore of prime importance to understand its reactivity. At present no biological counterpart has been reported for the pyruvate-oxalate conversion catalyzed by **2**. The chemical transformation as reported here, however, takes place at room temperature and physiological pH and should therefore be considered as a possible alternative pathway in the reactivity of pyruvate. The mechanism of this conversion is currently not clear. No other products could be detected by NMR during the reaction, which precludes the formulation of a mass balance for the reaction and clearly hampers a mechanistic interpretation. In any case, the pyruvate to oxalate conversion requires the scission of a C–C bond. On the other hand, the reactivity of zinc enzymes and their model complexes is often of hydrolytic nature. This can be attributed to the generation of a nucleophilic hydroxide species and/or the activation of a coordinated substrate towards attack of such a nucleophile.[3] The formation of oxalate from pyruvate via a hydrolytic mechanism is, however, difficult to envision. Further investigations have to be performed to address the mechanistic questions concerning this transformation.

7.4 Conclusions

The difference in applied steric bulk by the ligands **L1** and **L3** is reflected in the coordination chemistry of the two ligands towards $ZnCl_2$. Octahedral (**L1**) versus tetrahedral (**L3**) and trigonal pyramidal (**L1**) versus tetrahedral (**L3**) coordination geometries were obtained in the 1:1 and 2:1 ligand to metal complexes, respectively. The bridging binding mode of the two crystallographically characterized coordination polymers illustrates the intrinsic flexibility of the 3,3-bis(imidazol-2-yl)propionate ligand framework. The polymeric nature of the complexes could limit their biological relevance with respect to the 2-His-1-carboxylate facial triad in the case of zinc. On the other hand, attempts aimed at obtaining structurally more faithful mononuclear complexes, led to the observation of the unprecedented Zn-mediated pyruvate to oxalate conversion. This new, non-oxidative transformation of an important metabolic junction is intriguing and warrants further investigation.

7.5 Experimental Section

Air-sensitive organic reactions were carried out under an atmosphere of dry, oxygen-free N_2 using standard Schlenk techniques. THF and diethyl ether were dried over sodium benzophenone ketyl and distilled under N_2 prior to use. Methanol was dried over magnesium methoxide and distilled under N_2 prior to use. ^{1}H and ^{13}C NMR spectra were recorded on a Varian AS400, Varian Inova 300, or Varian Mercury 200 spectrometer, operating at 25 °C. Infrared spectra were recorded with a Perkin-Elmer Spectrum One FT-IR instrument. Elemental microanalyses were carried out by the Microanalytisches Laboratorium Dornis & Kolbe, Mulheim a.d. Ruhr, Germany. ESI-MS spectra were recorded on a Micromass LC-TOF mass spectrometer at the Biomolecular Mass Spectrometry group, Utrecht University. Bis(1-methylimidazol-2-yl)methane,[57] 3,3-bis(1-methylimidazol-2-yl)propionic acid (H**L1**), potassium and tetrabutylammonium 3,3-bis(1-methylimidazol-2-yl)propionate (K[**L1**] and [Bu_4N][**L1**]),[28] potassium 3,3-bis(1-ethyl-4-isopropylimidazol-2-yl)propionate (K[**L3**])[27] and zinc(bis-trimethylsilyl amide)[31] were prepared according to published procedures. All other chemicals were commercially obtained and used as received.

Benzyl bis(1-methylimidazol-2-yl)acetate (BnL5) (8): To a cooled solution of bis(1-methylimidazol-2-yl)methane (0.52 gram, 3.0 mmol) in dry THF (50 mL) at – 78 °C was added drop wise a solution of *n*-BuLi in hexanes (2.0 mL, 3.2 mmol). The reaction mixture was stirred for 1 hour at – 78 °C after which benzylchloroformate (1.19 mL, 3.5 mmol, 50 wt% solution in toluene) was added dropwise. During the addition, a white precipitate formed. The solution was allowed to warm to room temperature overnight. The reaction mixture was quenched with H_2O (20 mL) and all volatiles were removed *in vacuo*. The aqueous layer was extracted with diethyl ether (4 × 20 mL) and the combined organic layers were dried over $MgSO_4$, filtered and concentrated *in vacuo*. The crude oil was purified by column chromatography, (SiO_2, ethylacetate:methanol 2:1). The compound was isolated as a yellow oil in 62% yield (0.58 g, 1.9 mmol). ^{1}H NMR (300 MHz, CD_3CN, 25 °C): δ = 3.44 (s, 6H, NC*H*3), 5.23 (s, 2H, CH_2), 5.62 (s, 1H, C*H*), 6.85 (s, 2H, H_{im}), 6.96 (s, 2H, H_{im}), 7.35 (s, 5H, H_{Ph}) ppm. Anal. for $C_{17}H_{18}N_4O_2$ (310.35): calc. C 65.79, H 5.85, N 18.05; found C 65.88, H 5.74, N 17.92. IR (solid): ν = 3122.9, 2911.5, 1734.5, 1547.4, 1510.2, 1454.4, 1373.6, 1263.4, 1220.8, 1150.4, 978.2, 958.3, 907.1, 847.8, 785.7, 776.5, 740.1, 696.7, 683.5, 665.3 cm^{-1}. ESI-MS: *m/z* = 409.0 {[M-Cl]$^+$, calc. 409.0}.

[Zn(L1)$_2$] (1): To a hot, colorless solution of H**L1** (282 mg, 1.20 mmol) in dry acetonitrile (100 mL) was added a solution of $Zn[N(SiMe_3)_2]_2$ (232 mg, 0.60 mmol) in dry diethyl ether (20 mL) via cannula. The resulting colorless, clear solution was stirred for 60 h at elevated temperature during which gradually a white precipitate formed. The reaction mixture was concentrated *in vacuo* to give the crude product as a white powder. Recrystallization from an acetone/water mixture (4:1 *v/v*) gave the product as a colorless crystalline solid (230 mg, 72%). ^{1}H NMR (300 MHz, D_2O, 25 °C): δ = 2.69 (d, 2H, *J* = 6.3 Hz, CHCH_2), 3.74 (s, 6H, NCH_3), 4.93 (t, 1H, *J* = 6.0 Hz, C*H*CH$_2$), 6.69 (s, 2H, H_{im}), 7.00 (s, 2H, H_{im}) ppm. ^{13}C{^{1}H} NMR (50 MHz, D_2O, 25 °C): δ 30.2, 33.4, 43.6, 122.7, 125.7, 146.8, 177.2 ppm. Anal. for $C_{22}H_{26}ZnN_8O_4$ (531.90): calc. C 49.68, H 4.93, N 21.07; found C 49.76, H 5.06, N 20.97. IR (solid): ν = 3120.2, 2951.7, 2907.1, 2815.2, 1580.5, 1508.1, 1427.1, 1391.0, 1306.4, 1288.0, 1229.3, 1168.8, 1143.3, 1044.8, 956.9, 906.2, 769.3, 751.1 cm^{-1}. ESI-MS: *m/z* = 531.18 {[M+H]$^+$, calc 531.14}, 553.18 {[M+Na]$^+$, calc. 553.13}, 569.16 {[M+K]$^+$, calc. 569.10}.

[Zn(L1)Cl] (2): To a hot, colorless solution of K[**L1**] (255 mg, 0.93 mmol) in dry methanol (5 mL) was added a solution of $ZnCl_2$ (127 mg, 0.93 mmol) in methanol (5 mL) via cannula. Immediately upon addition a white precipitate formed and the suspension was stirred at elevated temperature for 1 h. The white precipitate was separated by centrifugation and washed with methanol (3 × 20 mL). The product was obtained as a white powder in almost quantitative yield (305 mg, 98%). ^{1}H NMR (300 MHz, D_2O, 25 °C): δ = 2.80 (d, 3H, *J* = 3.3 Hz, CHC*H*$_2$), 3.85 (s, 6H, NC*H*$_3$), 4.99 (t, 1H, CH_2C*H*), 6.99 (s, 2H, *H*$_{im}$), 7.14 (s, 2H, *H*$_{im}$) ppm. ^{13}C{^{1}H} NMR (50 MHz, D_2O, 25 °C): δ = 29.8, 33.4, 42.6, 122.5, 125.5, 146.1, 177.3 ppm. Anal. for $C_{11}H_{13}ClN_4O_2Zn$ (334.11): calc. C 39.55, H 3.92, N 16.77; found: C 39.46, H 4.05, N 16.85. IR (solid): ν = 3138.0, 3117.2, 1614.8, 1508.2, 1389.8, 1299.8, 1289.5, 1151.7, 1142.5, 1089.7, 976.2, 949.7, 796.3, 765.3, 736.1 cm^{-1}. ESI-MS: *m/z* = 296.94 {[M-Cl]$^+$, calc 297.03}, 332.92 {[M+H]$^+$, 333.01}, 413.97 {[3M-Zn-3Cl+H]$^{2+}$, calc. 414.09}, 531.02 {[2M-Zn-2Cl+H]$^+$, calc. 531.15}, 628.97 {[2M-Cl]$^+$, calc. 629.03}, 827.10 {[3M-Zn-3Cl]$^+$, calc. 827.17}.

[Zn(L1)Cl(H$_2$O)] (2·H$_2$O): Colorless crystals of complex **2·H$_2$O** suitable for X-ray diffraction were obtained upon standing of a concentrated solution of [Zn(**L1**)Cl] (**2**) in H_2O for several weeks. The obtained coordination polymer is insoluble in all common organic solvents and water of neutral pH. Anal. for $C_{11}H_{15}ClN_4O_3Zn$ (352.12): calc. C 37.52, H 4.29, 15.91; found C 37.44, H 4.27, N 15.97. IR (solid): ν = 3408.6, 3113.5, 3134.7, 1594.5, 1504.5, 1403.1, 1306.7, 1255.5, 1155.5, 1136.3, 1087.4, 983.7, 959.1, 934.9, 849.7, 764.6, 743.1, 717.6 cm^{-1}.

[Zn(L3)Cl] (3): To a colorless solution of $ZnCl_2$ (30 mg, 0.22 mmol) in dry methanol (10 mL) was added a solution of K[**L3**] (85 mg, 0.22 mmol) in dry methanol (15 mL) via cannula. The clear solution was stirred overnight at room temperature and evaporated *in vacuo*. The product was redissolved in dichloromethane and insoluble KCl was separated off by centrifugation. The solution was filtered over celite and concentrated *in vacuo* to give the product as a white powder (97 mg, 99%). Colorless crystals suitable for X-ray diffraction were obtained from a methanolic solution of **3** upon standing. ^{1}H NMR (300 MHz, D_2O, 25 °C): δ = 1.22 (d, 6H, *J* = 7.2 Hz, C*H*$_3$CHCH$_3$), 1.25 (d, 6H, *J* = 6.8 Hz, CH$_3$CHC*H*$_3$), 1.44 (t, 6H, *J* = 7.2 Hz, C*H*$_3$CH$_2$), 2.88 (d, 2H, *J* = 6.0 Hz, CHC*H*$_2$), 3.25 (m, 2H, CH$_3$C*H*CH$_3$), 4.21 (ABX$_3$, 2H, *J* = 7.2, C*H*HCH$_3$), 4.32 (ABX$_3$, 2H, *J* = 7.2, CH*H*CH$_3$), 5.02 (t, 1H, *J* = 5.7 Hz, C*H*CH$_2$), 6.99 (s, 2H, H$_{im}$) ppm. ^{13}C{^{1}H} NMR (100 MHz, CD_3OD, 25 °C): δ = 16.6, 22.1, 24.1, 28.0, 31.1, 42.9, 116.0, 146.2, 149.9, 175.7 ppm. Anal. for $C_{19}H_{29}ClN_4O_2Zn$ (446.32): calc. C 51.13, H 6.55, N 12.55; found: C 51.05, H 6.43, N 12.37. IR (solid): ν = 3101.4, 2967.9, 2873.7, 1626.6, 1572.8, 1494.8, 1448.9, 1464.1, 1381.1, 1324.8, 1257.2, 1175.8, 1153.0, 1027.6, 976.1, 801.2, 757.7, 660.5 cm^{-1}. ESI-MS: *m/z* = 409.13 {[2M-2Cl]$^{2+}$, calc 409.16}, 445.11 {[M+H]$^+$, calc. 445.13}, 483.04 {[M+K]$^+$, calc 483.09}, 631.21 {[3M-2Cl]$^{2+}$, calc. 631.22}, 853.29 {[2M-Cl]$^+$, calc. 853.29}, 889.20 {[2M+H]$^+$, calc. 889.26}, 1297.02 {[3M+H]$^+$, calc. 1297.42}.

[Zn(BnL5)Cl$_2$] (5): To a hot solution of **BnL5** (**8**) (259 mg, 0.84 mmol) in dry methanol (5 mL) was added a solution of anhydrous $ZnCl_2$ (115 mg, 0.84 mmol) dry MeOH (5 mL) via cannula. The reaction mixture was stirred at elevated temperature for 1 h and gradually the product formed as a white precipitate. The product was separated by centrifugation and obtained as a white powder in quantitative yield. Single crystals suitable for X-ray analysis were be obtained by slow evaporation of a solution of **5** in acetone. ^{1}H NMR (300 MHz, CD_3CN, 25 ^{o}C): δ = 3.79 (2, 6H, C*H*$_3$), 5.12 (s, 2H, C*H*$_2$), 5.60 (s, 1H, C*H*), 7.13 (d, 2H, *J* = 0.75 Hz, *H*$_{im}$), 7.22 (d, 2H, *J* = 0.75 Hz, *H*$_{im}$), 7.25 (m, 2H, *H*$_{Ph}$), 7.33 (m, 3H, *H*$_{Ph}$) ppm. ^{13}C{^{1}H} NMR (100 MHz, CD_3OD, 25 °C): δ = 34.9,

40.6, 69.7, 124.5, 126.5, 129.1, 129.5, 129.7, 136.1, 142.3, 166.2 ppm. Anal. for $C_{17}H_{18}Cl_2N_4O_2Zn$ (446.67): calc. C 45.71, H 4.06, N 12.54; found C 45.64, H 3.95, N 12.61. IR (solid): ν = 3122.9, 2911.5, 1734.5, 1547.4, 1510.2, 1454.4, 1373.6, 1263.4, 1220.8, 1150.4, 978.2, 958.3, 907.1, 847.8, 785.7, 776.5, 740.1, 696.7, 683.5, 665.3 cm^{-1}. ESI-MS: *m*/*z* = 409.0 {$[M\text{-}Cl]^+$, calc. 409.0}.

$[Zn_2(L1)_2(ox)]$ (7) (direct synthesis): To a solution of [Zn(**L1**)Cl] (**2**) (50 mg, 0.15 mmol) in water (5 mL) was added a solution of potassium oxalate hydrate (14 mg, 0.075 mmol) in water (3 mL). The solution was stirred overnight at room temperature, during which gradually a white precipitate formed. The precipitate was separated by centrifugation and washed three times with water (3 × 20 mL). The product was dried *in vacuo* and obtained as a white powder in 82% yield (42 mg, 0.061 mmol). Anal. for $C_{24}H_{26}N_8O_8Zn_2 \cdot 6H_2O$ (685.33): calc. C 36.33, H 4.83, N 14.12; found: C 36.45, H 4.50, N 14.25. IR (solid): ν = 3476.8, 3135.4, 1671.3, 1651.6, 1600.2, 1544.9, 1504.8, 1423.6, 1382.7, 1320.1, 1287.2, 1158.1, 1137.9, 985.1, 769.4, 745.1, 710.4 cm^{-1}.

$[Zn_2(L1)_2(ox)] \cdot 6H_2O$ (7), reaction of 2 with sodium pyruvate. NMR Reactions: Stock solutions of [Zn(**L1**)Cl] (20 mg, 0.06 mmol) in H_2O (1 mL) and sodium pyruvate (13.2 mg, 0.06 mmol) in H_2O (2 mL) were prepared. NMR tubes were filled with 0.1 mL of each stock solution and kept either at room temperature or heated to 50 °C. The NMR samples were analyzed at different times after mixing the reagents. Before acquisition of the NMR spectrum 0.4 mL of D_2O was added to the reaction mixture. Crystals usually deposited within two or three days in the NMR tube.
In the case of the catalytic runs, 0.1 mL of a solution containing 20 equivalents of sodium pyruvate was added to 0.1 mL of the [Zn(**L1**)Cl] stock solution and DMSO (5 eq, 11 μL) was added as internal standard. The reaction mixture was kept at 50 °C and the NMR spectrum was recorded with addition of 0.4 mL D_2O after 24 hours.
Preparative scale: To a solution of $ZnCl_2$ (37 mg, 0.27 mmol) and K[**L1**] (75 mg, 0.27 mmol) in H_2O (10 mL) was added sodium pyruvate (30 mg, 0.27 mmol). The solution was heated to 50 °C and gradually an off-white precipitate was formed. After a week, the product was separated by centrifugation (29 mg, 31%). The IR spectrum of the product was identical to independently synthesized $[Zn_2(\mathbf{L1})_2(ox)]$.

X-ray crystal structure determinations of $2 \cdot H_2O$, 3, 5, 6 and 7. Reflections were measured on a Nonius Kappa CCD diffractometer with rotating anode (graphite monochromator, λ = 0.71073 Å) at a temperature of 150 K. The structures were refined with SHELXL-97[58] against F^2 of all reflections. Non hydrogen atoms were refined with anisotropic displacement parameters. Geometry calculations and checking for higher symmetry were performed with the PLATON program.[59] Further details are given in Table 6.

$2 \cdot H_2O$: The structure was solved with SHELXS-97[60] using Direct Methods. All hydrogen atoms were located in the difference Fourier map and refined freely with isotropic displacement parameters.
3: The structure was solved with DIRDIF-99[61] using automated Patterson Methods. Refinement was performed as an inversion twin. All hydrogen atoms were located in the difference Fourier map and refined with a riding model.
5: The structure was solved with DIRDIF-99[61] using automated Patterson Methods. All hydrogen atoms were located in the difference Fourier map and refined with a riding model.
6: The structure was solved with SIR-97[62] using Direct Methods. All hydrogen atoms were located in the difference Fourier map and refined freely with isotropic displacement parameters.

7: The crystal was non-merohedrally twinned with a twofold rotation about the crystallographic *c*-axis as twin operation. This twin law was taken into account during the intensity integration using the program EvalCCD.[63] The structure was solved on the non-overlapping reflections with DIRDIF-99[61] using automated Patterson Methods. All hydrogen atoms were located in the difference Fourier map and refined with a riding model. The twin fraction refined to 0.127(3).

Table 6. Crystallographic data for compounds **2·H_2O**, **3**, **5**, **6**, **7**

Compound	[Zn(**L1**)Cl(H_2O)] (**2·H_2O**)	[Zn(**L3**)Cl] (**3**)	[$ZnCl_2$(**BnL5**)] (**5**)	[$ZnCl_2$(MIm_2CH_2)] (**6**)	[Zn_2(**L1**)$_2$(ox)]·6H_2O (**7**)
formula	$C_{11}H_{15}ClN_4O_3Zn$	$C_{19}H_{29}ClN_4O_2Zn$	$C_{17}H_{18}Cl_2N_4O_2Zn$	$C_9H_{12}Cl_2N_4Zn$	$C_{24}H_{26}N_8O_8Zn_2·6H_2O$
fw	352.09	446.28	446.62	312.50	793.36
crystal size [mm^3]	0.30×0.12×0.09	0.18×0.03×0.03	0.60×0.03×0.03	0.30×0.15×0.06	0.24×0.18×0.09
crystal color	colorless	colorless	colorless	colorless	colorless
crystal system	orthorhombic	monoclinic	monoclinic	monoclinic	triclinic
space group	$P2_12_12_1$ (no. 19)	Cc (no. 9)	C2/c (no. 15)	$P2_1/c$ (no. 14)	$P\bar{1}$ (no. 2)
a [Å]	8.7159(1)	10.1766(2)	35.5761(4)	7.3547(1)	9.9634(7)
b [Å]	10.1124(1)	23.8561(6)	7.4531(1)	14.9538(2)	12.0617(11)
c [Å]	15.1177(2)	9.1995(2)	14.6106(2)	12.3489(2)	14.8889(9)
α [°]	–	–	–	–	113.021(3)
β [°]	–	107.0078(14)	101.8858(5)	117.5968(6)	90.365(3)
γ [°]	–	–	–	–	102.513(3)
V [Å]	1332.45(3)	2135.72(8)	3790.97(8)	1203.62(3)	1599.4(2)
Z	4	4	8	4	2
D_{calc} [g/cm^3]	1.755	1.388	1.565	1.724	1.647
μ [mm^{-1}]	2.056	1.296	1.597	2.461	1.580
abs. corr.	multi-scan	multi-scan	multi-scan	multi-scan	multi-scan
abs.corr. range	0.71 – 0.84	0.86 – 0.96	0.85 – 0.96	0.74 – 0.86	0.64 – 0.87
$(\sin\theta/\lambda)_{max}$ [$Å^{-1}$]	0.65	0.65	0.60	0.65	0.65
refl (meas./unique)	21618 / 3063	11758 / 4644	28566 / 3424	27341 / 2759	35709 / 7342
param./restraints	241 / 0	251 / 2	237 / 0	193 / 0	438 / 0
R1/wR2 [I>2σ(I)]	0.0182 / 0.0447	0.0312 / 0.0694	0.0309 / 0.0704	0.0306 / 0.0793	0.0389 / 0.0867
R1/wR2 [all refl.]	0.0190 / 0.0452	0.0384 / 0.0723	0.0512 / 0.0786	0.0389 / 0.0852	0.0540 / 0.0947
S	1.062	1.041	1.081	1.089	1.083
Flack parameter[64]	– 0.006(7)	0.305(9)	–	–	–
res. density [$e/Å^3$]	– 0.36/0.19	– 0.27/0.41	– 0.31/0.43	– 0.54/1.23	– 0.79/0.51

7.6 References & Notes

1. Costas, M.; Mehn, M. P.; Jensen, M. P.; Que, L., Jr. *Chem. Rev.* **2004**, *104*, 939-986.
2. Koehntop, K. D.; Emerson, J. P.; Que, L., Jr. *J. Biol. Inorg. Chem.* **2005**, *10*, 87-93.
3. Parkin, G. *Chem. Rev.* **2004**, *104*, 699-768.
4. Stark, W.; Pauptit, R. A.; Wilson, K. E.; Jansonius, J. N. *Eur. J. Biochem.* **1992**, *207*, 781-791.
5. Vahrenkamp, H. *Acc. Chem. Res.* **1999**, *32*, 589-596.
6. Alsfasser, R.; Trofimenko, S.; Looney, A.; Parkin, G.; Vahrenkamp, H. *Inorg. Chem.* **1991**, *30*, 4098-4100.
7. Kitajima, N.; Hikichi, S.; Tanaka, M.; Moro-oka, Y. *J. Am. Chem. Soc.* **1993**, *115*, 5496-5508.
8. Looney, A.; Han, R.; McNeill, K.; Parkin, G. *J. Am. Chem. Soc.* **1993**, *115*, 4690-4697.
9. Beck, A.; Weibert, B.; Burzlaff, N. *Eur. J. Inorg. Chem.* **2001**, 521-527.
10. Chiu, Y.-H.; Canary, J. W. *Inorg. Chem.* **2003**, *42*, 5107-5116.
11. Hammes, B. S.; Kieber-Emmons, M. T.; Letizia, J. A.; Shirin, Z.; Carrano, C. J.; Zakharov, L. N.; Rheingold, A. L. *Inorg. Chim. Acta* **2003**, *346*, 227-238.
12. Hegelmann, I.; Beck, A.; Eichhorn, C.; Weibert, B.; Burzlaff, N. *Eur. J. Inorg. Chem.* **2003**, 339-347.
13. Maldonado Calva, J. A.; Vahrenkamp, H. *Inorg. Chim. Acta* **2005**, *358*, 4019-4026.
14. Mareque Rivas, J. C.; Torres Martín de Rosales, R.; Parsons, S. *Dalton Trans.* **2003**, 2156-2163.
15. Niklas, N.; Walter, O.; Alsfasser, R. *Eur. J. Inorg. Chem.* **2000**, 1723-1731.
16. Niklas, N.; Zahl, A.; Alsfasser, R. *Dalton Trans.* **2003**, 778-786.
17. Papish, E. T.; Taylor, M. T.; Jernigan III, F. E.; Rodig, M. J.; Shawhan, R. R.; Yap, G. P. A.; Jové, F. A. *Inorg. Chem.* **2006**, *45*, 2242-2250.
18. Smith, J. N.; Hoffman, J. T.; Shirin, Z.; Carrano, C. J. *Inorg. Chem.* **2005**, *44*, 2012-2017.
19. Smith, J. N.; Shirin, Z.; Carrano, C. J. *J. Am. Chem. Soc.* **2003**, *125*, 868-869.
20. Trösch, A.; Vahrenkamp, H. *Eur. J. Inorg. Chem.* **1998**, 827-832.
21. Trösch, A.; Vahrenkamp, H. *Inorg. Chem.* **2001**, *40*, 2305-2311.
22. Friese, S. J.; Kucera, B. E.; Que, L., Jr.; Tolman, W. B. *Inorg. Chem.* **2006**, *45*, 8003-8005.
23. Parkin, G. *Chem. Commun.* **2000**, 1971-1985.
24. Dowling, C.; Parkin, G. *Polyhedron* **1996**, *15*, 2463-2465.
25. Ghosh, P.; Parkin, G. *J. Chem. Soc., Dalton Trans.* **1998**, 2281-2283.
26. Bruijnincx, P. C. A.; Buurmans, I. L. C.; Gosiewska, S.; Lutz, M.; Spek, A. L.; Weckhuysen, B. M.; van Koten, G.; Klein Gebbink, R. J. M. *to be submitted* (Chapter 5 of this thesis).
27. Bruijnincx, P. C. A.; Lutz, M.; Spek, A. L.; Hagen, W. R.; Weckhuysen, B. M.; van Koten, G.; Klein Gebbink, R. J. M. *J. Am. Chem. Soc.*, accepted for publication (Chapter 3 of this thesis).
28. Bruijnincx, P. C. A.; Lutz, M.; Spek, A. L. ; van Faassen, E. L. ; Weckhuysen, B. M.; van Koten, G.; Klein Gebbink, R. J. M. *Eur. J. Inorg. Chem.* **2005**, 779-787 (Chapter 2 of this thesis).
29. Bruijnincx, P. C. A.; Viciano, M.; Lutz, M.; Spek, A. L.; Reedijk, J.; van Koten, G.; Klein Gebbink, R. J. M. *to be submitted* (Chapter 8 of this thesis).
30. Kervinen, K. ; Bruijnincx, P. C. A.; Beale, A. M.; Mesu, J. G.; van Koten, G.; Klein Gebbink, R. J. M.; Weckhuysen, B. M. *J. Am. Chem. Soc.* **2006**, *128*, 3208-3217.
31. Darensbourg, D. J.; Holtcamp, M. W.; Struck, G. E.; Zimmer, M. S.; Niezgoda, S. A.; Rainey, P.; Robertson, J. B.; Draper, J. D.; Reibenspies, J. H. *J. Am. Chem. Soc.* **1999**, *121*, 107-116.
32. Robert, V.; Lemercier, G. *J. Am. Chem. Soc.* **2006**, *128*, 1183-1187.
33. Peters, L.; Hübner, E.; Burzlaff, N. *J. Organomet. Chem.* **2005**, *690*, 2009-2016.

34. Addison, A. W.; Rao, T. N.; Reedijk, J.; van Rijn, J.; Verschoor, G. C. *J. Chem. Soc., Dalton Trans.* **1984**, 1349-1356.
35. Allen, F. H. *Acta Cryst.* **2002**, *B58*, 380-388.
36. Hammes, B. S.; Carrano, C. J. *Inorg. Chem.* **1999**, *38*, 4593-4600.
37. *Spartan SGI version 5.1.1*, Wavefunction Inc.: Irvine, CA, USA.
38. Otero, A.; Fernández-Baeza, J.; Antiñolo, A.; Tejeda, J.; Lara-Sánchez, A. *Dalton Trans.* **2004**, 1499-1510.
39. Abufarag, A.; Vahrenkamp, H. *Inorg. Chem.* **1995**, *34*, 2207-2216.
40. Arend, H.; Connelly, J. J. *J. Crystal Growth* **1982**, *56*, 642-644.
41. Curtis, N. F.; McCormick, I. R. N.; Waters, T. N. *J. Chem. Soc., Dalton Trans.* **1973**, 1537-1548.
42. Unexpected oxalate formation by Zn-complexes is not completely unprecedented. The reaction of $Zn(NO_3)_2$ with pyridine-2,4,6-tricarboxylic acid in the presence of pyridine at room temperature, resulted for instance in the formation of the Zn-oxalato polymer $[Zn(ox)(py)_2]\cdot H_2O$.[44] Another oxalato bridged zinc coordination polymer was obtained from the hydro(solvo)thermal reaction between $Zn(NO_3)_2$ and pyridine in ethanol or methanol. It was proposed that the oxalate resulted from ethanol oxidation and oxidative coupling of methanol for the two different solvents, respectively.[43] Clearly, different reaction mechanisms are operative in these cases.
43. Evans, O. R.; Lin, W. *Cryst. Growth Des.* **2001**, *1*, 9-11.
44. Ghosh, S. K.; Savitha, G.; Bharadwaj, P. K. *Inorg. Chem.* **2004**, *43*, 5495-5497.
45. Tallman, D. E.; Leussing, D. L. *J. Am. Chem. Soc.* **1969**, *91*, 6253-6256.
46. Tallman, D. E.; Leussing, D. L. *J. Am. Chem. Soc.* **1969**, *91*, 6256-6262.
47. Cheong, M.; Leussing, D. L. *J. Am. Chem. Soc.* **1989**, *111*, 2541-2549.
48. Jefford, C. W.; Knöpfel, W.; Cadby, P. A. *J. Am. Chem. Soc.* **1978**, *100*, 6432-6436.
49. Jefford, C. W.; Knöpfel, W.; Cadby, P. A. *Tetrahedron Lett.* **1978**, *38*, 3585-3588.
50. Nierop Groot, M. N.; de Bont, J. A. M. *Appl. Environ. Microbiol.* **1998**, *64*, 3009-3013.
51. Nierop Groot, M. N.; de Bont, J. A. M. *Appl. Environ. Microbiol.* **1999**, *65*, 5590-5593.
52. Smit, B. A.; Engels, W. J. M.; Alewijn, M.; Lommerse, G. T. C. A.; Kippersluijs, E. A. H.; Wouters, J. T. M.; Smit, G. *J. Agric. Food. Chem.* **2004**, *52*, 1263-1268.
53. Mahler, H. R.; Roberts, A. *J. Am. Chem. Soc.* **1950**, *72*, 5095-5098.
54. Meyer, K. *J. Biol. Chem.* **1933**, *103*, 39-49.
55. Niki, E.; Yamamoto, Y.; Saito, T.; Nagano, K.; Yokoi, S.; Kamiya, Y. *Bull. Chem. Soc. Jpn.* **1983**, *56*, 223-228.
56. Villablanca, M.; Cilento, G. *Biochim. Biophys. Acta* **1987**, *926*, 224-230.
57. Braussaud, N.; Ruther, T.; Cavell, K. J.; Skelton, B. W.; White, A. H. *Synthesis* **2001**, 626-632.
58. Sheldrick, G. M. *SHELXL-97. Program for crystal structure refinement*, University of Göttingen: Germany, 1997.
59. Spek, A. L. *J. Appl. Cryst.* **2003**, *36*, 7-13.
60. Sheldrick, G. M. *SHELXS-97. Program for crystal structure solution*, University of Göttingen: Germany, 1997.
61. Beurskens, P. T.; Admiraal, G.; Beurskens, G.; Bosman, W. P.; Garcia-Granda, S.; Gould, R. O.; Smits, J. M. M.; Smykalla, C. *The DIRDIF99 program system*, Technical Report of the Crystallography Laboratory, University of Nijmegen: The Netherlands, 1999.
62. Altomare, A.; Burla, M. C.; Camalli, M.; Cascarano, G. L.; Giacovazzo, C.; Guagliardi, A.; Moliterni, A. G. G.; Polidori, G.; Spagna, R. *J. Appl. Cryst.* **1999**, *32*, 115-119.
63. Duisenberg, A. J. M.; Kroon-Batenburg, L. M. J.; Schreurs, A. M. M. *J. Appl. Cryst.* **2003**, *36*, 220-229.
64. Flack, H. D. *Acta Cryst.* **1983**, *A39*, 876-881.

CHAPTER 8

Oxidative Double Dehalogenation of Tetrachlorocatechol by a Dinuclear Cu^{II} Complex: Formation of Chloranilic Acid

Abstract

The copper(II) coordination chemistry of the potentially tridentate 3,3-bis(1-methylimidazol-2-yl)propionate monoanion (**L1**) was explored. The 1:1 metal to ligand complexes were found to be dinuclear. A new coordination mode of the ligand was observed in which the carboxylato group is bridging between two copper(II) centers. The dinuclear complexes exhibit a very modest catecholase activity but show a surprising reactivity towards tetrachlorocatechol. The unprecedented, stoichiometric oxidative dehalogenation of tetrachlorocatechol to chloranilic acid is reported.

P. C. A. Bruijnincx, M. Viciano, M. Lutz, A. L. Spek, J. Reedijk, G. van Koten, R. J. M. Klein Gebbink, to be submitted for publication

8.1 Introduction

Copper containing metalloenzymes play a major role in the activation of dioxygen in Nature.[1] Currently, up to seven different types of copper enzymes can be discerned based on the active site structure of the enzymes, featuring mono-, di-, tri-, or tetranuclear copper centers.[2] The active site of so-called type-3 copper enzymes, for instance, consists of two copper(II) ions in close proximity, both of which are coordinated by three histidine residues. The type-3 copper enzymes are represented by the three enzymes hemocyanin, tyrosinase, and catechol oxidase, all of which are now characterized crystallographically.[3-5] Hemocyanin reversibly binds dioxygen for transport, while the other enzymes are involved in the oxidation of phenols to catechols (tyrosinase) and subsequent two-electron oxidation of the catechols to quinones (both tyrosinase and catechol oxidase). To understand the mechanisms by which these closely related enzymes catalyze their respective transformations, many structural and functional modeling studies have been reported. Most of these studies deal with model compounds of catechol oxidase,[6-11] which have recently been reviewed.[2]

We have earlier reported on copper[12,13] and iron[14,15] complexes of the monoanionic, substituted 3,3-bis(1-alkylimidazol-2-yl)propionate ligand family as biomimetic oxidation catalysts. Homogeneous and immobilized copper(II) complexes of the parent ligand **L1** (Figure 1) have for instance been tested in the oxidation of benzyl alcohol.[13] Whereas an 1:1 ligand to copper complex was found inside a zeolite framework,[13] we mainly observed 2:1 ligand to copper species ([Cu(**L1**)$_2$]) in solution and single crystal X-ray diffraction studies (Figure 1).[12]

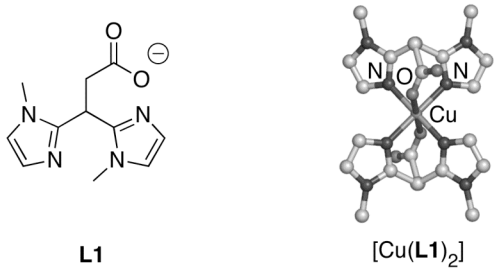

L1 [Cu(**L1**)$_2$]

Figure 1. Ligand **L1** and the 2:1 metal to ligand complex [Cu(**L1**)$_2$].[12]

Here, we have expanded our studies on the coordination chemistry of **L1** with copper(II) ions and report on new dinuclear copper(II) complexes derived from **L1**. A study of the catecholase activity of these complexes resulted in the unexpected and unprecedented formation of chloranilic acid from tetrachlorocatechol. This observation has environmental relevance. Tetrachlorocatechol is, in fact, part of a bigger group of pollutants, such as chlorinated phenols, guaiacols (2-methoxyphenols) and catechols, which are found in the low-molecular weight fraction of waste generated by, for instance, the paper bleaching industry.[16,17] These highly chlorinated organic compounds include some of the most toxic and persistent organic pollutants. A copper-mediated oxidative dehalogenation reaction, which provides a new entry into the chemical degradation of these pollutants, is described in here.

8.2 Results

Synthesis of copper(II) complexes. The coordination chemistry of **L1** towards copper(II) ions was found to be stoichiometry dependent, as was previously observed for other transition metal cations, such as zinc(II).[18] In Chapter 2, we have reported on complex [Cu(**L1**)$_2$] (Figure 1), which can be obtained by the addition of two equivalents of **L1** to a copper(II) source.[12] A different complex, however, is obtained when only one equivalent of **L1** is used. The reaction of equimolar amounts of Cu(OTf)$_2$ and K[**L1**] resulted in the isolation of a light-blue complex. According to elemental analysis, a complex of the stoichiometry [Cu$_2$(**L1**)$_2$](OTf)$_2$ ([**1**](OTf)$_2$) is formed. Previous studies showed that the positions of the symmetric and asymmetric carboxylato stretch vibrations in the IR spectrum are indicative of the binding mode of the ligand.[12,18] The IR spectrum of powderous [**1**](OTf)$_2$, however, showed a distinct absorption pattern that had not previously been observed. The asymmetric and symmetric stretch vibrations were found at 1555 and 1433 cm^{-1}, respectively. As a result, the $\Delta(\nu_{as}-\nu_s)$ amounts to only 122 cm^{-1}. This is substantially less than $\Delta(\nu_{as}-\nu_s)_{ionic}$ (188 cm^{-1}) and points to a bridging carboxylato group.[19] Furthermore, the four sharp vibrations observed at 1259, 1224, 1148, and 1028 cm^{-1} were indicative of the presence of non-coordinated triflate anions.[20-22] Further insight into the structure of [**1**](OTf)$_2$ was obtained from its ESI-MS spectrum recorded in acetonitrile. Major ions were observed at *m*/*z* = 295.99 and 740.94, corresponding to the dimeric cations [Cu$_2$(**L1**)$_2$]$^{2+}$ (calc. 296.03) and [Cu$_2$(**L1**)$_2$(OTf)]$^+$ (calc. 741.02), respectively. In addition, a signal at *m*/*z* 518.63 was observed, which can be attributed to a trimeric copper species [Cu$_3$(**L1**)$_3$(OTf)]$^{2+}$ (calc. 518.53). The molar conductivity of 243 cm^2 mol^{-1} Ω^{-1} for a 1 mM of **1** in acetonitrile fits well in the reported range for 2:1 electrolytes.[23] In addition, a d-d transition was observed at 636 nm in the electronic spectrum of **1** in acetonitrile. Based on this data, we conclude that in solution a dinuclear species [Cu$_2$(**L1**)$_2$]$^{2+}$ prevails. The proposed structure of this dication is depicted in Figure 2, consistent with the carboxylato group bridging two copper centers and non-coordinated triflate anions.

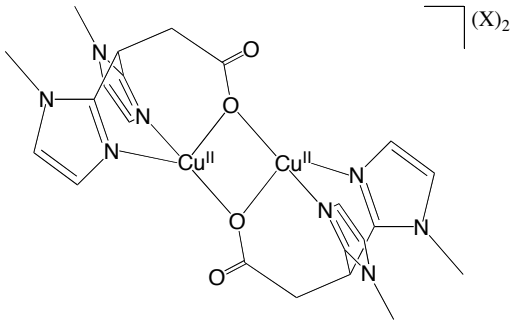

Figure 2. Proposed structure of the dication [Cu$_2$(**L1**)$_2$]$^{2+}$, X = OTf or PF$_6$.

For solubility reasons, the triflate anion in [**1**](OTf)$_2$ was exchanged for a PF_6^- anion by the addition of excess potassium hexafluorophosphate to an aqueous solution of [**1**](OTf)$_2$. The resulting light-blue powder of composition [Cu$_2$(**L1**)$_2$](PF$_6$)$_2$ ([**1**](PF$_6$)$_2$) has similar

spectroscopic properties as [**1**](OTf)$_2$ and hence the same dinuclear structure is inferred. Unfortunately, all attempts at obtaining single crystals of either [**1**](OTf)$_2$ or its PF_6 analog failed.

Catecholase activity. The dinuclear character of [Cu_2(**L1**)$_2$](X)$_2$ (X = OTf, PF_6) in solution prompted us to study the catecholase activity of these complexes in the oxidation of benchmark substrate 3,5-di-*tert*-butylcatechol (H_2dtbc) to 3,5-di-*tert*-butylbenzoquinone (dtbq) in acetonitrile solution. The product dtbq has a strong absorption band at about 395 nm and, therefore, the reaction can be easily monitored by UV-Vis spectroscopy. As complex [**1**](OTf)$_2$ dissolves only very slowly in acetonitrile, the studies described below have been performed with [**1**](PF_6)$_2$. To estimate the catecholase type activity of [**1**](PF_6)$_2$, a solution of the catalyst in acetonitrile was treated with 50 eq of H_2dtbc. The dtbq formation was followed in time by UV-Vis spectroscopy (Figure 3). The results show that complex [**1**](PF_6)$_2$ does catalyze the oxidation of H_2dtbc, but only with a very modest activity (5.2 TON after 120 min).

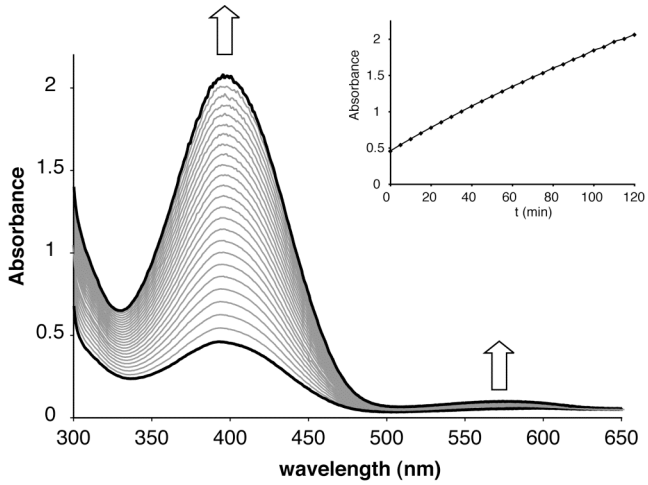

Figure 3. Oxidation of 3,5-di-*tert*-butylcatechol by [**1**](PF_6)$_2$ monitored by UV-Vis spectroscopy. Spectra were recorded at regular time intervals (5 min) over a period of 120 min. The inset shows the increase in absorption in time.

The activity was tested at different substrate concentrations. Michealis-Menten type substrate saturation behavior, which is commonly observed at higher substrate concentrations in related model studies,[2,3,24] was not observed and the reaction rate was found to be rather independent of substrate concentration in the range studied (10 – 100 eq). This phenomenon has been observed before[7,11,25] and a particularly strong binding of the substrate to the catalyst was proposed as a possible explanation.[11]

Tetrachlorocatechol binding studies. The mode of binding of catechols to the dinuclear dication [**1**]$^{2+}$ was studied by the addition of tetrachlorocatechol (H_2tcc) to a solution of [**1**](PF_6)$_2$ in acetonitrile. Tetrachlorocatechol has a higher oxidation potential than H_2dtbc,[26,27] due to its electron withdrawing substituents, and is commonly used as a pseudo-

substrate resistant to oxidation. Upon titration of a solution of [**1**]$(PF_6)_2$ with H_2tcc, a new band appears at 430 nm and concomitantly the intensity of the d-d transition decreases (Figure 4). The spectral changes correspond to the observed color change of the solution from blue to yellow upon addition of H_2tcc. The two isosbestic points at 581 and 785 nm indicate the presence of only two absorbing species in solution. These marked changes are consistent with previously observed UV-Vis spectral changes upon titration of dinuclear copper(II) complexes with tetrachlorocatechol[2,28,29] and indicate the binding of the catechol to the complex.

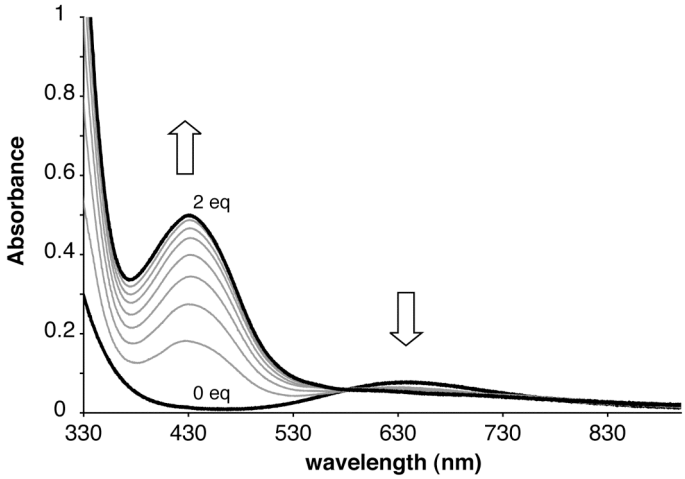

Figure 4. UV-Vis spectral changes upon addition of tetrachlorocatechol (0-2 eq in 0.25 eq increments) to a solution of [**1**]$(PF_6)_2$ in acetonitrile. Arrows indicate a decrease or increase in absorption upon addition.

In order to get further insight into the binding mode of the tetrachlorocatechol, we tried to obtain single crystals of the adduct. The crystallization solutions, however, gradually changed color and went from yellow to brown to green over the course of several weeks. A crystal structure determination on the green crystals that were obtained, revealed that the tetrachlorocatechol was no longer intact. Instead, a chloranilato (ca) moiety was found that bridges two copper(II) centers to form [Cu_2(ca)Cl_2(H**L1**)$_2$] (**2**) (Figure 5).

Crystal structure of [Cu^{II}_2(ca)Cl_2(HL1)$_2$]·8MeCN·2H_2O. Green crystals of **2·8MeCN·2H_2O** suitable for X-ray diffraction were obtained from an acetonitrile solution of [**1**]$(PF_6)_2$ and one equivalent of tetrachlorocatechol (H_2tcc) upon standing. The molecular structure of **2·8MeCN·2H_2O** is depicted in Figure 5, with selected bond lengths and angles presented in Table 1.

The crystal structure of **2·8MeCN·2H_2O** consists of discrete chloranilato bridged dimers in which the chloranilato dianion is positioned on an inversion center and is bound as a bis-bidentate bridging ligand. Each copper(II) atom is facially capped by a protonated, neutral H**L1** ligand. A chlorido anion completes the $N_2O_2O'Cl$ donor set for each copper, resulting in a severely distorted octahedral coordination geometry around the copper(II) center. The basal plane is defined by the two nitrogen donor atoms and the chloranilato

oxygens donor atoms. The copper atom is displaced 0.2713(2) Å above this plane towards the chlorido anion. The complex is centrosymmetric with the crystallographic inversion center coinciding with the center of the chloranilato ring. The intramolecular Cu···Cu separation is 7.7628(5) Å. The chloranilato moiety is planar and the structural features show delocalization of the negative charges to the lower and upper regions of the ring. This is reflected in the C12–C13 and C12a–C14 bond lengths (1.393(2) and 1.398(2) Å) and the C13–O3 and C14–O4 bond lengths (1.2627(19) and 1.259(2) Å). The C13–C14 bond length is 1.530(2) Å, indicative of a single bond. All these features result in essentially equal Cu–O distances and a symmetric binding mode of the dianion. Some end-capped dimeric [Cu_2(ca)] structures have been reported before and the observed bond lengths of the dicopper(II)-chloranilato moiety in the structure of **2·8MeCN·2H$_2$O** compare well to the reported values.[30-34] These end-capped dimeric complexes were all synthesized via self-assembly of their components, i.e. they were obtained from mixtures of chloranilic acid, a copper(II) source, and a bi- or tridentate nitrogen donor ligand.

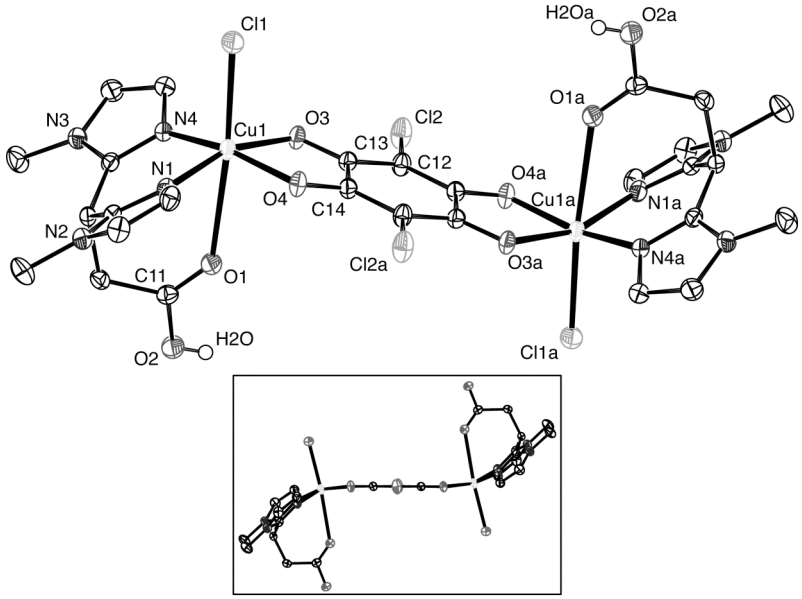

Figure 5. Molecular structure of [Cu^{II}_2(ca)Cl_2(H**L1**)$_2$] (**2·8MeCN·2H$_2$O**) in the crystal. All C–H hydrogen atoms and co-crystallized acetonitrile and water solvent molecules have been omitted for clarity. Displacement ellipsoids are drawn at the 50% probability level. Symmetry operation a: 1 – x, 1 – y, 1 – z. The inset offers a side-view of the dimer showing the planarity of the bridging chloranilato dianion.

The neutral H**L1** ligand is coordinated to copper through both 1-methylimidazole-*N* donor atoms and the carbonyl-*O* of the acid group. This is supported by the C–O bond lengths of 1.210(2) and 1.326(2) Å for C11–O1 and C11–O2, respectively, and the involvement of O2 in a hydrogen bonding interaction of the OH group of the acid with a co-crystallized water molecule, cf. Figure 6. The Cu–$O_{carbonyl}$ distance in **2·8MeCN·2H$_2$O** (2.7911(12) Å) is much longer than the Cu-$O_{carboxylato}$ distance observed in the related [Cu^{II}(**L1**)$_2$]·2H_2O (2.400 Å),[12] in which the monoanionic **L1** ligand is coordinated via its carboxylato-*O* anion.

The two co-crystallized water molecules are involved in identical hydrogen bonding patterns that connect the dimeric units into a one-dimensional ladder-like structure (Figure 6, Table 2). The carboxylic acid proton H2O is involved in a hydrogen bond with oxygen O5 of a lattice water molecule. The water molecule is in turn involved in a hydrogen bond donor with a chlorido anion of a second dimer. Finally, the water molecule forms an additional hydrogen bond with one of the co-crystallized acetonitrile molecules.

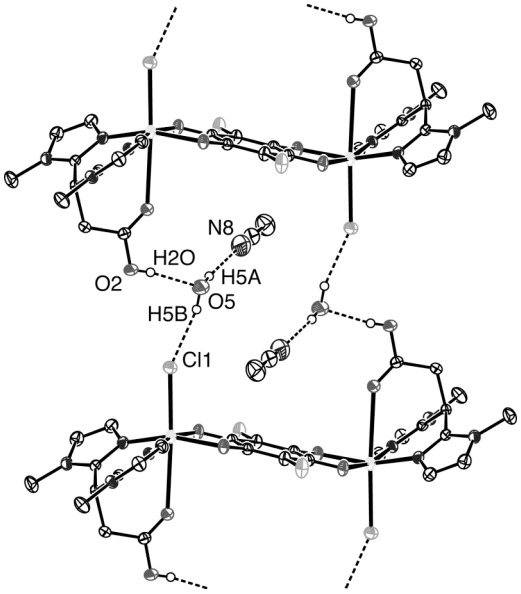

Figure 6. Hydrogen bonding network of **2·8MeCN·2H$_2$O** resulting in a ladder-like structure. All C–H hydrogen atoms and co-crystallized solvent molecules that do not participate in hydrogen bonding have been omitted for clarity.

Table 1. Selected bond lengths (Å) and angles (°) for [Cu$^{II}_2$(ca)Cl$_2$(H**L1**)$_2$]·8MeCN·2H$_2$O (**2·8MeCN·2H$_2$O**). Symmetry operation a: 1 – x, 1 – y, 1 – z

	Bond length		Angle		Angle
Cu1–Cl1	2.5171(5)	Cl1–Cu1–O1	174.62(3)	Cl1–Cu1–O3	96.99(4)
Cu1–N1	1.9607(14)	O3–Cu1–N1	161.09(6)	Cl1–Cu1–O4	95.53(4)
Cu1–N4	1.9541(14)	O4–Cu1–N4	165.93(6)	Cl1–Cu1–N1	101.06(4)
Cu1–O1	2.7911(12)	O1–Cu1–N1	77.88(5)	Cl1–Cu1–N4	97.59(4)
Cu1–O3	2.0234(12)	O1–Cu1–N4	77.19(5)	O4–Cu1–N1	91.85(5)
Cu1–O4	2.0027(12)	O1–Cu1–O3	84.66(5)	N1–Cu1–N4	90.60(6)
		O1–Cu1–O4	89.79(4)	N4–Cu1–O3	92.57(5)
				O3–Cu1–O4	80.79(5)
			Chloranilato bond lengths		
C11–O1	1.210(2)	C13–O3	1.2627(19)	C13–C12	1.393(2)
C11–O2	1.326(2)	C14–O4	1.259(2)	C12–C14a	1.398(2)
				C13–C14	1.530(2)

Table 2. Selected hydrogen bond lengths (Å) and angles (°) for $[Cu^{II}_2(ca)Cl_2(H\mathbf{L1})_2]\cdot 8MeCN\cdot 2H_2O$ (**2·8MeCN·2H$_2$O**) and $[Cu^{II}(ca)(H\mathbf{L1})(H_2O)]$ (**3**). Symmetry operations for **3**: i) – x, – y, – z; ii) 1 – x, 1 – y, 1 – z; iii) 1 + x, 1 + y, 1 + z

	Donor–H ··· Acceptor	D–H	H ··· A	D ··· A	D–H ··· A
2·8MeCN·2H$_2$O	O2–H2O ··· O5	0.73(3)	1.91(3)	2.627(2)	170(3)
	O5–H5A ··· N8	0.93(3)	2.04(3)	2.932(3)	161(3)
	O5–H5B ··· Cl1	0.87(3)	2.28(3)	3.1111(18)	159(3)
3	O1–H1O ··· O42^{i}	0.71(5)	2.05(5)	2.742(3)	166(5)
	O1–H2O ··· O21^{ii}	0.85(5)	2.07(5)	2.919(3)	173(5)
	O11–H11O ··· O32^{iii}	0.96(5)	1.65(5)	2.594(3)	169(5)

Chloranilic acid formation. The observed conversion of tetrachlorocatechol to chloranilic acid is very unusual. Since tetrachlorocatechol is stable in acetonitrile under ambient conditions, [**1**](PF$_6$)$_2$ apparently mediates the stoichiometric oxidative dehalogenation of tetrachlorocatechol to chloranilic acid (Scheme 1). Both the protons and chloride anions that are released during the reaction can be found in the final product. The monoanionic ligands **L1** are coordinated as their conjugated acids H**L1** and the chloride anions are each found coordinated to one of the copper(II) ions of the dimer. The reaction can also be performed at larger scale. Upon addition of tetrachlorocatechol to a blue solution of [**1**](PF$_6$)$_2$ in acetonitrile/water (100:1 *v*/*v*) an immediate color change to brown-yellow was observed and after stirring the reaction for a week under ambient conditions a green solution was obtained. The product was finally collected as a green crystalline solid in 41% yield. It was analyzed by elemental analysis and the spectroscopic data were compared with those of independently synthesized [Cu$_2$(ca)Cl$_2$(H**L1**)$_2$] (**2**) (*vide infra*). No product is obtained when the reaction is performed under an argon atmosphere or under water-free conditions, illustrating the requirement of water and dioxygen for formation of **2**.

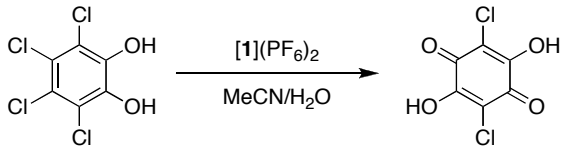

Scheme 1. Chloranilic acid formation in the reaction of [**1**](PF$_6$)$_2$ with tetrachlorocatechol.

Independent synthesis of [Cu$^{II}_2$(ca)Cl$_2$(HL1)$_2$] (2). The dinuclear chloranilato-copper(II) complex **2** can also be directly synthesized from its components. The addition of chloranilic acid to a solution containing equimolar amounts of $CuCl_2\cdot H_2O$ and [Bu$_4$N][**L1**] in methanol resulted in the precipitation and isolation of **2** as a dark green powder. The IR spectrum of **2** is identical to the one obtained for the isolated product from the reaction of [**1**](PF$_6$)$_2$ and tetrachlorocatechol (*vide supra*). The carboxylato group of **L1** is protonated upon formation of the complex, as indicated by the asymmetric stretch vibration at 1731 cm^{-1}. Vibrations at 1525 cm^{-1} and 1383 cm^{-1} can be attributed to the chloranilato group and agree

well with the approximate D_{2h} symmetry of this group.[30] The electronic spectrum of a powder sample of **2**, which has a green color, shows two absorptions at 403 and 629 nm, which can be attributed to a charge transfer band and a d-d transition, respectively.[30]

The complex is insoluble in acetonitrile. Interestingly, dissolution of green **2** in methanol yielded a blue-purple solution, whereas in DMF a pinkish-purple solution was obtained. Two absorptions are observed in the UV-Vis absorption spectrum of a solution of **2** in DMF, i.e. one at 518 nm (ε = 725 M^{-1} cm^{-1}) and a less intense transition at 679 nm (ε =150 M^{-1} cm^{-1}). The transition at 518 nm can be assigned to a chloranilato-to-copper charge transfer transition of a chloranilato moiety with *ortho*-benzoquinone character.[30] Credence for this assignment and further insight into the structure of the pink-purple chromophore was obtained from an X-ray crystal structure determination of single crystals of [Cu(ca)(H**L1**)(H_2O)] (**3**) grown from a solution of **2** in acetonitrile/methanol (*vide infra*). Apparently, a new equilibrium of both mono- and dinuclear species is established upon dissolution of **2**, which ultimately results in the crystallization of mononuclear complex **3**. Ions from both dinuclear and mononuclear species are observed in the ESI-MS spectrum of **2**. The higher extinction coefficient associated with the mononuclear pink-purple chromophore, however, causes the coloration of the solution.

Magnetic and EPR properties of 2. The EPR spectrum of a powder sample of independently synthesized **2** recorded at room temperature and 77 K showed an anisotropic signal with $g_{\|}$ = 2.2633 and $g_{\perp}$ = 2.0606 (average g value of 2.13). The EPR envelope is typical of isolated S = 1/2 spin systems with axial symmetry and the signals correspond to the $\Delta M_s = \pm 1$ allowed transitions. Variable temperature magnetic susceptibility data were collected for a powder sample of **2** at 0.1 Tesla in the temperature range of 2 – 300 K. The plot of $\chi_M T$ and χ_M versus temperature is shown in Figure 7.

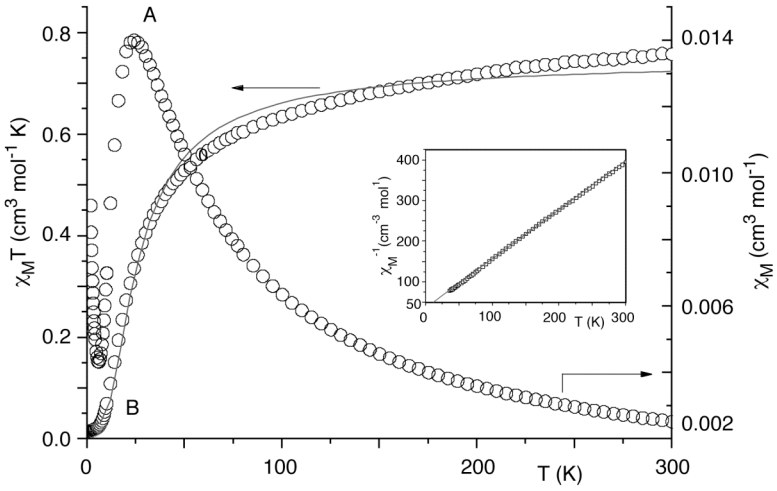

Figure 7. Plots of χ_M versus T (A) and $\chi_M T$ versus T (B) for **2** in the range of 2 to 300 K in 0.1 T field. The inset shows the plot of χ_M^{-1} versus T with the corresponding fitting.

The $\chi_M T$ product of **2** at 300 K is 0.76 cm^3 K mol^{-1}, which is in agreement with the spin-only value for two non-interacting S = 1/2 copper(II) centers (0.75 cm^3 K mol^{-1}). The $\chi_M T$ value decreases more pronounced from 65 K to 0.02 cm^3 K mol^{-1} at 5 K and is characteristic of antiferromagnetic coupling of the two copper(II) ions. The temperature dependency of the magnetic susceptibility of **2** was fit to the Curie-Weiss expression with a C value of 0.83 cm^3 K mol^{-1} and a θ value of -29.79 K. The negative θ value is again indicative of antiferromagnetic coupling between the metals.

The experimental $\chi_M T$ data were fitted to the equation for dinuclear copper compounds derived from the Hamiltonian $H = J(\mathbf{S}_1 \cdot \mathbf{S}_2)$ given as follows:[35]

$$\chi_i' = \frac{\chi_i}{1 - (2zJ'/Ng^2\beta^2)\chi_i}$$

where zJ' are the intermolecular interactions and χ_i is the magnetic susceptibility, considering the paramagnetic impurities (ρ) and the temperature independent paramagnetism (TIP) of the Cu(II) ions. The best fitted parameters are g = 2.13 (from the EPR experimental data), J = – 34.35 cm^{-1}, zJ' = – 0.098 cm^{-1}, and ρ = 0.023% (from a fit of the experimental data) with a reliability factor R of 4.4 x 10^{-4}. A TIP of $60 \cdot 10^{-6}$ cm^3 mol^{-1} (for each copper(II) ion) was taken into account. The negative J value arises from the antiferromagnetic interactions between the two metal centers and is typical for chloranilato bridged dinuclear copper(II) complexes.[31,32,36]

Crystal structure of [Cu^{II}(ca)(HL1)(H_2O)] (3). Purple crystals of **3** suitable for X-ray diffraction were obtained from a blue-purple solution of **2** in an acetonitrile/methanol mixture upon standing. The molecular structure of **3** is depicted in Figure 8, with selected bond lengths and angles presented in Table 3.

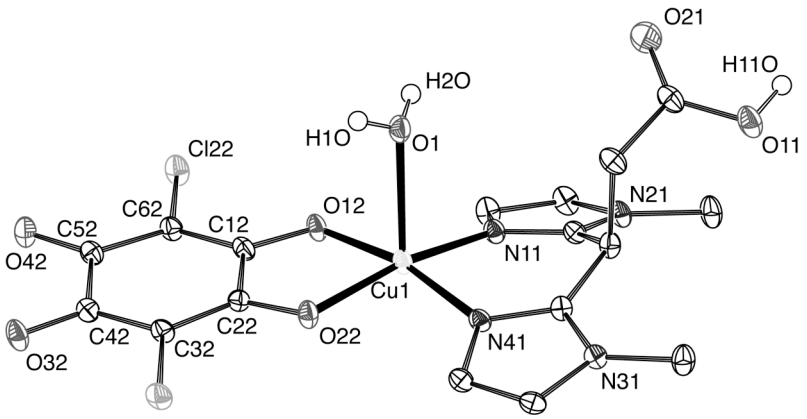

Figure 8. Molecular structure of [Cu^{II}(ca)(H**L1**)(H_2O)] (**3**) in the crystal. All C–H hydrogen atoms have been omitted for clarity. Displacement ellipsoids are drawn at the 50% probability level.

The crystal structure consists of a mononuclear, five-coordinate copper(II) complex, in which the dianionic chloranilato ligand acts as a bidentate terminal ligand. The protonated, neutral H**L1** ligand is coordinated in an *N*,*N*-bidentate fashion to the copper center by its 1-

methylimidazole-*N* donor atoms. The acid functionality is pointing away from the metal center, i.e. is non-coordinated, and is involved in hydrogen bonding interactions (*vide infra*). A water molecule completes the coordination sphere around copper, resulting in an N_2O_2O' donor set for the copper ion. The coordination geometry around the metal center is slightly distorted square pyramidal with a τ value[37] of 0.01. The basal plane is made up by the two chloranilato oxygen atoms and the two nitrogen donor atoms of the H**L1** ligand. The water molecule occupies the apical position. The copper atom is displaced 0.2024(3) Å from the best least-squares plane through the equatorial atoms towards the water molecule. The slight distortion from ideal symmetry is illustrated by the increased O1–Cu1–N41 and O1–Cu1–O22 angles (102.75(8) and 101.11(8) Å, respectively). These are the result of the water molecule being involved in two hydrogen bonding interactions, which move the oxygen atom slightly from the center of the pyramid. The structural features of **3** compare well to those reported for $[Cu^{II}(ox)(Hbip)(H_2O)]$,[38] which features the related 3,3-bis(imidazol-2-yl)propionate (Hbip) ligand and has an oxalato group as the other bidentate, dianionic ligand. Similar Cu–N and Cu–OH_2 distances are found in both complexes.

As a result of the different binding mode of the chloranilato anion, i.e. terminal bidentate in **3** vs. bis-bidentate in **2**, the observed sequence of C–C and C–O bond lengths are different. The C–O bond lengths in **3** are 1.272(3) Å (C12–O12) and 1.267(3) Å (C22–O22) for the coordinated (anionic) oxygens atoms and 1.227(3) Å (C52–O42) and 1.243(3) Å (C42–O32) for the non-coordinated (carbonyl) ones. The single C–C bond lengths observed for C12–C22 and C42–C52 together with the intermediate C–C distances for the other C–C bond lengths in the chloranilato ring, indicate charge delocalization over the lower and upper regions of the ring. These structural features are similar to those observed in the few other reported copper complexes with a terminal bidentate chloranilato ligand.[30,33,39-41]

Table 3. Selected bond lengths (Å) and angles (°) for $[Cu^{II}(ca)(H\mathbf{L1})(H_2O)]$ (**3**)

	Bond length		Angle		Angle
Cu1–O1	2.302(2)	O1–Cu1–N11	91.35(9)	O12–Cu1–N11	93.49(8)
Cu1–N11	1.971(2)	O1–Cu1–N41	102.75(8)	N11–Cu1–N41	90.85(9)
Cu1–N41	1.950(2)	O1–Cu1–O22	101.11(8)	N41–Cu1–O22	90.03(8)
Cu1–O12	1.9485(19)	O1–Cu1–O12	88.56(8)	O22–Cu1–O12	83.21(8)
Cu1–O22	1.9700(19)	O12–Cu1–N41	167.80(9)		
		O22–Cu1–N11	166.99(9)		
		chloranilato bond lengths			
C12–O12	1.272(3)	C12–C22	1.518(4)	C42–C52	1.550(4)
C22–O22	1.267(3)	C22–C32	1.390(4)	C52–C62	1.418(4)
C52–O42	1.227(3)	C32–C42	1.407(4)	C62–C12	1.375(4)
C42–O32	1.243(3)				

Three different hydrogen bonding interactions are observed in the crystal structure of **3** (Table 4, Figure 9). The carboxylic acid group oxygen of H**L1** acts as a hydrogen bond donor to the non-coordinated chloranilato oxygen O32 of a second monomeric unit and in this way an infinite, ladder-like linear chain is formed along the [1,1,1] body diagonal. The infinite linear chain is connected via two hydrogen bonds to a second infinite chain. The water molecule is the donor of two single hydrogen bonds to both the carbonyl oxygen O21 of the acid group and the other non-coordinated chloranilato oxygen O42. The two linear chains run anti-parallel to each other and the strand is further held together by a π-π stacking interaction between the chloranilato rings with an interplanar distance of 3.49 Å.

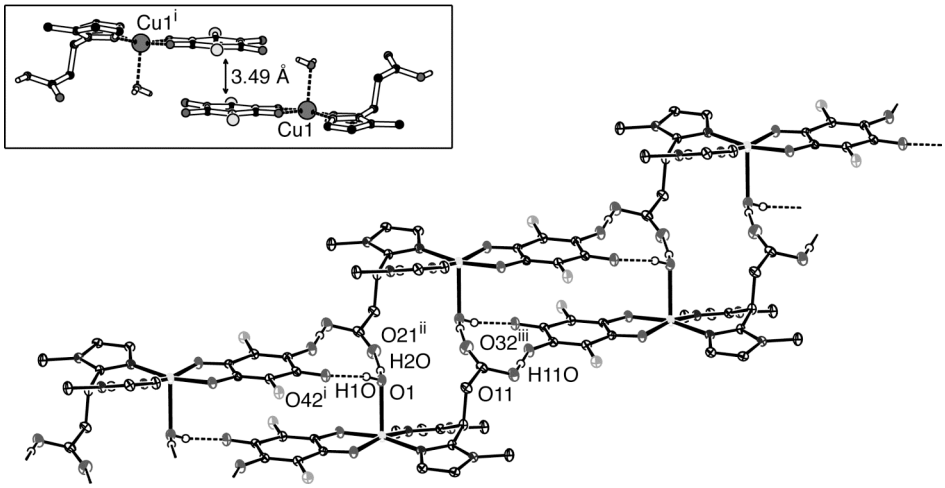

Figure 9. Hydrogen bonding network of **3** resulting in infinite strands; all C–H hydrogen atoms have been omitted for clarity. Inset: π-π stacking in the crystal structure of **3**. Symmetry operations: i) – x, – y, – z; ii) 1 – x, 1 – y, 1 – z; iii) 1 + x, 1 + y, 1 + z.

8.3 Discussion

The copper(II) coordination chemistry of ligand **L1** and the reactivity with tetrachlorocatechol as outlined here is summarized in Figure 10.

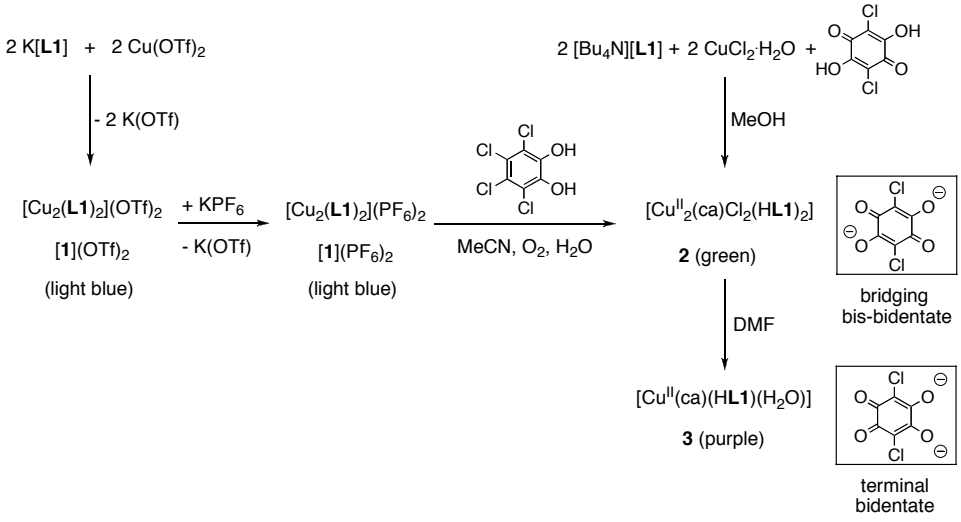

Figure 10. Synthesis and reactivity of copper(II) complexes **1**-**3**.

The isolation of a chloranilato-bridged dinuclear copper(II) complex from a reaction mixture containing [**1**]$(PF_6)_2$ and tetrachlorocatechol was rather unexpected and is very unusual. In fact, the observed oxidative dehalogenation is, to the best of our knowledge, the first report of this type of chemical degradation of tetrachlorocatechol. Dehalogenation has been reported in reactions of Cu^{I} complexes with tetrachlorobenzoquinone. Chlorido bridged dinuclear Cu^{II} complexes were found as one of the products in these reactions.[42,43] These conversions are the consequence of the well-established instability of tetrachlorobenzoquinone with respect to both reduction and dehalogenation.[17,44,45] The principal products of this conversion are tetrachlorocatechol and chloranilic acid. In contrast to tetrachlorobenzoquinone, tetrachlorocatechol is commonly used as a chemically inert catechol derivative because of its stability with respect to oxidation. Indeed, the formation of stable complexes with this electronically deactivated (pseudo)-substrate has been used to advantage in modeling studies.[11,42,46] The downside of this chemical stability is the limited biodegradation of tetrachlorocatechol as mentioned before.

A plausible mechanism for the surprising transformation of tetrachlorocatechol to chloranilic acid we have observed in the present study, involves its initial oxidation to tetrachlorobenzoquinone by [**1**]$(PF_6)_2$ (Scheme 2). Subsequently, two consecutive nucleophilic attacks of water result in dehalogenation and chloranilic acid formation with the release of two equivalents of HCl. In the presence of dioxygen the Cu^{1} ions formed in the first step are reoxidized to Cu^{II} and the dimeric complex **2** can be assembled. Importantly, the chloranilic acid product has a low acute toxicity and is unlikely to pose a major environmental threat.[17]

Further development of the stoichiometric reaction reported here might provide a new entry in the chemical oxidation and dechlorination of halogenated aromatics for waste treatment or remediation processes.[47-49]

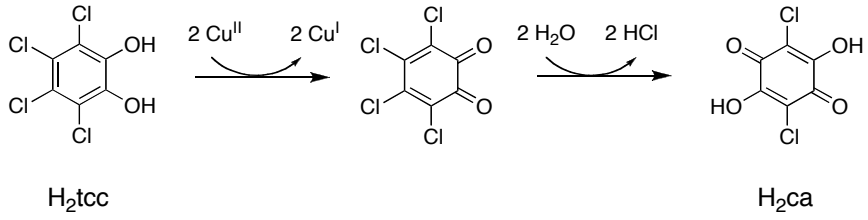

Scheme 2. Proposed mechanism for the degradation of tetrachlorocatechol (H_2tcc) to chloranilic acid (H_2ca).

Interestingly, there is biological precedent for the observed formation of chloranilic acid from tetrachlorocatechol. It has been reported that the lignin-degrading white-rot fungus *Coriolus versicolor* converts tetrachloroguaiacol to tetrachlorocatechol and finally degrades the latter to, amongst other products, chloranilic acid.[16] The enzyme that is thought to be involved in this transformation is laccase. Laccase has a so-called type-4 copper active site,[2] which comprises a trinuclear copper cluster that is composed of a type-2 mononuclear and type-3 dinuclear copper site. In this light, the reactivity of [**1**]$(PF_6)_2$ towards

tetrachlorocatechol can be regarded as a functional model of the laccase involved in the dechlorination of tetrachlorocatechol.

8.4 Conclusions

The dinuclear character of [**1**](X)$_2$ (X = OTf, PF_6), which was obtained from the reaction of stoichiometric amounts of K[**L1**] and Cu(OTf)$_2$ followed by anion exchange for the PF_6 complex, prompted us to study its catecholase activity. Although the catecholase activity is modest, a different and surprising conversion of tetrachlorocatechol into chloranilic acid was discovered. A structure determination of single crystals obtained from a solution containing tetrachlorocatechol and dinuclear [**1**](PF_6)$_2$ revealed the formation of a dinuclear copper compound containing a bridging bis-bidentate chloranilato ligand. This ligand results from a stoichiometric, oxidative double dehalogenation of tetrachlorocatechol by a homogeneous copper complex to yield chloranilic acid. This conversion is unprecedented and provides an interesting new opportunity for the degradation of persistent organic pollutants such as polychlorinated aromatic hydrocarbons. Furthermore, it is interesting to note that the supporting H**L1** ligand shows a flexible coordination chemistry, which ranges from N_2O-binding as a monoanionic ligand in [**1**](PF_6)$_2$, via N_2O(H) binding as a neutral ligand in [Cu_2(ca)Cl_2(H**L1**)$_2$] (**2**), to bidentate N_2-binding in [Cu(ca)(H**L1**)(H_2O)] (**3**).

8.5 Experimental Section

Infrared spectra were recorded with a Perkin-Elmer Spectrum One FT-IR instrument. Elemental microanalyses were carried out by the Microanalytisches Laboratorium Dornis & Kolbe, Mulheim a.d. Ruhr, Germany. ESI-MS spectra were recorded on a Micromass LC-TOF mass spectrometer at the Biomolecular Mass Spectrometry group, Utrecht University. Solution UV-Vis spectra were recorded on a Varian Cary 50, diffuse reflectance UV-Vis spectra on a Perkin-Elmer Lambda 900. Magnetic susceptibility measurements (2-300 K) were carried out using a Quantum Design MPMS-5 5T SQUID magnetometer (measurements carried out at 0.1 T). Data were corrected for magnetization of the sample holder and for diamagnetic contributions, which were estimated from Pascal's constants. X-band powder EPR spectra were obtained on polycrystalline samples with a JEOL RE2X EPR spectrophotometer with DPPH (g = 2.0036) as reference. The potassium and tetrabutylammonium salts of 3,3-bis(1-methylimidazol-2-yl)propionate (**L1**) were prepared according to a published procedure.[12] Tetrachlorocatechol was recrystallized from toluene before use. All other chemicals were commercially obtained and used as received.

[Cu^{II}_2(L1)$_2$](OTf)$_2$ ([**1**](OTf)$_2$): To a solution of K[**L1**] (289 mg, 1.06 mmol) in warm, dry methanol (10 mL) was added a solution of Cu(OTf)$_2$ (384 mg, 1.06 mmol) in dry methanol (5 mL) and the resulting deep blue solution was stirred at 50 ºC for 30 minutes during which a light blue precipitate formed. The suspension was allowed to cool to room temperature and was stirred overnight, after which the blue precipitate was separated via centrifugation. The precipitate was washed twice with dry methanol (2 × 20 mL) and the product was obtained as a blue powder (391 mg, 82%). $C_{24}H_{26}Cu_2F_6N_8O_{10}S_2$ (891.72) calc. C 32.33, H 2.94, N 12.57; found C 32.46,

H 3.10, N 12.38. IR (solid) ν = 3139.2, 2963.8, 1555.5, 1516.2, 1433.6, 1412.4, 1320.0, 1258.4, 1223.8, 1148.0, 1028.3, 958.9, 768.9, 752.9 cm^{-1}. UV-Vis (acetonitrile, ε [M^{-1} cm^{-1}]): λ_{max} = 636 (100) nm. Conductivity (1 mM in acetonitrile): Λ_M = 243 cm^2 mol^{-1} Ω^{-1}. ESI-MS: *m/z* = 295.99 {$[Cu_2(L1)_2]^{2+}$, calc. 296.03}, 445.98 {$[Cu(L1)(OTf)+H]^+$, calc. 445.99}, 518.63 {$[Cu_3(L1)_3(OTf)]^{2+}$, calc. 518.53}, 740.94 {$[Cu_2(L1)_2(OTf)]^+$, calc. 741.02}, 1186.30 {$[Cu_3(L1)_3(OTf)_2]^+$, calc. 1186.00}.

$[Cu^{II}_2(L1)_2](PF_6)_2$ ([1]$(PF_6)_2$): To a blue solution of [**1**]$(OTf)_2$ (408 mg, 0.46 mmol) in water (35 mL) was added a solution of KPF_6 (840 mg, 5 eq) in water (10 mL) and immediately a light-blue precipitate formed. The suspension was stirred for 10 min and the light-blue precipitate was separated via centrifugation. The precipitate was washed three times with water (3 × 20 mL) and the product was obtained as a light-blue powder (365 mg, 90%). $C_{22}H_{26}Cu_2F_{12}N_8O_4P_2$ (883.51) calc. C 29.91, H 2.97, N 12.68; found C 29.82, H 3.10, N 12.54. IR (solid) ν = 3157.1, 2962.0, 1555.1, 1527.2, 1515.8, 1433.1, 1411.0, 1320.2, 1289.1, 1213.8, 1171.4, 1148.9, 1092.4, 976.1, 958.4, 837.1, 818.7, 767.6, 742.8 cm^{-1}. UV-Vis (acetonitrile, ε [M^{-1} cm^{-1}]): λ_{max} = 639 (100) nm. Conductivity (1 mM in acetonitrile): Λ_M = 231 cm^2 mol^{-1} Ω^{-1}. ESI-MS: *m/z* = 296.00 {$[Cu_2(L1)_2]^{2+}$, calc 296.03}, 737.03 {$[Cu_2(L1)_2(PF_6)]^+$, calc. 737.03}, 1052.06 {$[Cu_3(L1)_3(PF_6)+F]^+$, calc. 1052.06}.

$[Cu_2(ca)Cl_2(HL1)_2]$ (2): To a blue solution of [**1**]$(PF_6)_2$ (77 mg, 0.09 mmol) in acetonitrile (6 mL) was added a solution of tetrachlorocatechol (H_2tcc) (22 mg, 0.09 mmol) in acetonitrile/water (5 mL, 100:1 *v*/*v*) and an immediate color change to yellow-brown was observed. The solution was stirred under ambient conditions for 8 days at room temperature, during which the color gradually changed from yellow-brown to green. The solution was filtered and concentrated to 3 mL. Green crystals of the composition $[Cu_2(ca)Cl_2(H\mathbf{L1})_2]\cdot 6H_2O$ grew upon standing after several weeks (35 mg, 41%). $C_{28}H_{28}Cu_2Cl_4N_8O_8\cdot 6H_2O$ (981.57) calc. C 34.26, H 4.11, N 11.42; found C 34.65, H 4.26, N 11.65. IR (solid) ν = 3419.7, 3135.3, 1732.0, 1522.2, 1504.6, 1383.4, 1286.0, 1148.3, 756.2 cm^{-1}.

$[Cu_2(ca)Cl_2(HL1)_2]$ (direct synthesis) (2): To a colorless solution of $[Bu_4N]$[**L1**] (438 mg, 0.92 mmol) in methanol (15 mL) was added $CuCl_2\cdot H_2O$ (157 mg, 0.92 mmol) and the blue solution was stirred for 5 minutes. To this solution was added a red solution of chloranilic acid (98 mg, 0.46 mmol) in methanol (5 mL) and an immediate color change to dark blue-green was observed. The solution was stirred overnight at room temperature, during which gradually a green precipitate formed. The crude product was separated by centrifugation and washed with methanol (3 × 5 mL) and diethyl ether (3 × 20 mL). The product was obtained as a dark green powder (354 mg, 88%). $C_{28}H_{28}Cu_2Cl_4N_8O_8$ (873.47) calc. C 38.50, H 3.23, N 12.83; found C 38.64, H 3.28, N 12.72. IR (solid) ν = 3144.3, 3102.4, 2961.3, 1730.7, 1525.9, 1505.3, 1383.8, 1290.5, 1178.1, 1151.2, 1136.1, 861.3, 784.4 cm^{-1}. UV-Vis (DMF, ε [M^{-1} cm^{-1}]): λ_{max} = 518 (725), 679 (150) nm. UV-Vis (diffuse reflectance): λ_{max} = 403, 629 nm. ESI-MS: *m/z* = 400.03 {$[Cu_2(ca)(HL1)_2]^{2+}$, calc. 400.00}, 504.00 {$[Cu(ca)(HL1)+H]^+$, calc. 503.97}, 799.13 {$[Cu_2(ca)(L1)_2+H]^+$, calc. 798.99}.

Catecholase activity and tetrachlorocatechol titrations. To a solution of [**1**]$(OTf)_2$ or [**1**]$(PF_6)_2$ in acetonitrile (2 mL, 0.75 mM) in a quartz cuvette was added 0.1 mL of an acetonitrile solution containing either 10, 20, 50 or 100 eq of 3,5-di-*tert*-butylcatechol. Upon addition of the substrate the blue solution immediately turned yellow. Quinone formation was monitored by recording the characteristic absorption at 395 nm. The reactions were performed under ambient conditions.

The titrations of [**1**](OTf)$_2$ and [**1**](PF$_6$)$_2$ with tetrachlorocatechol were performed through incremental additions of 10 μL aliquots of a 37.5 mM solution of tetrachlorocatechol in acetonitrile (0.25 eq) to a solution of the copper(II) complex in acetonitrile (0.75 mM, 2mL). UV-Vis spectra were recorded after each addition.

X-ray crystal structure determination of 2·8MeCN·2H$_2$O and 3. Reflections were measured on a Nonius Kappa CCD diffractometer with rotating anode (graphite monochromator, λ = 0.71073 Å) up to a resolution of $(\sin\theta/\lambda)_{max}$ = 0.65 Å^{-1}. Intensities were integrated with EvalCCD[50] using an accurate description of the experimental setup for the prediction of the reflection contours. The structures were refined with SHELXL-97[51] against F^2 of all reflections. Non hydrogen atoms were refined with anisotropic displacement parameters. All hydrogen atoms were located in the difference Fourier map. The O-H hydrogen atoms were refined freely with isotropic displacement parameters; all other hydrogen atoms were refined with a riding model. Geometry calculations and checking for higher symmetry were performed with the PLATON program.[52]

X-ray crystal structure determination of 2·8MeCN·2H$_2$O. $C_{28}H_{28}Cl_4Cu_2N_8O_8\cdot 8MeCN\cdot 2H_2O$, Fw = 1237.93, green block, 0.24 × 0.21 × 0.18 mm^3, monoclinic, $P2_1/c$ (no. 14), a = 10.1857(4), b = 11.0587(3), c = 27.1239(14) Å, β = 109.560(2)°, V = 2878.9(2) Å^3, Z = 2, D_x = 1.428 g/cm^3, μ = 0.99 mm^{-1}. 55363 Reflections were measured at a temperature of 150 K. The reflections were corrected for absorption and scaled on the basis of multiple measured reflections with the program SADABS[53] (0.79-0.84 correction range). 6601 Reflections were unique (R_{int} = 0.0418). The structure was solved with the program DIRDIF-99[54] using automated Patterson Methods. 361 Parameters were refined with no restraints. R1/wR2 [I>2σ(I)]: 0.0299/0.0745. R1/wR2 [all refl.]: 0.0398/0.0789. S = 1.040. Residual electron density between – 0.33 and 0.51 e/Å^3.

X-ray crystal structure determination of 3. $C_{17}H_{16}Cl_2CuN_4O_7$, Fw = 522.78, dark purple block, 0.30 × 0.30 × 0.15 mm^3, triclinic, $P\bar{1}$ (no. 2), a = 7.6753(3), b = 11.5330(4), c = 12.0878(4) Å, α = 111.707(2), β = 101.398(2), γ = 90.896(1)°, V = 969.88(6) Å^3, Z = 2, D_x = 1.790 g/cm^3, μ = 1.45 mm^{-1}. 13998 Reflections were measured at a temperature of 110 K. The crystal appeared to be non-merohedrally twinned with a twofold rotation about the crystallographic *b*-axis as twin operation. This twin operation was taken into account during the integration of the intensities and the refinement as a HKLF5 refinement.[55] An absorption correction was not applied due to the twinning. 4424 Reflections were unique (R_{int} = 0.0676). The structure was solved with non-overlapping reflections with the program DIRDIF-99[54] using automated Patterson Methods. 295 Parameters were refined with no restraints. R1/wR2 [I>2σ(I)]: 0.0390/0.0975. R1/wR2 [all refl.]: 0.0434/0.1002. S = 1.177. The twin fraction refined to 0.371(3). Residual electron density between – 0.72 and 0.62 e/Å^3.

8.6 References

1. Solomon, E. I.; Chen, P.; Metz, M.; Lee, S.-K.; Palmer, A. E. *Angew. Chem. Int. Ed.* **2001**, *40*, 4570-4590.
2. Koval, I. A.; Gamez, P.; Belle, C.; Selmeczi, K.; Reedijk, J. *Chem. Soc. Rev.* **2006**, *35*, 814-840.
3. Klabunde, T.; Eicken, C.; Sacchettini, J. C.; Krebs, B. *Nat. Struct. Biol.* **1998**, *5*, 1084-1090.
4. Matoba, Y.; Kumagai, T.; Yamamoto, A.; Yoshitsu, H.; Sugiyama, M. *J. Biol. Chem.* **2006**, *281*, 8981-8990.
5. Volbeda, A.; Hol, W. G. *J. Mol. Biol.* **1989**, *209*, 249-279.
6. Yang, C.-T.; Vetricheivan, M.; Yang, X.; Moubaraki, B.; Murray, K. S.; Vittal, J. J. *Dalton Trans.* **2004**, 113-121.
7. Selmeczi, K.; Réglier, M.; Giorgi, M.; Speier, G. *Coord. Chem. Rev.* **2003**, *245*, 191-201.

8. Merkel, M.; Möller, N.; Piacenza, M.; Grimme, S.; Rompel, A.; Krebs, B. *Chem. Eur. J.* **2005**, *11*, 1201-1209.
9. Koval, I. A.; Selmeczi, K.; Belle, C.; Philouze, C.; Saint-Aman, E.; Gautier-Luneau, I.; Schuitema, A. M.; van Vliet, M.; Gamez, P.; Roubeau, O.; Lüken, M.; Krebs, B.; Lutz, M.; Spek, A. L.; Pierre, J.-L.; Reedijk, J. *Chem. Eur. J.* **2006**, *12*, 6138-6150.
10. Granata, A.; Monzani, E.; Casella, L. *J. Biol. Inorg. Chem.* **2004**, *9*, 903-913.
11. Ackermann, J.; Meyer, F.; Kaifer, E.; Pritzkow, H. *Chem. Eur. J.* **2002**, *8*, 247-258.
12. Bruijnincx, P. C. A.; Lutz, M.; Spek, A. L.; van Faassen, E. L.; Weckhuysen, B. M.; van Koten, G.; Klein Gebbink, R. J. M. *Eur. J. Inorg. Chem.* **2005**, 779-787 (Chapter 2 of this thesis).
13. Kervinen, K.; Bruijnincx, P. C. A.; Beale, A. M.; Mesu, J. G.; van Koten, G.; Klein Gebbink, R. J. M.; Weckhuysen, B. M. *J. Am. Chem. Soc.* **2006**, *128*, 3208-3217.
14. Bruijnincx, P. C. A.; Buurmans, I. L. C.; Gosiewska, S.; Lutz, M.; Spek, A. L.; van Koten, G.; Klein Gebbink, R. J. M. *to be submitted* (Chapter 5 of this thesis).
15. Bruijnincx, P. C. A.; Lutz, M.; Spek, A. L.; Hagen, W. R.; Weckhuysen, B. M.; van Koten, G.; Klein Gebbink, R. J. M. *J. Am. Chem. Soc.*, accepted for publication (Chapter 3 of this thesis).
16. Iimura, Y.; Hartikainen, P.; Tatsumi, K. *Appl. Microbiol. Biotechnol.* **1996**, *45*, 434-439.
17. Remberger, M.; Hynning, P.-Å.; Neilson, A. H. *Environ. Sci. Technol.* **1991**, *25*, 1903-1907.
18. Bruijnincx, P. C. A.; Lutz, M.; den Breejen, J. P.; Spek, A. L.; van Koten, G.; Klein Gebbink, R. J. M. *to be submitted* (Chapter 7 of this thesis).
19. Deacon, G. B.; Phillips, R. J. *Coord. Chem. Rev.* **1980**, *33*, 227-250.
20. Gejji, S. P.; Hermansson, K.; Lindgren, J. *J. Phys. Chem.* **1993**, *97*, 3712-3715.
21. Gosiewska, S.; Cornelissen, J. L. M.; Lutz, M.; Spek, A. L.; van Koten, G.; Klein Gebbink, R. J. M. *Inorg. Chem.* **2006**, *45*, 4214-4227.
22. Johnston, D. H.; Shriver, D. F. *Inorg. Chem.* **1993**, *32*, 1045-1047.
23. Geary, W. J. *Coord. Chem. Rev.* **1971**, *7*, 81-122.
24. Rompel, A.; Fischer, H.; Meiwes, D.; Büldt-Karentzopoulos, K.; Dillinger, R.; Tuczek, F.; Witzel, H.; Krebs, B. *J. Biol. Inorg. Chem.* **1999**, *4*, 56-63.
25. Monzani, E.; Quinti, L.; Perotti, A.; Casella, L.; Gullotti, M.; Randaccio, L.; Geremia, S.; Nardin, G.; Faleschini, P.; Tabbì, G. *Inorg. Chem.* **1998**, *37*, 553-562.
26. Stallings, M. D.; Morrison, M. M.; Sawyer, D. T. *Inorg. Chem.* **1981**, *20*, 2655-2660.
27. Harmalker, S.; Jones, S. E.; Sawyer, D. T. *Inorg. Chem.* **1983**, *22*, 2790-2794.
28. Reim, J.; Krebs, B. *J. Chem. Soc., Dalton Trans.* **1997**, 3793-3804.
29. Torelli, S.; Belle, C.; Hamman, S.; Pierre, J.-L.; Saint-Aman, E. *Inorg. Chem.* **2002**, *41*, 3983-3989.
30. Folgado, J. V.; Ibáñez, R.; Coronado, E.; Beltrán, D.; Savariault, J.-M.; Galy, J. *Inorg. Chem.* **1988**, *27*, 19-26.
31. Fujii, C.; Mitsumi, M.; Kodera, M.; Motoda, K.-I.; Ohba, M.; Matsumoto, N.; Okawa, H. *Polyhedron* **1994**, *13*, 933-938.
32. Gallert, S.; Weyhermüller, T.; Wieghardt, K.; Chaudhuri, P. *Inorg. Chim. Acta* **1998**, *274*, 111-114.
33. Kawahara, M.; Kabir, M. K.; Yamada, K.; Adachi, K.; Kumagai, H.; Narumi, Y.; Kindo, K.; Kitagawa, S.; Kawata, S. *Inorg. Chem.* **2004**, *43*, 92-100.
34. Pierpont, C. G.; Francesconi, L. C.; Hendrickson, D. N. *Inorg. Chem.* **1977**, *16*, 2367-2376.
35. Kahn, O., *Molecular Magnetism*. Wiley-VCH: New York, 1993.
36. Chaudhuri, P.; Oder, K. *J. Chem. Soc., Dalton Trans.* **1990**, 1597-1605.
37. Addison, A. W.; Rao, T. N.; Reedijk, J.; van Rijn, J.; Verschoor, G. C. *J. Chem. Soc., Dalton Trans.* **1984**, 1349-1356.

38. Akhriff, Y.; Server-Carrió, J.; Sancho, A.; García-Lozano, J.; Escrivá, E.; Folgado, J. V.; Soto, L. *Inorg. Chem.* **1999**, *38*, 1174-1185.
39. Zheng, L.-M.; Schmalle, H. W.; Ferlay, S.; Decurtins, S. *Acta Cryst.* **1998**, *C54*, 1578-1580.
40. Reinoso, S.; Vitoria, P.; San Felices, L.; Lezama, L.; Gutiérrez-Zorilla, J. *Acta Cryst.* **2005**, *E61*, m1925-m1927.
41. Kawata, S.; Kumagai, H.; Adachi, K.; Kitagawa, S. *J. Chem. Soc., Dalton Trans.* **2000**, 2409-2417.
42. Börzel, H.; Comba, P.; Pritzkow, H. *Chem. Commun.* **2001**, 97-98.
43. Alilou, E. H.; Giorgi, M.; Pierrot, M.; Reglier, M. *Acta Cryst.* **1992**, *C48*, 1612-1614.
44. Remberger, M.; Hynning, P.-Å.; Neilson, A. H. *Ecotoxicol. Environ. Saf.* **1991**, *22*, 320-336.
45. Fang, X.; Schuchmann, H.-P.; von Sonntag, C. *J. Chem. Soc., Perkin Trans. 2* **2000**, 1391-1398.
46. Karlin, K. D.; Gultneh, Y.; Nicholson, T.; Zubieta, J. *Inorg. Chem.* **1985**, *24*, 3727-3729.
47. Sorokin, A.; Séris, J.-L.; Meunier, B. *Science* **1995**, *268*, 1161-1166.
48. Sen Gupta, S.; Stadler, M.; Noser, C. A.; Ghosh, A.; Steinhoff, B.; Lenoir, D.; Horwitz, C. P.; Schramm, K.-W.; Collins, T. J. *Science* **2002**, *296*, 326-328.
49. Lente, G.; Espenson, J. H. *Green Chem.* **2005**, *7*, 28-34.
50. Duisenberg, A. J. M.; Kroon-Batenburg, L. M. J.; Schreurs, A. M. M. *J. Appl. Cryst.* **2003**, *36*, 220-229.
51. Sheldrick, G. M. *SHELXL-97. Program for crystal structure refinement*, University of Göttingen: Germany, 1997.
52. Spek, A. L. *J. Appl. Cryst.* **2003**, *36*, 7-13.
53. Sheldrick, G. M. *SADABS: Area-Detector Absorption Correction, V2.10*, University of Göttingen: Germany, 1999.
54. Beurskens, P. T.; Admiraal, G.; Beurskens, G.; Bosman, W. P.; Garcia-Granda, S.; Gould, R. O.; Smits, J. M. M.; Smykalla, C. *The DIRDIF99 program system*, Technical Report of the Crystallography Laboratory, University of Nijmegen: The Netherlands, 1999.
55. Herbst-Irmer, R.; Sheldrick, G. M. *Acta Cryst.* **1998**, *B54*, 443-449.

SUMMARY & PERSPECTIVE

Natural metalloenzymes usually operate with high selectivity and atom efficiency under ambient conditions and in aqueous solution. It is for these reasons that metalloenzymes and enzymes in general continue to inspire synthetic chemists in their search for selective and benign catalysts and reagents. The study of these metalloenzymes through small synthetic analogues could lead to the development of bio-inspired catalysts that work under the principles of green chemistry and can thus help to make our society a more sustainable one.

The work described in this thesis is concerned with the modeling of non-heme iron enzymes that are involved in dioxygen activation. More specifically, the research focused on the versatile group of non-heme iron enzymes characterized by the 2-His-1-carboxylate facial triad at their active site (Figure 1). These enzymes catalyze a remarkably broad spectrum of oxidative transformations. Not only are selective oxidations still a synthetic challenge, many of the transformations catalyzed by this group of enzymes are unprecedented in synthetic chemistry.

Chapter 1 of this thesis provides a concise background to this interesting group of metalloenzymes and the diverse oxidative transformations they catalyze. Reflecting the interdisciplinary character of bioinorganic research, contributions from enzymology, protein crystallography, spectroscopy and modeling studies, amongst others, have resulted in a wealth of structural and as well as mechanistic information for these metalloenzymes. Several recent developments in the field expand the exciting new chemistry of these systems and are discussed as well.

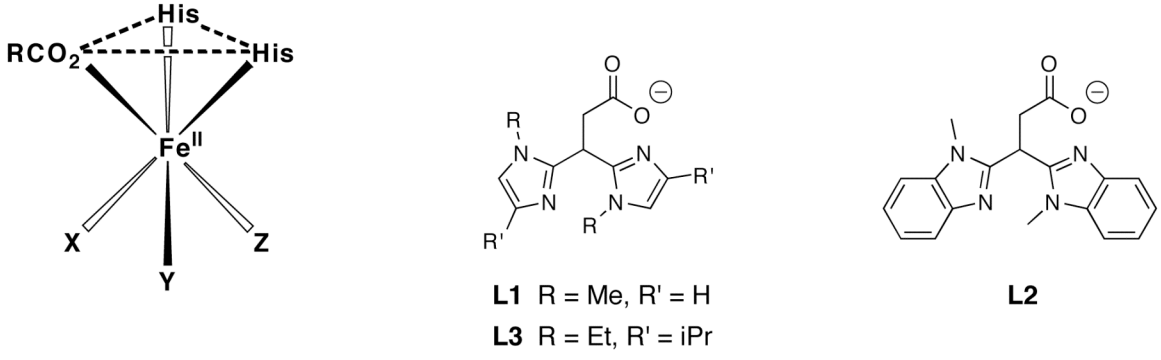

Figure 1. Schematic representation of the 2-His-1-carboxylate facial triad (left) and the new biomimetic *N,N,O* ligands **L1**, **L2**, and **L3**.

The approach to the study of small synthetic analogues of the facial triad taken in this research focused on the synthesis of ligands that would faithfully mimic the coordination environment found at the active site of these enzymes. The general structural predisposition of tripodal ligands makes them particularly suited for the facial capping of transition metals.

In Chapter 2 a general synthetic route towards the parent members **L1** and **L2** of a new family of tripodal, tridentate mononanionic *N*,*N*,*O* ligands is presented (Figure 1). The ligands incorporate the biologically relevant imidazole and carboxylato donor groups, which are combined into a single ligand framework. The applied synthetic route is relatively straightforward, allows for facile modification of the *N*,*N*-backbone and thus offers the possibility of further expansion of the ligand family. The facial capping potential of the ligands was studied using copper(II) as the spectroscopically rich probe metal. Two neutral, octahedral complexes of the type $[CuL_2]$ were isolated and characterized crystallographically. The crystal structures show that the desired facial capping mode can be attained by the new ligands and renders them suitable candidates for mimicking the 2-His-1-carboxylate facial triad.

In Chapter 3, the non-heme iron enzymes and in particular the subgroup of the extradiol cleaving catechol dioxygenases are the subject of attention. Since the enzymes of the facial triad family use a stepwise mechanism in which the substrate binds prior to dioxygen, iron(II/III)-catecholato complexes with the ligands **L1**, **L2** and the bulkier ligand **L3** were synthesized as mimics of the enzyme-substrate (E–S) complex (Figure 2). An additional advantage of constructing models of the E–S complex rather than the resting state of the enzyme is that the addition of the bidentate, anionic substrate allows for the stabilization and isolation of mononuclear complexes. This is otherwise difficult to achieve in homogeneous solution. Mononuclear ferrous and ferric complexes with both tetrachlorocatechol (H_2tcc) and 3,5-di-*tert*-butylcatechol (H_2dtbc) were synthesized to allow the study of both structure and function of these complexes, respectively. The complexes were characterized with a variety of techniques including UV-Vis and EPR spectroscopy, and ESI-MS. The crystal structure of $[Fe^{III}$(**L3**)(tcc)(H_2O)] showed that the ligands accurately mimic the facial triad and that close structural models of the E–S complex are obtained (Figure 2).

The dioxygen reactivity of the ferrous-Hdtbc complexes was found to proceed in two distinct steps. First, the complexes convert rapidly to the corresponding iron(III) complexes upon exposure to air. In the second slower step oxidative cleavage of the catechol takes place to yield, next to the quinone auto-oxidation product, both extradiol and intradiol cleavage products in roughly equal amounts. Extradiol type cleavage by biomimetic iron complexes is rare and these iron-catecholato complexes thus belong to the rather exclusive class of complexes capable of this. They are actually the first complexes with a mixed *N*/*O* donor set that display this type of reactivity.

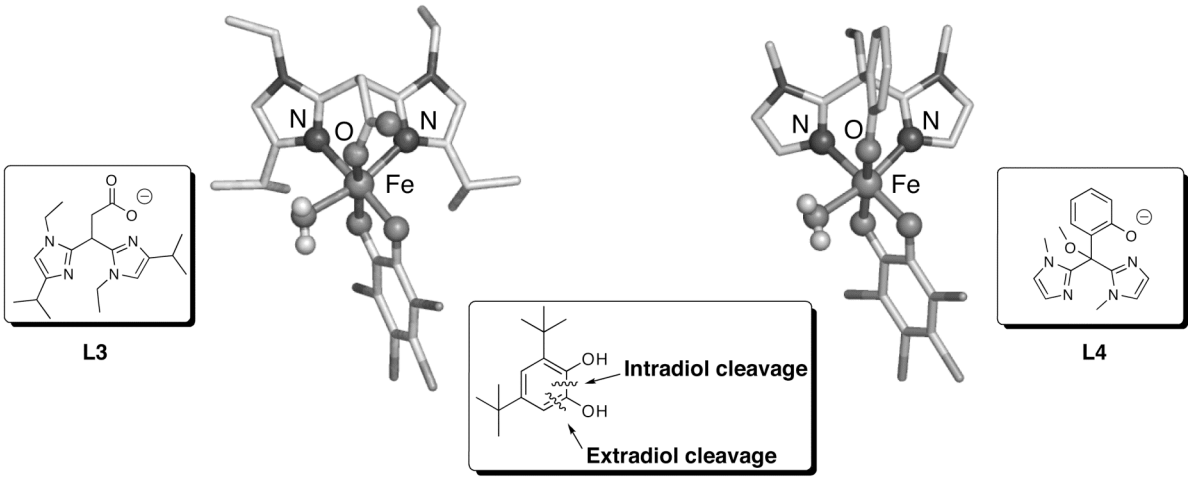

Figure 2. Structural and functional models of the extradiol (left) and intradiol (right) cleaving catechol dioxygenases.

The related *intradiol* cleaving catechol dioxygenases are the subject of Chapter 4. The active site structure of the E–S complexes of these non-heme iron enzymes differs from their extradiol counterparts in the coordinated monoanionic residue. In this case, the iron metal center is coordinated by two histidines and one tyrosine. To gain more insight into the factors determining the regioselectivity of catechol cleavage, mononuclear iron(III)-catecholato complexes with ligand **L4** (Figure 2) were synthesized and fully characterized. The tripodal monoanionic *N*,*N*,*O* ligand **L4** is similar to **L1**-**L3**, but incorporates a phenolato instead of a carboxylato group. Crystallographically characterized [Fe^{III}(**L4**)(tcc)(H_2O)] presents the closest structural model of the intradiol dioxygenase E–S complex to date (Figure 2). The complex [Fe^{III}(**L4**)(dtbc)] slowly reacts with air resulting in oxygenative cleavage of the catechol substrate. Both extradiol and intradiol type cleavage are again observed in equal amounts. Comparison of the results on the model complexes described in Chapters 3 and 4 leads to the conclusion that neither the exact ligand donor set nor the metal valency are the decisive factors for regioselective cleavage of catecholic substrates.

The more practical application of biomimetic non-heme iron complexes as homogeneous oxidation catalysts is the focus of the Chapters 5 and 6. Chapter 5 describes the synthesis and full characterization of the ferrous complexes [Fe(**L1**)$_2$] and [Fe(**PrL1**)$_2$](X)$_2$ (X = OTf, BPh_4). Ligand **PrL1** is the neutral, propyl ester precursor of **L1** (Figure 3). Different binding modes were observed for **PrL1** in the crystal structures of [Fe(**PrL1**)$_2$](BPh_4)$_2$ and [Fe(**PrL1**)$_2$($MeOH$)$_2$](OTf)$_2$, depending both on the chosen anion and the crystallization conditions. In the former complex a tridentate *N*,*N*,*O* coordination is observed (Figure 3), whereas in the latter the ligand coordinates in an *N*,*N*-bidentate fashion. [Fe(**L1**)$_2$] was found to be inactive in the oxidation of alkenes. [Fe(**PrL1**)$_2$](OTf)$_2$, on the other hand, is an active catalyst capable of both epoxidation and *cis*-dihydroxylation of various olefins using hydrogen peroxide as the oxidant. The differences in reactivity are attributed to the more facile ligand exchange in the case of the complex with neutral ligand **PrL1**.

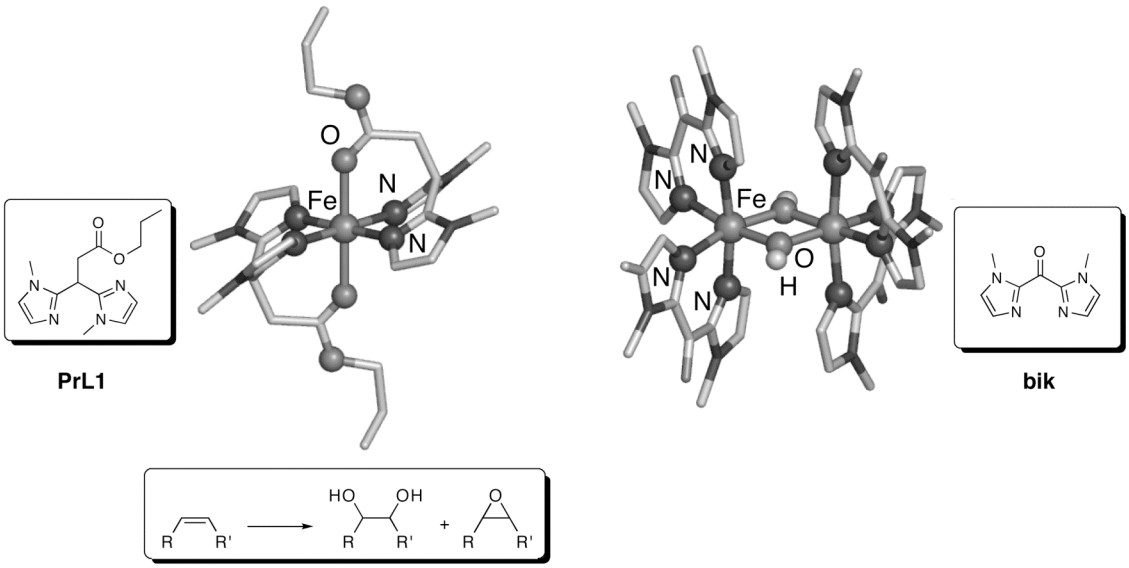

Figure 3. The mononuclear complex $[Fe^{II}(\mathbf{PrL1})_2]^{2+}$, its reactivity in the oxidation of alkanes, and the dinuclear complex $[Fe^{III}_2(\mu\text{-}OH)_2(\mathbf{bik})_4]^{4+}$.

The iron coordination chemistry and subsequent reactivity of the simple bidentate ligand bis(1-methylimidazol-2-yl)ketone (**bik**), which is a precursor of the ligands **L1**-**L3** and **PrL1**, are described in Chapter 6. An antiferromagnetically coupled dinuclear iron complex with an $[Fe^{III}_2(\mu\text{-}OH)_2]$ core was constructed via self-assembly and characterized crystallographically (Figure 3). The dinuclear complex does not persist in methanol solution and spontaneously reduces to yield a $[Fe^{II}(\mathbf{bik})_3]^{2+}$ species. The readily accessible, air-sensitive complex $[Fe^{II}(\mathbf{bik})_3](OTf)_2$ catalyzes the oxidation of alkanes with *t*-BuOOH. Interestingly, a very high 3°/2° value of 29.6 was obtained in the oxidation of adamantane, which suggests the involvement of a selective metal-based oxidant. On the other hand, a low alcohol/ketone ratio and low retention of configuration in the oxidations of cyclohexane and *cis*-1,2-dimethylcyclohexane, respectively, suggest that free radicals dominate the oxidation. Using H_2O_2 in combination with $[Fe^{II}(\mathbf{bik})_3](OTf)_2$ results in the stereoselective oxidation of various olefins, albeit with moderate efficiency.

In the last part of this thesis the zinc(II) and copper(II) coordination chemistry of the substituted 3,3-bis(1-alkylimidazol-2-yl)propionate ligand family was explored. The 2-His-1-carboxylate facial triad is also found in several different zinc containing enzymes like, e.g., thermolysin and carboxypeptidase. Chapter 7 describes efforts directed at modeling these enzymes with the ligands **L1** and **L3**. Rather than the facial capping observed in the iron complexes, a bridging coordination mode of the ligand was observed when these ligands were reacted with one equivalent of $ZnCl_2$. The complexes $[Zn(\mathbf{L1})Cl(H_2O)]$ and $[Zn(\mathbf{L3})(Cl)]$ were characterized crystallographically and in both cases a coordination polymer was obtained (Figure 5). The difference in applied steric bulk by the different ligands is reflected in the coordination number of the zinc atom, i.e. five-coordinate in the case of **L1** and four-coordinate with **L3**. In an interesting twist, an oxalato bridged coordination polymer was

obtained from a reaction mixture of [Zn(**L1**)Cl] and sodium pyruvate. This transformation constitutes the first non-oxidative formation of oxalate from pyruvate.

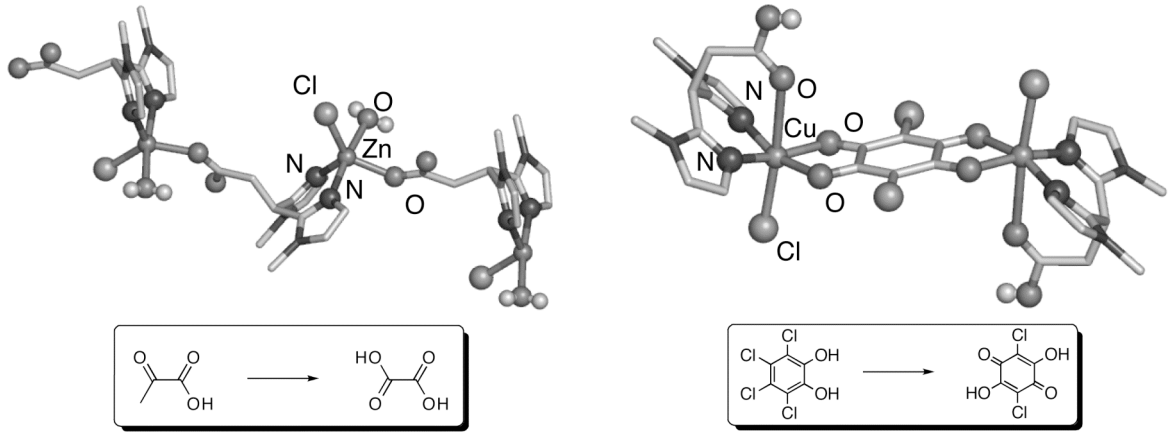

Figure 4. Unique reactivities of pyruvate (left) and tetrachlorocatechol (right) mediated by a zinc(II) and copper(II) complex of **L1**, respectively.

Finally, in Chapter 8 the copper(II) coordination chemistry of **L1** was further investigated. Dinuclear complexes were obtained with weakly or non-coordinating anions and a new coordination mode of the ligand was observed in which the carboxylato moiety is *O*-bridging between two metal centers. The dinuclear complexes were tested as functional models of catechol oxidase, but exhibited a very modest catecholase activity. Crystallization experiments, however, revealed a surprising reactivity with the pseudo-substrate tetrachlorocatechol. The crystallographic characterization of $[Cu_2(ca)Cl_2(H\mathbf{L1})_2]$ (ca, chloranilato) showed the unprecedented, stoichiometric oxidative dehalogenation of tetrachlorocatechol to chloranilic acid (Figure 4). Tetrachlorocatechol belongs to a larger group of persistent polychlorinated aromatics and the discovered reactivity might provide a new entry for the degradation of these organic pollutants. The copper complexes described in Chapter 8 also further illustrate the general coordinative flexibility of the new ligands, which enables them to coordinate either as monoanionic or neutral *N*,*N*,*O*(H)-tridentate ligands or as monoanionic or neutral *N*,*N*-bidentate ligands.

Concluding remarks and Perspective

In conclusion, the efforts devoted to the modeling of non-heme iron enzymes described in this thesis have resulted in the synthesis of biomimetic complexes of high structural fidelity, in particular of the 2-His-1-carboxylate facial triad. In addition to reproducing the structural characteristics of the active site, some of the complexes can also be regarded as functional models of the enzymes under scrutiny and have provided valuable insights into their mechanism of operation.

The new family of *N,N,O* ligands proved to be very versatile and the relatively straightforward synthesis allows for their broad use and for further expansion of the family. In Nature, the facial triad in the enzymes provides the iron metal center with a platform that enables the generation of a powerful oxidant such as the high-valent iron-oxo species. The actual chemo-, regio- and stereoselectivity of the enzymatic reaction is often brought about by the precise positioning of the substrate, via for example hydrogen bonds and π-stacking, and/or the acid-base chemistry mediated by second sphere residues. The design of second-generation ligands of the family could include such molecular recognition elements that orient the substrate and in this way steer the outcome of the reaction. The incorporation of functionalities capable of these non-covalent interactions into the ligand framework might also allow for the stabilization and characterization of the reactive intermediates. A second goal would be the synthesis of enantiopure ligand family members that would allow for the development of enantioselective oxidation catalysts. The ligand framework offers many possibilities for both types of modifications by organic synthetic methodologies in a modular approach.

The synthesized iron-catecholato complexes model the active site of the extradiol cleaving catechol dioxygenases after substrate binding. Such five-coordinate intermediates with a substrate or a cofactor bound in a bidentate fashion to the iron metal center are quite characteristic for this group of non-heme iron enzymes and can be found in many of the other subgroups of the 2-His-1-carboxylate facial triad family. These observations, therefore, illustrate the significance of the model systems described here. Further modeling studies could be extended to other subfamilies, such as the α-ketoglutarate dependent dioxygenases which couple substrate oxidation to oxidative decarboxylation of the cofactor. This is an interesting strategy and the synthesis and study of the reactivity of iron α-keto acid complexes of the new ligands could in this way lead to practical oxidation catalysts that use dioxygen as oxidant, which is an ultimate goal of biomimetic oxidation catalysis. Some of the reactions catalyzed by the non-heme iron enzymes are without precedent in synthetic chemistry. The fact that some of these reactivities, such as oxygenative catechol cleavage and *cis*-dihydroxylation, can be reproduced with simple, small synthetic analogues holds great promise for the future.

Finally, the excursions into the coordination chemistry of the new ligands with other transition metals such as copper and zinc have revealed interesting and unprecedented reactivities and further broadened the scope of the ligand system. These results exemplify the apparently unique steric and electronic properties of a '2-His-1-carboxylate' coordination environment and call for a further extension of the chemistry of the ligands developed in this thesis.

GRAPHICAL ABSTRACT

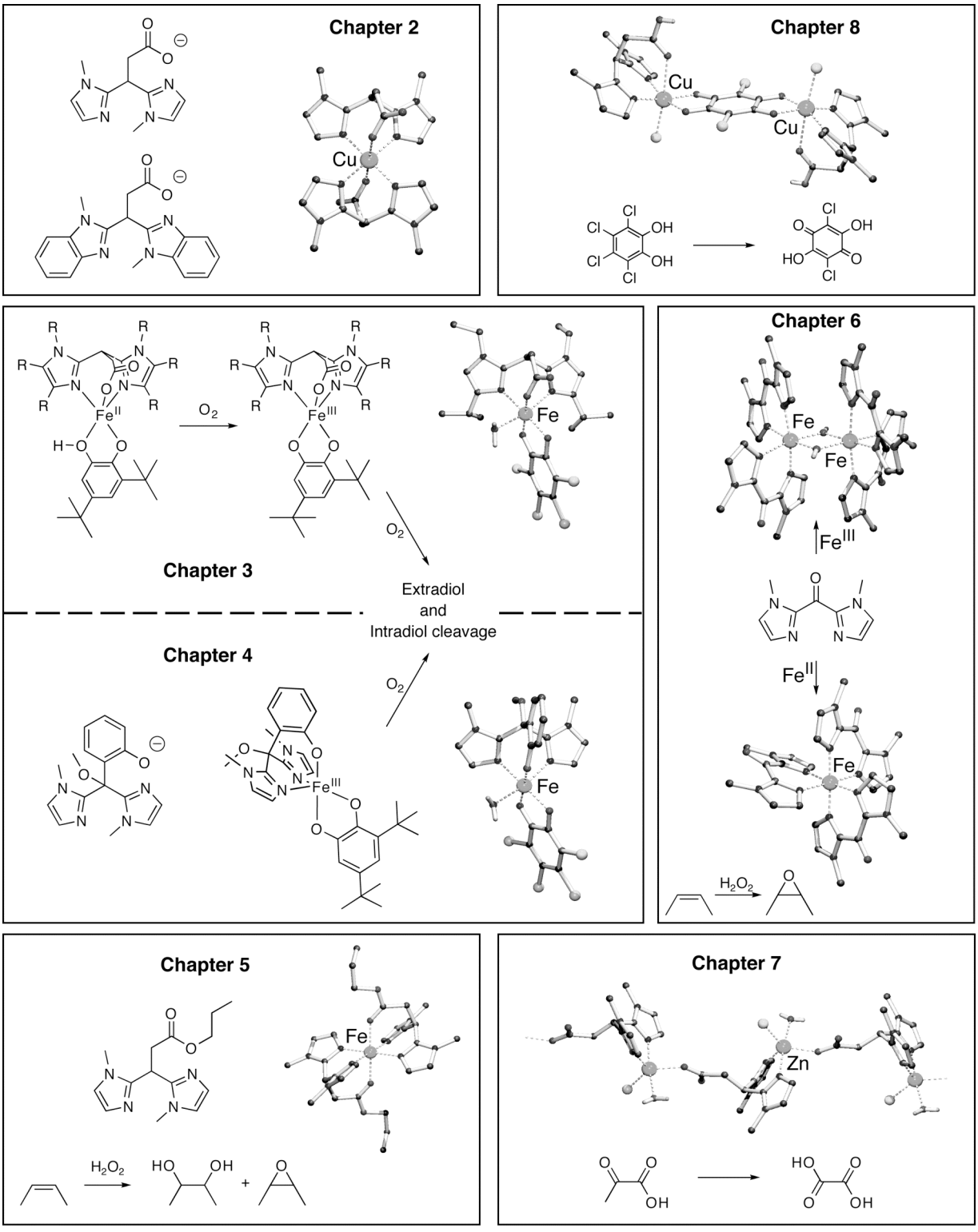

SAMENVATTING & PERSPECTIEF

In de natuur werken metaalenzymen onder milde omstandigheden en in waterige oplossingen, meestal met een grote selectiviteit en atoomefficiëntie. Juist om deze redenen vormen deze metaalenzymen, of meer in het algemeen alle enzymen, een aanhoudende inspiratiebron voor synthetisch chemici op zoek naar selectieve en milieuvriendelijke katalysatoren en reagentia. Het onderzoek naar metaalenzymen d.m.v. de studie van synthetische modelverbindingen kan zo leiden tot de ontwikkeling van op de natuur geïnspireerde katalysatoren, die werken volgens de principes van de groene chemie en zo bijdragen aan een duurzamere samenleving. Het onderzoek dat wordt beschreven in dit proefschrift betreft model studies van niet-heem-ijzerbevattende enzymen, die zijn betrokken bij het activeren van moleculaire zuurstof. In het bijzonder was de studie gericht op de veelzijdige groep niet-heem-ijzerbevattende enzymen, waarvan het actieve centrum gekenmerkt wordt door de aanwezigheid van de zogenaamde 2-His-1-carboxylaat faciale triade (Figuur 1). Deze enzymen katalyseren een opmerkelijk breed palet aan oxidatieve omzettingen. Niet alleen zijn veel van deze oxidatiereacties nog steeds een synthetische uitdaging, vele zijn zelfs ongekend in de synthetische chemie.

In Hoofdstuk 1 wordt een beknopte achtergrond van deze interessante groep enzymen en de diverse hierdoor gekatalyseerde reacties gepresenteerd. De bijdragen vanuit o.a. de enzymologie, eiwitkristallografie, spectroscopie en modelstudies weerspiegelen het multidisciplinaire karakter van de bioanorganische chemie en hebben geleid tot een schat aan structurele en mechanistische informatie over deze enzymen. Verschillende recente ontwikkelingen, die de spannende chemie van deze groep enzymen nog verder hebben verbreed, worden ook besproken.

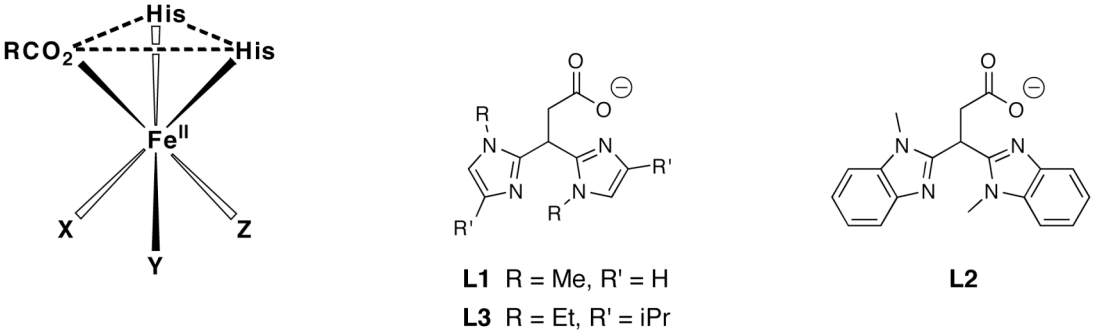

Figuur 1. Schematische weergave van de 2-His-1-carboxylaat faciale triade en de nieuwe biomimetische *N*,*N*,*O*-liganden **L1**, **L2** en **L3**.

De in dit onderzoek genomen benadering van de studie naar synthetische modellen van de faciale triade concentreerde zich op de synthese van liganden, die getrouw de coördinatie-eigenschappen van het actieve centrum nabootsen. De algemene structurele eigenschap van tripodale liganden, bijvoorbeeld, maakt hen uitermate geschikt voor faciale coördinatie van overgangsmetaalionen. Hoofdstuk 2 beschrijft een algemene syntheseroute voor de moederverbindingen **L1** en **L2** van een nieuwe familie tripodale, tridentate, monoanionische *N*,*N*,*O*-liganden. Deze liganden verenigen de biologisch relevante imidazool- en carboxylaatgroepen in één enkele ligandstructuur. De toegepaste syntheseroute is redelijk ongecompliceerd, staat eenvoudige modificatie van het *N*,*N*-geraamte toe en biedt zo de mogelijkheid tot verdere uitbreiding van de ligandfamilie. De potentie van de liganden om een metaalion faciaal te coördineren werd getest met behulp van koper(II), een metaalion met een rijk scala aan spectroscopische eigenschappen. Twee octaëdrische [CuL_2] complexen werden geïsoleerd en de structuur van deze complexen werd bepaald d.m.v. Röntgendiffractie. De kristalstructuren laten zien dat de gewenste faciale coördinatie van de liganden mogelijk is en dit maakt hen goede kandidaten voor het nabootsen van de 2-His-1-carboxylaat faciale triade.

In Hoofdstuk 3 vormen de niet-heem-ijzerbevattende enzymen en in het bijzonder de subgroep van de extradiol-klievende catecholdioxygenases het onderwerp. Aangezien de enzymen van de faciale triade familie een 'geordend' mechanisme gebruiken, wat betekent dat het binden van het substraat vooraf gaat aan het activeren van zuurstof, werden ijzer(II/III)-catecholaatcomplexen met de liganden **L1**, **L2** en het sterisch meer gehinderde ligand **L3** gesynthetiseerd als model voor het enzym-substraat (E–S) complex (Figuur 2). Bijkomend voordeel van de keuze om deze E–S-complexen te modelleren, was dat mononucleaire ijzercomplexen eenvoudiger te stabiliseren en te isoleren zijn door de toevoeging van de bidentate, anionische substraten, iets wat anders moeilijk te bewerkstelligen is in een homogeen systeem. Mononucleaire ijzer(II)- en ijzer(III)-verbindingen met zowel tetrachlorocatechol (H_2tcc) als 3,5-di-*tert*-butylcatechol (H_2dtbc) werden gesynthetiseerd om respectievelijk hun structuur en reactiviteit te bestuderen. De verbindingen werden gekarakteriseerd m.b.v. verschillende technieken, waaronder UV-Vis- en EPR-spectroscopie en ESI-MS. De kristalstructuur van [Fe(**L3**)(tcc)(H_2O)] liet zien dat op een accurate manier de faciale triade nagebootst wordt en dat nauwkeurige structurele modellen van het E–S-complex verkregen zijn (Figuur 2).

De reactiviteit van de ijzer(II)-complexen met zuurstof bleek in twee stappen te verlopen. In de eerste stap worden de verbindingen bij blootstelling aan de lucht snel omgezet in de overeenkomstige ijzer(III)-complexen. In de tweede, langzamere stap wordt de catechol oxidatief gekliefd en worden, naast het quinone autooxidatieproduct, zowel extradiol- als intradiol-gekliefde producten aangetroffen in ongeveer gelijke hoeveelheden. Biomimetische ijzercomplexen die het substraat op extradiol-wijze klieven zijn zeldzaam. De hier beschreven ijzer-catecholaatverbindingen behoren zo tot de exclusieve groep ijzercomplexen met deze reactiviteit en vormen bovendien het eerste voorbeeld met een gemengde *N*/*O* donorset.

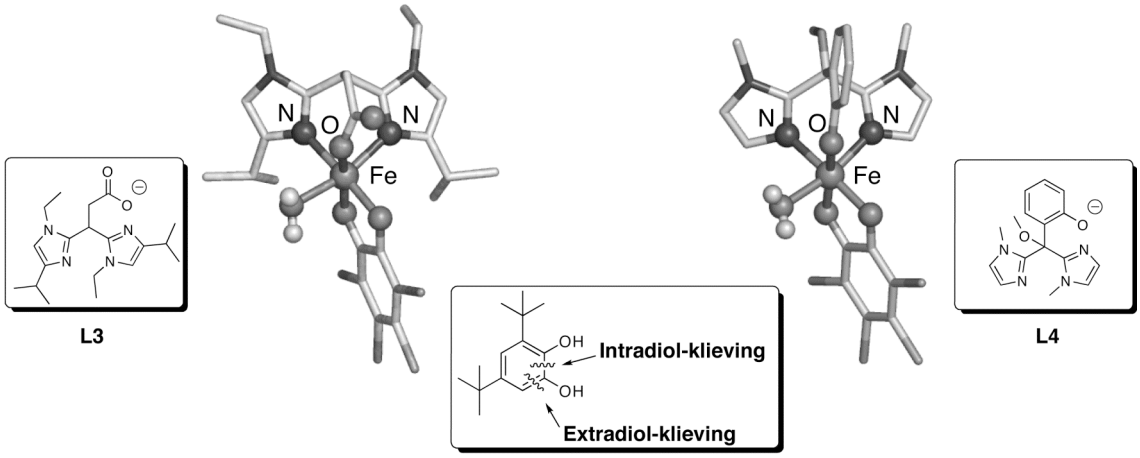

Figuur 2. Structurele en functionele modellen voor de extradiol- (links) en intradiol-klievende (rechts) catecholdioxygenases.

De verwante, *intradiol*-klievende catecholdioxygenases zijn het onderwerp van Hoofdstuk 4. Het actieve centrum van het E–S-complex van deze groep niet-heem-ijzerbevattende enzymen verschilt van hun extradiol tegenhangers in het gecoördineerde monoanionische residu. In dit geval is het ijzer(III)-metaalion gecoördineerd aan twee histidines en een tyrosine residu. Om meer inzicht te krijgen in de factoren die de regioselectiviteit van het catecholklieven bepalen, werden mononucleaire ijzer(III)-catecholaatverbindingen met het ligand **L4** gesynthetiseerd en gekarakteriseerd (Figuur 2). Het tripodale, monoanionische ligand **L4** is vergelijkbaar met de liganden **L1**-**L3**, maar bevat een fenolaatgroep i.p.v. een carboxylaatgroep. Het kristallografisch gekarakteriseerde complex [Fe^{III}(**L4**)(tcc)(H_2O)] is het tot nu toe meest nauwkeurige structurele model van het intradiol E–S-complex (Figuur 2).

[Fe^{III}(**L4**)(dtbc)] reageert langzaam met zuurstof uit de lucht, wat resulteert in het klieven van het catecholsubstraat. Wederom worden zowel extradiol- en intradiol-gekliefde producten waargenomen in vergelijkbare hoeveelheden. Een vergelijking van de resultaten van de modelverbindingen uit de Hoofdstukken 3 en 4 leidt tot de conclusie dat noch de precieze ligandsamenstelling, noch de valentie van het metaalatoom beslissende factoren zijn voor het regioselectieve klieven van het catecholsubstraat.

Een meer praktische toepassing van biomimetische niet-heem-ijzercomplexen als homogene oxidatiekatalysatoren wordt gepresenteerd in de Hoofdstukken 5 en 6. Hoofdstuk 5 beschrijft de synthese en karakterisering van de ijzer(II)-verbindingen [Fe(**L1**)$_2$] en [Fe(**PrL1**)$_2$](X)$_2$ (X = OTf, BPh_4). Het ligand **PrL1** is de ongeladen propylesteranaloog van **L1** (Figuur 3). Afhankelijk van zowel het gekozen anion als van de kristallisatiecondities bindt dit ligand het ijzer(II)-atoom op verschillende manieren, zoals aangetoond in de kristalstructuren van [Fe(**PrL1**)$_2$](BPh_4)$_2$ en [Fe(**PrL1**)$_2$($MeOH$)$_2$](OTf)$_2$. In het eerstgenoemde complex coördineerde het ligand op een tridentate *N*,*N*,*O*-wijze (Figuur 3), daar waar in het laatstgenoemde complex een *N*,*N*-bidentate coördinatiewijze werd gevonden. [Fe(**L1**)$_2$] is niet actief in de oxidatie van alkenen. [Fe(**PrL1**)$_2$](OTf)$_2$, echter, is een actieve katalysator en is in staat tot epoxidatie en *cis*-

dihydroxylering van verschillende olefines met waterstofperoxide als oxidant. De verschillen in reactiviteit van deze complexen kunnen worden toegeschreven aan de eenvoudigere liganduitwisseling in het geval van de complexen met het ongeladen ligand **PrL1**.

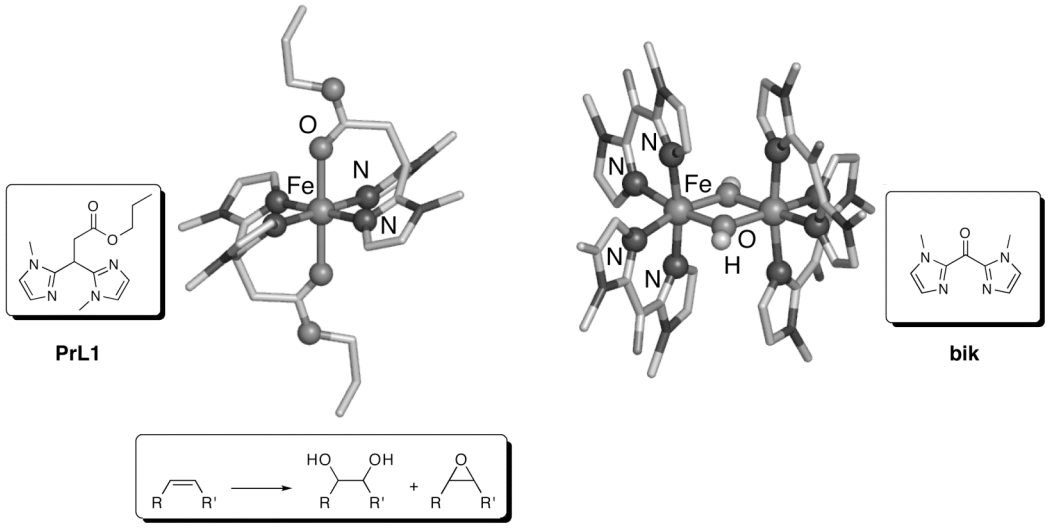

Figuur 3. De mono- en dinucleaire complexen $[Fe^{II}(\mathbf{PrL1})_2]^{2+}$ en $[Fe^{III}{}_2(\mu\text{-}OH)_2(\mathbf{bik})_4]^{4+}$.

De ijzercoördinatiechemie van het eenvoudige, bidentate ligand bis(1-methylimidazol-2-yl)keton (**bik**), alsmede de reactiviteit van diens ijzercomplexen staan centraal in Hoofdstuk 6. Een antiferromagnetisch gekoppeld, dinucleair ijzercomplex met een $[Fe^{III}{}_2(\mu\text{-}OH)_2]$ kern werd verkregen via zelf-assemblage en de structuur van dit complex werd bepaald d.m.v. Röntgendiffractie. De dinucleaire verbinding houdt geen stand in methanol en reduceert spontaan tot een $[Fe^{II}(\mathbf{bik})_3]^{2+}$ deeltje. Het eenvoudig te synthetiseren, luchtstabiele $[Fe^{II}(\mathbf{bik})_3](OTf)_2$ complex katalyseert de oxidatie van alkanen met *tert*-butyl waterstofperoxide. Opmerkelijk is dat een zeer hoge 3°/2° waarde van 29.6 werd gevonden in de oxidatie van adamantaan, wat de betrokkenheid van een selectief, metaalgebaseerde oxidant suggereert. Aan de andere kant wijzen een lage alcohol/keton-verhouding en een laag behoud van configuratie in de oxidaties van respectievelijk cyclohexaan en *cis*-1,2-dimethylcyclohexaan op een dominante rol van vrije radicalen in de oxidatiereacties. De combinatie van H_2O_2 en $[Fe^{II}(\mathbf{bik})_3](OTf)_2$ resulteert in stereospecifieke oxidatie van olefines, zoals bijvoorbeeld cycloocteen en styreen, zij het met matige efficiëntie.

In het laatste deel van dit proefschrift is de zink(II)- en koper(II)-coördinatiechemie van de nieuwe ligandfamilie verder verkend. De 2-His-1-carboxylaat faciale triade is ook gevonden in het actieve centrum van verscheidene zinkenzymen, zoals bijvoorbeeld thermolysine en carboxypeptidase. Hoofdstuk 7 beschrijft de inspanningen gericht op het synthetiseren van modelverbindingen met de liganden **L1** en **L3** voor deze enzymen. In plaats van de faciale coördinatie van de liganden, zoals eerder gevonden voor de ijzerverbindingen, werd een bruggende coördinatiewijze gevonden voor de liganden wanneer deze met een equivalent $ZnCl_2$ werden gereageerd. Van zowel $[Zn(\mathbf{L1})Cl(H_2O)]$ als $[Zn(\mathbf{L3})Cl]$ werd de kristalstructuur bepaald

en in beide gevallen werd een coördinatiepolymeer gevonden (Figuur 4). Het coördinatiegetal van het zinkatoom, vijfgecoördineerd voor **L1** en viergecoördineerd voor **L3**, weerspiegelt het verschil in sterische hindering veroorzaakt door beide liganden. Opmerkelijk was de isolatie van een oxalaat-gebrugde coördinatiepolymeer uit een reactiemengsel van [Zn(**L1**)Cl] en natriumpyruvaat. Deze omzetting is de eerste niet-oxidatieve transformatie van pyruvaat tot oxalaat.

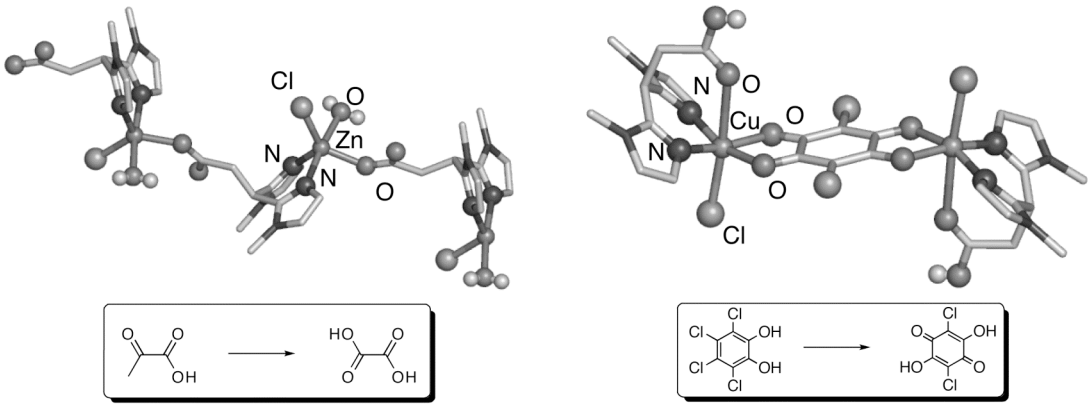

Figuur 4. Unieke reactiviteiten van pyruvaat (links) en tetrachlorocatechol (rechts), gestuurd door respectievelijk een zink- en koperverbinding van ligand **L1**.

Als laatste is in Hoofdstuk 8 de koper(II)-coördinatiechemie van **L1** verder onderzocht. Dinucleaire complexen met opnieuw een andere coördinatiewijze van het ligand werden verkregen met zwak- of niet-coördinerende anionen, waarbij de carboxylaatgroep is gebrugd tussen twee metaalionen. Deze dinucleaire complexen werden getest als functionele modellen voor catechol oxidase, maar vertoonden slechts een geringe catecholase-activiteit. Kristallisatie-experimenten onthulden echter een verrassende reactiviteit met het pseudosubstraat tetrachlorocatechol. De structuur van $[Cu_2(ca)Cl_2(H\mathbf{L1})_2]$ (ca, chloranilaat) bracht de ongekende, oxidatieve dehalogenering van tetrachlorocatechol tot chloranilzuur aan het licht (Figuur 4). Tetrachlorocatechol behoort tot een grotere groep van hardnekkige polygechloreerde aromaten en de gevonden reactiviteit biedt mogelijk een nieuwe optie voor de afbraak van deze schadelijke organische verbindingen. De kopercomplexen uit Hoofdstuk 8 illustreren ook de algemene, coördinatieve flexibiliteit van de nieuwe liganden. Deze flexibiliteit zorgt ervoor dat ze op zowel monoanionische of neutrale tridentate *N*,*N*,*O*(H)-wijze als op monoanionische of neutrale bidentate *N*,*N*-wijze kunnen coördineren.

Algemene Conclusies en Perspectief

Concluderend hebben de inspanningen gericht op het modelleren van niet-heem-ijzerbevattende enzymen zoals beschreven in dit proefschrift geleid tot de synthese van modelverbindingen van grote structurele getrouwheid, in het bijzonder van de 2-His-1-carboxylaat faciale triade. Naast de reproductie van de structurele kenmerken van het actieve centrum, kunnen sommige van de complexen ook beschouwd worden als functionele modellen

van de onderhavige enzymen en hebben zo tot waardevolle inzichten in hun werkingsmechanismen geleid.

De nieuwe familie van *N*,*N*,*O*-liganden blijkt erg veelzijdig en de relatief eenvoudige synthese laat een breed gebruik en verdere uitbreiding van de familie toe. In de Natuur biedt de faciale triade het ijzerion een platform, dat de vorming van een krachtige oxidator, zoals een hoogvalent ijzer-oxo intermediair, mogelijk maakt. De eigenlijke chemo-, regio-, en stereoselectiviteit van de enzymatische reactie wordt echter vaak bepaald door de precieze positionering van het substraat m.b.v. bijvoorbeeld waterstofbruggen en π-pakking en/of de zuur/base-chemie van zgn. tweede-schilresiduen. Het ontwerp van tweede-generatie liganden van deze familie zou zulke moleculaire herkenningselementen, die het substraat specifiek positioneren, kunnen opnemen en zo de uitkomst van de reactie bepalen. Deze functionaliteiten zouden ook de vorming en stabilisering van reactieve intermediairen mogelijk kunnen maken. Een tweede doel zou de synthese van chirale varianten van de liganden zijn, met het oog op de ontwikkeling van enantioselectieve oxidatiekatalysatoren. Het geraamte van het ligand biedt vele mogelijkheden voor beide soorten aanpassingen d.m.v. synthetisch organische methoden.

De gesynthetiseerde ijzer-catecholaatcomplexen staan model voor het actieve centrum van de extradiol-klievende catecholdioxygenases na binding van het substraat. Deze vijfgecoördineerde E–S-complexen zijn vrij karakteristiek voor de superfamilie van niet-heem-ijzerbevattende enzymen met de 2-His-1-carboxylaat faciale triade en kunnen ook in veel van de andere subgroepen gevonden worden. De verkregen resultaten zinspelen zodoende op een bredere toepasbaarheid van deze systemen. Verdere modelstudies zouden daarom kunnen worden uitgebreid tot andere subgroepen, zoals bijvoorbeeld de α-ketoglutaraatafhankelijke dioxygenases. Deze enzymen maken gebruik van een interessante strategie en koppelen de oxidatieve decarboxylering van de cofactor met oxidatie van het substraat. De synthese en studie naar de reactiviteit van ijzer-α-ketozuur verbindingen met de nieuwe liganden zouden zo kunnen leiden tot praktische oxidatiekatalysatoren die moleculaire zuurstof gebruiken als oxidant, het ultieme doel van de biomimetische oxidatiekatalyse.

Sommige van de reacties die worden gekatalyseerd door de natuurlijke systemen zijn ongekend in de synthetische chemie. Het feit dat sommige van deze reactiviteiten, zoals het oxidatief klieven van catecholen en *cis*-dihydroxyleringen, kunnen worden gereproduceerd met deze simpele synthetische modelverbindingen houdt een grote belofte voor de toekomst in.

Ten slotte hebben de uitweidingen in de coördinatiechemie van de liganden met andere overgangsmetalen zoals koper en zink geleid tot de ontdekking van interessante en ongekende reactiviteiten en hebben op deze wijze de scope van de ligandfamilie verder vergroot. Deze resultaten illustreren de schijnbaar unieke sterische en elektronische eigenschappen van een 2-His-1-carboxylaat coördinatieomgeving en vragen om een verder onderzoek naar de chemie van de liganden ontwikkeld in dit proefschrift.

DANKWOORD

Na zo'n viereneenhalf jaar is het dan zover, het werk is gedaan en alles is opgeschreven. Nu is het hoog tijd om iedereen te bedanken die mijn promotieonderzoek en alles daaromheen tot een onvergetelijke tijd hebben gemaakt. Het is echt waar, onderzoek doe je niet alleen en daarom wil ik een graag een aantal mensen bijzonder bedanken voor hun wetenschappelijke bijdrage aan dit proefschrift. Minstens net zo belangrijk is echter het leven buiten het lab. Mijn familie, vrienden en collega's wil ik dan ook bedanken voor hun steun, interesse en alle gezelligheid waardoor deze jaren niet alleen onvergetelijk maar ook ongelofelijk plezierig waren.

Als eerste wil ik graag mijn promotoren prof. dr. Gerard van Koten, prof. dr. Bert Klein Gebbink en prof. dr. Bert Weckhuysen noemen. Beste Gerard, bedankt voor de mogelijkheid die je me geboden hebt om in jouw groep ook mijn promotieonderzoek te doen en de vrijheid die je me daarin gegeven hebt. De kritische blik op mijn manuscripten en de suggesties op het juiste moment heb ik zeer gewaardeerd. Niet alleen je grote kennis van de chemie en je bijzondere chemische intuïtie, maar ook je kijk op andere zaken waren niet alleen erg leerzaam, maar ook inspirerend.

Beste Bert K., jij hebt net je eigen 'promotie' achter de rug. Je begon als mijn co-promotor en staat nu als mijn promotor in het boekje. Toen je me als hoofdvakstudent vroeg om na mijn buitenlandse stage terug te komen naar Utrecht voor een promotieonderzoek, moest ik er even over nadenken, maar ik heb er zeker geen spijt van gehad. Ik waardeer het zeer dat je deur altijd openstond voor 'even een klein vraagje' en voor het nodige advies, maar ook dat je me de ruimte hebt gegeven om dingen te proberen en paden te begaan die misschien niet altijd oorspronkelijk de bedoeling waren. Bedankt ook voor het nauwkeurig en snel corrigeren van mijn manuscripten, waardoor het lukte om dit proefschrift op tijd af te krijgen. Ik wens je veel succes met de nieuwe, spannende onderzoeksrichting die we nu met onze groep inslaan.

Beste Bert W., ik heb de samenwerking met jouw en de vakgroep Anorganische Chemie & Katalyse als een zeer plezierig en erg leerzaam deel van dit project ervaren. Al verschillen onze werelden in het Went en het Kruyt soms wat van elkaar wat betreft achtergrond, technieken en (vak)taal (al klonk het Vlaams mij als bijna-Belg erg prettig in de oren), de meerwaarde van ons gezamenlijke project spreekt, denk ik, uit de resultaten. Ik kijk met plezier terug op onze werkbesprekingen. Jouw enthousiasme zorgde ervoor dat ik altijd met een zeer positief gevoel uit het Went terugkwam.

Graag bedank ik ook de overige stafleden van de vakgroep OCC, dr. Johann Jastrzebski, dr. Gerard van Klink (weer een Brabander minder!), dr. Berth-Jan Deelman en dr. Jaap Boersma voor alle hulp, adviezen en suggesties over de jaren. Johann, bedankt dat ik altijd bij je terecht kon voor allerlei wetenschappelijke, maar vooral ook voor praktische en computerproblemen, die je vaak ter plekke voor me oploste. Ook wil ik graag Henk Kleijn

van harte bedanken voor alle bestellingen, hulp bij weigerende apparaten en alle andere dingen die je voor je rekening neemt. Om dezelfde redenen zou ik ook Ed Vlietstra van harte willen bedanken. Een vakgroep als de onze kan niet bestaan zonder goede secretariële ondersteuning, op het laatst van Milka en de jaren daarvoor van Margo. Margo, heel erg bedankt voor alle hulp en alle dingen die je in de loop van de tijd geregeld hebt, op het laatst zelfs nog vanuit het bestuursgebouw (toen ik, zoals gewoonlijk, weer eens wat aan de late kant was met allerlei zaken). Hester, ook jij bedankt voor de dingen die je (vaak even tussendoor) voor me regelde.

Zoals gezegd: onderzoek doe je niet alleen. Vele samenwerkingen hebben bijgedragen aan het onderzoek dat beschreven is in de verschillende hoofdstukken. Allereerst wil ik 'mijn' studenten Inge Buurmans, Johan den Breejen en Stefan Oosterhout bedanken voor hun inzet en voor het verzette werk. Ik heb het erg leuk gevonden om jullie te begeleiden. Inge, jouw enthousiasme en harde werken leidde tot mooie resultaten die uiteindelijk onderdeel zijn geworden van twee hoofdstukken van dit proefschrift. Johan, de zinkchemie waar je mee worstelde was niet eenvoudig, maar door jouw volharding is het een leuk stuk geworden. Veel succes met je eigen promotieonderzoek.

Een belangrijk onderdeel van dit project was de samenwerking met de vakgroep Anorganische Chemie & Katalyse. Dr. Kaisa Kervinen en later ook dr. Gerbrand Mesu wil ik dan ook van harte bedanken voor de leuke samenwerking, die uiteindelijk geleid heeft tot een mooie paper met geïmmobiliseerde complexen. Ook de twee weken bij het synchrotron in Grenoble waren een aparte, maar erg leuke ervaring. Thanks, also to dr. Andy Beale for being good company during the (long) night shifts. Fouad Soulimani zou ik graag willen bedanken de verrichte Raman metingen. Jaap Bergwerff en dr. Ferry Winter wil ik graag bedanken voor de gezelligheid tijdens onze studie en later als aio's.

Mijn grote dank gaat uit naar de kristallografen dr. Martin Lutz, dr. Duncan Tooke en prof. dr. Ton Spek voor het bepalen van de vele kristalstructuren. Het proberen te groeien van mooie kristallen heeft me heel wat uurtjes gekost, maar door jullie grote expertise en geduld zijn er uiteindelijk veel structuren in dit boekje terechtgekomen en was het zeker de moeite waard. Martin, hoe vaak zag ik je niet met een vragend gezicht de hoek om komen? Soms was de uitkomst een (grote) verrassing, soms precies waar we naar op zoek waren. Uiteindelijk ben je bij alle experimentele hoofdstukken van dit proefschrift betrokken geraakt en graag wil ik je dan ook hartelijk bedanken voor de prettige samenwerking en je enthousiasme voor mijn onderzoek.

Prof. dr. Fred Hagen van de Technische Universiteit Delft wil ik graag bedanken voor de soepele en succesvolle samenwerking op het gebied van de EPR spectroscopie. De metingen aan mijn ijzerverbindingen hebben leuke resultaten opgeleverd en vormen een belangrijk onderdeel van de hoofdstukken 3 en 4. Dr. Ernst van Faassen zou ik graag willen bedanken voor het opnemen van de koper EPR spectra en de goede samenwerking. Ronald van Ooijen wil ik graag bedanken voor de vele massaspectrometrische metingen die hij voor en met mij heeft gedaan en de bereidheid om er altijd nog snel even één extra te meten.

Marta Viciano, dr. Manuel Quesada, dr. Stefania Tanase en prof. dr. Jan Reedijk van de Universiteit Leiden dank ik hartelijk voor de bepaling van de magnetische eigenschappen van

sommige van mijn verbindingen en voor de prettige samenwerking. Dr. Sergio Bambirra en dr. Andries Bruins van de Rijksuniversiteit Groningen wil ik graag bedanken voor hun hulp bij de anaërobe massaspectrometrische metingen. Helaas is het maar bij één trip naar het hoge noorden gebleven en was er geen tijd meer voor de andere geplande metingen. Jan den Boesterd, Ingrid van Rooijen en Aloys Lurvink wil ik graag bedanken voor hun behulpzaamheid en creativiteit bij het maken van de vele posters en het omslag van dit proefschrift.

Het grootste deel van de tijd sta je echter toch gewoon achter de zuurkast op het lab en vooral door de leuke (werk)sfeer en de gezelligheid zijn de vier jaar omgevlogen. De vakgroep Organische Chemie & Katalyse was door alle borrels, sinterklaasvieringen, etentjes, labstaps, kerstdiners, congressen, de NIOK cup en alle andere activiteiten tijdens en na werktijd een geweldige plaats om te werken. Als eerste wil ik graag Bart, Guido (nog een laatste dan?), Silvia, Kees, Aidan, Margo, Hester, en de Angry Beavers Alexsandro, Preston en Elena bedanken voor alle gezelligheid tijdens de vele avonden, die op de een of andere manier altijd in de Filemon leken te eindigen. Alle aio's, post-docs en studenten van Zuid I, Catelijne (het is echt een stuk stiller zonder jou), Rob C. (mijn oude mentor), Silvia, Henk, Peter, Nilesh, Marcella, Sipke, Dennis, Marcel, Kamil en Morgane: het was een plezier om met jullie op het lab te staan. Jeroen en Sipke wil ik in het bijzonder bedanken voor hun hulp bij alle mogelijke NMR problemen. Bedankt ook: Erwin, Birgit, Thomas, Jerôme, Maaike, Rob K., Monika, Jeroen, Anne, Marianne, Judith, Alexey, Joep, Patrick, Jie, Nesibe, Harm, Niels, Silvester, Michel, Martijn, Sander, Sara, Koen en de buren van de FOC, Kees, Jan, Layo, Jacco en alle anderen voor alle hulp, de samenwerking, discussies en het broodnodige geouwehoer op zijn tijd.

Gelukkig was er naast al dat werk nog genoeg tijd voor een leven naast de chemie, al was dat tijdens de laatste loodjes helaas wat minder dan ik had gewild. Bart, Odile, Belén, Anil, Robert, Seza, Reinier, Irene, en Monica wil ik graag bedanken voor de getoonde interesse en voor alle leuke dingen die voor de nodige afleiding zorgden, van de pubquiz tot copieuze etentjes. Joost, ook al zien we elkaar niet al te vaak, ik vind het altijd erg gezellig. Daan, Robert en Michel: Ik ben blij dat onze vriendschap ook aan deze kant van de plas overeind is gebleven, it's good to be a Florida Gator (dat weekendje moet er trouwens nu toch echt eens van komen).

Dat een groot deel van mijn leven zich nog in Roosendaal afspeelt, komt vooral ook doordat de oude Gertrudis groep na al die jaren gelukkig nog steeds (deels) intact is. Bart, Raymond, Stijn, Jeroen, Daan, Ruud, Rudy, Bram, Edwin, Thijs en Rob, bedankt voor de getoonde interesse (ja, ik kan nu heel goed titreren) en natuurlijk alle genoten gezelligheid van de vele vakanties en weekendjes tot het doornemen van de week onder het genot van een pilske. Ik hoop dat we dat nog lang vol kunnen houden. Voor de sportieve ontspanning was er het voetbal. Al weet ik nog steeds niet precies waarom dat nou per se zo vroeg op de zondagochtend moest, toch wil ik graag Frank, Bas, Raymond, Stijn, Brooij, Bart, Johan, Mario, Ivo, Sandra, Chantal, Mariska, Kristel en alle teamgenoten van 't achtste bedanken voor alle lol tijdens de wedstrijden, de weekendjes weg en alle goede feestjes. Wat waren we

goed (in de derde helft)! Helaas was het op het eind niet meer goed te combineren, ik mis het toch wel een beetje.

Bart en Robert, jullie zijn al een aantal keer voorbijgekomen. Ik vind het erg fijn dat jullie mijn paranimfen willen zijn. Bart, het was lange weg tot hier en ik ben blij dat we hem samen hebben afgelegd. Al lijkt het erop dat we nu (eindelijk?) andere dingen gaan doen, ik reken erop dat dat niet uit zal maken. Robert, ook onze levens hebben zich sinds die druilerige voetbalmiddag in Gainesville vrijwel parallel aan elkaar voltrokken (al werd ik uiteindelijk werkloos en jij assistent-professor). Allebei bedankt voor jullie vriendschap en beiden veel succes met jullie eigen promoties.

I would also like to thank Anna, Ján, Renáta, Milan, Lukáš and Jakub of the Gosiewski family for the warm welcome in the family and the pleasant stays in Bratislava. Andrej, thank you for all the enjoyable evenings and for introducing me to all the local specialities.

Een goede thuisbasis is erg belangrijk. Ik wil dan ook graag mijn ouders, Marloes, Dennis, Oma en de rest van de familie bedanken voor hun steun, interesse en de gezelligheid bij familiegelegenheden. Oma, erg fijn dat U er bij bent op mijn promotie.

Pa en ma, dit proefschrift is niet voor niets aan jullie opgedragen. Bedankt voor alle hulp, liefde en de onvoorwaardelijke steun. Dat ik tot hier gekomen ben, heb ik voor een groot deel aan jullie te danken.

Dit boekje is echter niet het belangrijkste dat ik aan mijn aio periode in Utrecht overhoud. Lieve Silvia, bedankt voor alle steun, hulp en liefde in de afgelopen periode. Toen ik meer dan vier jaar geleden begon, deelden we slechts een kantoor en twee labbanken, nu delen we ons leven. Het zit er eindelijk op. Na twee promoties hebben we nu alle tijd om van dat leven samen iets moois te maken.

Pieter

CURRICULUM VITAE

De schrijver van dit proefschrift werd geboren op 9 april 1979 te Roosendaal. Na het behalen van het VWO diploma in 1997 aan het Gertrudis Lyceum, begon hij datzelfde jaar met de studie Scheikunde aan de Universiteit Utrecht. Na een bijvak Fysisch-Organische Chemie (prof. dr. L. W. Jenneskens) en een hoofdvak Organische Synthese (prof. dr. G. van Koten), verbleef de schrijver zes maanden aan het Scheikunde departement van de University of Florida voor een onderzoeksstage in de Bio-Anorganische Chemie (prof. dr. M. J. Scott). Het doctoraal examen werd afgelegd in augustus 2002 met het judicium cum laude.

Van september 2002 tot september 2006 verrichtte de schrijver het in dit proefschrift beschreven onderzoek als Assistent in Opleiding in de vakgroep Organische Chemie & Katalyse onder de supervisie van prof. dr. G. van Koten en prof. dr. R. J. M. Klein Gebbink. Het onderzoek werd financieel ondersteund door de toponderzoekschool NRSC-C en bestond uit een gezamenlijk project met de vakgroep Anorganische Chemie & Katalyse van prof. dr. B. M. Weckhuysen. Delen van het onderzoek hier beschreven werden gepresenteerd op verschillende nationale en internationale bijeenkomsten, zoals de 'Netherlands' Chemistry and Catalysis' Congressen (NCCC), de '7th European Biological Inorganic Chemistry Conference' (EUROBIC-7, Garmisch-Partenkirchen, Duitsland) en de '12th International Conference on Biological Inorganic Chemistry' (ICBIC-12, Ann Arbor, VS) en werd onderscheiden met een Faustus Poster Award (ICBIC-12) en een Best Lecture Award (NCCC7).

The author of this thesis was born on April 9, 1979, in Roosendaal, the Netherlands. After graduating from high school at the Gertrudis Lyceum in 1997, he went on to study Chemistry at Utrecht University that same year. After a minor in Physical-Organic Chemistry (prof. dr. L. Jenneskens) and a major in Organic Synthesis (prof. dr. G. van Koten), the author spent six months at the chemistry department of the University of Florida (USA) for a research project on Bioinorganic Chemistry (prof. dr. M. J. Scott). He obtained his MSc degree in 2002 with the distinction cum laude.

From September 2002 until September 2006 the author worked as a PhD student in the Organic Chemistry & Catalysis group under the supervision of prof. dr. G. van Koten and prof. dr. R. J. M. Klein Gebbink on the research described in this thesis. The research project was financially supported by the National Research School Combination-Catalysis (NRSC-C) and consisted of a joint collaboration with the Inorganic Chemistry & Catalysis group of prof. dr. B. M. Weckhuysen. Parts of the research described in this thesis were presented at several national and international meetings, including the Netherlands' Chemistry and Catalysis conferences (NCCC), the 7th European Biological Inorganic Chemistry Conference (EUROBIC-7, Garmisch-Partenkirchen, Germany), and the 12th International Conference on Biological Inorganic Chemistry (ICBIC-12, Ann Arbor, USA). The author was awarded a Faustus Poster Award (ICBIC-12) and a Best Lecture Award (NCCC7) for these presentations.

LIST OF PUBLICATIONS

Bis(1-methylimidazol-2-yl)propionates and Bis(1-methylbenzimidazol-2-yl)propionates: A New Family of Biomimetic N,N,O Ligands. Synthesis, Structures and Cu^{II} Coordination Complexes
P. C. A. Bruijnincx, M. Lutz, A. L. Spek, E. E. van Faassen, B. M. Weckhuysen, G. van Koten, and R. J. M. Klein Gebbink, *Eur. J. Inorg. Chem.* **2005**, 779-787. (Chapter 2)

Dichloro(di-2-pyridylamine)zinc(II): A Redermination at 110K
M. Lutz, A. L. Spek, P. C. A. Bruijnincx, R. J. M. Klein Gebbink, and G. van Koten, *Acta Cryst.* **2005**, *E61*, m1813-m1815.

Zeolite Framework Stabilized Copper Complex Inspired by the 2-His-1-Carboxylate Facial Triad Motif yielding New Oxidation Catalysts
K. Kervinen, P. C. A. Bruijnincx, A. M. Beale, J. G. Mesu, G. van Koten, R. J. M. Klein Gebbink and B. M. Weckhuysen, *J. Am. Chem. Soc.* **2006**, *128*, 3208-3217.

Novel Enantiopure non-C_2-symmetric NCN-Pincer Palladium Complexes with L-Proline Chiral Auxiliaries: mer η_3-N,C,N vs. Square Planar η_4-N,C,N,O Coordination
S. Gosiewska, M. Huis in 't Veld, J. J. M. de Pater, P. C. A. Bruijnincx, M. Lutz, A. L. Spek, G. van Koten, and R. J. M. Klein Gebbink, *Tetrahedron: Asymmetry* **2006**, *17*, 674-686.

Modeling the 2-His-1-carboxylate Facial Triad: Iron-Catecholato Complexes as Structural and Functional Models of the Extradiol Cleaving Dioxygenases
P. C. A. Bruijnincx, M. Lutz, A. L. Spek, W. R. Hagen, B. M. Weckhuysen, G. van Koten, and R. J. M. Klein Gebbink, *J. Am. Chem. Soc.,* accepted for publication. (Chapter 3)

Iron(III)-Catecholato Complexes as Structural and Functional Models of the Intradiol Cleaving Catechol Dioxygenases
P. C. A. Bruijnincx, M. Lutz, A. L. Spek, W. R. Hagen, G. van Koten, and R. J. M. Klein Gebbink*, J. Am. Chem. Soc.*, submitted for publication. (Chapter 4)

Dendritic Host Molecules with a Polycationic Core and an Outer Shell of Dodecyl Groups
R. van de Coevering, P. C. A. Bruijnincx, R. J. M. Klein Gebbink, and G. van Koten, *Eur. J. Org. Chem*, submitted for publication.

Iron(II) Complexes with Bio-Inspired N,N,O Ligands as Oxidation Catalysts: Olefin Epoxidation and cis-Dihydroxylation
P. C. A. Bruijnincx, I. L. Buurmans, S. Gosiewska, M. Lutz, A. L. Spek, G. van Koten, and R. J. M. Klein Gebbink, to be submitted. (Chapter 5)

Oxidative Double Dehalogenation of Tetrachlorocatechol by a Cu^{II} Complex
P. C. A. Bruijnincx, M. Viciano, M. Lutz, A. L. Spek, J. Reedijk, G. van Koten, and R. J. M. Klein Gebbink, to be submitted. (Chapter 8)

Mononuclear Non-Heme Iron Enzymes with the 2-His-1-Carboxylate Facial Triad: Recent Developments in Enzymology and Modeling Studies
P. C. A. Bruijnincx, G. van Koten, and R. J. M. Klein Gebbink, manuscript in preparation. (Chapter 1)

Mono- and Dinuclear Iron Complexes with Bis(1-methylimidazol-2-yl)ketone (bik): Structural Characterization and Catalytic Oxidation Studies
P. C. A. Bruijnincx, I. L. C. Buurmans, M. Quesada, M. Viciano, S. Tanase, M. Lutz, D. C. Tooke, A. L. Spek, J. Reedijk, G. van Koten, and R. J. M. Klein Gebbink, manuscript in preparation. (Chapter 6)

Structure and Reactivity of Zinc Complexes of the Biomimetic N,N,O Ligand Family of Substituted 3,3-Bis(1-methylimidazol-2-yl)propionates: The Formation of Oxalate from Pyruvate
P. C. A. Bruijnincx, M. Lutz, J. P. den Breejen, A. L. Spek, G. van Koten, and R. J. M. Klein Gebbink, manuscript in preparation. (Chapter 7)